Numerical modelling and upscaling of modified salinity waterflooding

Bonto, Maria

Publication date:
2021

Document Version
Publisher's PDF, also known as Version of record

DTU Compute
DHRTC

Numerical modelling and upscaling of modified salinity waterflooding

PhD Thesis

2021

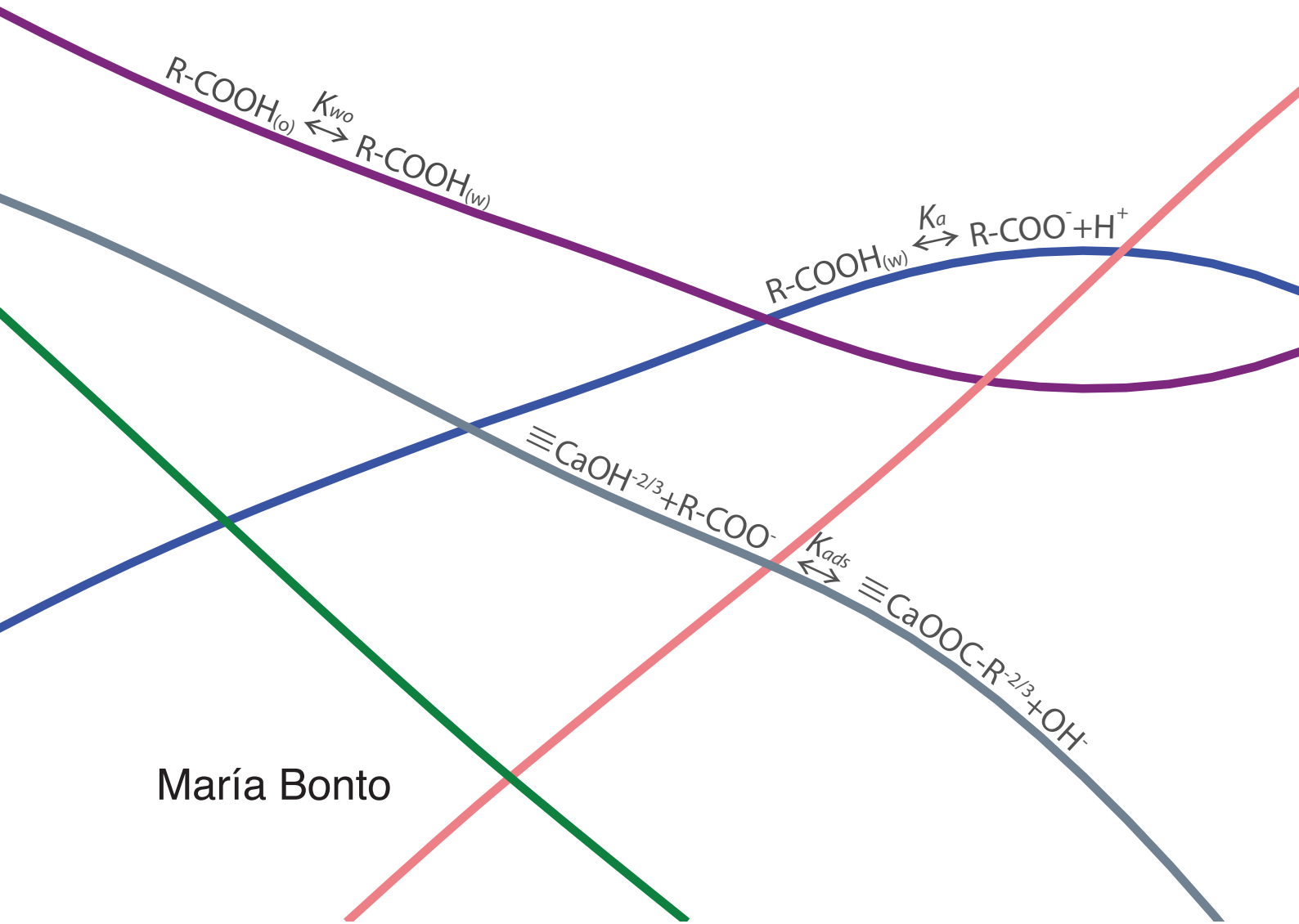

María Bonto

Numerical modelling and upscaling of modified salinity waterflooding

PhD Thesis
December 2021

By
María Bonto
Department of Applied Mathematics and Computer Science (DTU COMPUTE) and
Danish Hydrocarbon Research and Technology Centre (DHRTC)
Technical University of Denmark (DTU)

Supervised by
Dr. Hamid M. Nick
Danish Hydrocarbon Research and Technology Centre (DHRTC)
Technical University of Denmark (DTU)

Co-supervised by
Dr. Ali A. Eftekhari
Danish Hydrocarbon Research and Technology Centre (DHRTC)
Technical University of Denmark (DTU)

Cover photo: Hamid Nick, 2021
Published by: DTU, Danish Hydrocarbon Research and Technology Centre, Elektrovej, Building 375, 2800 Kgs. Lyngby, Denmark
https://www.oilgas.dtu.dk/

“The first step toward wisdom is the realization that the laws of the universe don’t care about you. The next is the realization that this does not imply that life is meaningless, because people care about you, and vice versa.” – Steven Pinker (Enlightenment Now)

To my mother, father, and grandmother

Preface

This thesis has been prepared at the Danish Hydrocarbon Research and Technology Centre (DHRTC) and the Department of Applied Mathematics and Computer Science (DTU COMPUTE) at the Technical University of Denmark (DTU) in partial fulfillment of the requirements for the degree of Ph.D. This work, part of the Advanced Waterflooding project at the DHRTC, has been carried out from 2018 to 2021 under the supervision of senior researcher Hamid M. Nick and researcher Ali A. Eftekhari. The project has also included a three-month external stay at the King Abdullah University of Science and Technology (KAUST) under the supervision of Prof. Tadeusz Patzek and Dr. Maxim Yutkin.

María Bonto

Kongens Lyngby, December 2021

Acknowledgments

Fortunately, this PhD project was not a solo journey. During this adventure, I interacted with many people who have, in different ways, left their fingerprints either explicitly on the thesis or myself and my attitude towards diverse aspects of life.

A special mention goes to my supervisors for granting me their unconditional academic and personal support. Hamid, thank you for believing in me! You have entrusted me with many opportunities during these years and pushed me towards new research areas and activities I was not comfortable with, helping me nurture the antidote to my shyness. Although you may be demanding and hope that your students harvest achievements, you have invested time to show us that rejection or failure is not an apocalypse. Besides encouraging and inspiring me research-wise, I am amazed by your energy levels. You are a vivid example that academia is not equivalent to sedentary life. You motivated me and my peers to be physically active and I thank you for that. Although I am sure you will not use me as a future reference for volleyball or frisbee, please remember my positive attitude and table tennis skills. Ali (alias Ehsan), I am thrilled by your knowledge, optimism, and patience. If I were to compare this thesis to a house, you represent its foundation. I have bothered and asked you so many questions that I am still wondering how you continued keeping the door open for me. Words fall short every time I try to articulate a sentence expressing my gratitude for all the things you have taught me. In many ways, I feel like a toddler whom you taught to walk. I will never forget your moral support and feedback when I felt so unhappy after my oral presentation at the Interpore conference in Valencia. What I will, for sure, forget is the look on your face when angry. But perhaps that is because I have rarely seen you angry, or if you were, it was always hidden behind a huge smile.

I also thank Prof. Tadeusz Patzek and Dr. Maxim Yutkin for inviting and hosting me at KAUST University for my external stay. It was an enriching experience both scientifically and personally. Going there to perform streaming potential measurements taught me the importance of understanding the experimental protocols for carrying out modelling work. Maxim, I cannot thank you enough for your patience to show me around in the laboratory, your eagerness to engage in scientific discussions, and your critical (yet constructive) feedback. I must admit that when I first met you at EAGE in Copenhagen, still an MSc student, I was intimidated by your seriousness. It was such a (nice) surprise to get to KAUST and discover that you are so kind and actually laugh. I also thank Sirisha Kamireddy for helping me with the experiments. All people at ANPERC are kindly acknowledged for making me feel welcome and for sharing all the tricks and tips to make the most out of my three-month stay in Thuwal, Jeddah.

All my colleagues at the DHRTC are thanked for contributing to the nice work and research environment. I cherish all the fruitful conversations and memories at the conferences and seminars organized by the centre. I will not forget the Christmas dinners where I was introduced to the Danish dishes and taught how to correctly place the different ingredients to obtain a tasty *smørrebrød*. Aslaug Glad and Ulla Hoffmann are thanked for translating the summary of this thesis to Danish. I apologize to my officemates, Helton, Aslaug, and Hamed if in the last months of my PhD there were times I was unbearable. Prof. Alexander Shapiro is also thanked for introducing me to the DHRTC midway through my MSc where I eventually ended up carrying out my research activities. DTU COMPUTE is also thanked for hosting me as a PhD student.

Besides great mentors, I was also lucky enough to be surrounded by many great friends. Moein, Meen, Maiya, and Mirhossein (Yes! That your name starts by “M” is a requirement for being selected for a PhD with Hamid) thank you for your advice, scientific collaboration, and for showing me the bits and pieces of the PhD life. When Behzad and Mohsen started their project, I stopped feeling like a spoiled child and felt that it was time to offer to others what has been previously offered to me. And when I thought I was too ahead in my PhD project and too busy to get emotionally invested, Ali, Helton, and Mohammad landed DHRTC. Ali, on behalf of everyone, I apologize for bullying you for your every

day's lunch. Thank you all for the moments we spent together, you were the perfect people for this journey!

A special mention goes to my friend and previous colleague Samira. I felt almost heartbroken when I returned from my external stay and found out you were no longer going to be my officemate. You can have the credit for the "cake club" but then I will take it for the "catalyst theory" and "push-ups challenge". Ashish, thank you for being such a good friend. You have provided invaluable support almost from the first day I arrived in Denmark. Thank you for always being honest with me, even if painful at times.

Due to Covid-19, my home was also my workplace for a great part of the PhD. Thank you, Guille, for bearing me 24/7 and for providing so much trust, confidence, and joy to my life. You are the special ingredient of this thesis! Thanks to you I kept a balanced lifestyle, so beneficial to my mood and attitude, during this project. Javier, thank you for almost fostering me and being there for me unconditionally from the moment we met. I came to Denmark in the first place because that option was pointed to me through you. But most importantly, I want to thank my parents and grandma for their extreme sacrifice during my upbringing. I would have not written this thesis if you had not imprinted in me values such as hard work and persistence.

Summary

Unraveling the mechanisms controlling the two-phase flow dynamics in porous media, stemming from the interactions between the rock and in situ fluids, is essential to many subsurface applications. The injection of a modified salinity brine within hydrocarbon reservoirs, by disturbing the existing equilibrium conditions, may induce a shift in the relative mobility of the aqueous and oleic phases, eventually boosting the (oil) production. In carbonate fields, the success of modified salinity waterflooding (MSW) is determined by interactions between the calcite, brine, and crude oil, as described in Chapter 1. Resembling a jigsaw puzzle, this thesis, consisting of five chapters, illustrates the overall (calcite-brine-crude oil) system behavior under different chemical and temperature conditions by assembling the contributions arising from the calcite-brine and brine-oil sub-interfaces.

Chapter 2 reviews the surface complexation models (SCM) for the calcite-water interface. Different SCMs are assessed against a database of critically evaluated electrokinetic measurements. The models, despite their contrasting electrostatic description of the interface, may fit equally well zeta potential data. However, the premises that the models are built upon (and their effect on surface sites and reactions definition) considerably affect their prediction performance at variable ionic composition. The SCMs, once tuned to zeta potential measurements, showed a weak agreement with proton charge and dynamic retention data of natural samples. Apart from electrokinetic measurements, other types of experiments (e.g., single-phase flooding tests) must be considered to obtain the equilibrium constants of the surface reactions. Applying the SCMs at subsurface conditions is possible, provided that the effect of temperature on the surface reactions is considered. In Chapter 3, the equilibrium constants of the calcite surface reactions are estimated assuming that they follow a temperature dependency described by the van't Hoff equation. The reaction enthalpies are obtained by fitting a reactive transport model to a combination of high-temperature streaming potential and single-phase flooding tests. Analogous to the calcite-water system, the interactions and charge development at the oil-brine interface can also be described by SCMs. However, compared to calcite, whose surface sites are easily expressed in terms of its lattice ions, the complex composition of the crude oil challenges the definition of the (oil) surface. An SCM that considers the oil surface as represented by a network of acid and base groups, linearly dependent on the crude oil total acid and base number, respectively, is defined in Chapter 4. A third type of adsorption site is included to account for the surface charge exhibited by non-polar oil. The model is consistent with several zeta potential measurements reported for different types of crude oil. Additional insight into the distribution of polar species at the oil-brine interface under different salinity and temperature conditions could further refine the model. In Chapter 5, the speciation and electrokinetic behavior at the calcite-brine and brine-oil interfaces are linked to the mineral wetting conditions. The developed model is used to explain the improved oil recovery obtained at the core scale during spontaneous imbibition tests on fairly homogeneous chalk samples. By coupling the formulations of calcite-brine and oil-brine interfaces, Chapter 6 provides a unifying approach to holistically describe the calcite-brine-oil interactions. Additional key interactions between the oil and brine are included (e.g., acid partitioning and ionization), which allow to explicitly define and quantify the adsorption of acid polar groups from the crude oil on the calcite surface. Applying the model to simulate the adsorption of oleic acids on outcrop chalk reveals that the traditional approach of characterizing the acidity of the crude oil in terms of a single pseudocomponent (e.g., acid number) is not an adequate measure of adsorbable polar groups; predictive capabilities may only be achieved provided the acids in the crude oil are identified and their affinity for the calcite surface and the brine phase is (experimentally) resolved.

This comprehensive description of the calcite-brine-crude oil system serves as a valuable tool for assisting in interpreting the outcome from core flooding experiments and designing laboratory and field tests in the context of MSW in carbonates. The models and conclusions derived from this thesis are easily transferable to other subsurface applications such as storage of fluids within the subsurface or groundwater remediation.

Resumé

Forståelsen af de mekanismer dynamikken ved to-fase-strømnings i porøse medier, fra interaktionerne mellem bjergarten og in situ væsker, er afgørende for mange underjordiske applikationer. Injektionen af en modificeret saltholdig saltvandsopløsning i kulbrintereservoirer, ved at forstyrre de eksisterende ligevægtsbetingelser, kan inducere et skift i den relative mobilitet af de vandige og olieholdige faser, hvilket øger olieproduktionen. I karbonatfelter bestemmes succesen af modificeret saltholdighedsvandoversvømmelse (MSW) af interaktioner mellem calcit, saltlage og råolie, som beskrevet i kapitel 1. Denne afhandling består af fem kapitler. Kapitel 1 illustrerer den overordnede (calcit-saltlage-råolie) systemadfærd under forskellige kemiske og temperaturforhold ved at samle bidragene fra calcit-saltlage og saltlage-olie-undergrænseflader.

Kapitel 2 gennemgår overfladekomplekserings-modellerne (SCM) for calcit-vand-grænsefladen. Forskellige SCM'er vurderes mod en database med kritisk evaluerede elektrokinetiske målinger. På trods af deres kontrasterende elektrostatiske beskrivelse af grænsefladen kan modellerne passe lige så godt til zeta-potentiale data. De præmisser, som modellerne er bygget på, påvirker deres forudsigelsesydelse ved variabel ionsammensætning. SCM'erne, da de var indstillet til zeta-potentialemålinger, viste en svag overensstemmelse med protonladning og dynamiske retentionsdata for naturlige prøver. Bortset fra elektrokinetiske målinger skal andre typer eksperimenter (f.eks. enkeltfasede oversvømmelsestest) overvejes for at opnå ligevægtskonstanterne for overfladereaktionerne. Det er muligt at anvende SCM'erne ved underjordiske forhold, forudsat at temperaturens effekt på overfladereaktionerne tages i betragtning. I kapitel 3 estimeres ligevægtskonstanterne for calcitoverfladereaktionerne under antagelse af, de følger en temperaturafhængighed beskrevet af van't Hoff-ligningen. Reaktionsentalpierne opnås ved at tilpasse en reaktiv transportmodel til en kombination af højtemperaturstrømningspotentiale og enkeltfasede oversvømmelser. Analogt med calcit-vand-systemet kan interaktionerne og ladningsudviklingen ved olie-brine-grænsefladen også beskrives af SCM'er. Sammenlignet med calcit, hvis overfladesteder let kan udtrykkes i form af dets gitterioner, udfordrer den komplekse sammensætning af råolien definitionen af (olie) overfladen. En SCM, der betragter olieoverfladen som repræsenteret af et netværk af syre- og basegrupper, lineært afhængig af henholdsvis råoliens totale syre- og basetal, er defineret i kapitel 4. En tredje type absorptionssted er inkluderet for at tage højde for overfladeladningen udvist af ikke-polær olie. Modellen er i overensstemmelse med adskillige zeta-potentialemålinger rapporteret for forskellige typer råolie. Indsigt i fordelingen af polære arter ved olie-saltlagegrænsefladen under forskellige saltholdigheds- og temperaturforhold kunne yderligere forfine modellen. I kapitel 5 er artsdannelsen og den elektrokinetiske adfærd ved grænsefladerne mellem calcit-saltlage og saltlage-olie forbundet med de mineralske befugtningsbetingelser. Modellen bruges til at forklare den forbedrede olieudvinding opnået på kerneskalaen under spontane imbibitionstests på kridtprøver. Ved at koble formuleringerne af calcit-saltlage- og olie-saltlage-grænseflader giver kapitel 6 en samlende tilgang til beskrivelse af calcit-saltlage-olie-interaktionerne. Yderligere nøgleinteraktioner mellem olien og saltvand er inkluderet (f.eks. syreopdeling og ionisering), som gør det muligt eksplicit at definere og kvantificere adsorptionen af sure polære grupper fra råolien på calcitoverfladen. Anvendelse af modellen til at simulere adsorptionen af oliesyrer på kridt afslører, at tilgangen til at karakterisere surheden af råolien i form af en enkelt pseudokomponent (eg. syretal) ikke er et tilstrækkeligt mål for absorberbare polære grupper; forudsigelsesevner kan kun opnås, hvis syrerne i råolien er identificeret, og deres affinitet til calcitoverfladen og saltvandsfasen er (eksperimentelt) opløst.

Beskrivelsen af calcit-saltlage-råolie-systemet tjener til at fortolke resultatet fra kerneoversvømmelseseksperimenter og designe laboratorie- og feltforsøg i forbindelse med MSW i karbonater. Modellerne og konklusionerne fra denne afhandling er let overførbare til andre underjordiske applikationer såsom opbevaring af væsker i undergrunden eller grundvandsoprensning.

Contents

1 Introduction

1.1 Rationale

The low prospects for discovering new oil reserves emphasize the need to improve the production of the existing ones. Denmark, an oil producer since 1972, has seen a steady decline in its hydrocarbon production for the past 15 years[1]. The offshore location and characteristics of the Danish reservoirs limit the type of enhanced oil recovery (EOR) techniques that can be used to boost production. Most of the oil in the North Sea is sheltered in chalk formations. Danish reservoir chalk consists primarily of calcite (>95% $CaCO_3$) sprinkled with minor amounts of silica and kaolinite. Compared to other calcium carbonate-containing rocks (e.g., limestone), North Sea chalk has a higher porosity (up to 45%) and lower permeability (<5 mD)[2]. Many of the Danish reservoirs have been waterflooded, as the light oil in these fields results in favorable water to oil mobility ratio. The high specific area (>2 m^2/g)[3] and low permeability of the chalk restrict the applicability of popular chemical EOR techniques (e.g., polymer flooding) to further increase the oil recovery. CO_2 injection was selected as a promising EOR method for the Danish fields, but the non-availability of captured CO_2 eventually made such a project unfeasible[4]. The expertise on water injection in the North Sea bolsters the possibility of increasing the oil recovery through modified/low salinity waterflooding (MSW/LSW). The implementation of MSW/LSW is not expected to considerably increase the operational complexity as, in addition, and compared to a normal waterflood, it would only require filtration equipment to tailor the water chemistry. Moreover, as to other EOR techniques that rely on complex chemicals, the environmental impact of MSW is anticipated to be lower since the injection fluid is simply seawater, depleted or enriched in certain ions. Nonetheless, finding the right brine composition to be injected in a field characterized by a particular temperature, crude oil type, and mineralogy such that it leads to increased oil recovery has been a great research question for the last 20 years.

The injection of a foreign brine within the reservoir disrupts its equilibrium conditions, triggering different types of interactions and processes that guide the system towards a new equilibrium. For instance, MSW may promote calcite dissolution and change the pore connectivity, releasing some of the oil and leading to increased oil recovery[5]. On the other hand, some brine recipes may lead to supersaturation conditions resulting in the precipitation of secondary phases, e.g., magnesite, anhydrite. Adsorption/desorption processes at the calcite surface may also result in a shift in the affinity/wettability of the calcite surface for the oil phase, leading to an increase in the oil mobility and final oil recovery[6,7]. The mechanical properties of the chalk are contingent not only on dissolution/precipitation episodes[8–10] but also on the adsorption of certain ions (e.g., sulfate)[11] at the mineral surface; the chalk can then become weaker and drive increased compaction[12], squeezing out the oil from the pores. The injection of a new brine may also alter the mechanical balance of reservoir particles, leading to the release of fines[13]; these fines may block some pore throats, diverting the flow of the injection water and improving the sweep efficiency[14]. Besides rock-water interactions, MSW may prompt the rearrangement or affinity of crude oil components and aqueous species at the oil-brine interface with implications for the (oil-brine) interfacial properties[15,16] and the development of emulsions[17,18], with effects on both the sweep efficiency and mobility. Additional interactions and possible mechanisms responsible for EOR during MSW have been thoroughly discussed in recent review papers[19,20]. While these mechanisms are often

treated and regarded as exclusive, in fact they may all be related to the surface speciation and electrokinetic behavior at the calcite-brine and brine-oil interfaces.

Core flooding and spontaneous imbibition tests assess the success and extent of MSW by recording the volume of oil produced during the injection of a modified salinity brine with respect to seawater (SW) or formation water (FW). Since these experiments try to mimic the reservoir conditions and history, restoring the initial wettability of the core represents a crucial step. The core samples are prepared with a representative initial FW saturation and crude oil followed by "aging" at relevant temperature conditions. Once initialized, the cores may undergo a different injection/imbibition sequence (e.g., SW followed by MSW) depending on the experimental design. The oil recovery during each stage will depend heavily on the initial wetting conditions of the core. Although core flooding experiments are the preferred method in the oil and gas community to evaluate the potential of MSW for EOR, they show several limitations. First, these types of experiments are time-consuming (especially for tight chalk samples) and require expensive resources such as reservoir rock material and fluids. Alternatives such as performing flooding experiments on shorter cores[21] or microfluidic devices[22] have been proposed to tackle in a faster way the effect of the sample initialization protocols, brine composition, crude oil properties, mineralogy, or temperature on oil recovery. A second limitation is that core flooding experiments only quantify the increase in the oil recovery but do not provide any knowledge/information on the mechanisms leading to it. The progress in imaging these centimeter-scale displacement processes allows now to complement the limited information from core flooding tests with valuable insight on the processes occurring at the pore scale[23]. Additional experiments (e.g., electrokinetic measurements[24], contact angle[25], atomic force microscopy[26]) targeting different length scales are usually carried out to bring additional information and sustain the different hypotheses on the recovery mechanisms. Yet, most experimental results reflect the combined response of multiple interactions. Interpreting these results using mathematical models may be essential to isolate and quantify the different interactions in the crude oil-brine-calcite system or to identify the mechanisms and processes dictating the recovery profiles[27,28].

Besides relevant experimental data, the implementation of MSW at a larger scale requires also the development of numerical models that can forecast oil production. The traditional approach for modelling MSW assumes that the change in the salinity levels increases oil recovery due to a shift in the wetting conditions[29]. The shift in the wetting conditions is accounted for through two sets of relative permeability and capillary pressure curves (i.e., one for the initial equilibrium condition with the FW/SW and the other for the final equilibrium condition with the MSW) obtained by history matching core flooding experiments. Nonetheless, this approach may not be suitable for carbonates, where oil recovery is rather dictated by the specific composition and not the ionic strength[30]. Thus, for carbonates, models that specifically account for the brine composition are required as describing the contrasting affinity of different ions in the brine towards the calcite surface is imperative. Surface complexation models (SCMs) represent the state-of-the-art approach for modelling ion adsorption and associated charge development at both mineral-fluid and fluid-fluid interfaces. While the definition of the adsorption sites at the calcite surface is quite apparent based on its crystallography, the treatment of the crude oil surface is much more uncertain due to its complex composition. Because of their versatility to account for different chemical and temperature conditions, SCMs are often coupled to the flow equations to describe and anticipate reactive transport processes such as those during MSW. Yet, the performance and prediction of the models are often bound to the experimental data used for their optimization. The pore-scale interactions described through SCM may be linked to different processes (e.g., wettability alteration, fines migration), representing a pillar for the development of mechanistic models for MSW, which are needed to anticipate the outcome at core and field scale. These mechanistic models could eventually assist in designing the optimal brine composition for a particular reservoir with a specific crude oil and mineralogy.

The understanding and description of the interactions of chalk with aqueous species and organic components have implications beyond EOR. In North-West Europe, chalk formations hold enormous volumes of water, supplying more than 60% of the drinking water of Northern France, England, Belgium, Denmark, and the Netherlands[31,32]. Depleted chalk oil fields are also likely to be repurposed for CO_2 storage applications. Thus, chemistry representations of calcite-brine-organic phase interactions during MSW may be integrated into transport models to also describe the flow of contaminants or CO_2 migration plume to ensure groundwater quality or CO_2 containment, respectively.

1.2 Objectives

The overall ambition behind this thesis is to develop predictive models that overcome some of the limitations of the existing models for MSW in carbonate formations by improving the description and formulation of the interactions between the calcite, brine, and crude oil. Thus, the main objectives targeted in this study are:

1. Propose a thermodynamic model that can predict the adsorption and electrokinetic behavior at the calcite-water interface under non-isothermal conditions and in the presence of ions relevant to MSW.
2. Develop a surface complexation model for the oil-brine interface that can account for the contrasting electrokinetic behavior of different crude oil.
3. Develop a mechanistic model for the wettability alteration based on the interactions at the calcite-brine and brine-oil interfaces.
4. Provide a holistic model to describe calcite-brine-crude oil interactions and the adsorption of polar acidic groups on the calcite surface.

1.3 Chapter outline

This thesis consists of five main chapters (Chapters 2 to 6).

Chapter 2 offers a review of the SCMs used to illustrate the interactions at the calcite-water interface. This section discusses the main differences between the models in terms of their electrostatic representation of the interface, surface sites, and reactions. Three different SCMs are implemented and used to predict the electrokinetic behavior of natural and synthetic calcite in aqueous solutions. The performance of the models is evaluated against a large database of compiled zeta potential measurements. Some of the uncertainties related to electrokinetic experiments on calcite systems are also discussed.

Chapter 3 addresses and quantifies the effect of temperature on calcite surface speciation in aqueous environments by interpreting with an SCM the variation of the zeta potential with temperature. The enthalpies of the surface reactions, inferred by assuming a temperature dependency of the equilibrium constants according to the van't Hoff equation, are further refined using the recorded ion concentration history of the effluent during the injection of aqueous solutions through chalk or limestone samples. The obtained enthalpies are also assessed against microcalorimetry measurements on chalk powders.

Chapter 4 introduces the main aspects that govern the crude oil electrokinetic behavior and gives an overview of previous modelling approaches for describing the charge development at the oil-water interface. An SCM that considers particularities of the crude oil, i.e., total acid and base number, is defined to describe the reactivity at the oil-water interface. The model is tested against zeta potential measurements reported in the literature.

Chapter 5 provides a mechanistic model to assess the shift in the wetting conditions of calcite in equilibrium with a specific crude oil and FW triggered by the injection of a modified salinity brine. The proposed parameter, which depends on the surface speciation and electrokinetic behavior at the brine-rock and oil-brine interface, indicates the relative increase/decrease of the available adsorption sites at

the calcite surface (in presence of MSW with respect to FW) that may bind polar groups from the crude oil. The suggested parameter is evaluated at the conditions (e.g., temperature, solution composition) of different spontaneous imbibition tests and represented against the remaining oil saturation recorded at the end of these experiments.

Chapter 6 presents a model to describe the adsorption of polar acid groups from the crude oil on water-saturated calcite. The model is validated against both batch and dynamic adsorption experiments and highlights the limitations of describing the acidity of crude oil in terms of a single “acid number” pseudocomponent.

The main findings of this thesis are summarized in Chapter 7, which also includes suggestions and recommendations for future work.

2 Electrokinetic behavior of artificial and natural calcites: a review of experimental measurements and surface complexation models

The surface charge of calcite in aqueous environments is essential to many industrial and environmental applications. Electrokinetic measurements are usually used to assess the calcite charging behavior and characterize its electrical double layer (EDL). Numerous surface complexation models (SCMs) have been proposed to interpret the effect of different surface interactions on the zeta potential. Because of their versatility, SCMs have also become important tools in reactive transport modeling. The research on enhanced oil recovery within the last decade has led to an increased number of publications reporting both zeta potential measurements and SCMs for calcite. Nonetheless, the measurements are often inconsistent and the reasons for choosing one model over another are unclear. In this work, we review the models proposed for calcite and address their main differences. We first collect a large number of published zeta potential measurements and then we fit a Diffuse Layer, Basic Stern, and Charge-Distribution Multi-Site Complexation models to a selected reliable dataset. For each model, we maintain a similar number of adjustable parameters. After optimizing the parameters of the models, we systematically compare their prediction capabilities against data obtained in monovalent and divalent electrolyte systems containing calcium, magnesium, sulfate, or carbonate. We show that, often, the discrepancies between the models and the experimental data can be explained by different levels of disequilibrium. Nonetheless, assumptions used in the development of the models may significantly reduce their extrapolability to variable chemical conditions. The poor agreement between the models tuned to electrokinetic data with surface charge measurements and dynamic retention from single-phase flowthrough tests show that zeta potential may not be the best type of data to characterize ion binding at the calcite surface. Including the effect of mineral impurities and temperature on the calcite surface speciation and electrokinetic behavior prevail as main challenges for reactive transport modeling.

This chapter is a revised layout of the article: M. Bonto, A.A. Eftekhari, H.M. Nick. Electrokinetic behavior of artificial and natural calcites: a review of experimental measurements and surface complexation models. In revision.

2.1 Introduction

The reactivity of calcite in natural environments is governed primarily by its surface hydration layer[33–36] and associated charge development[37]. In aqueous systems, calcite may undergo dissolution, precipitation, adsorption, or ion exchange[38]. These physicochemical reactions that take place at the interface between the mineral lattice and bulk solution not only affect the fluid composition but also shift the surface charge of the carbonate. According to the DLVO (Derjaguin, Landau, Verwey, and Overbeek) theory[39,40], any shift in the electrical charges reshapes the balance between attractive and repulsive forces, which governs both the colloidal properties of the mineral and its interaction with other substrates[41–43]. For instance, altering the calcite charge by adsorbing specific organics at its surface has important applications in the synthesis of nanomaterials[44–52], can improve the separation and recovery of other valuable minerals by flotation[53], inhibit its growth to avoid scaling issues[54,55], increase the efficiency of underground water remediation methods[56], or improve colloidal stability[57,58]. Decreasing the ionic strength or adding specific ions in natural water systems can also change calcite wettability[59–61], promote the release of fines[14,62], and affect the mechanical properties of the porous media (e.g.,[8,9,11,63]), all of them having an impact on the flow/extraction/storage of fluids/energy within the subsurface. Given the pivotal role of the calcite surface charge in many industrial and environmental processes, numerous studies have attempted to determine experimentally the main parameters that control the charging behavior.

The charge at the calcite surface leads to the development of an electrical double layer (EDL) consisting of a region with strongly bound ions (also known as Stern layer) and a diffuse layer with mobile ions. The charge at mineral-water interfaces, and thus the characteristics of their EDL, are commonly assessed through potentiometric acid-base titrations. Nonetheless, the application of this method to calcite systems is challenged by the fast dissolution at low pHs[64,65]. As an alternative, electrokinetic techniques can be used to estimate the zeta potential (ζ), which represents the potential at the boundary between stagnant and mobile ions (also known as the shear or slip plane). Although the absolute value of the zeta potential is lower than the surface potential[66], it gives a good indication of the electrostatic forces. Given the wide implications of the calcite electrokinetic behavior, zeta potential measurements proliferate in the literature. However, the synergy between the interactions in the calcite-water system may challenge deciphering these experiments and the role of individual reactions. Surface complexation models[67–72] (SCMs) are usually used to interpret experimental results by breaking down and quantifying the contribution of different surface interactions to the overall measured zeta potential. These mathematical models, initially developed to describe the reactivity of oxide-water interfaces, assume that the energy of adsorption is a contribution of a chemical and an electrostatic term [73,74]. Despite their generalized use, some aspects of these SCMs are still questioned; the unclear thermodynamic significance of the relationship between the apparent and intrinsic equilibrium constants[74,75] or the lack of validation of the equilibrium constants over diverse experimental conditions are among the main concerns[74,76,77]. For oxide-water interfaces[78–81], several publications[74,76,78,82] attempted to provide consistent model parameters. Westall and Hohl[78] compared the performance of these models for describing material balance data obtained on crystalline oxides in presence of simple aqueous solutions. They observed that after the fitting procedure all models showed similar goodness of fit and that the obtained parameters were not univocal. When it comes to the calcite-water interface, the number of publications reporting and modeling electrokinetic measurements has been steadily increasing. However, since the validation of the models is usually limited to showing fitted trends or prediction of only a few experimental measurements, there is no clear evidence on the advantages or benefits of choosing one model over another. However "the adsorption models and surface stability constants should be tested over a wide range of experimental conditions before they are regarded as acceptable"[77]. The goal of this work is to review and compare the existing surface complexation models for calcite and to evaluate their capabilities for predicting reported electrokinetic data of both natural and synthetic samples. Lastly, we assess whether the models, once tuned to zeta potential measurements, are

consistent with the few published net proton charge data or can replicate the effluent concentration from single-phase core flooding tests.

2.2 Models

Several surface complexation models, well-established for describing ion binding and surface charge of oxide minerals, have also been tailored to illustrate the reactive behavior of calcite. Van Cappellen et al.[70] applied a constant capacitance model (CCM) to correlate the dissolution kinetics of calcium carbonate with the chemical speciation at the mineral-aqueous solution interface. Pokrovsky et al.[83,84] further refined this model by assuming that the complexation reactions at the mineral surface are analogous to those in the bulk solution and by considering data from surface titration, electrokinetics, and dissolution rates. The model could reproduce the surface speciation of calcite/aqueous solution at different pHs. Later, Wolthers et al.[67] applied a Charge-Distribution Multi-SIte complexation model (CD-MUSIC); this model, initially developed by Hiemstra and Van Riemsdijk[85] and Hiemstra et al.[86] for oxide surfaces, provided a meticulous representation of the calcite surface by incorporating sites with different coordination (e.g., face, edge, and corner sites), thus, reactivity. The model showed a fair agreement with a wide dataset of electrokinetic measurements reported in the literature. Hiorth and coworkers[5] were among the first to apply a diffuse layer model (DLM) to describe the calcite electrokinetic behavior. Heberling et al.[68,87] proposed a Basic Stern model (BSM) constrained by surface diffraction data and both equilibrium and non-equilibrium zeta potential measurements. Although these models (i.e., CCM, CD-MUSIC, DLM, BSM) rely on common fundamentals (e.g., definitions of surface sites and reactions), the representation of the electrical double layer (EDL) prevails as the main distinctive feature. All these proposed models, implemented in different speciation software, have been widely used for both environmental[88–93] and enhanced oil recovery[5,27,71,72,94–106] applications (Figure 2.1). The main constituents of the surface complexation models are discussed in more detail hereafter.

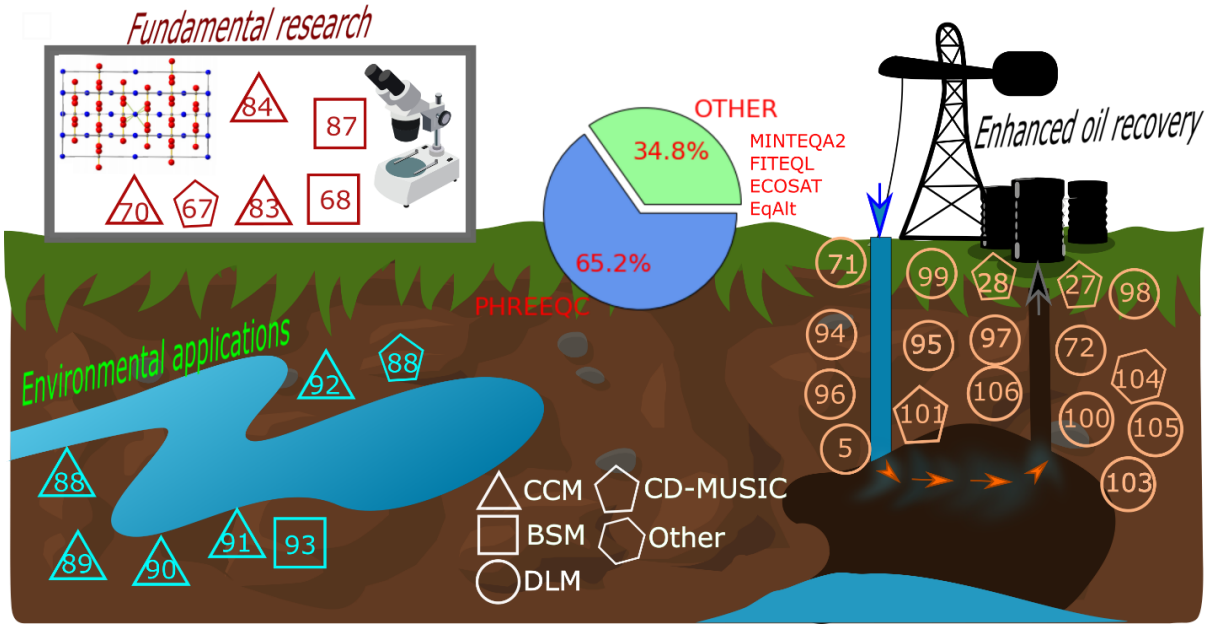

Figure 2.1. Summary of publications involving surface complexation modeling of calcite-water systems for different disciplines. The numbers in each shape represent the reference number and the shapes represent the type of model. The pie chart shows the main software used for surface complexation modeling and the calculated percentages consider only the publications and models reviewed in this chapter.

2.2.1 Surface sites

The reactive behavior of calcite is strongly governed by the predominant $\{10\bar{1}4\}$ crystal surface exposed to solution[46,47]. The existing surface models are developed mainly for this cleavage plane, which is characterized by a sequence of an equal number of intertwined calcium and carbonate sites.

Generally, these models consider a surface site density of 4.95 sites/nm^2 according to the calcite crystallography; yet, some exceptions exist (e.g., ref [5]), which propose a different surface site density to improve the match of the models with electrokinetic data. Apart from the CD-MUSIC model proposed by Wolthers et al.[67], which included different types of sites depending on their crystallographic coordination, all other models consider only the face sites. In agreement with experimental evidence from X-ray reflectivity (XRR)[35,36,107,108], X-ray photoelectron spectroscopy (XPS)[33], and molecular dynamics (MD) simulations[36], these calcium and carbonate reactive sites are assumed to be hydrated. When the calcite $\{10\bar{1}4\}$ cleavage plane forms, one Ca-O bond is broken for each calcium and carbonate ion; this leaves the calcium at the surface undercoordinated (coordination number of 5) with respect to the bulk, where it has an octahedral geometry[107,109]. Existing evidence suggests that a first water layer completes the calcium ion coordination shell and a second layer hydrates the surface carbonate ion by hydrogen bonding between the water and the carbonate oxygen[36]. In some cases, this hydration layer, ordered by both chemical and steric effects[109], was reported to consist of up to three different water molecules[110]. Likewise, the lower surface energy of hydrated calcite compared to non-hydrated one[111,112] supports the affinity of water towards the calcite surface. Early XPS measurements hinted at the existence of bound water to the reactive sites[33]. However, since hydrogen is not visible in the XPS spectra, these measurements could not distinguish whether the sites were covered by hydroxyl species or a water molecule. The best-fitted model to X-ray reflectivity data[108] suggested that these were hydroxyl groups and not water molecules. Later, Fenter and Sturchio[109] argued that the calcium at the calcite surface cannot complete its coordination shell by adsorbing a hydroxyl ion and that molecular adsorption of water is needed to properly terminate any valence imbalance caused when the surface is created. While most SCMs for calcite assume that water dissociates when adsorbed at the surface, DFT and MD simulations suggest that associative adsorption of water is more favorable[113–116].

A distinctive feature between the models is the definition of the surface sites, in particular their charge. The models that assume one unit charge per bond result in surface sites with integer charges. Many publications consider neutral surface sites[69,94,117] in agreement with the model proposed by van Cappellen and coworkers[70]; the adsorption of hydroxyl and proton (dissociative adsorption of water) to the positive and negative surface terminations, i.e., $\equiv Ca^+$ and $\equiv CO_3^-$, results in the existence of neutral hydroxylated ($\equiv CaOH^o$) and protonated ($\equiv CO_3H^o$) surface sites. Considering molecular adsorption of water, Hiorth et al.[5] defined $\equiv CaOH_2^+$ and $\equiv CO_3^-$ surface sites. On the other hand, the models that consider that the charge is distributed over all the oxygens that coordinate to the cation[118] define surface sites and surface complexes with fractional charges. In the CD-MUSIC model, the charge of the surface sites depends on their coordination number with other atoms and therefore on the crystallographic structural planes[85]. For the $\{10\bar{1}4\}$ calcite cleavage plane, considering a symmetric distribution of charge over the surrounding bonds and a coordination number of six for the calcium and carbonate in the bulk, the charge per Ca-O and CO_3-Ca bond is +1/3 and -1/3, respectively (calculated as the charge of an ion divided by its coordination number). Upon (dissociative) adsorption of water, the surface sites become $\equiv CaOH^{-2/3}$ and $\equiv CO_3H^{+2/3}$. Others suggest that since $CaCO_3$ is not purely ionic, the effective charge on the Ca is slightly lower than 1/3, around 0.25[68]. Considering these assumptions and dissociative adsorption of water, Song et al.[71,72] defined $\equiv CaOH^{-0.75}$ and $\equiv CO_3H^{+0.75}$ reactive sites. Heberling et al.[68] argued that the model was insensitive to the defined fractional charge, and to simplify charge calculations they defined $\equiv CaOH^{-0.5}$ and $\equiv CO_3H^{+0.5}$ sites. The model was later revised and the surface sites were updated to $\equiv CaOH^{-0.5}$ and $\equiv CO_3^{-0.5}$ [93].

2.2.2 Representation of the calcite-water interface

The peculiarity of each SCM relies mainly on the description of the EDL. In the CCM, the calcite-water interface is described as consisting of only a Stern layer (no diffuse layer); ions adsorb in the surface

plane and the charge and potential are linearly related through a capacitance, C [F/m^2] (Figure 2.2-a). The DLM also contemplates ion adsorption in the surface plane. The charge at the surface is completely neutralized by a diffuse layer (Figure 2.2-b) where the electrical potential and the ion density are related through the Poisson-Boltzmann equation (e.g., ref [119]):

$$\nabla^2\psi = \frac{d^2\psi}{dx^2} = -\frac{F}{\varepsilon_r\varepsilon_0}\sum_i m_i z_i exp\left(-\frac{z_i F\psi}{RT}\right) \tag{2.1}$$

where ψ [V] is the potential, x [m] is the distance, F [96485.33 C/mol] is Faraday's constant, ε_0 [8.854·10^{-12} F/m] is the vacuum permittivity, ε_r is the dielectric permittivity of the medium (78.5 for liquid water at 25ºC), m_i [mol/m^3] and z_i [-] are the concentration and charge of ion *i*, respectively, *R* [8.314 J/mol] is the ideal gas constant, and *T* [K] is the temperature.

Integrated once, eq. (2.1) becomes:

$$\left(\frac{d\psi}{dx}\right)^2 = \frac{2RT}{\varepsilon_r\varepsilon_0}\sum_i m_i\left[exp\left(-\frac{z_i F\psi}{RT}\right) - 1\right] \tag{2.2}$$

The surface charge density, σ [C/m^2], and electric field at a surface are related through Gauss' law:

$$\sigma = -\varepsilon_0\varepsilon_r\frac{d\psi}{dx} \tag{2.3}$$

Combining eqs. (2.2) and (2.3) results in the Grahame equation[120]:

$$\sigma = \pm\left\{2RT\varepsilon_r\varepsilon_0\sum_i m_i\left[\exp\left(-\frac{z_i F\psi}{RT}\right) - 1\right]\right\}^{1/2} \tag{2.4}$$

For symmetrical electrolytes, eq. (2.4) yields:

$$\sigma = -\left\{2RT\varepsilon\varepsilon_0 m_i\left[2cosh\left(\frac{zF\psi}{RT}\right) - 2\right]\right\}^{1/2} \tag{2.5}$$

Rewritting eq. (2.5) by considering the identity $\cosh(x) = 2sinh^2(x/2) + 1$ results in a charge-potential relationship also known as the Gouy-Chapman double-layer equation (e.g.,refs [121,122]):

$$\sigma = -(8RT\varepsilon\varepsilon_0 m_i)^{1/2} sinh\left(\frac{zF\psi}{2RT}\right) \tag{2.6}$$

The latter equation (eq. 2.6) is usually included in publications describing the implementation of the SCMs (e.g., refs [64,123]) in terms of the ionic strength ($I = \frac{1}{2}\sum_i m_i z_i^2$) instead of concentration. However, even in monovalent background electrolytes, the dissolution of calcite represents a source of divalent ions that would force the use of the general mathematical expression (eq. 2.4). Lützenkirchen et al.[122] showed that the charge-potential relationship is implemented differently in surface speciation codes and that eq. (2.4) is invoked in PHREEQC and ECOSAT. The diffuse layer thickness depends on the ionic strength and its characteristic length scale is approximated through the Debye length, κ^{-1} [m] (eq. 2.7):

$$\kappa^{-1} = \sqrt{\frac{\varepsilon\varepsilon_0 RT}{2IF^2}} \tag{2.7}$$

The BSM (Figure 2.2-c) and CD-MUSIC model (Figure 2.2-d) are a combination of the CCM and DLM as they consider both a compact layer of ions (Stern layer) and a diffuse layer. While in the CCM and DLM all ions are located at the surface, BSM and CD-MUSIC model allow placing the charge in different electrostatic planes, depending on the affinity of the ion for the mineral surface. Within the

CD-MUSIC framework, Wolthers et al.[67] described the calcite-water interfacial region as consisting of three discrete electrostatic planes, i.e., the 0-plane that cuts through the surface oxygens and where only (de)protonation occurs, the 1-plane or Inner Helmholtz plane (IHP) where inner-sphere complexation reactions take place and the 2-plane or Outer Helmholtz plane (OHP). Ions that can disrupt the hydration layer and displace a water molecule from the calcite surface are placed in the Inner Helmholtz Plane (IHP); these surface species are called inner-sphere complexes. Ions with less affinity for the calcite surface that cannot displace the hydration sheath sit further away from the surface, in the OHP. The charge and potential between the 0- and 1- and 1- and 2- planes are related through two capacitances (i.e., C_1 and C_2 [F/m^2]) and the onset of the diffuse layer is located at the 2-plane. In the Basic Stern model for calcite proposed by Heberling et al., the interface consists of the surface plane and the β-plane. As in the CD-MUSIC model, protons and hydroxyls adsorption are the only interactions at the surface, whereas all remaining interactions occur as outer-sphere complexes within the β-plane. The equations relating the charge and potential in the diffuse region are the same as for the DLM.

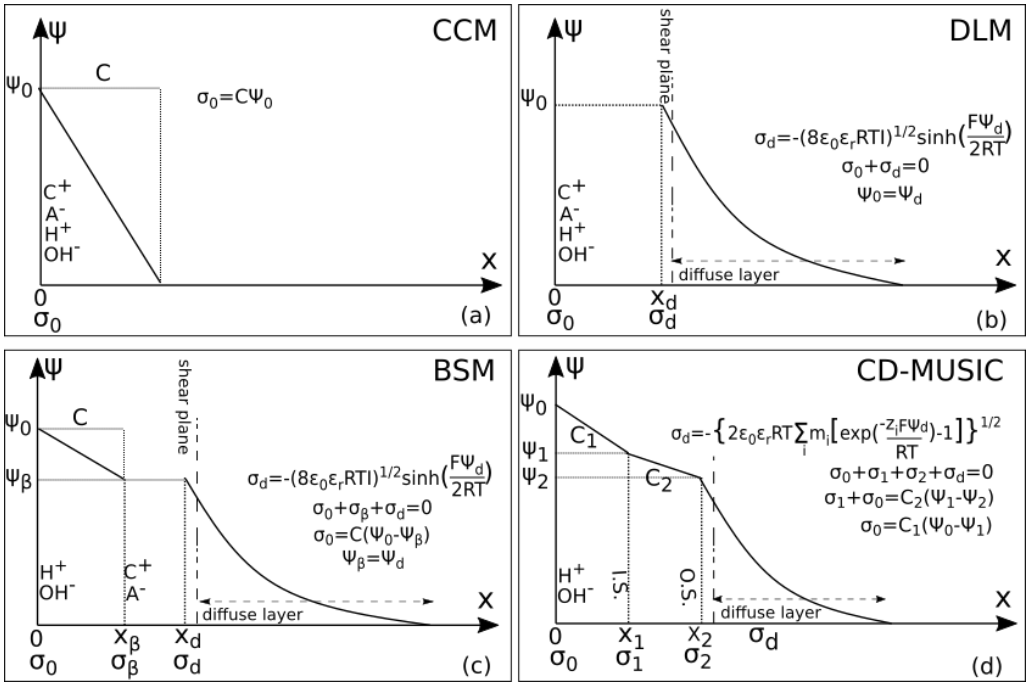

Figure 2.2. Schematics of the potential profile across mineral-water interfaces and charge-potential relationships according to CCM, DLM, BSM, and CD-MUSIC models. In the figures, x [m] represents the thickness of the interfacial region and ψ the potential. Note that the shear plane is located at an unknown distance from the OHP (d- or 2-plane). The species placed in each plane, i.e., C^+, A^-, H^+, and OH^- represent cations, anions, proton, and hydroxyl, respectively. For the CD-MUSIC models, the adsorbed species are represented by inner and outer spheres (I.S. and O.S. respectively) depending on whether the adsorption process involves the displacement of water molecules; these I.S. and O.S. can be either cations or anions.

Electrokinetic techniques measure the potential at the shear plane, which is located at an unknown distance from the onset of the diffuse layer. Thus, predicting the zeta potential with the SCM necessarily involves assumptions concerning this distance. Since the shear plane distance is usually used as an adjustable parameter, contrasting values can be found in the literature for specific interfaces (e.g., refs [42,68,124]). Although it has been previously shown that the location of the shear plane location is proportional to the square root of the ionic strength and relatively independent of the mineral type[125], it seems that the surface topography may have a great effect on this parameter[126]. Nonetheless, to reduce the number of adjustable parameters it is often assumed that the zeta potential coincides with the potential at the OHP.

The capacitance of the electrical double layer (EDL) can be computed as the sum of a rigid and diffuse layer (eq. 2.8). This corresponds to the Stern synthesis of the Helmholtz-Perrin and Gouy-Chapman models, respectively [127,128].

$$\frac{1}{C_{EDL}} = \frac{1}{C_H} + \frac{1}{C_{GC}} \tag{2.8}$$

where C_{EDL} [F/m^2] is the capacitance of the double layer, C_H is the Helmholtz capacitance and C_{GC} is the Gouy-Chapman capacitance. The first component is the Helmholtz capacitance due to the chemisorption of hydroxide groups or protons, potential determining ions, and the attraction of counterions. This capacitance comes from the contribution of the adsorbed ions[128] and is considered to depend on their molecular size. The Gouy-Chapman capacitance arises from the electrolytes in the diffuse layer and depends on the ionic strength. Although the diffuse layer capacitance is governed by the electrolyte concentration, it usually has a high value[78] making the Helmholtz capacitance the leading term[127]. The integral capacitance of the Helmholtz layer depends on the degree of structure in the hydration sheath at the surface and, therefore, on the nature of the surface. Ideally, all physical and chemical properties of the mineral-water interface required in a mechanistic model could be experimentally explored and no fitting parameters would be necessary. At present, the electrical capacitance, C [F/m^2], resulting from segregation of charge into discrete planes in the EDL cannot be directly measured[129,130] and is therefore treated as a fitting parameter in many surface complexation models[68,88,93] or estimated from the dielectric permittivity and the dimension of the interfacial region[73] as given by eq. (2.9):

$$C = \frac{\varepsilon_0 \varepsilon_r}{x} \tag{2.9}$$

where x [m] denotes the thickness of the interfacial region. The dielectric permittivity close to an interface does not depend only on the solvent but also on its hydrophilicity/hydrophobicity[131]. Because the water at the calcite surface is highly ordered, the permittivity of the Stern layer is believed to have an intermediate value between the permittivity of ice ($\varepsilon_{r,\text{ice}}$=6) and that of bulk water ($\varepsilon_{r,\text{water}}$=78.5)[104,132]. Although SCMs assume a constant value for the dielectric permittivity of water, this parameter is a tensor and is, therefore, space-dependent. A local permittivity can be defined only if the electric field inside the medium does not vary appreciably[133]. In some cases, it has been shown that the permittivity of a polar fluid may increase and not decrease as it is commonly assumed[133]; including the dielectric profile in a mean-field description of ion distribution at a charged interface instead of using a constant value, results in a better reproducibility of the double-layer capacitance[131].

In the simpler models (i.e., CCM), the capacitance values should be obtained for each experimental condition and they cannot be extrapolated to other electrolyte systems than those they were obtained for. However, the capacitance in the triple-layer models (including CD-MUSIC models) may, a priori, be suitable for different chemical circumstances[78]. For a TLM, two Helmholtz capacitances need to be specified, one for the IHP (C_1) and one for the OHP (C_2). For oxide-water interfaces the value of the IHP capacitance has been more widely addressed whereas the C_2 capacitance was simply assumed similar to C_1[74,82,132,134,135]; this is because, during the development of the SCMs, many models were calibrated using proton charge data. However, for calcite systems, usually characterized through electrokinetics, the C_2 capacitance plays a bigger role in the performance of the model. Some publications (e.g., ref [136]) have also fixed the capacitance of the OHP by considering eq. (2.9) and assuming that the distance between the IHP and OHP is equivalent to the molecular size of water molecules or that of the adsorbing ions. The high capacitance values for the calcite-water interface, traditionally defined to accommodate high surface charge densities [67,83], result in very thin EDLs that could not shelter even a water molecule. Van Cappellen et al.[70] defined a relationship between the ionic strength and the capacitance value (eq. 2.10):

$$C = \frac{\sqrt{I}}{\alpha} \tag{2.10}$$

where *I* represents the ionic strength expressed in mol/L and α is a constant that depends on the dielectric properties of the EDL. A constant of 0.006 was defined to fit the surface charge of rhodochrosite and Pokrovsky et al.[83] later used this constant to define a capacitance for calcite ranging from 5 F/m^2 at an ionic strength of 0.001 M to 160 F/m^2 at 1 M. The same approach was later used by Lakshtanov and Stipp[90] who used a fixed capacitance value of 15 F/m^2 in a CCM to model the adsorption of nickel onto calcite. Wolthers et al.[67] defined high capacitance values (C_1=C_2=100 F/m^2) and independent of the ionic strength to model the surface charge and zeta potential of calcite. Lower values (C_1=1.3 and C_2=4.5 F/m^2) were later proposed by Sø et al.[88] for the same CD-MUSIC model. Heberling et al.[68] obtained a capacitance of 0.45 F/m^2 by fitting a BSM to zeta potential measurement of calcite suspensions considering a salinity-dependent shear plane distance in 0.1 M NaCl and different CO_2 partial pressures; this capacitance was later updated by Li et al.[93] to 1.24 F/m^2 by assuming that the potential at the onset of the diffuse layer coincides with the electrokinetic potential. A lower capacitance value (0.13 F/m^2), defined by eq. (2.9), was proposed by Yutkin et al.[104]. Figure 2.3-a shows a comparison of the capacitances proposed for calcite and those of several metal (hydr)oxides. The two capacitance values inserted for the metal hydr(oxides) correspond to the minimum and maximum values obtained in different electrolytes and reviewed by Sverjensky et al.[135]. Figure 2.3-b shows the capacitance of calcite as a function of ionic strength as proposed by Van Cappellen et al.[70] and Pokrovsky et al.[83]. Except for the value proposed by Wolthers et al.[67], the capacitances for the calcite-water interface shown in Figure 2.3-a are within the range of other (hydr)oxide minerals; the reported capacitances are also between 0.1–2.8 F/m^2, a range that would yield more realistic values of the Stern layer thickness that is envisioned to be somewhere around 3.5 Å[68,132].

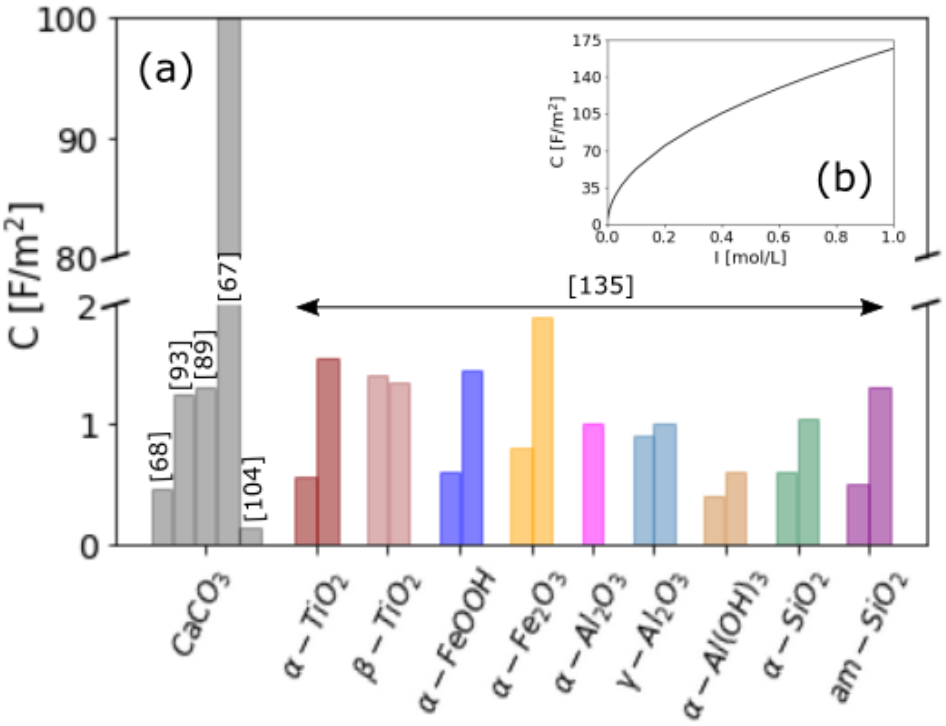

Figure 2.3. (a) Capacitances values reported for the calcite ($CaCO_3$) -water interface (from left to right, Heberling et al.[68], Li et al. [93], Sø et al.[89], Wolthers et al.[67] and Yutkin et al.[104]) in comparison with the values gathered and reviewed by Sverjensky et al. [135] for several metal (hydr)oxides in monovalent systems. (b) Variation of the capacitance for the calcite-water interface with the ionic strength as proposed by Van Cappellen et al.[70] and Pokrovsky et al.[83].

2.2.3 Surface reactions

Although reflectivity data suggests that, over a wide pH, the calcite surface speciation can be explained solely by de(protonation) reactions[108], numerous electrokinetic measurements indicate that proton and

hydroxyl are not responsible for the calcite charging behavior. It rather seems that, through dissolution, pH governs the concentration of calcite lattice ions, Ca^{2+} and CO_3^{2-}, in solution, which are ultimately the potential determining ions (PDI) that determine the polarity of the zeta potential[137–139]. The first SCMs applied to calcite defined de(protonation) of the reactive sites and interactions of the surface with Ca^{2+}, CO_3^{2-}, and HCO_3^-. But besides these ions, calcite is known to interact with trace elements and divalent ions commonly present in natural environments (e.g., refs [91,140–143]). Numerous electrokinetic measurements in the presence of Mg^{2+} and SO_4^{2-} ions were reported in the last decade within the field of enhanced oil recovery (EOR). To compare the models for predicting these data, we first need to define relevant surface reactions with these ions. Sulfate and magnesium affect calcite dissolution and precipitation[144–146], the uptake of foreign ions[147], and its wettability[148,149]. These effects may even be reinforced when both ions are present and act together[150,151]. MD simulations[152] have shown that the adsorption of sulfate at the calcite surface is energetically favorable and the desolvation of the surface during the adsorption process hints at inner-sphere complexation. Sulfate may also integrate into the calcite lattice to substitute the carbonate or combine with calcium ions to form calcium sulfate, precipitating together with $CaCO_3$. Through chromatographic wettability tests[30,153], it was also shown that SO_4^{2-} has a higher affinity for the calcite surface than other ions. The substitution of Ca^{+2} by Mg^{+2} was found to be particularly feasible in the presence of a hydration layer but less likely to occur on the $\{10\bar{1}4\}$ plane[154], which is the surface plane considered in the SCMs; besides, SCMs are more pertinently used to explain superficial adsorption and not a 3D incorporation of the ion within the bulk. Kerisit et al.[116] showed that, although both magnesium and calcium adsorb preferentially as inner-sphere complexes, magnesium results in a more stable inner-sphere complex because of its strong interaction with both the surface and water. On the contrary, others[155] showed that Ca^{+2}, Mg^{+2}, and SO_4^{2-} sit further away from the surface and do not disturb the interfacial water structure (suggesting outer-sphere complexation).

Monovalent ions/background electrolye (e.g., Na^+, Cl^-) have been traditionally regarded as "indifferent ions" for the calcite surface. The constant point of zero charge (PZC) obtained from titrations on calcite particles in four different NaCl concentrations (1×10^{-4}-1×10^{-1} M)[57] supports this hypothesis. However, streaming potential measurements on three types of limestones in presence of NaCl solutions (0.05-3 M) led to opposite findings and showed that Estaillades limestone experienced a reversal in the sign of the zeta potential with increasing NaCl concentration[137] whereas Portland limestone showed a shift in the isoelectric point (IEP) at different NaCl concentrations[156]. These observations imply that Na^+ adsorption is driven also by a chemical component and not only by an electrostatic contribution. AFM and MD indicate the presence of Na^+ in the calcite Stern layer[157,158] but the easiness of Na^+ removal from the surface suggests weak adsorption. The evidence regarding the type of surface complex the sodium forms with the calcite is not conclusive; whereas Ricci et al.[157] showed that Na^+ is placed beyond the hydration layer, Liu et al.[155] indicated that Na^+ can disrupt the hydration layer and adsorb on the calcite crystal. Heberling et al.[68] have probably been the first to include explicit interactions between the Na^+ and Cl^- with the calcite surface[68,71,87] and they were later implemented also in DLM[71,72] and CD-MUSIC models[101]. A recent publication[105] has shown that defining an explicit interaction between the calcite and the background electrolyte improved the agreement between the SCM and the experimental data.

Although the adsorption at the calcite-water interface is a complex process through which ions bind at different distances depending on the hydration sheath of both cations and calcite, SCMs adopt a simple approach to define the surface interactions; these surface reactions are most likely not a true representation of the complexation that occurs at the calcite-water interface. In the simpler models (i.e., CCM and DLM) all ions adsorb at the surface as inner-sphere complexes. In the CD-MUSIC model for calcite[67], Wolthers et al. assumed inner-sphere complexation for the calcium and carbonate species and showed that considering outer-sphere complexation resulted in only slightly lower potentials. On the

other hand, Heberling et al.[68] carried out surface diffraction measurements and could not find any indication of calcium nor carbonate inner-sphere complexation; hence, they assumed all surface species as outer-sphere complexes. In the DLM, CCM, and BSM, upon adsorption, the charge of the ion is entirely placed within one plane. In the CD-MUSIC model, depending on the structure of the surface complex, the charge of the ion can be fractionally assigned to different planes. For instance, the charge of the central atom of the oxyanions (e.g., HCO_3^-, CO_3^{2-}, SO_4^{2-}) may be partially neutralized by the oxygen at the calcite surface and the remaining fraction in the 1- or 2-plane depending on the type of surface complex (i.e., inner- or outer-sphere).

Besides inner/outer-sphere complexation, the models also exhibit differences in associating specific ions with certain sites. Van Cappellen and coworkers[70] compared the equilibrium constants of the dissolved $CaHCO_3^+$ and $CaOH^+$ complexes and suggested that the adsorption of divalent metals at carbonate sites is strongly favored over binding at calcium sites. Thus, most models consider that cations are bound to the surface through the oxygen of the calcite carbonate group in agreement with MD simulations and X-ray reflectivity data (e.g., refs [108,115,157]). Some exceptions exist, which assume that anions and cations adsorb on the carbonate and calcite groups[71,72], respectively, or that all surface groups, irrespective of the type, can bind both anions and cations[68].

2.3 Experimental data

Electrophoresis (EP) and streaming potential (SP) are the most popular methods used to measure the zeta potential of calcite; electrokinetic sonic amplitude (ESA) has also been employed on calcite suspensions, but to a lower extent. These methods allow to indirectly determine the zeta potential either from the electrophoretic mobility of particles (EP), dynamic mobility spectrum (ESA), or the coupling coefficient (SP). In the EP measurements, the test sample consists of a suspension containing an electrolyte of interest and a certain concentration of solids. When an electric field is applied, particles move in the static liquid and the electrophoretic mobility is determined from the speed of the particle in the applied electric field strength (V/m). The movement of the particles towards the anode and cathode gives the polarity of the zeta potential. Depending on the size of the particles and properties of the solvent, the electrophoretic mobility can be converted to zeta potential through different equations (e.g., Hückel, Smoluchowski, O'Brien-White)[159]. During the streaming potential measurements, the electrolyte of interest is flooded through the sample (either intact core rock samples or packed beds of rock agglomerates/powder) by applying a pressure gradient. The fluid motion drags the ions in the diffuse layer downstream leading to a streaming current and, therefore, to a streaming potential. At the same time, the streaming potential causes a conduction current in the opposite direction. At steady state, when the conduction current and streaming current are equivalent and cancel out, a streaming potential coupling coefficient can be defined as the ratio between the measured potential difference, ΔV [V], and pressure drop, ΔP [Pa]. The zeta potential is then usually obtained from the streaming potential coupling coefficient through the Helmholtz-Smoluchowski equation. In the ESA measurements, particles move due to the action of an alternating electric field that generates sound waves. The dynamic particle mobility spectrum can then be used to determine the zeta potential and particle size[160]. This technique can be used in more concentrated colloids systems compared to EP. Further description of these and other methods can be found in Hunter[161].

To test the models, we first collected a wide dataset of electrokinetic measurements. Table 2.1 gathers some fundamental details of these experiments. The table entries regarding particle size and solids concentration are not relevant to SP measurements performed on intact core samples.

Table 2.1. Zeta potential measurements of calcite in presence of diverse electrolyte solutions. SSA denotes specific surface area.

Ref.	Type of calcite	Method	Pulverized/ Particle size [μm]	Conc. Solids (wt.%)	ssa m^2/g	Equilibration procedure and experimental details
156	Portland LS (96.6%)	SP	NA	NA	—	0.05/0.5/2.0 M NaCl solution equilibrated with atmospheric CO_2 and limestone particles until conductivity and pH reached a constant value (pH≈8.2). The equilibrated solution was then modified with different divalent ions (Ca^{2+}, Mg^{2+}, SO_4^{2-}) and uploaded in the SPM (closed) setup.
		EP	Yes/—	1.0	—	Limestone cleaned with methanol for 48 h and then pulverized. Particles equilibrated with the electrolyte solution (0.05 M NaCl+ Ca^{2+}) and atmospheric CO_2. Prior sampling from the supernatant, the suspension was allowed to settle for 1 h.
162	Synthetic	EP	Yes/ 2.3-3	0.05	—	Calcite particles mixed with different aqueous solutions containing Na^+, Cl^-, Mg^{2+}, and SO_4^{2-} (I=10^{-4}-10^{-2} M) at ambient pressure and temperature. The pH of the electrolyte solution and calcite suspensions was adjusted by adding HCl/NaOH. Short equilibration times resulted in time-dependent zeta potential values.
163	Middle Eastern carbonate	EP	Yes/—	1	—	Rock particles (clean or surface treated with crude oil) were equilibrated in deionized water and sonicated for 5 minutes. The pH of the suspensions was fixed to 7.5 by NaOH/HCl titrations. NaCl, KCl, $MgCl_2$, $CaCl_2$, Na_2SO_4, or Na_3PO_4 were added to the calcite suspensions to achieve different electrolyte concentrations (300-1000 ppm). The pH was re-adjusted to 7.5 and after a short time, measurements were taken at 25 and 80ºC.
53	Natural (>97%)	EP	Yes/5.0	0.05	—	0.01 M KCl calcite suspensions at fixed pH by HCl/NaOH titrations. No information on equilibration time nor CO_2 atmosphere.
164	Artificial Biogenic calcite	EP	Yes/ <10.0	0.288	—	Ground, sieved, and washed calcite was equilibrated with 0.03 M KCl or 0.03 M KCl/$CaCl_2$ mixtures in a closed system for 24 h.
57	Synthetic	ESA	Yes/ <1.1	20	8.5	Suspensions of different solids concentrations were prepared by mixing calcite particles in different electrolyte solutions (0-0.5 M NaCl background electrolyte in presence/absence of CO_2); pH fixed by adding HCl/NaOH. Suspensions were stirred for 45 min and allowed to equilibrate for 15 min before pH was checked again and adjusted when necessary.
165	Synthetic	EP	Yes/—	2	—	Calcite particles were mixed with $MgCl_2$ and NaCl aqueous solutions of different concentrations (10^{-5}-1.0 M) were sonicated for 30 s. Samples were left equilibrating for 2 h before measurements were taken. No information on the CO_2 atmosphere.
166	Precipitated $CaCO_3$	EP	Yes/—	—	—	Calcite suspensions adjusted for pH, ionic strength (0.01, 0.05, and 0.15 M) and pCa by HCl/NaOH, NaCl and $CaCl_2$, respectively. No information on the CO_2 atmosphere.
68	Synthetic calcite	EP	Yes/ <1.0	—	—	Calcite suspensions in 0.1 M NaCl equilibrated with controlled CO_2 phase (P_{CO2}= $10^{-5.2}$, $10^{-3.4}$and 1 atm). Equilibration times from 1 day up to a month depending on the CO_2 partial pressure and solution composition. pH was adjusted by HCl/NaOH titrations.
167	Synthetic calcite (99%)	ESA	Yes/0.7	25	8.63	Calcite particles equilibrated in a closed system with $CaCl_2$ electrolytes (0-10^{-2}) M and sonicated vigorously for 60 minutes. Bottles were agitated at room temperature for 5 days.
93	Iceland Spar	SP	Yes/>25	NA	—	Measurements performed in NaCl solutions (0.001, 0.01, 0.05 M) in the pH range 5.5-10.5 (adjusted with HCl/NaOH) and equilibrated with atmospheric CO_2.

168	Carbonate 1 (98.37%) Carbonate 2 (98.34%)	SP	NA	NA	–	Aqueous solutions pre-equilibrated for 2 weeks (no mention to CO_2 phase) with rock particles of the same kind as the core sample in the streaming potential setup. Measurements performed on fully saturated samples and at residual oil saturation with mixed solutions of different ionic strength and single electrolyte systems (10^{-3}-0.5 M NaCl and $CaCl_2$ solutions).
169	LS 1 (82%) LS 2 (98%) LS 3 (71%) LS 4 (47%)	EP	Yes/3-5	1.0	–	Limestone powders were treated by ultrasonic cleaning with ethanol and distilled water successively. Calcite particles were added to 10^{-4}-1 M single electrolyte systems (NaCl, $MgCl_2$, $CaCl_2$) and dilutions of formation water of an oil reservoir from China. Suspensions were sonicated for 2 minutes and the pH was adjusted to 8 by HCl/NaOH additions. No information on the CO_2 atmosphere. The effect of surfactant and naphtenic acid adsorption on the limestone response on the zeta potential was also studied.
170	LS (100%)	EP	Yes/1-20	1.0	–	Calcite particles mixed with electrolyte solutions of several ionic strengths (0.035-3.65 M) were placed in a sonicator bath for 20 min and then allowed to equilibrate for 1 day. The pH of the suspensions was adjusted by HCl/NaOH titrations and then the solution was stirred for 5 min and allowed to rest for another 20 min. The pH was monitored until it reached a constant value.
137	Ketton LS (97%) Estaillades LS (97%) Portland LS (96.6%)	SP	NA	NA	–	0.5/2.0 M NaCl solutions were first equilibrated with atmospheric CO_2 and limestone particles until conductivity and pH reached a constant value (pH≈8.2). The equilibrated solutions were then modified with different divalent ions Ca^{2+}, Mg^{2+}, SO_4^{2-} and uploaded in the SP (closed) setup.
171	Natural calcite (Broken Hill, Australia)	EP	Yes/<2.0	0.01	–	Calcite particles were mixed with $NaClO_4$, $NaClO_4$/$CaClO_4$, or $NaClO_4$/ Na_2CO_3 electrolytes of constant ionic strength ($2\cdot10^{-3}$ M) and fixed pH ($HClO_4$/ NaOH titrations). The suspensions were equilibrated for 30 min in an open system.
139	Natural (Orgon, France) Synthetic	EP	Yes/0.75 Yes/2.0	4.0	7.1 22.3	Calcite particles equilibrated with 10^{-3}-10^{-1} M NaCl (in some cases divalent ions such as Ca^{2+}, Mg^{2+}, and SO_4^{2-} were also added) at different pHs fixed by HCl/NaOH titrations. Suspensions were mechanically shaken for 24 hours while pH and conductivity were checked for invariability. Measurements were carried out on dilutions of the original calcite suspension. They observed that equilibrium is reached (for pHs<10) after one hour of stirring.
172	Natural (Norvijaur, Sweden)	EP	Yes/5.0	0.028	10.3	$2\cdot10^{-3}$ M $NaClO_4$ solutions with different pHs (NaOH/HCl titrations) with and without sodium oleate were equilibrated with calcite powder for about 30 minutes. No special precautions were taken to exclude CO_2.
173	Natural (99%) Natural (99.75%) Natural Synthetic 1 Synthetic 2	EP	Yes/3.0 Yes/3.0 Yes/2.5 Yes/– Yes/–	0.01-0.2	4 2.5 2.0 – –	Different sample preparation procedures and experimental protocols (e.g., open system, closed, stirring mode, solids concentration) were tested.
174	Synthetic	EP	Yes/<0.4	–	–	Suspensions of calcite in single electrolyte systems ($5\cdot10^{-4}$ – 0.05 M NaCl, $CaCl_2$, $MgCl_2$, Na_2SO_4, and Na_2CO_3) were prepared 1-1.5 h before each run. Equilibration performed in a closed system (no CO_2 gas phase).
175	Synthetic	EP	Yes/1.0	0.01-0.03	–	Calcite particles were equilibrated with binary electrolyte systems (NaCl+ $CaCl_2$/$MgCl_2$/Na_2SO_4/Na_2CO_3) of fixed ionic strength (0.1 M) in a controlled CO_2 atmosphere (P_{CO2}=$10^{-3.4}$ and 1.0 atm). Suspensions were left to equilibrate until the predicted pH reached the equilibrium value calculated with Phreeqc. Sample equilibration typically occurred within 1-4 days.

72	Synthetic (99.5%) Iceland Spar (99.9%) Indiana LS (93%) Middle East carb. (86.7%)	EP	Yes/1.0	0.01-0.03	–	Ground calcite particles were mixed with binary electrolyte systems (NaCl + $CaCl_2$/$MgCl_2$/Na_2SO_4) of 0.1 M fixed ionic strength or with more complex brine mixtures (e.g., seawater-like solutions and dilutions of this) and left to equilibrate under controlled CO_2 atmosphere ($10^{-3.4}$ atm).
138	Synthetic	SP	Yes/ 106-150	NA	–	Mixed electrolyte solutions (NaCl + $NaHCO_3$/$CaCl_2$) were loaded in the SP setup and flushed through the calcite pack in a closed system. 48 h were initially needed to equilibrate the solution with the core, whereas 15 h were needed to equilibrate upon adding acid/base. The pH was adjusted through NaOH/HCl or $Ca(OH)_2$/H_2CO_3 titrations.
176	Synthetic	EP	Yes/ 2.2	0.02	17.0	Samples were equilibrated in 0.001 M NaCl reaching a pH of 8.6. Then, the suspensions were titrated with HCl/NaOH to reach desired pH values. No information on equilibration time nor CO_2 atmosphere.
	Natural		Yes/ 2.8		6.6	
177	Precipitated calcite, vaterite, and aragonite	EP	Yes/20	0.4	6.4	Calcite particles equilibrated in 0.001 M NaCl solutions for a few hours until the pH reached 8.3. The pH was then adjusted by NaOH/HCl titrations and ζ measurements were performed just after the titration.
178	Chalk (>96%) Stevns Klint, Denmark	ESA	Yes/–	4.0	2.0	0.573 M NaCl solution was equilibrated with chalk particles through stirring for 2 days. Series of tests were performed by gradually adding $CaCl_2$ or Na_2SO_4 (0-0.12 M) to the suspension while the pH was kept constant at 8.4 by adding NaCl/NaOH. No information on the CO_2 gas phase.
6	Chalk(>96 %) Stevns Klint, Denmark	ESA	Yes/–	4.0	2.0	0.573 M NaCl solution equilibrated with chalk particles through stirring for 2 days. Series of tests were performed by gradually adding 0-0.12 M $CaCl_2$ with(out) 0.012 M Na_2SO_4 to the suspension while keeping the pH constant to 8.4 by adding NaCl/NaOH. The suspension was stirred for 2 minutes after new chemicals were added to achieve a new equilibrium before the measurement. No information on the CO_2 gas phase.
60	Chalk(>96 %) Stevns Klint, Denmark	ESA	Yes/–	4.0	2.0	0.573 M NaCl solution equilibrated with chalk particles through stirring for 2 days. No information on the CO_2 phase. Series of tests were performed by gradually adding (0-0.12 M) $MgCl_2$ or Na_2SO_4 into the suspension while the pH was kept constant by adding NaCl/NaOH. The suspension was stirred for 2 minutes after new chemicals were added to achieve a new equilibrium before the measurement.
179	Chalk	SP	Yes/ 0.5-5.0	NA	1.8-3.5	0.001 M NaCl electrolyte solution flushed through the chalk powder pack while the pH was adjusted by additions of HCl/NaOH. No information on the CO_2 partial pressure nor equilibration time.
98	Indiana limestone	EP	Yes/<53	1.0	1.0	Rock particles mixed with single electrolyte systems (NaCl, KCl, $CaCl_2$, $MgCl_2$, Na_2SO_4) of fixed ionic strength (0.04 M) and brine mixtures mimicking formation water (3.27 M), seawater (0.65 M), and low salinity water (0.04 M) were sonicated for 30 minutes. No information on the CO_2 phase. The suspension was allowed to sit for a minimum of 2 h after which the supernatant solution was drawn out, filtered through 70 nm filter paper used for pH and ζ measurements at 25 and 40ºC.
180	Limestone	EP	Yes/–	0.4	–	Electrolyte mixtures of different salinities (5500-55000 ppm) containing Na^+, Ca^{2+}, Mg^{2+}, Cl^-, HCO_3^-, SO_4^{2-} and different pHs (adjusted by HCl/NaOH titrations) were mixed with rock powder and equilibrated for 2 days. Samples were centrifuged to separate the supernatant, and measurements were performed at 25 and 50 ºC. No information on the CO_2 gas phase.
181	Carbonate (80%)	SP	NA	NA	–	Core pre-saturated with brine mixtures containing Na^+, Ca^{2+}, Mg^{2+}, Cl^-, HCO_3^-, and SO_4^{2-} (ionic strength between 0 and 1.15 M) were mounted in the SP setup. No information on the required equilibration time nor CO_2 atmosphere. Measurements performed at 25 and 60ºC.

[182]	Natural (100%)	EP	Yes/–	0.4	–	Ground calcite particles were equilibrated for 2 days with single electrolyte systems (NaCl, $CaCl_2$, $MgCl_2$, and Na_2SO_4) of different ionic strength (0.098-0.15 M). pH was adjusted by HCl/NaOH titrations. The suspensions were centrifuged to separate the supernatant, and measurements were carried out at 50 and 80ºC. No information on the CO_2 gas phase.
[183]	Several carbonate reservoir core samples	SP	NA	NA	–	Rock samples were equilibrated in a closed system for at least 24 h with electrolyte mixtures containing HCO_3^-, Na^+, Mg^{2+}, Ca^{2+}, Cl^-, K^+, Li^+, Br^- and SO_4^{2-} (ionic strength between 0.01 and 4.3 M). Experiments were conducted either on fully water-saturated samples or at residual oil saturation at ambient conditions and 70, 80, and 100ºC.
[184]	Ketton LS (97%) Estaillades LS (97%) Portland LS (96.6%)	SP	NA	NA	–	Clean limestone samples were equilibrated by flooding a core sample with at least 4 pore volumes of 0.05 M NaCl aqueous solution. The electrolyte solution was pre-equilibrated with carbonate particles and atmospheric CO_2 for 4-8 weeks until a pH of 8.2 was reached. Measurements performed from 20 to 120ºC in 0.01 M and 0.5 M NaCl.
[185]	Iceland spar	EP	Yes/ 0.45	–	–	Calcite particles aged/treated in model oil (stearic acid + toluene) were equilibrated during 24 h with seawater and modified seawater compositions (ionic strength of 0.57 M). No information on the CO_2 gas phase.
[186]	Iceland spar	EP	Yes	–	–	Clean calcite particles or calcite aged in model oil (toluene with stearic acid) were equilibrated for 24 h with mixed electrolyte systems containing Na^+, Ca^{2+}, Mg^{2+}, SO_4^{2-}, Cl^- (ionic strength of 0.574 M). CO_2 access was supposed to be prevented but this could not be completely removed.
[187]	Synthetic	ESA	Yes/7	11.1	0.77	Calcite particles equilibrated with a Na_2SO_4/$NaNO_3$ mixture (ionic strength of 0.12 M) and air (atmospheric CO_2). Measurements performed at a pH of 12.4 fixed with $Ca(OH)_2$ titrations.

2.4 Methodology

The synergy between the interactions taking place at the calcite surface complicates quantifying the contribution of each one of them to the zeta potential. To assess the role of individual surface reactions, fitting the models to reliable experimental data by optimizing equilibrium constants is required. Once the equilibrium constants are obtained, the model would, ideally, have predictive capabilities and could anticipate the outcome for systems with variable conditions. Nonetheless, the prediction capabilities may be dependent on the SCM type. Westall and Hohl[78] remarked that the parameters derived for simpler models (e.g., CCM and DLM) are strongly dependent on the experimental conditions (e.g., ionic strength and electrolyte concentration) they were inferred for. On the other hand, the equilibrium constants derived for triple-layer models could be applicable over a wider ionic strength range because many of the interactions are explicitly defined and the value of the potential at the OHP can be used as an estimate of the electrokinetic potential. The objective of this work is twofold. First, we assess whether the models, once tuned to a particular dataset, can predict electrokinetic data over different chemical conditions. Second, by comparing the performance of three different SCMs against multiple datasets we evaluate whether a particular model describes better the zeta potential of calcite in presence of different electrolytes, ionic strength, and pH. To do so, we implement the following models:

1. BSM proposed by Heberling et al.[68]. To implement this model we adopt the modifications proposed by Heberling et al.[87] and Li et al.[93]. Thus, we consider that there is no stagnant zone within the diffuse region and that the zeta potential coincides with the potential at the OHP (2- or d-plane). To preserve a similar number of adjustable parameters for all models, we limit the interaction of the anions with the calcium sites and that of the cations with carbonate sites; these interactions are kept as defined in refs.[87,93]. Since we simplify the model by reducing the number of surface reactions defined in the original work, the capacitance value is also left as a fitting

parameter but constraining its value between 0.1-2.5 F/m^2 to ensure Stern layer thicknesses within a reasonable range[68].

2. CD-MUSIC model proposed by Wolthers et al.[67]. For the implementation of this model, we consider only the face sites and the capacitances proposed by Sø et al.[88] (C_1=1.3 F/m^2 and C_2=4.5 F/m^2). The net charge distribution in the surface plane, IHP, and OHP (Δz_0, Δz_1, and Δz_2, respectively) is not used as an adjustable parameter but kept the same as in the original work.
3. DLM as proposed by Brady et al.[94]. We assume that the zeta potential coincides with the potential at the onset of the diffuse layer (d-plane). For the initial estimates of the equilibrium constants in the optimization, we consider the values proposed by Tetteh et al.[98].

The CCM is not tested against zeta potential measurements because its assumption of only a Stern layer is not consistent with the concept of the shear plane, thus the theory behind electrokinetic phenomena. The CD-MUSIC and BSM models taken from Wolthers et al.[67] and Heberling et al.[68], respectively, do not define surface reactions with magnesium and sulfate ions. We include these interactions in both models in analogy with the already existing surface interactions for calcium and carbonate. To compare the models under the same circumstances we obtain their parameters by fitting them to the experimental data from Song et al.[71,72]. We appraised this experimental dataset as the most reliable for the following reasons: (1) it provides a detailed description of the equilibration procedure; (2) the equilibration with pure/partial CO_2 atmosphere was assessed through pHs measurements and compared with theoretical pHs predictions; (3) it does not only report the solids concentration of the initial suspension, but it explicitly characterizes the particle concentration in the supernatant, which is the fraction used in the electrophoresis measurements; (4) it evaluates the particle concentration range that leads to constant zeta potential; (5) the measurements in four mixed electrolyte systems, e.g., NaCl + $CaCl_2$/$MgCl_2$/Na_2CO_3/Na_2SO_4 allow obtaining the equilibrium constants of all reactions defined; (6) the measurements, performed on synthetic calcite, allow establishing a baseline for the zeta potential of pure calcite. Nonetheless, this data also carries some uncertainty because the particle concentration range that resulted in constant zeta potential was only investigated for a calcite/0.1 M $CaCl_2$ suspension in the absence of a CO_2 gas phase; this solids weight fraction may be questionable for the measurements performed in a pure CO_2 atmosphere, where dissolution effects become more relevant.

To fit the three models to the chosen experimental dataset, we use a least-squares optimization algorithm implemented in Python ("leastsq" method)[188]. Thus, we write and run the Phreeqc input files from Python. The optimization algorithm adjusts the parameters in an iterative process until the sum of the squared errors between the measured and calculated zeta potential is minimized and the parameters converge to values within a certain specified tolerance. The used algorithm also allows the estimation of the uncertainty of the optimized parameters from the inverse of the Hessian matrix. The surface reactions defined in each model, the initial estimates of the parameters assigned in the optimization, and the optimized values (including uncertainty), are shown in Table 2.2 as log K and log K_{opt}, respectively.

The fitted models along with the experimental data used in the optimization are shown in Figure 2.4. A plot displaying the confidence interval of the models has been included in Appendix A.1. To address the importance of the interaction with the background electrolyte, we perform the optimization of the models with(out) an additional interaction with Na^+. We only kept the interaction with the cation (Na^+) as after a first optimization we observed, for the three models, that the reaction defined for Cl^- does not affect the residuals. In the BSM, Heberling and coworkers[68,87,93] defined a reaction between the calcite and Na^+ and we could not satisfactorily fit the model to the experimental data by dismissing this interaction. For this reason, the performance of the BSM models is always shown including the reaction with Na^+. After the optimization, the three models display a similar residual mean squared error (RMSE). The CD-MUSIC and BSM models, with 7 adjustable parameters each, have an RMSE of 2.78 and 2.87 mV respectively, whereas the DLM, with 6 adjustable parameters has an RMSE of 3.05 mV.

Increasing the number of adjustable parameters by adding a reaction with Na^+ decreases the RMSE of the CD-MUSIC and DLM to 1.73 and 2.48 mV, respectively. In general, the poorer match is obtained for the $NaCl/Na_2SO_4$ system and the measurement in the absence of any divalent ion (NaCl=0.1 M) at low CO_2 partial pressure ($10^{-3.4}$ atm). The equilibrium constant for the reaction with sulfate is also the one that shows the highest uncertainty. This could be an indication that the complexation of the calcite surface with the sulfate does not proceed as envisioned by the reactions we defined; it may also mean that sulfate is not a PDI for the calcite surface as concluded by Mahrouqi et al.[137]. Despite the apparent satisfactory trend between models and experimental data, the models may be overfitted given the fairly low ratio of experimental datapoints to fitting parameters (34 to 7). Thus, to address whether these models can describe the calcite electrokinetic behavior at variable conditions, in the next section, we show the performance of the models for the different experimental datasets gathered in Table 2.1.

Table 2.2. Surface reactions defined in each SCMs and optimized equilibrium constants (with uncertainties). The initial values assigned in the optimization are the equilibrium constants (log K at 25ºC) defined in the original publications that reported/revised the models. The first reaction for each interaction type (marked with [(a)]) corresponds to that defined in the DLM by Brady et al.[94] and the initial values for the equilibrium constants are taken from Tetteh et al.[98]; the second reaction for each interaction type (marked with [(b)]) and the initial log K values correspond to those defined in the CD-MUSIC model by Wolthers et al.[67]. The reactions for Mg^{2+} and SO_4^{2-} were defined analogously to those for Ca^{2+} and CO_3^{2-} and the initial log K values for those reactions were taken from the Lawrence Livermore National Laboratory database, llnl.dat, distributed with Phreeqc (marked with *). Capacitances for this model: C_1=1.3 F/m^2 and C_2=4.5 F/m^2. The third reaction for each interaction type (marked with [(c)]) and the initial log K values correspond to the Basic Stern model proposed by Li et al.[93]. The optimization shifted only slightly the value of the capacitance proposed by Li et al. (from 1.24 to 1.20 F/m^2). The net charge distributed, Δz_i, in plane i is irrelevant for DLM as all ions adsorb in the surface place. The net charge in the 2-plane (CD-MUSIC) is zero as all surface species are considered inner-sphere complexes. For all models, we considered a stoichiometric site density at the calcite surface of 4.95 #/nm^2.

		Reactions	log *K* [25ºC]	log K_{opt} [25ºC]	Δz_0	Δz_1
Calcium sites	R2.1. Protonation	$\equiv CaOH^o + H^+ \leftrightarrow \equiv CaOH_2^+$ (a)	11.85	14.11±1.09	NA	NA
		$\equiv CaOH^{-0.667} + H^+ \leftrightarrow \equiv CaOH_2^{+0.333}$ (b)	12.85	14.04±0.16	1	0
		$\equiv CaOH^{-0.5} + H^+ \leftrightarrow \equiv CaOH_2^{+0.5}$ (c)	0.5	0.15±0.03	1	0
	R2.2. Interaction with bicarbonate	$\equiv CaOH^o + HCO_3^- \leftrightarrow \equiv CaCO_3^- + H_2O$ (a)	5.8	4.53±1.15	NA	NA
		$\equiv CaOH^{-0.667} + CO_3^{2-} + H^+ \leftrightarrow \equiv CaHCO_3^{-0.667} + OH^-$ (b)	10.15	9.24±0.39	0.6	-0.6
		$\equiv CaOH^{-0.5} + H^+ + HCO_3^- \leftrightarrow \equiv CaOH_3CO_3^{-0.5}$	0.54	1.53±0.10	1	-1
	R2.3. Interaction with carbonate	NA	NA	NA	NA	NA
		$\equiv CaOH^{-0.667} + CO_3^{2-} \leftrightarrow \equiv CaCO_3^{-1.667} + OH^-$ (b)	1.55	0.81±0.14	0.6	-1.6
		$\equiv CaOH^{-0.5} + H^+ + CO_3^{2-} \leftrightarrow \equiv CaOH_2CO_3^{-1.5}$ (c)	-6.57	-6.57	1	-2
	R2.4. Interaction with sulfate	$\equiv CaOH_2^+ + SO_4^{2-} \leftrightarrow \equiv CaSO_4^- + H_2O$ (a)	2.1	0.05±0.09	NA	NA
		$\equiv CaOH^{-0.667} + SO_4^{2-} \leftrightarrow \equiv CaSO_4^{-1.667} + OH^-$ (b)	2.1*	0.04±0.10	1.4	-2.4
		$\equiv CaOH^{-0.5} + H^+ + SO_4^{2-} \leftrightarrow \equiv CaOH_2SO_4^{-1.5}$ (c)	0.54	1.71±0.13	1	-2
Carbonate sites	R2.5. Deprotonation	$\equiv CO_3H^o \leftrightarrow \equiv CO_3^- + H^+$ (a)	-5.1	-2.76±0.21	NA	NA
		$\equiv CO_3H^{+0.667} \leftrightarrow \equiv CO_3^{-0.333} + H^+$ (b)	-3.58	-3.12±0.27	-1	0
		NA	NA	NA	NA	NA
	R2.6. Interaction with calcium	$\equiv CO_3H^o + Ca^{2+} \leftrightarrow \equiv CO_3Ca^+ + H^+$ (a)	-4.4	-1.9±0.21	NA	NA
		$\equiv CO_3H^{+0.667} + Ca^{2+} \leftrightarrow \equiv CO_3Ca^{+1.667} + H^+$ (b)	-2.80	-2.15±0.28	-1	2
		$\equiv CO_3^{-0.5} + Ca^{2+} \leftrightarrow CO_3Ca^{+1.5}$ (c)	1.68	2.42±0.06	0	2
	R2.7. Interaction with magnesium	$\equiv CO_3H^o + Mg^{2+} \leftrightarrow \equiv CO_3Mg^+ + H^+$ (a)	-4.4	-2.11±0.25	NA	NA
		$\equiv CO_3H^{+0.667} + Mg^{2+} \leftrightarrow \equiv CO_3Mg^{+1.667} + H^+$ (b)	-2.20*	-2.38±0.37	-1	2
		$\equiv CO_3^{-0.5} + Mg^{2+} \leftrightarrow CO_3Mg^{+1.5}$ (c)	1.68	2.37±0.06	0	2
	R2.8. Interaction with sodium	NA	NA	NA	NA	NA
		NA	NA	NA	NA	NA
		$\equiv CO_3^{-0.5} + Na^+ \leftrightarrow CO_3Na^{+0.5}$	0.56	1.66±0.02	0	1

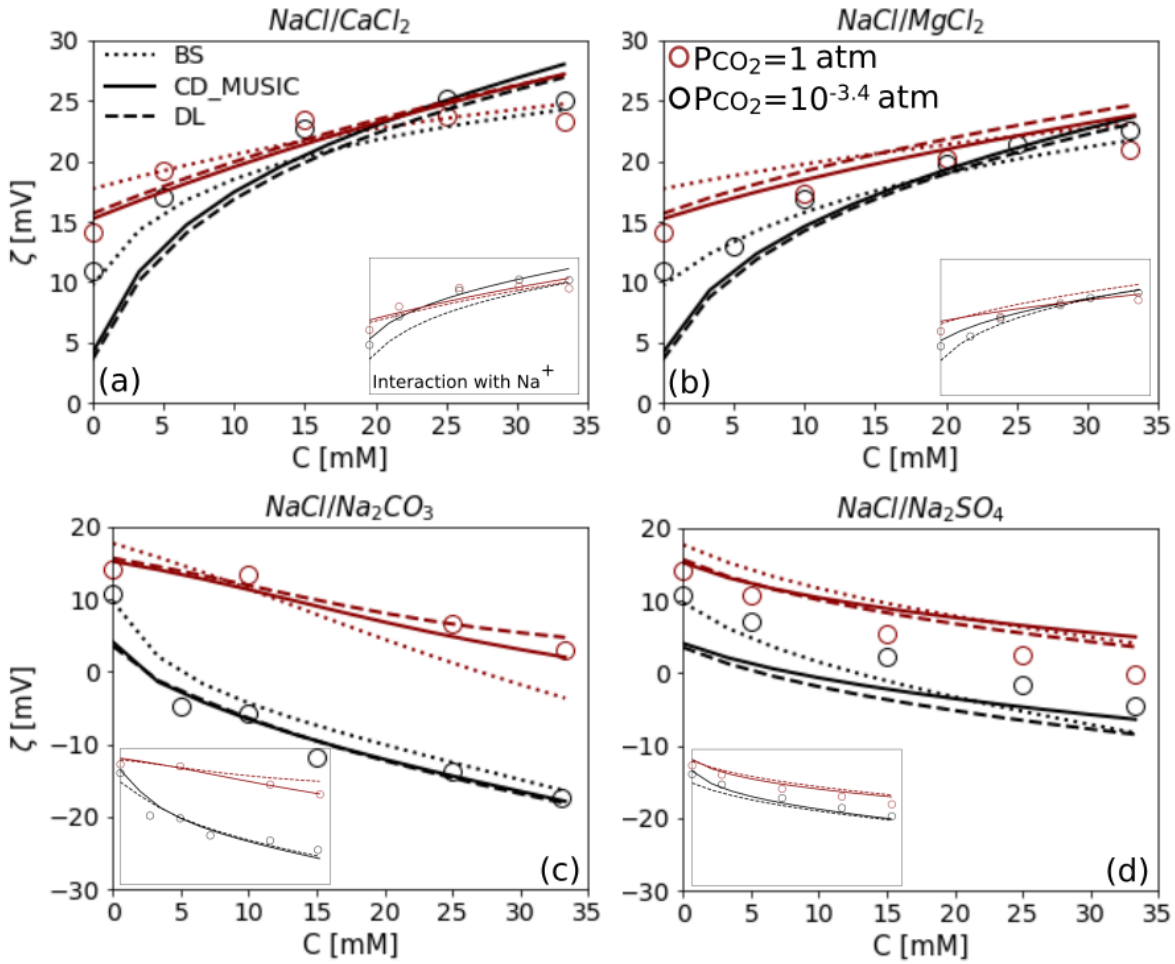

Figure 2.4. Models optimized to zeta potential measurements on synthetic calcite suspensions at fixed ionic strength (0.1 M), partial and pure CO_2 atmosphere (black and red circles, respectively) and (a) $NaCl/CaCl_2$ (b) $NaCl/MgCl_2$ (c) $NaCl/Na_2CO_3$ (d) $NaCl/Na_2SO_4$ electrolyte mixtures. For the calculations, we considered 1% wt. calcite and a ssa of 2 m^2/g. Inner plots, with the same axis limits as the outer plots, show the fit of the CD-MUSIC and DLM when an explicit interaction between the background electrolyte (e.g., Na^+) and the calcite is defined. The residual mean squared error for the BSM, CD-MUSIC, and DLM are 2.87, 2.78, and 3.05 mV. Considering an additional interaction between calcite and Na^+ decreases the RMSE of the CD-MUSIC and DLM to 1.73 and 2.48 mV, respectively. Note that the BSM model is always shown considering explicit interaction between the calcite and the Na^+ ion as without this interaction we could not satisfactorily fit the model to this data.

2.5 Results

The zeta potential for calcite suspensions in monovalent (mostly NaCl) and divalent electrolytes (containing either calcium, magnesium, sulfate, or carbonate) are shown in Figures 2.5 to 2.9. We collected and grouped the experimental data into different panels based on the ionic strength, electrolyte concentration, or equilibration procedure. The empty markers in all figures correspond to measurements on synthetic calcite whereas the filled ones to natural samples. The source of each dataset together with a brief experimental description can be found in the figure caption; for further details on the experimental procedure, the reader is referred to Table 2.1. In each plot, the zeta potential predicted by the BS, DL, and CD-MUSIC models is represented by dotted, dashed, and solid lines, respectively.

2.5.1 Monovalent electrolytes

The zeta potential of calcite in monovalent systems shows contrasting trends (see Figure 2.5). Opposite to the dataset that we considered in the optimization, many other publications report a negative zeta potential at equilibrium conditions with atmospheric CO_2 (pH≈8.3). The calcite reactivity in aqueous solutions, readily boosted when exposed to CO_2, challenges the equilibrium assumption, and even subtle changes in the experimental procedure can trigger disequilibrium. Thus, the recorded scattering is

partially a consequence of the lack of a "universal" robust protocol for carrying out zeta potential measurements on calcite systems.

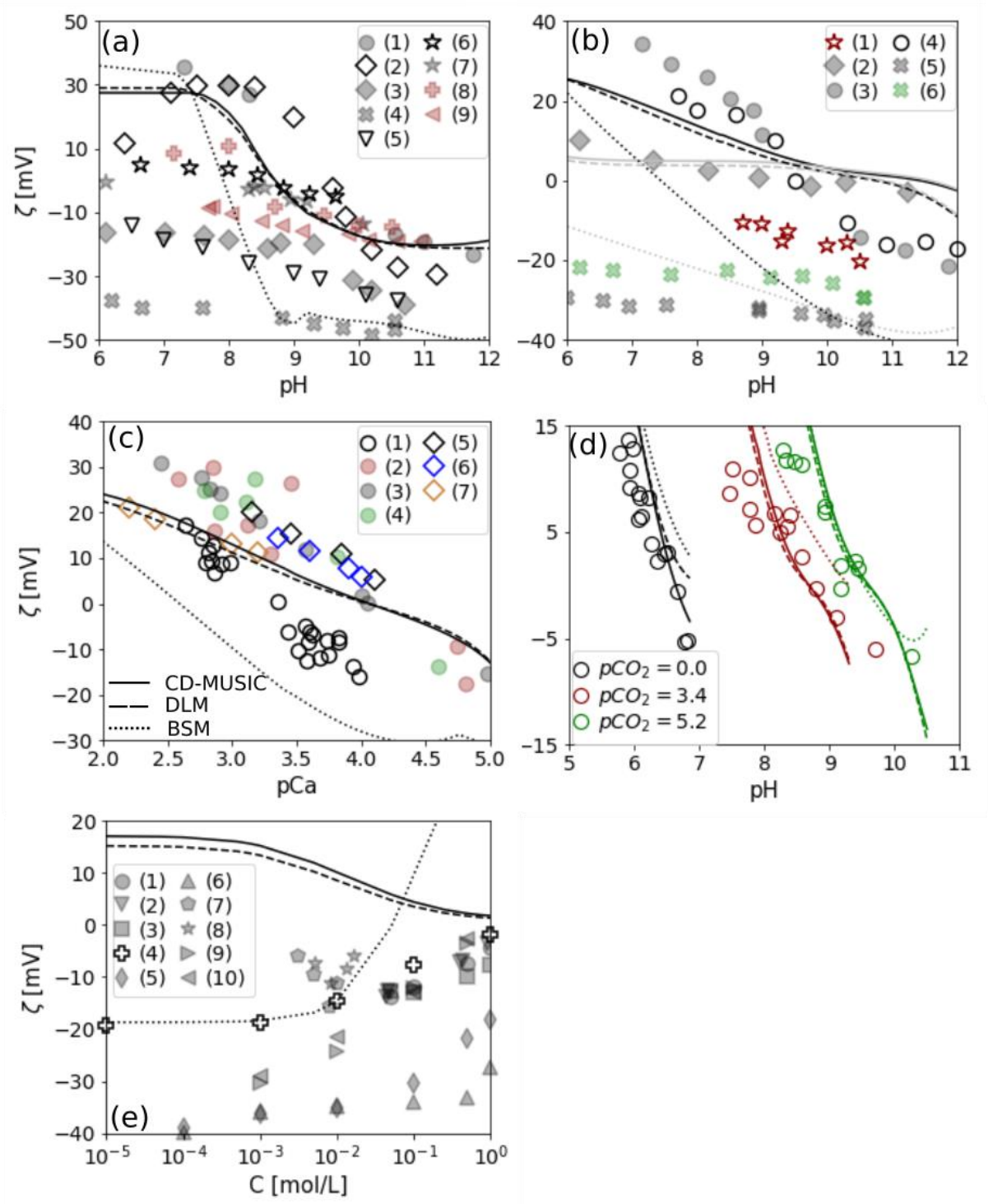

Figure 2.5. Zeta potential of calcite in monovalent electrolyte systems. For all panels, the solid, dashed, and dotted lines correspond to the prediction of the CD-MUSIC, DLM, and BSM, respectively. **(a)** ζ measurements at different pHs and 0.001-0.002 M monovalent electrolyte suspensions. The datasets represent (1) EP measurements of 0.001 M NaCl/natural calcite suspensions – data from [139]; (2), (3) EP measurements of suspensions consisting of 0.001 M NaCl and synthetic and natural calcite particles, respectively – data from [176]; (4) SP measurements on a packed bed of synthetic calcite saturated with 0.001 M NaCl – data from [93]; (5) EP measurements of a 0.001 M NaCl/synthetic calcite suspension – data from [177]; (6), (7) SP measurements of synthetic calcite and chalk in 0.001 M NaCl, respectively – data from [179]; (8) EP measurements of natural calcite particles in 0.002 M $NaClO_4$ – data from [171]; (9) EP measurements of natural calcite particles in 0.002 M $NaClO_4$ – data from [172]. The lines correspond to the prediction of the models when considering equilibrium conditions of calcite particles (4% wt., ssa=7.1 m^2/g) with the solution and a CO_2 gas phase; equilibrium reached only between pHs 7-10. **(b)** ζ measurements

at different pHs and 0.01-0.05 M monovalent electrolyte suspensions. The datasets represent: (1) EP measurements in 0.03 M KCl/synthetic calcite suspensions – data from [164]; (2) EP measurements on synthetic calcite particles in 0.01 M KCl – data from [53]; (3), (4) EP measurements of natural and synthetic calcite, respectively, in 0.01 M NaCl – data from [139]; (5), (6) SP measurements on natural calcite samples in 0.01 and 0.05 M NaCl, respectively – data from [93]. The lines show the prediction of the model assuming equilibrated (black lines) and non-equilibrated (gray-lines) calcite suspensions (4% wt., ssa=22.3 m^2/g) in the absence of CO_2. **(c)** Dependence of the calcite zeta potential on the equilibrium pCa. The datasets represent: (1) EP measurements of synthetic calcite particles in 0.01 M NaCl against the equilibrium calcium concentrations at different pHs adjusted with HCl/NaOH titrations – data from [139]; (2), (3), (4) EP measurements of synthetic calcite particles in 0.001, 0.01, and 0.1 M NaCl, respectively, against the equilibrium calcium concentration at different pHs adjusted with HCl/NaOH titrations – data from [139]; (5), (6), (7) EP measurements of synthetic calcite particles in 0.01, 0.05, and 0.15 M NaCl, respectively against the equilibrium calcium concentrations at different pHs adjusted with HCl/NaOH titrations – data from [166]. The lines correspond to the prediction of the models assuming equilibration of the calcite particles (4% wt., ssa=22.3 m^2/g) with atmospheric CO_2 and electrolyte solution (0.01 M NaCl). **(d)** ζ of synthetic calcite particles (1% wt., ssa=2 m^2/g) in 0.1 M NaCl and controlled CO_2 atmosphere – data from [68]. **(e)** ζ at increasing monovalent electrolyte concentration. The datasets represent: (1), (2), (3) SP measurements in NaCl solutions on Ketton, Estaillades, and Portland limestone samples, respectively – data from [137]; (4) EP measurements on NaCl/synthetic calcite particles suspensions – data from [165]; (5), (6) – EP measurements on suspensions consisting of NaCl/natural carbonate samples containing 82% and 98% calcite, respectively – data from [169]; (7), (8) – EP measurements on Middle Eastern carbonate samples in KCl and NaCl solutions, respectively – data from [163]; (9), (10) – SP measurements in NaCl solutions on two different carbonate samples with 98.37% and 98.34% calcite content, respectively –data from [168]. The lines represent the prediction of the models considering equilibration of the calcite core (ssa=2 m^2/g) with the electrolyte solution and CO_2 gas phase.

Different equilibration procedures affect the solution composition, yielding conflicting zeta potentials. Figure 2.5-a shows measurements performed in the presence/absence of CO_2 at different pHs and ionic strengths between 1 and 2 mM. The lines represent the prediction of the models when considering equilibrium at the fixed pH between the calcite, electrolyte solution, and atmospheric CO_2. Nonetheless, considering the experimental conditions by Pierre et al. (4% wt. solids, 23.1 m^2/g ssa), equilibrium could just be achieved at pHs between 7 and 10. At pHs lower than 7 in presence of atmospheric CO_2, the high proton concentration would lead to calcite dissolution. The dissolution of the whole amount of calcite included in the equilibrium calculations leads to a constant (high) calcium concentration, resulting in the constant ζ predicted between pHs 6-7. The three models show a fairly steady zeta potential in this pH range, supporting the observations that the calcite zeta potential is governed by the pCa and not by the pH [137]. Above a pH of 10, the conversion of HCO_3^- to CO_3^{2-} disrupts the equilibrium conditions with atmospheric CO_2 and a high transfer rate of CO_2 to solution would be necessary to keep the system in equilibrium. However, considering that in most of these experiments, during the equilibration, the CO_2 transfer to solution simply takes place by diffusion, the experimental timescales and volumes may be insufficient to ensure equilibration with the atmospheric CO_2 at such alkaline conditions. Figure 2.5-b shows the prediction of the models considering that the electrolyte solution is in equilibrium with the calcite particles (black lines) or out of equilibrium (gray lines). When the system is considered out of equilibrium, the predicted zeta potential by the DLM and CD-MUSIC is rather constant as no source of calcium is included in the calculations. Figure 2.5-c shows the variation of the zeta potential with the pCa. The calcium source in these datasets is the calcite dissolution due to NaOH/HCl titrations in calcite suspensions with monovalent electrolytes. The three models predict a linear decrease in the zeta potential with the pCa when equilibrium between calcite, electrolyte, and CO_2 is assumed. The performance of the models to account for changes in the CO_2 atmosphere is shown in Figure 2.5-d against experimental measurements at total/partial CO_2 atmosphere. This particular dataset was originally used in the development of the BSM model. Given the similarities between these measurements and the optimization dataset, the three models predict relatively well the zeta potential under the three CO_2 conditions. Figure 2.5-e shows the prediction of the models at increasing NaCl concentration. The CD-MUSIC and DLM are consistent with the double layer compression at increasing ionic strength, thus a tendency of the zeta potential towards zero; however, these models predict a positive zeta potential at the equilibrium pH in NaCl solutions, consistent with the optimization dataset, but opposite to all other gathered datasets. On the contrary, since the BSM assumes that the calcite negative surface charge is neutralized by adsorption of both divalent and monovalent ions in the β-plane, the predicted zeta potential steadily increases with increasing NaCl concentration.

2.5.2 Systems with added calcium

Figure 2.6 displays zeta potential measurements obtained in the presence of electrolytes containing calcium.

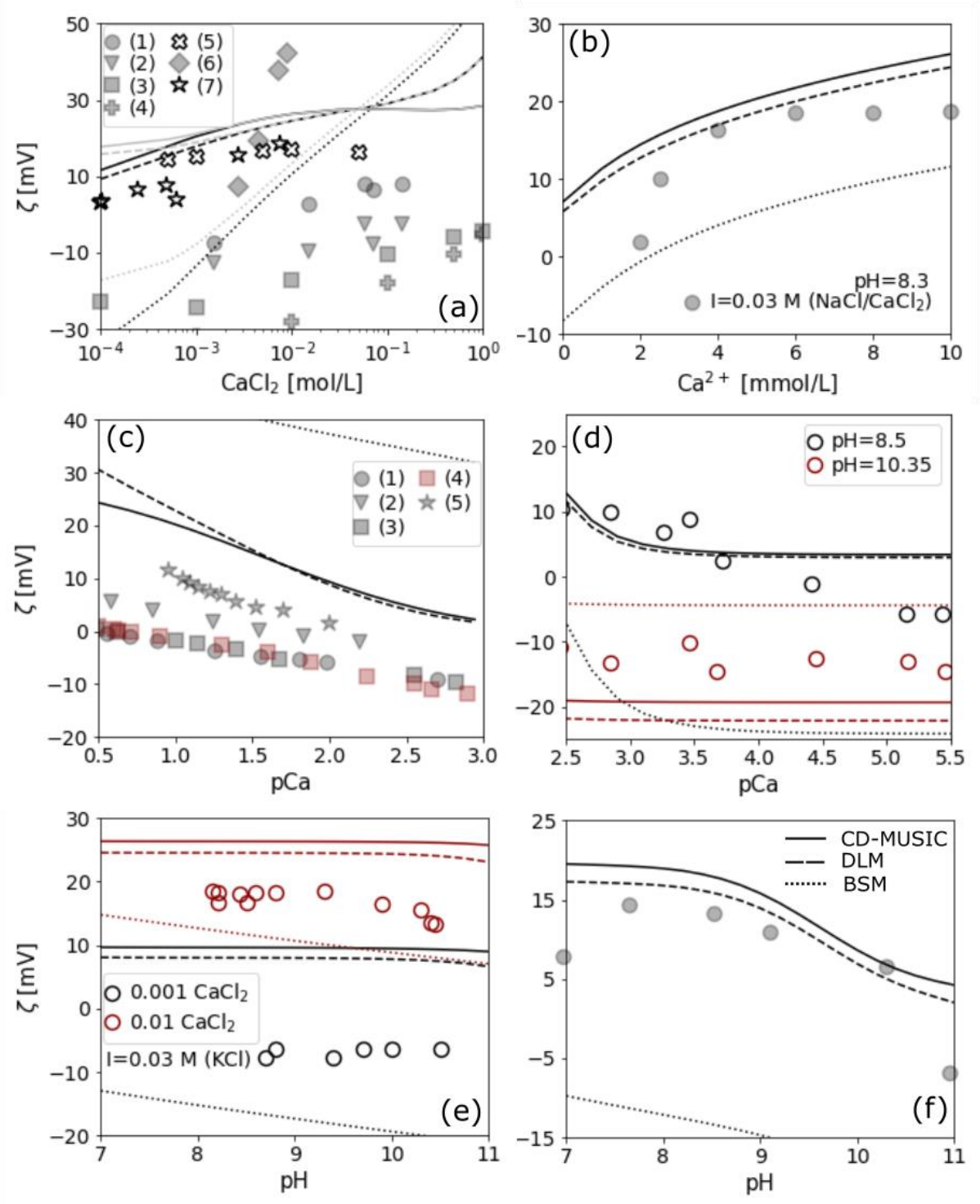

Figure 2.6. Zeta potential measurements in electrolyte systems containing Ca^{2+}. **(a)** ζ measurements at increasing $CaCl_2$ concentration. The datasets represent: (1), (2) SP measurements of two different carbonate samples with 98.37% and 98.34% calcite content, respectively – data from [168]; (3), (4) EP measurements on suspensions consisting of $CaCl_2$/natural carbonate samples containing 82% and 98% calcite, respectively – data from [169]; (5) EP measurements on synthetic calcite/$CaCl_2$ suspensions–data from [174]; (6) EP measurements on suspensions consisting of calcite/$CaCl_2$ and pH adjusted to 8.0 – data from [163]; (7) EP measurements on synthetic calcite/$CaCl_2$ suspensions – data from [167]; The black lines correspond to the prediction of the models considering a core (ssa=2 m^2/g) in a closed SP system (no CO_2 gas phase) while the gray lines correspond to an open system where the calcite/$CaCl_2$ suspension is in equilibrium with atmospheric CO_2 (pCO_2=-3.44). **(b)** ζ of natural calcite

particles (4% wt., ssa=7.1 m^2/g) at increasing calcium concentration, 0.03 M ionic strength (fixed with NaCl), and pH adjusted to 8.3 by HCl/NaOH titrations. **(c)** ζ of natural calcite samples against the equilibrium pCa. The datasets represent (1), (2), (3) SP measurements in 0.5 M NaCl and variable $CaCl_2$ concentration of Ketton, Estaillades, and Portland limestone samples, respectively – data from [137]; (4) SP measurements in 0.05 M NaCl and variable $CaCl_2$ concentration of Portland limestone – data from [156]; (5) EP measurements in 0.573 M and variable $CaCl_2$ concentration at pH=8.4 (fixed by HCl/NaOH titrations) – data from [178]. The lines represent the prediction of the models considering that the solution is in equilibrium with the calcite particles (1% wt., ssa=2 m^2/g) and atmospheric CO_2 gas phase. **(d)** ζ of synthetic calcite particles in 0.01 NaCl/$CaCl_2$ electrolyte solutions at fixed pH by HCl/NaOH titrations– data from [139]. The lines represent the prediction of the models assuming, initially, equilibrium between the solution (at the specific pH) with CO_2 followed by equilibration with the calcite particles (4% wt., ssa=22.3 m^2/g) and readjustment of the pH in a closed system. **(e)** ζ measurements (EP) of synthetic calcite particles $CaCl_2$/KCl electrolyte mixture of fixed ionic strength (I=0.03 M). The lines represent the prediction of the model considering equilibrium between the calcite particles (1% wt., ssa=2 m^2/g) with the electrolyte solution (no CO_2 gas phase) at the fixed pH [164]. **(f)** ζ measurements at different pHs of natural calcite particles at $5 \cdot 10^{-4}$ M $CaClO_4$ and a fixed ionic strength of $2 \cdot 10^{-3}$ M adjusted with $NaClO_4$ – data from [171]. The lines represent the prediction of the models assuming, initially, equilibrium between the electrolyte solution, calcite (1% wt., ssa=2 m^2/g), and atmospheric CO_2 followed afterward by acid/base titration in a closed system (no CO_2 gas-phase considered).

Figure 2.6-a includes experiments performed in single $CaCl_2$ electrolyte systems. The zeta potential in presence of calcium is significantly greater (more positive) than in NaCl electrolytes. Despite this, some natural samples in presence of high $CaCl_2$ concentration still show a negative zeta potential. To isolate the effect of calcium on the calcite zeta potential and discard any pH or ionic strength effects, Pierre et al.[139] performed experiments at constant ionic strength and fixed pH (Figure 2.6-b). Additional experiments in mixed NaCl/$CaCl_2$ systems up to salinities close to those for seawater are shown in Figure 2.6-c. Interestingly, measurements performed at variable pCa but fixed pH (Figure 2.6-d) imply that the zeta potential is governed not only by the added calcium concentration but also by the pH, given the large variation in the zeta potential between the two pHs. However, we would expect different ζ-pCa trends if the zeta potential was reported against the equilibrium pCa instead. At pHs around 8, for the same amount of Ca added to the solution, the equilibrium calcium concentration is still expected to be higher than above pHs of 10, which would explain the higher zeta potential values. Moreover, as discussed in the previous section, above pHs of 10, equilibrium with the CO_2 is unlikely to be sustained. On the other hand, experiments in a closed system at two different calcium concentrations show no change in the zeta potential with the pH (Figure 2.6-e). In this case, because the experiments were not performed in the presence of CO_2, the lower calcite dissolution leads to minor changes in the equilibrium calcium concentration with pH, resulting in steadier zeta potential. Figure 2.6-f shows zeta potential measurements at equilibrium conditions in a mixed $NaClO_4$/$CaClO_4$ electrolyte. The prediction of the CD-MUSIC and DLM considering equilibrium conditions with atmospheric CO_2 is in fair agreement with the experiments up to a pH of 10; hereafter, a non-equilibrium environment probably dominates.

2.5.3 Systems with added magnesium

The affinity of magnesium for the calcite surface has been usually assessed by carrying out experiments comparable to those performed with calcium. Figure 2.7 shows that magnesium has a similar effect as calcium on the zeta potential of calcite. As also observed for the systems with calcium, the measurements at increasing electrolyte concentration (Figure 2.7-a) show a larger scatter, most likely because of the different provenance of the samples and different equilibrium conditions. Figure 2.7-b shows measurements in binary electrolyte systems (NaCl+$MgCl_2$) at several ionic strengths, whereas those at fixed pH and constant ionic strength are shown in Figure 2.7-c. In the last panel (Figure 2.7-d), we show the prediction of the model for experiments performed in a $MgSO_4$/NaCl mixed system at several ionic strengths. As was the case for monovalent and calcium-containing systems, the BSM prediction shows the highest discrepancy with the experimental data, whereas the CD-MUSIC and DLM perform similarly.

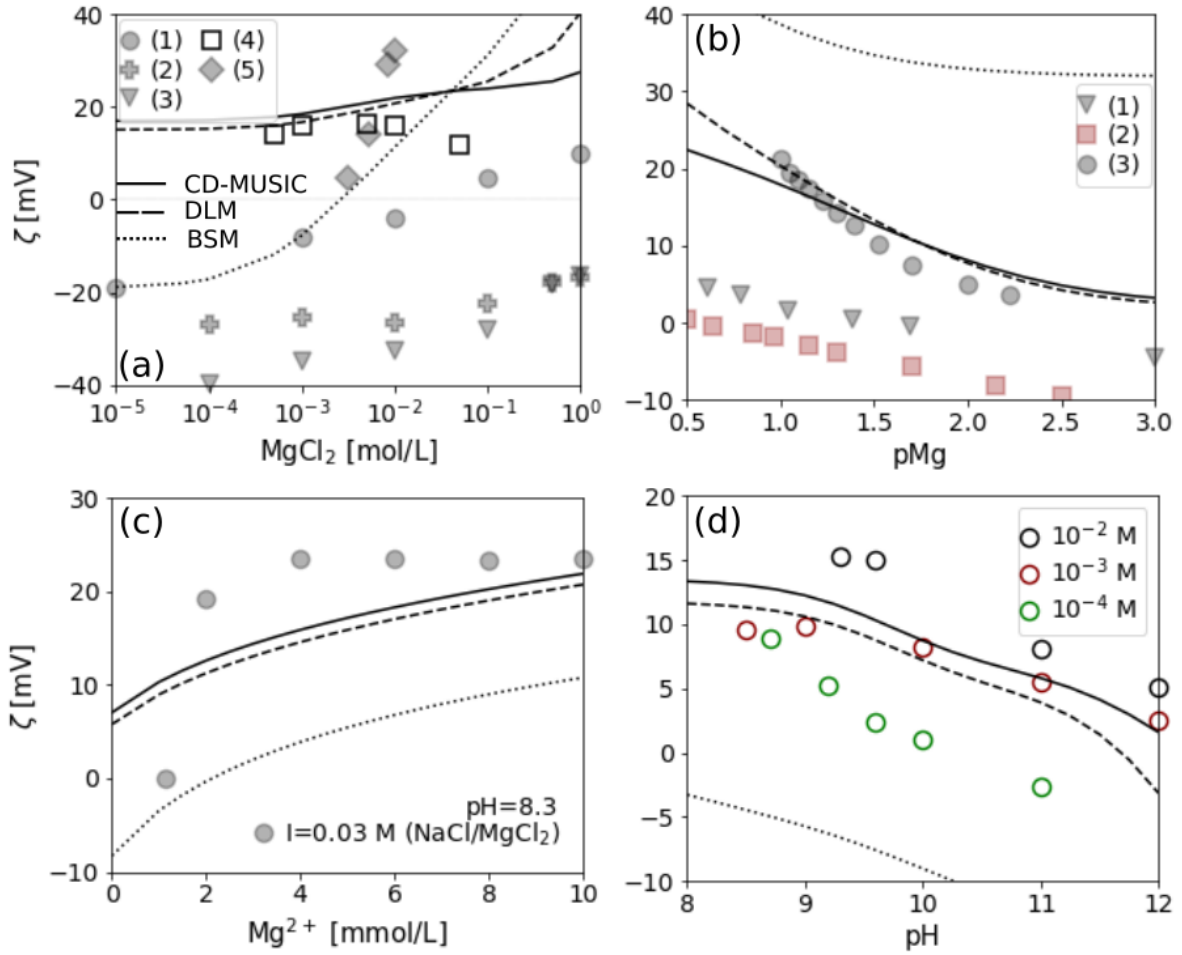

Figure 2.7. Zeta potential measurements of calcite in presence of electrolyte solutions containing Mg^{2+}. **(a)** ζ measurements of calcite particles at increasing $MgCl_2$ concentration. The datasets represent (1) EP measurements on synthetic calcite particles– data from [165]; (2), (3) EP measurements on carbonate rock particles containing 82% and 98% calcite, respectively – data from [169]; (4) EP measurements of synthetic calcite suspensions – data from [174]; (5) EP measurements on natural calcite suspensions – data from [163]. The lines represent the prediction of the models assuming equilibration of the calcite suspension (1% wt., ssa=2 m^2/g) with atmospheric CO_2. **(b)** ζ of carbonate rock samples in NaCl/$MgCl_2$ electrolyte mixtures. The datasets represent (1) SP measurements on an Estailades limestone sample in 0.5 M NaCl and increasing $MgCl_2$ concentration – data from [137]; (2) SP measurements on a Portland limestone sample in 0.05 M NaCl and increasing $MgCl_2$ concentration – data from [156]; (3) EP measurements on suspensions consisting of chalk powder in 0.573 M NaCl and varying $MgCl_2$ concentration and a pH fixed to 8.4 by HCl/NaOH additions – data from [60]. The lines represent the prediction of the models assuming equilibrium between the calcite suspension (1% wt., ssa=2 m^2/g) and atmospheric CO_2. **(c)** ζ of natural calcite particles (4% wt., ssa=7.1 m^2/g) at increasing $MgCl_2$ concentration, ionic strength fixed to 0.03 M with NaCl, and pH adjusted to 8.3 by HCl/NaOH titrations – data from [139]. The lines represent the prediction of the models assuming that, initially, the electrolyte solution is in equilibrium with the calcite particles and atmospheric CO_2 followed by the pH adjustment in a closed system (no CO_2). **(d)** ζ of artificial calcite particles in mixed electrolyte systems containing Na^+, Cl^-, Mg^{2+}, and SO_4^{2-} of different pHs (adjusted with NaOH/HCl titrations) and ionic strengths – data from [162]. The lines represent the prediction of the model assuming that the calcite suspension (1% wt., ssa=2 m^2/g) was initially equilibrated with CO_2, followed by acid/base titration in a closed system (no CO_2).

2.5.4 Systems with added sulfate

Less experimental data is available for systems containing sulfate (Figure 2.8) compared to those containing monovalent salts or calcium and magnesium. The experiments, both those performed in single salt (Na_2SO_4) systems (Figure 2.8-a) and binary electrolyte systems (Figure 2.8-b and -c), show a decrease in the zeta potential at increasing sulfate concentrations. Nonetheless, the sulfate affinity for the calcite surface seems to decrease at higher pH (Figure 2.8-d). The effect of sulfate on the zeta potential of calcite was also thoroughly discussed by Mahrouqi et al. They suggested that the presence of sulfate only alters the equilibrium conditions, thus the Ca concentration, but does not undergo a

strong interaction with the calcite surface[137]. Their hypothesis could justify the great uncertainty of the optimized equilibrium constant for sulfate. However, a different structure for the sulfate complex, e.g., bidentate instead of monodentate, may also result in a more robust equilibrium constant and closer agreement with the experimental data. Although the DLM and CD-MUSIC models generally capture the trends of the zeta potential in electrolyte systems containing sulfate, a great discrepancy can be identified for the BSM. Since at increasing Na_2SO_4 electrolyte concentration the molality of Na^+ is always twice as high as SO_4^{2-} molality, the effect of the latter on reducing the zeta potential is screened by the opposite positive effect of the former. Moreover, a degree of disagreement between the modeled and experimental system was identified for the measurements in Figure 2.8-b; an equilibrium calcium concentration of 11.41 mM is reported at equilibrium conditions[187] whereas our theoretical calculations suggest a much higher Ca concentration (18 mM), which could explain the greater zeta potential predicted by the models.

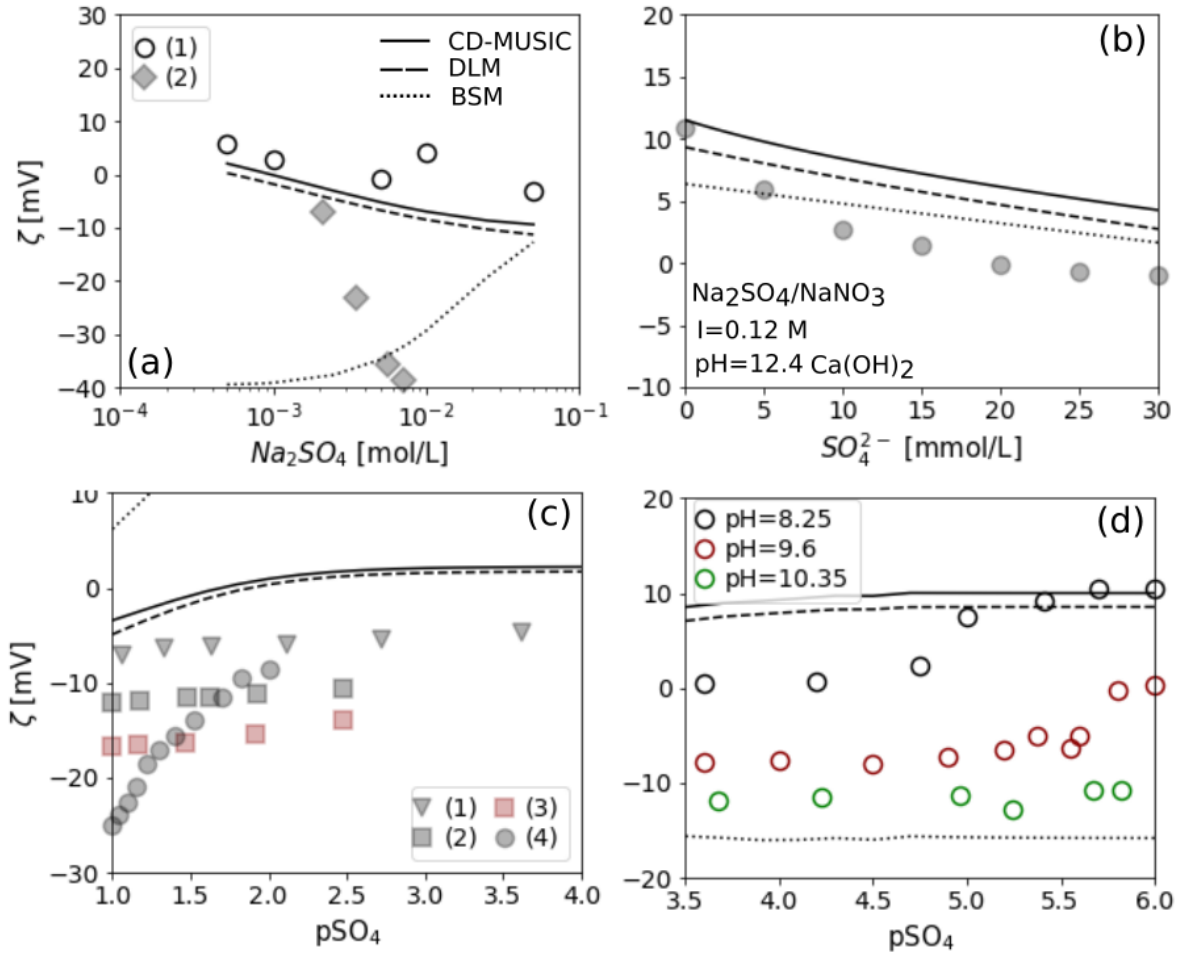

Figure 2.8. Zeta potential measurements of calcite in presence of electrolyte solutions containing SO_4^{2-}. **(a)** ζ of calcite at increasing Na_2SO_4 concentration. The datasets represent (1) EP measurements on synthetic calcite suspensions – data from [174]; (2) EP measurements on carbonate rock suspensions – data from [163]. The lines represent the prediction of the models assuming that the calcite particles (1% wt., ssa=2 m^2/g) are in equilibrium with the solution (no CO_2 gas phase). **(b)** ζ of calcite particles at increasing sulfate concentration, pH=12.40 adjusted with $Ca(OH)_2$, measured equilibrium calcium concentration Ca_{eq}≈11 mM±1.5 mM and ionic strength of 0.12 M fixed with $NaNO_3$ – data from [187]. The lines represent the prediction of the models assuming initial equilibration of the calcite particles (11% wt., ssa=0.77 m^2/g) with atmospheric CO_2 followed by titration in a closed system (calculated Ca_{eq} 18.09 mM). **(c)** ζ of carbonate rock samples in NaCl/Na_2SO_4 electrolyte mixtures. (1), (2) SP measurements on Estailades and Portland limestone samples, respectively, in 0.5 M NaCl and increasing Na_2SO_4 concentration – data from [137]; (3) SP measurements on a Portland limestone sample in 0.05 M NaCl and increasing $MgCl_2$ concentration – data from [156]; (4) EP measurements on suspensions consisting of chalk powder in 0.573 M NaCl and varying Na_2SO_4 concentration and a pH fixed to 8.4 by HCl/NaOH additions – data from [60]. The lines represent the prediction of the models assuming equilibrium between the calcite particles (1% wt., ssa=2 m^2/g), electrolyte solution, and atmospheric CO_2. **(d)** ζ of synthetic calcite particles at fixed pH (adjusted with HCl/NaOH titrations), 0.01 M NaCl background electrolyte

concentration, and variable sulfate concentration – data from [139]. The lines represent the prediction of the model assuming an initial equilibration step of the calcite particles (4% wt., ssa=22.3 m^2/g) with the electrolyte solution followed by titration and equilibration in the absence of CO_2.

2.5.5 Systems with added bi(carbonate)

Figure 2.9 gathers measurements obtained in presence of added bi(carbonate). Figure 2.9-a shows that an increase in the HCO_3^-/CO_3^{2-} concentration leads to a decrease in the zeta potential whereas Figure 2.9-b includes experimental data obtained in a closed system at different pHs. The prediction of the DLM and CD-MUSIC is in good agreement with these datasets obtained on synthetic calcite but shows a great mismatch with the experimental data obtained on natural calcite (Figure 2.9-c). The iron and magnesium content of this natural sample[171] could be a plausible reason for the displayed discrepancy as these impurities could bind divalent ions and affect the equilibrium pH. It was previously shown that the presence of only 0.05% Fe oxide coating was necessary to considerably increase the retention of divalent metals on calcite[189]. The BSM cannot capture the trends of the zeta potential in presence of carbonate ions as, similarly as for the sulfate-containing systems, the effect of carbonate ions is completely screened by the sodium concentration. This was somewhat expected, given the low binding constants for bi(carbonate) that were defined in the original work[68,87,93] and that we used as an initial guess in the optimization.

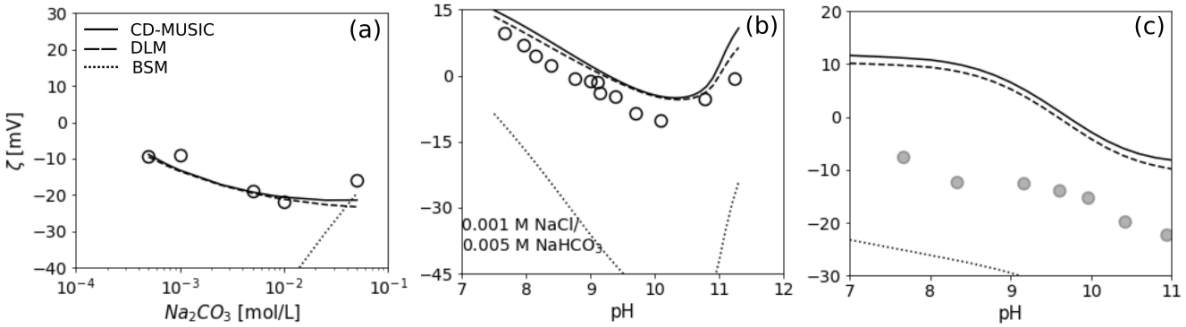

Figure 2.9. Zeta potential measurements of calcite in presence of electrolyte solutions containing CO_3^{2-}/HCO_3^-. **(a)** ζ of synthetic calcite particles at increasing Na_2CO_3 concentration. The lines represent the prediction of the models assuming equilibrium between the calcite particles with the electrolyte solution (no CO_2 gas phase). **(b)** Zeta potential measurements of synthetic calcite particles in a 0.001 M NaCl/0.005 M $NaHCO_3$ electrolyte mixture (no CO_2 gas phase) at fixed pH adjusted with $H_2CO_3/Ca(OH)_2$. The lines represent the prediction of the models assuming that calcite particles (1% wt., ssa=2 m^2/g) are in equilibrium with only the electrolyte solution (no CO_2). **(c)** Zeta potential of natural calcite particles in a $1.5 \cdot 10^{-3}$ M $NaClO_4/5 \cdot 10^{-4}$ M Na_2CO_3 electrolyte mixture – data from [171]. The lines represent the prediction of the model assuming that the calcite particles (1% wt., ssa= 2 m^2/g) were initially equilibrated with atmospheric CO_2 followed by the acid/base titration in a closed system (no CO_2).

2.6 Discussion

2.6.1 SCM vs zeta potential data

The scattered reported zeta potentials challenge any assessment related to the prediction capabilities of the SCMs. The DLM and CD-MUSIC models showed very similar behavior and predicted relatively well the ζ of synthetic samples. On the contrary, the BSM considers a strong interaction between the calcite and the background electrolyte concentration, displaying major discrepancies for measurements performed at an ionic strength considerably different than that of the optimization dataset. Sometimes, a successful fit to a certain dataset may just be a consequence of overfitting and does not ensure that the model can be extrapolated to other systems. To better observe the differences/similarities between the models, we show their surface speciation prediction (Figure 2.10) for a suspension consisting of calcite particles equilibrated in a closed system with 0.001 M NaCl solution that was initially in contact with atmospheric CO_2 (similar to the equilibration procedure considered for the modeled trends in Figure 2.5-b). The BSM (Figure 2.10-a), optimized to the same experimental data as the other two models, yields a completely different surface speciation. Because one of the assumptions of this model is that

the calcite surface is negatively charged, negative surface species (e.g., $\equiv CaOH^{-0.5}$and $\equiv CO_3^{-0.5}$) dominate in the modeled pH interval (6-12). This negative surface charge is neutralized by positive calcium and sodium surface species. Although the $\equiv CO_3Ca^{+1.5}$ species decrease as the equilibrium calcium in solution drops at higher pHs, the $\equiv CO_3Na^{+0.5}$ species increase throughout the entire pH range; this is because the Na^+ concentration in solution rises as a result of the NaOH additions to reach alkaline conditions. The interaction of the carbonate sites with sodium ions explains the predicted, sometimes irregular, zeta potential. Although Heberling and coworkers[68,87,93] fitted the BSM against electrokinetic data–both equilibrium (EPM) and non-equilibrium (SP) measurements–as part of its development, they prioritized its consistency with surface diffraction data. Nonetheless, this strong interaction between Na^+ and calcite has not been previously reported, which explains why in most publications Na^+ is treated as an indifferent ion towards the calcite surface. On the other hand, according to the CD-MUSIC (Figure 2.10-b) and DLM (Figure 2.10-c), most surface species consist of protonated calcium surface sites that are balanced by negatively deprotonated carbonate sites (overlapping golden and black lines). Since these oppositely charged surface sites counterbalance, the zeta potential is governed by the surface species resulting from the interaction of calcite with HCO_3^-/CO_3^{2-} and Ca^{2+}. The similar surface speciation is consistent with their almost identical zeta potential prediction. Thus, although these models assume a different description of the EDL, the reactions proceed comparably in both models (analogous to solution complexation). Considering also the rather similar initial binding constants used in the optimization, the models show a similar outcome even at variable chemical conditions.

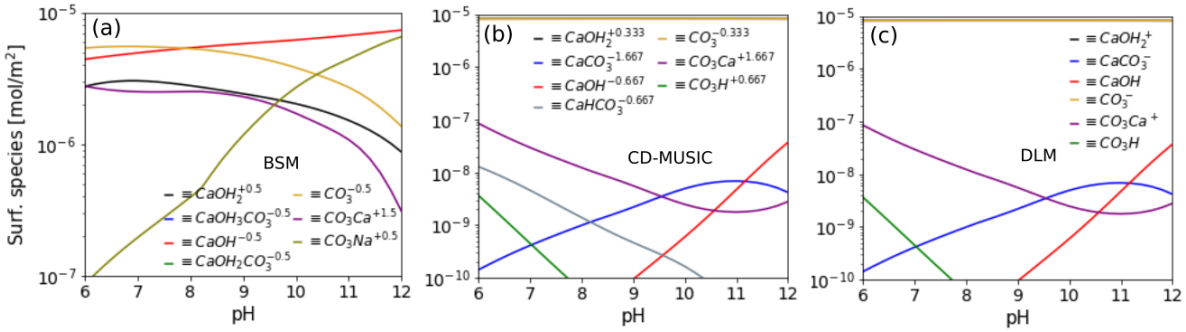

Figure 2.10. Surface speciation for the (a) BSM (b) CD-MUSIC and (c) DLM. The surface speciation corresponds to a calcite suspension with 4% solids content and ssa of 7.1 m^2/g. To model the chemical system we initially assumed a 0.001 M NaCl electrolyte solution in equilibrium with atmospheric CO_2; hereafter we considered that the electrolyte solution was mixed with the calcite particles in a closed system (no CO_2) and NaOH/HCl was added to reach the desired pH.

In general, the parameters obtained for the CD-MUSIC and DLM are applicable at variable chemical conditions. However, the susceptibility to compositional changes in the solution due to exchange with CO_2 questions the similarity between the modeled and actual (experimental) systems. In open systems, the solution composition is governed by the calcite-water-gas phase equilibrium[190]. The dissolution of CO_2 and formation of carbonic acid will lead to calcite dissolution affecting the Ca^{2+} equilibrium concentration, which eventually controls the calcite charging behavior. If the CO_2 partial pressure is not measured or properly controlled, it is hard to estimate the pCO_2 in the bulk fluid, which controls the surface pH[190]. In cases in which the pH is fixed, it should be clearly stated whether the changes in the proton concentration come from changing the CO_2 partial pressure or from acid/base titrations; these yield different H^+, Ca^{2+}, HCO_3^-, CO_3^{2-}, and CO_2(aq), thus, different surface charge characteristics[66]. Another important factor is the proper identification of all the chemicals added to the system. The type and concentration of the background electrolyte impact the dissolution rates[191], thus equilibration times, and the nature of the acid/base used in the titration also affects the charging behavior[138]. Knowing the equilibration times can also be conclusive when comparing two different experimental datasets. Equilibration times of two minutes[6,60] compared to one hour[139] or even weeks[37] can partially explain or shed light on the differences between different experimental datasets. Thus, to assess the performance

of a surface complexation model to describe the electrokinetic behavior of calcite requires a proper characterization of the chemical system at the time of the measurements. For instance, the (dis)agreement between the real and modeled system can be assessed for the data from Pierre et al.[139] as they reported the equilibrium calcium concentration at different pHs. Figure 2.11-a shows the measured calcium equilibrium concentration for synthetic and natural calcite samples in NaCl electrolytes at different pHs in a 4% wt. calcite suspension. The lines correspond to the theoretical equilibrium calcium concentrations calculated with Phreeqc using "phreeqc.dat" database considering three different equilibration scenarios. The first scenario, which considers equilibrium of the suspension with atmospheric CO_2 at different pHs, overpredicts the calcium concentration in solution at pHs below 8 for the synthetic calcite system. Equilibration scenario 2, i.e, calcite suspension initially equilibrated with CO_2 followed by NaOH/HCl titration in a closed system (no CO_2), shows the best match of the calcium concentration in solution for the synthetic calcite system. Considering the same scenario as (2) but with 0.5% $MgCO_3$ results in a reduced Ca concentration in solution.

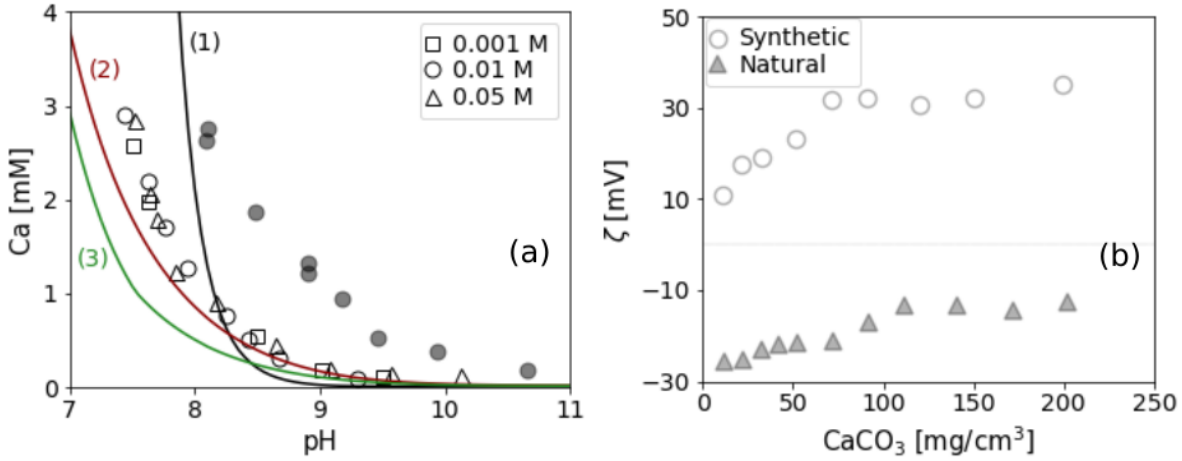

Figure 2.11. Factors introducing variability in zeta potential measurements. **(a)** Calcium equilibrium concentration for synthetic (empty markers) and natural calcite (filled markers); data from[139]. The lines correspond to the total predicted calcium concentration depending on the equilibration procedure: (1) calcite particles in equilibrium with the electrolyte solutions between pH 7-10 (adjusted with HCl/NaOH) and atmospheric CO_2. (2) calcite suspension equilibrated with atmospheric CO_2 (open system) followed by the equilibration at the desired pH in a closed system (3) same as (2) but considering 0.5% $MgCO_3$ (impurity reported for the natural sample). **(b)** Zeta potential variation with the solids concentration for synthetic and natural (98.5% calcite) samples -data from[173].

Theoretical calculations cannot explain the much higher equilibrium calcium concentration for the natural calcite system. We suspect several reasons that could cause this behavior. First, the increased calcium concentration could be an experimental flaw during the ion composition analysis. To collect samples for calcium analysis, the supernatant was obtained by suspension centrifugation, followed by acidification and dilution. If the supernatant was not properly filtrated and still contained some calcite particles, these may represent an additional source of calcium, which could explain the measured high Ca concentration. Nonetheless, this experimental artifact could have also potentially occurred with the synthetic sample, which would then still not explain the difference between the calcium concentration in the natural and synthetic systems. Another plausible option could be that impurities in the natural sample affect the calcium equilibrium concentration. The natural sample is reported to have 0.5% impurities out of which 0.4% corresponds to $MgCO_3$. Impurities may affect not only the calcite dissolution kinetics[192], hence equilibration times, but also its solubility. For instance, Mg-containing calcites are known to be more soluble[193] and in the SP measurements performed by Mahrouqi et al.[184], limestones leading to a higher equilibrium Mg concentration showed also the highest calcium concentration. Thus, the magnesium content could partially explain the higher solubility of the natural calcite samples. An additional point to consider is that Pierre et al.[139] observed that during the equilibration procedure of the calcite with the electrolyte, the calcium concentration undergoes a sudden

increase leading to supersaturation conditions; this stage is then followed by a surface recrystallization process where equilibrium conditions are restored. Nonetheless, as the Mg content increases, a greater supersaturation was observed to be needed to trigger calcite nucleation or (Mg-calcite nucleation)[194], which could affect the surface recrystallization process. Besides inorganic impurities, natural samples may also present strongly adhered organic layers that could considerably affect the calcite surface reactivity[90,195,196].

The effect of different experimental conditions on the zeta potential of calcite has been previously discussed by Siffert and Simbel[173]. They showed that the zeta potential depends on the equilibration procedure, sample preparation, and solids concentration (Figure 2.11-b). In the EP measurements, the solids concentration is among the most underreported parameter and its effect was emphasized also recently[162]. Most publications report the particle content (e.g., solids concentration) of the initial suspension and not of the supernatant that is taken for the electrophoretic analysis. Disequilibrium may be induced during the supernatant sampling or suspension dilution, which can eventually lead to samples undersaturated with respect to calcite. The effect of the sample preparation, e.g., particle washing, on the electrokinetic measurements was also thoroughly discussed in several other papers (e.g.,refs [67,138,164]). The equilibration of the calcite suspension with the gas phase represents another undervalued factor in the experimental protocols. Unless working in an inert system, considering the difficulty to completely avoid the CO_2 from different equilibration stages or sample preparation, the best way to ensure stable and reproducible conditions could be establishing a proper equilibration with the CO_2 by gas bubbling; nonetheless, this may be challenging to perform in the closed SP setup. Direct comparison between EP and SP measurements of natural samples may also be troublesome, as in the former the grinding of the sample leaves freshly created surface sites exposed to the solution. Additionally, since EP measurements are strongly affected by the solids content of the suspension, a particle concentration range leading to constant chemical conditions and zeta potential should be first identified [197].

The presence of impurities and their effect on the calcite reactivity and solution composition also confronts the prediction of the zeta potential of natural samples. Accommodating the effect of impurities in the surface complexation modeling of calcite is a fairly unexplored area. A common practice is to obtain a set of parameters that can match experiments performed on specific samples so to avoid explicitly accounting for the impurities. Nonetheless, this approach results in site/sample-specific models with limited applicability to other systems. Wolthers et al.[67] described measurements on both natural and synthetic calcite samples by defining unequal carbonate and calcium surface site density or considering non-stoichiometric calcite dissolution. As far as we are aware, there is only one work[72] that has attempted to tailor a model developed for pure (synthetic) calcite to natural systems. The proposed approach consisted of using the surface coverage with impurities as an adjustable parameter. Based on this surface fraction, a new type of surface site is defined; these sites undergo a reaction with “generic impurities” and result in a negative surface species to account for the more negative zeta potential of calcite measured in presence of silica or organic layers. Thus, the total number of surface sites stays constant as the third type simply decreases the calcite sorption sites. Yet, this approach does not lead to a universal formulation as it considers that all impurities have the same effect, e.g., that of decreasing the zeta potential and it would still be necessary to fit the model (e.g., the surface coverage adjustable parameter) to comply with specific conditions.

Although it may require a thorough characterization of the system, a more general approach for natural samples could be to consider additive ion binding[198]. However, in many cases, the additive approach is not sufficient to describe a binary or mixed system as the dissolution of secondary phases or impurities may lead to aggregation, surface precipitation, or coprecipitation, having an effect not only on the solution composition but also on the sorption properties of calcite[199–201]. Compared to calcite, the modeling of binary oxide systems has received wider attention, and a “patchwise approach” is usually

adopted; this consists of treating the overall surface as a combination of two different homogeneous surfaces. Different patchwise models/alternatives (e.g.,[202–204]) have been proposed for modeling ion binding at heterogeneous hydr(oxide) surfaces depending on the degree of interaction between the patches. Koopal et al.[204] considered three types of chemical heterogeneity, i.e., random, isolated, or interacting patches. The different alternatives proposed to model the charging and adsorption behavior in mixed/binary systems depend on the ionic strength, which governs the diffuse layer thickness, and the size of the patches. Still, the main difficulty is probably obtaining the real effect that impurities have on the zeta potential. The traditional equations to convert mobility to zeta potential, e.g., Smoluchowski, assume that the particles are uniformly charged[205] whereas the presence of impurities may lead to a non-uniform surface charge distribution. Thus, the obtained average zeta potential does not provide information on the local surface charge that eventually governs the colloidal behavior. Rotational electrophoresis[206] or AFM[207] are some of the alternatives that could be used to characterize the charge heterogeneity of surfaces. Additionally, apart from impurities, another factor that can contribute to the great zeta potential variability of natural calcite samples is the surface topography. The position of the slip plane, greatly affected by the surface roughness, determines the zeta potential value. While the assumption that the zeta potential coincides with the potential at the OHP may hold for smooth surfaces, it may not be valid for rough particles[126].

2.6.2 Is electrokinetic data consistent with other measurements?

2.6.2.1 Proton charge measurements

Obtaining binding constants from zeta potential measurements entails several important assumptions about the location of the slip plane or, depending on the model, capacitances values. To better constrain the value of the equilibrium constants and description of the EDL, several publications recommended the combined use of surface charge titrations and electrokinetic measurements (e.g., refs [208–211]). Although compared to other minerals, charge titrations reported for calcite are scarce, we checked whether the models, initially tuned to electrokinetic data, agree with the few published measurements (Figure 2.12).

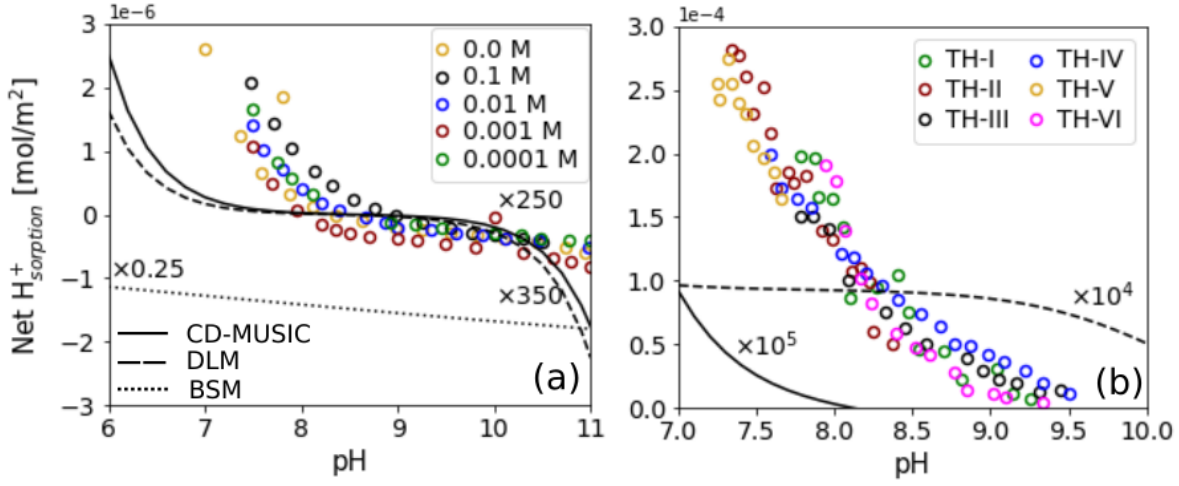

Figure 2.12. Net proton charge density for calcite: (a) measurements obtained in different NaCl electrolyte concentrations and HCl/NaOH titration –data from [57]. The prediction of the models (lines) assumes equilibrium of the solution with atmospheric CO_2 and non-equilibrium with respect to calcite. (b))Acidimetric titrations (TH) at several solid/liquid ratios in KCl solutions – data from [38]. The prediction of the models (CD-MUSIC and DLM) assumes equilibrium of the calcite with the electrolyte solution in the absence of a gas phase. BSM is not shown as it predicts a negative surface charge in the entire studied range. In both panels, the CD-MUSIC and DLM predictions were significantly lower than the measurements and for enhanced visualization purposes their prediction is magnified.

Although the two found datasets coincide that, near-neutral pH conditions, calcite is positively charged, Villegas et al.[38] (data shown in panel b) record surface charge densities two orders of magnitude higher than those measured by Eriksson et al.[57] (data shown in panel a). The inconsistency between these two experimental datasets can be only partially explained by differences in the experimental protocol; Villegas et al.[38] carried the equilibration procedure in a closed system in the absence of CO_2 whereas Eriksson et al.[57] did not control the CO_2 atmosphere nor the equilibrium conditions. For both datasets, the predicted net proton charge density with the CD-MUSIC and DLM models is significantly inferior to the experimental measurements and for visualization purposes, the predicted surface charge was magnified; a lower deprotonation constant would be required to obtain a better match with this experimental data. The negative surface charge predicted by the BSM throughout the entire studied pH range was expected as in the development of the model, Heberling et al.[68] assumed that, between pHs 6-11, calcite is negatively charged and the carbonate sites are deprotonated[68].

Moreover, the experimental data from Villegas et al.[38] exceeds the maximum theoretical adsorption corresponding to the number of calcite surface sites (8.2 μmol/m^2). The maximum adsorption reported would require a surface site density of approximately 150 #/nm^2, which is 30 times higher than the value of 4.95 #/nm^2 theoretically reported[67,68] and used in the three models. The increased proton sorption was explained through a H^+/Ca^{2+} ion-exchange mechanism, which results in a "dynamic rearrangement" of the most superficial calcite layers.

2.6.2.2 Single-phase flow experiments

When coupled to the fluid flow equations, SCMs can describe reactive transport processes. In many cases, models calibrated with zeta potential data are used to describe dynamic retention experiments. We assess the consistency between measured and predicted ion concentrations in the effluent during single-phase flooding tests. We also evaluate whether models calibrated to the same zeta potential may result in significantly different ion transport behavior. The species transport in porous media can be described according to eq. (2.11):

$$\frac{\partial}{\partial t}(\varphi c_i + (1-\varphi)\rho_s a_s q_i) + \nabla \cdot (\boldsymbol{u_w} c_i) + \nabla \cdot (-\varphi D_i \nabla c_i) = R_i \tag{2.11}$$

where t [s] is the time, φ [-] is the porosity, c_i [mol/m^3] is the concentration of species i, ρ_s [kg/m^3] is the mineral density, a_s [m^2/kg] is the specific surface area of the rock, q_i [mol/m^2] is the number of moles of species i adsorbed per unit surface area of rock, u_w [m/s] is the velocity of the water phase, D_i [m^2/s] is the diffusion coefficient of species i in the water phase and R_i is a source/sink term. Considering that in these experiments the Péclet number ($Pe = \frac{Lu_w}{D} \gg 1$, where L is a characteristic length scale) is high, i.e., the transport by advection dominates, the contribution of diffusion in eq. (2.11) is assumed negligible.

To solve this equation in one dimension we coupled the geochemical reaction module PhreeqcRM[212] that solves the chemical equilibrium and updates the concentrations at each time-step, with FiPy[213], a finite volume partial differential equations solver developed for Python. For all cases, we set a uniform mesh of 50 cells along the 1D domain, which was considered equal to the length of the cores.

Figure 2.13 shows the performance of the three models at predicting the calcium and magnesium concentration history from single-phase flooding tests performed on carbonate cores at room temperature. The three models predict similar effluent concentration profiles and show a poorer agreement with the experimental data obtained on chalk samples (panel a) compared to limestone (panel b). This was quite surprising, as the chalk considered for these experiments consisted of 99% calcite while a higher degree of chemical heterogeneity would be expected for the Middle Eastern limestone (although the authors do not report mineralogical composition). Nonetheless, as discussed in the previous section, it is not always the content but the identity of the impurities that has a greater effect

on the ion binding. For instance, it has been previously hypothesized that chalk, although relatively clean may contain nanoclays with a large specific area and that a relatively small amount is necessary to boost its adsorption properties[214,215]. Moreover, the binding constants optimized to synthetic calcite may not be the most appropriate to describe the dynamic retention on natural samples, where transport may be governed by local surface charges and not by an average surface potential[216]. To better understand whether the binding constants tuned to zeta potential data provide a good agreement with the dynamic retention tests, experiments on core samples containing synthetic calcite powder/aggregates should be considered. Unfortunately, we have not come across such experiments.

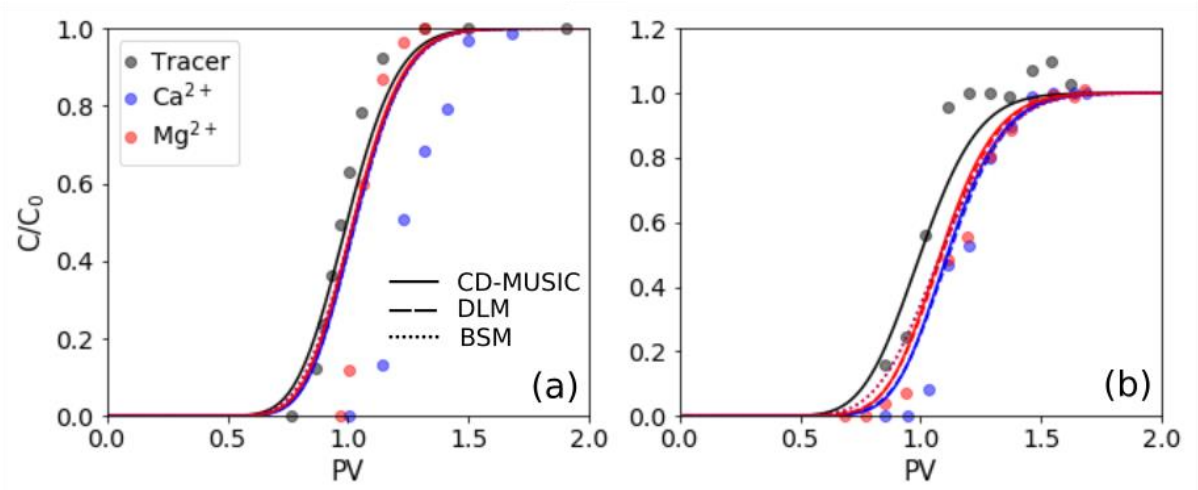

Figure 2.13. Performance of the models at predicting the effluent concentration (Ca, Mg, and tracer) after the injection of several pore volumes (PV) during single-phase flooding experiments performed at room temperature. **(a)** Experiments performed on chalk cores (length=7 cm) at room temperature and 0.2 ml/min injection rate; experimental data from [60]. **(b)** Experiments performed on Middle Eastern chalk cores (length=4.91 cm) at room temperature and 0.1 ml/min injection rate. Note that the measured tracer concentration, beyond the initial injection (tracer) concentration, increases the uncertainty of this dataset. Experimental data from [217]. For both datasets, the cores were initially saturated with NaCl solution (≈0.5 M) while the injection brine contained 0.013 M magnesium, calcium, and thiocyanate (tracer). Both panels include seven curves, e.g., one corresponding to the tracer concentration plus the Ca and Mg prediction for each model.

2.6.3 Effect of temperature on electrokinetic phenomena and surface reactions

The versatility of SCMs to account for changes in the aqueous chemistry makes them an essential tool for reactive transport modeling. However, many reactive transport models are relevant to subsurface applications involving temperatures typically higher than those at ambient conditions. SCMs may describe the adsorption behavior at higher temperatures provided that the effect of temperature on the equilibrium constants of the surface interactions is known. Commonly, these equilibrium constants are assumed to follow a temperature dependence according to van't Hoff equation (eq. 2.12).

$$\frac{\partial \ln K_i}{\partial T} = \frac{\Delta H_{r,i}}{RT^2} \tag{2.12}$$

where $\ln K_i$ represents the natural logarithm of the equilibrium constant, K_i of reaction i and $\Delta H_{r,i}$ [J/mol] is the reaction enthalpy. Assuming a constant ΔH_r, the definite integral of eq. (2.12), allows calculating the equilibrium constant (of a specific surface reaction) at any temperature based on the equilibrium constant at room temperature and the enthalpy of the reaction.

Several publications (e.g., refs [218–220]) have previously acknowledged the limited research on the temperature effect on the surface protonation/adsorption and obtained thermodynamic parameters for the surface reactions of metal oxides. However, to obtain such information for calcite, measurements in different electrolyte systems are first needed. Al Mahrouqi et al.[184], estimated the zeta potential at high temperatures (up to 120°C) by streaming potential measurements in NaCl solutions; the effect of temperature on the inferred zeta potential seemed to fade as the electrolyte concentration increased from 0.01 M to 0.5 M. Figure 2.14 summarizes zeta potential measurements performed at higher temperatures

at different pHs (panel a), for several limestone samples (panel b), in single electrolyte systems (panel c) and at variable ionic strength (panel d).

In a recent paper, Bonto et al.[221] reported enthalpies for some of the surface interactions of calcite in aqueous solutions (e.g., de/protonation, reactions with Ca^{2+}/CO_3^{2-}). The reaction enthalpies were inferred by fitting the CD-MUSIC model proposed by Wolthers et al.[67] to the streaming potential measurements carried out by Mahrouqi et al.[184] and assuming that the equilibrium constants followed the temperature-dependence given by van't Hoff equation. Despite the consistency of these inferred enthalpies with microcalorimetry data, additional experimental data is required to obtain more robust and model-independent values. Molecular dynamics computations may represent an important tool for resolving the energy patterns of the surface reactions[66]. Besides the thermodynamics of the surface reactions, the effect of temperature on the capacitance of the calcite-water interface is also a topic that deserves further consideration.

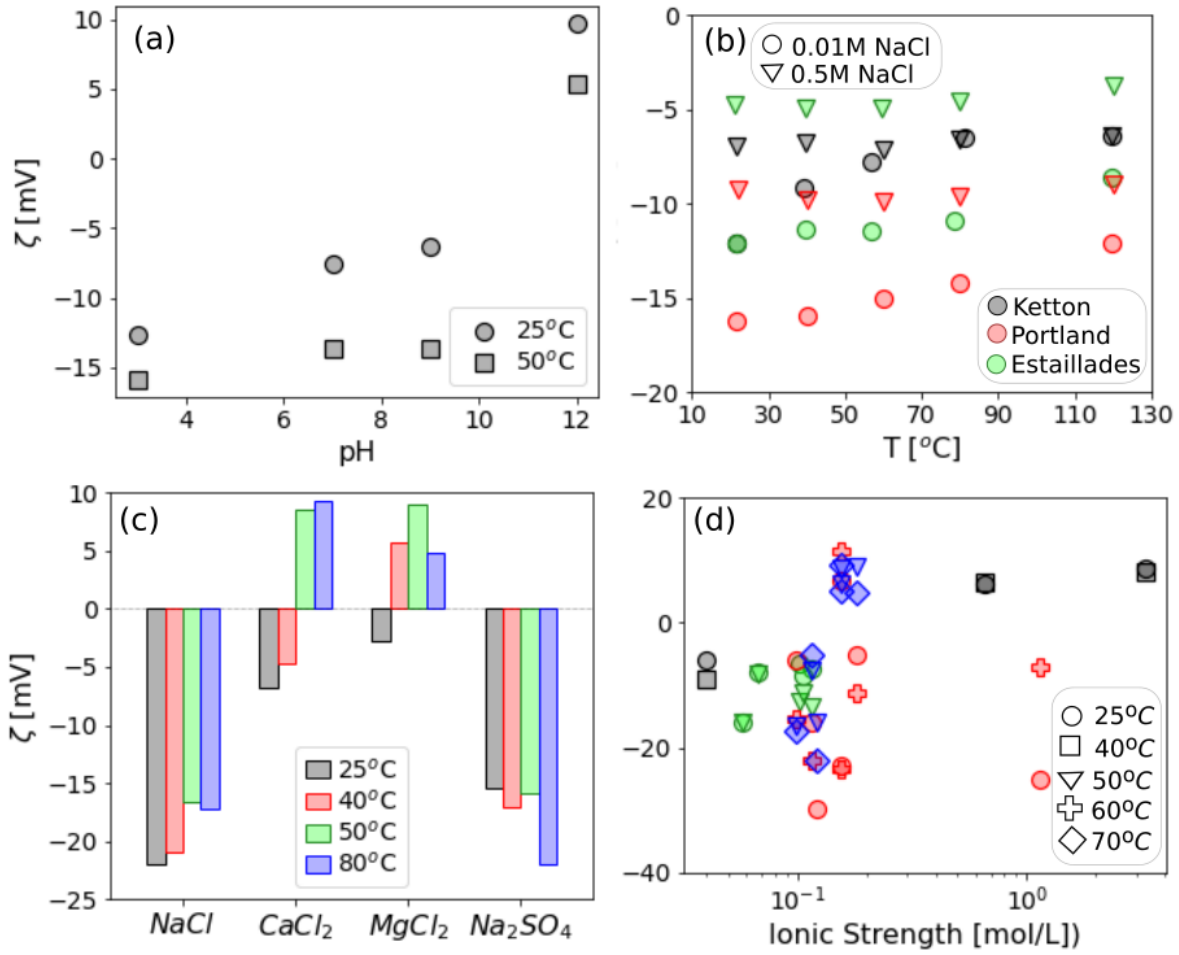

Figure 2.14. Zeta potential measurements performed at different temperatures and **(a)** at different pHs [180] **(b)** on different carbonate samples [184] **(c)** in single electrolyte systems; the data at 25 and 40°C is from [98] and that at 50 and 80°C is from [182] **(d)** at different ionic strengths; the color of the markers represents the source of the data, i.e., black – [98]. , green – [180] , red – [181] , blue – [182]. Figure adapted from [221].

2.7 Uncertainties and final remarks

The main requisite for the assessment of the performance of different SCMs is high-quality and consistent experimental data. The collected zeta potential measurements on calcite show an important degree of variability. The large scattering in the reported ζ comes from different levels of disequilibrium/equilibration procedures or the presence of impurities in natural samples. A clear

description of the experimental procedure is needed to ensure the repeatability/reproducibility of the experiments and the consistency between the real (experimental) and modeled systems. The vague description of the equilibration steps and sample/suspension characteristics (e.g., exchange with CO_2, specific surface area, solids concentration) leads to a heavily undetermined system where too many parameters are left to the modeler's assumptions. The only way to ensure that the modeled system is representative of the experimental one is by reporting at least pH and the solution composition at equilibrium. The most under-reported experimental details are conditions of equilibration of the calcite suspension with a gas phase and solids content (EP).

Although fitted to the same experimental dataset, the main assumptions in the development of the models played a massive role in their performance at different chemical conditions. The assumption that the calcite negative surface charge is neutralized by both monovalent and divalent ions has a great effect on the predictions of the BSM. This assumption leads to the definition of a strong interaction between calcite and sodium ions, impacting significantly, and often negatively, the predicted zeta potentials. Despite their different description of the EDL, the DLM and CD-MUSIC models resulted in similar predictions for all the datasets considered; this akin behavior is most likely because they rely on comparable assumptions (e.g., the reactions occur analogously to those in solution). Thus, among the three models, the DLM represents the most efficient approach to predict the experimental observations; with less adjustable parameters and no fractional charges, this model can describe the experimental data just as well as the CD-MUSIC model. This, of course, does not mean that the DLM offers the best description of the calcite-water interface. First, electrokinetic data alone may not be the best option to obtain the binding constants or electrical double layer properties as it requires assumptions regarding the location of the slip plane distances and capacitances values; this was also proven by the fact that the (de)protonation constants cannot explain the few published net proton charge data. Second, if spectroscopic methods brought more insights into the structure of the surface complexes then probably the CD-MUSIC model could be better constrained, reducing the degrees of freedom on the net charge distributed in the different planes.

Despite capturing the main zeta potential trends at increasing pH and ion concentration, further work is required to see how the models, developed for pure synthetic calcite, can be applied to natural samples. The current approach consisting of fitting the models to specific carbonate samples justifies the many different binding constants that proliferate in the literature. Patchwise models, as those proposed in the literature on metal oxides, could maybe lead to a more general approach to model chemically heterogeneous carbonate samples. Moreover, the surface charge heterogeneity of natural samples may justify the poor performance of the models tuned to zeta potential to describe the dynamic retention in single-phase flowthrough tests. Establishing a general framework for the electrokinetic behavior of natural samples and addressing the temperature effect on the surface reactions will be pivotal in the development of advanced reactive transport models for calcite-rich aqueous environments.

3 Thermodynamic analysis of the temperature effect on calcite surface reactions in aqueous environments

Reactive transport models for subsurface applications, particularly those for modified salinity waterflooding (MSW) in carbonates, have to be equipped with thermodynamic models that can reliably predict/describe adsorption phenomena at variable temperature conditions. To advance the understanding of the calcite reactivity at high temperatures, combining experimental and modelling studies is required. Therefore, we used a surface complexation model (SCM) to describe the reactivity at the calcite-water interface and obtained the enthalpies of the surface reactions by fitting the SCM to either high-temperature electrokinetic data obtained through streaming potential measurements on limestone samples or to the effluent concentration from single-phase flooding experiments. We assumed that the equilibrium constants of the surface reactions follow a temperature dependence according to van't Hoff equation. Our calculations suggest that calcite protonation is more exothermic compared to other minerals (e.g., silica, hematite) and that the adsorption of Ca^{2+}, Mg^{2+}, and SO_4^{2-} are all endothermic, with SO_4^{2-} having the highest reaction enthalpy. We further show that the inferred enthalpies were in agreement with enthalpy changes from published microcalorimetry experiments. Despite the consistency with microcalorimetry data, the obtained enthalpies are not undisputable and additional data are necessary to unequivocally constrain the temperature effect on the calcite surface reactivity.

This chapter is a revised layout of the article: M. Bonto, H.M. Nick, A.A. Eftekhari. Thermodynamic analysis of the temperature effect on calcite surface reactions in aqueous environments. Energy & Fuels, 2021.

3.1 Introduction

Increasing evidence from core flooding studies on carbonates suggests that the residual oil left after primary/secondary recovery could be mobilized by injecting an aqueous fluid with a composition different than that of the in-situ (formation) water[222–224]. Unfortunately, there is no universal brine recipe that can guarantee an increase in oil recovery and other factors, such as temperature[61], crude oil properties[183], and mineralogy[225,226], govern the production outcome. The myriad of factors involved justifies the countless mechanisms reported for the so-called "low salinity effect"[19]. Besides the water composition, temperature is the only variable that can be somewhat manipulated to shift the oil-brine-rock system to a new thermodynamic state that leads to higher oil recovery. This is the subject of the present study. The dependence of the modified salinity waterflooding (MSW) performance on site-specific conditions challenges not only the selection of suitable (oil field) candidates that could benefit from this enhanced oil recovery (EOR) but also the prediction of a "successful" water composition for a particular oil field. Several studies have tackled this problem by seeking a link between the interactions in the crude oil-brine-rock system, the wettability alteration, and eventually, the additional oil recovery[94,100,101]. Surface complexation models (SCMs) are commonly used to describe these interactions at both the oil-brine[227] and calcite-brine[69,228] interfaces. SCMs can be used in combination with analytical[27] or numerical[100,229,230] flow models for history matching purposes and eventually as predictive tools. Several publications have proposed different surface complexation models to describe the reactivity at the calcite surface[67,94,104,175]. These models have been validated mostly against experimental data at room temperature, hence, their description of adsorption or surface charge development at the rock-brine interface at higher temperature is uncertain.

The effect of temperature on reactions occurring at mineral surfaces can be deduced by performing surface charge[231] or adsorption measurements[232] at several temperatures. The data is then fitted either to adsorption isotherms or SCMs to obtain the corresponding equilibrium constants. The enthalpies of the reactions are finally inferred by considering that the equilibrium constants follow a temperature dependence according to van't Hoff equation[233] (eq. 3.1):

$$\frac{\partial \ln K_i}{\partial T} = \frac{\Delta H_{r,i}}{RT^2} \tag{3.1}$$

where $\ln K_i$ represents the natural logarithm of the equilibrium constant, K_i of reaction i, T [K] is the temperature, $\Delta H_{r,i}$ [J/mol] is the reaction enthalpy, and R is the ideal gas constant (8.314 J·mol^{-1}·K^{-1}).

Potentiometric techniques are widely used to assess ion sorption and charge development at oxide mineral/water interfaces. Nonetheless, the fast dissolution of calcite during acid-base titrations impacts unpredictably the proton balance in solution, challenging the surface charge estimation. Thus, quantifying the extent of adsorption reactions at the calcite surface and obtaining their thermodynamic parameters, i.e., K and ΔH_r, relies primarily on zeta potential (ζ) measurements. Zeta potential measurements are inherent to electrokinetic phenomena, hence, tightly linked to the electrical double layer (EDL) around charged particles. The EDL arises from the segregation of charge into a rigid layer with strongly bound ions (also known as Stern layer) and a diffuse layer with mobile ions. ζ is the potential at an unknown distance from the onset of the diffuse layer, also known as the shear plane, which represents the boundary between stagnant and mobile ions. Temperature can significantly affect ion adsorption at the interface, impacting both the surface charge density and zeta potential. However, performing and acquiring reliable zeta potential measurements of calcite in aqueous fluids at high temperatures is also troublesome as reaching a stable equilibrium solution requires controlling precisely the CO_2 atmosphere that is in equilibrium with the calcite suspension. Although the zeta potential of natural and synthetic calcite samples at room temperature has been extensively evaluated in the literature[6,60,164,175], only a few papers report measurements at higher temperatures[98,182–184,234,235]; except for Mahrouqi et al.[184], each study reports the zeta potential at two different temperatures. Figure 3.1

shows the effect of temperature on zeta potential measurements at varying ionic strength (panel a), pH (panel b), electrolyte type (panel c), and sample provenance (panel d). Discrepancies in the reported zeta potential values are not unusual and temperature can accentuate them even further.

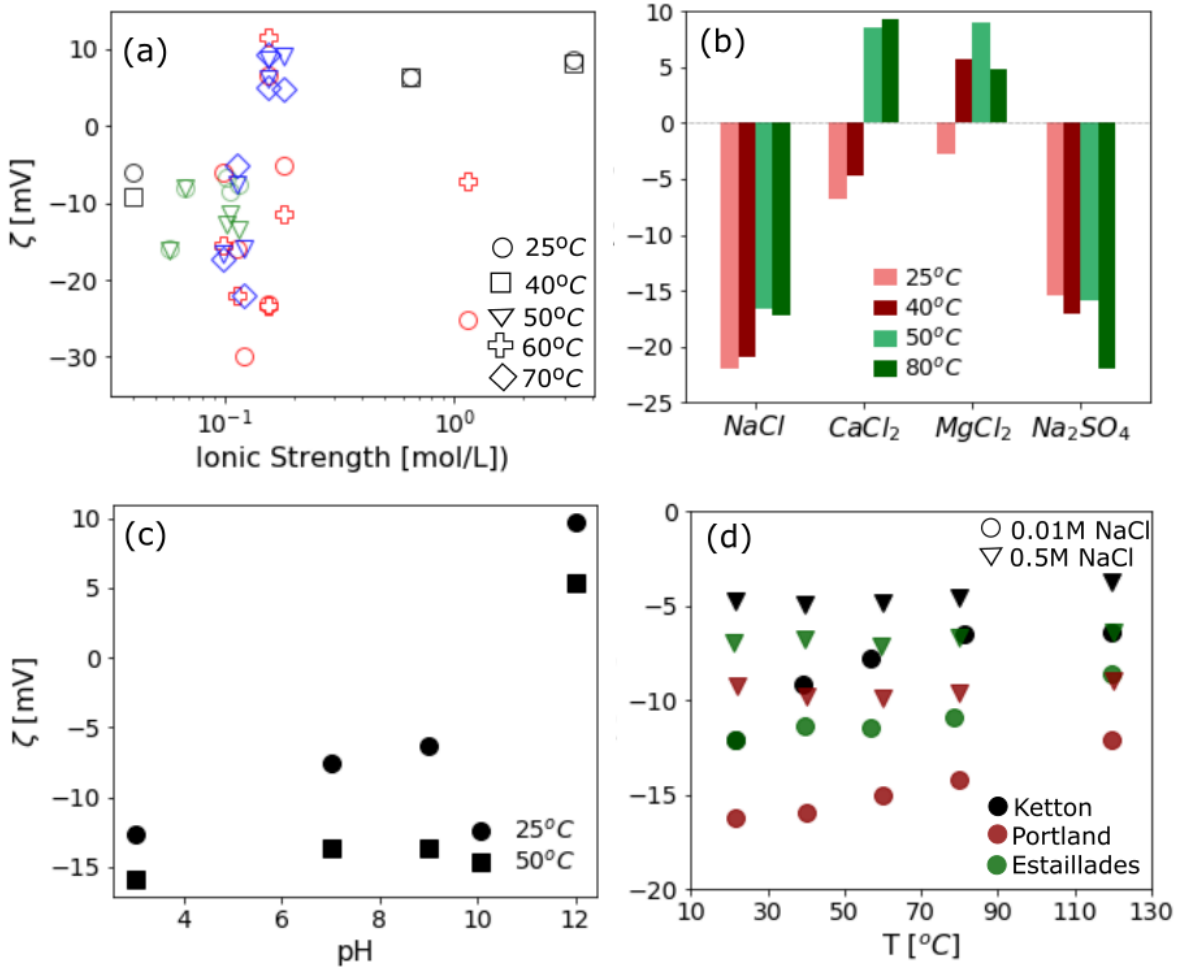

Figure 3.1. Temperature effect on zeta potential measurements (a) at different ionic strength in single electrolyte systems (e.g., NaCl, $CaCl_2$, $MgCl_2$, Na_2SO_4) or mixed aqueous solutions containing Na^+, Cl^-, Mg^{2+}, Ca^{2+}, SO_4^{2-}; the color of the markers represents the source of the data, i.e., black – data from ref.[98], green – data from ref.[234], red – data from ref.[181], blue – data from ref.[182] (b) in single electrolyte systems; the data at 25 and 40 °C is taken from ref.[98] and those at 50 and 80 °C from ref.[182] (c) at different pHs[234] in an aqueous solution containing Na^+, Cl^-, Mg^{2+}, Ca^{2+}, Sr^{2+}, SO_4^{2-}, and HCO_3^- (d) on different carbonate samples[184]. Reproduced from[236]. Copyright 2021 EAGE.

Other authors have suggested the use of microcalorimetry to characterize the enthalpy of the surface reactions[237]. The equilibrium constants at different temperatures can then be derived from the equilibrium constants at standard conditions and the enthalpy of the reactions according to eq. (3.1). Several publications have reported microcalorimetry measurements on chalk-brine-oil systems at 75°C[238,239]. These measurements, however, captured the overall enthalpy change occurring in the system, and the enthalpy change associated with each interaction at the chalk surface, e.g. (de)protonation, and adsorption of Mg^{2+} and Ca^{2+}, was not individually assessed. Other approaches, such as molecular dynamics[148,149], may also help advance the understanding of the temperature effect on the surface reactivity.

The scarce available experimental data explains why most SCMs applied to calcite assume either no temperature effect on the surface reactivity or an effect analogous to solution complexation. Some of the models that do report enthalpy for the reactions by considering either analogy with solution complexation or measurements at two different temperatures (up to 50°C) are summarized in Figure

3.2. Since these models were optimized using experimental data obtained on different carbonate samples (e.g., limestone, synthetic calcite, chalk) and experimental conditions, their equilibrium constants at 25ºC are quite diverse. This means that even though two models may consider similar reaction enthalpies, they may still show contrasting surface speciation and electrokinetic behavior at a given temperature. It is important to note that none of these models were thoroughly tested against experimental data at higher temperatures (>40ºC).

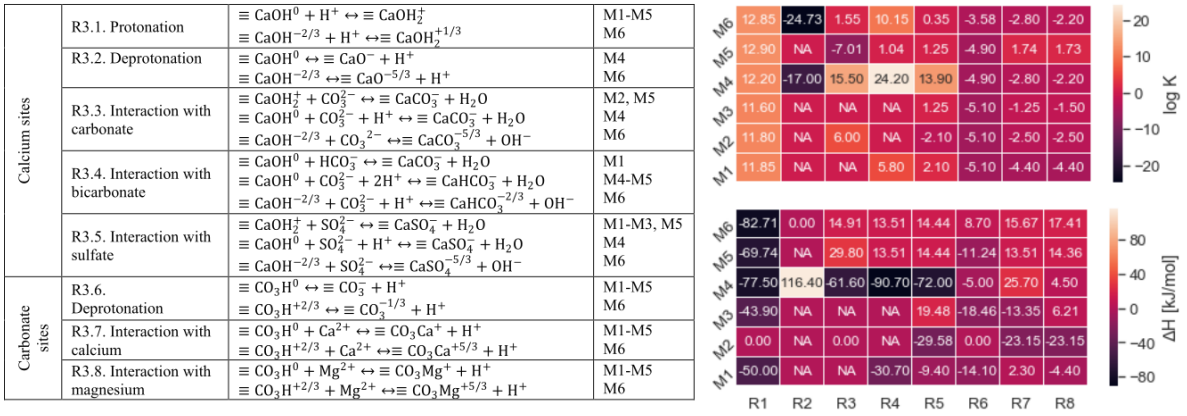

Figure 3.2. Main parameters defined in several SCMs reported in the literature: surface reactions (left), equilibrium constants (upper right), enthalpy of reaction (lower right). For further details on the models, the reader is referred to refs[98,99] (M1), ref[97](M2), ref[240] (M3), ref[103] (M4), ref[5] (M5), and refs[27,67,101] (M6). Some models (M2, M3, and M5) do not report directly the enthalpy of reactions but log *K* at several temperatures. In this case, the enthalpies were inferred by assuming a temperature dependence according to van't Hoff equation.

The main objective of this work is to improve the understanding and description of the calcite reactivity in presence of aqueous solutions at higher temperatures, representative of subsurface environments. To do so, we derive a set of enthalpies for the surface reactions by fitting an SCM to reported electrokinetic data obtained at high temperatures through streaming potential measurements. To validate these enthalpies, we further check their consistency with published data on enthalpy changes recorded through microcalorimetry and ion adsorption in flowthrough experiments. The obtained parameters are critically discussed and compared with thermodynamic data inferred for the surface speciation of other minerals. We also discuss the experimental uncertainties at temperatures higher than ambient conditions and provide some recommendations that could help in the development of versatile adsorption models that can be pertinently applied to a wide range of temperatures**.**

3.2 Methodology

To describe the calcite reactivity in an aqueous environment we consider a Charge Distribution MultiSite Complexation (CD-MUSIC) model (M6 in Figure 3.2) implemented in the geochemical software PHREEQC [241]. In this SCM, initially applied to calcite by Wolthers et al.[67], ions are located in different discrete electrostatic planes, i.e., surface/0-, inner/1-, and outer/2- Helmholtz planes (IHP and OHP, respectively) depending on their affinity for the surface. A schematic of the EDL description is shown in Figure 3.3. At the surface, only (de)protonation occurs whereas inner- and outer-sphere complexes are located at the IHP or OHP. Thus, the adsorption of ions at the calcite-water interface results in charged surface species, and each electrostatic plane experiences a net charge change, Δz_i, depending on the structure of the surface complex. For instance, considering the adsorption of calcium as proposed by Wolthers et al.[67] (e.g., reaction R3.7 corresponding to M6 in Figure 3.2), involves the deprotonation of the surface ($\Delta z_0 = -1$), whereas Ca^{2+} is located at the IHP ($\Delta z_1 = 2$). For all surface reactions, we kept the charge distribution from the original reference[67]. The excess surface charge leads to the development of a potential with respect to the bulk and the charge density and potential at the different planes are related through two capacitances (i.e., C_1 and C_2). The total Gibbs energy of adsorption of ions is given by a chemical contribution (proportional to the temperature-dependent

equilibrium constants) and an electrostatic component (proportional to the net charge change and the potential at plane i, Δz_i and ψ_i [V], respectively)[73,85]. The relationship between the reaction quotient, Q, and the intrinsic equilibrium constant, K, of an adsorption reaction is given by eq. (3.2):

$$Q = K\exp\left(-\sum \frac{\Delta z_i F}{RT}\psi_i\right) \tag{3.2}$$

where F [96485 C/mol] is the Faraday constant and the variation of K with temperature is given by eq. 1. Assuming a constant enthalpy of reaction, ΔH_r, and considering the definite integral of eq. (3.1) between 25ºC and any temperature, T, the relationship in eq. (3.2) can be re-written as a function of the equilibrium constant at 25ºC (=298 K) and reaction enthalpy (eq. 3.3):

$$Q = K_{@298\,K}\exp\left(-\frac{\Delta \mathrm{H}_r}{R}\left(\frac{1}{T}-\frac{1}{298}\right)\right)\exp\left(-\sum \frac{\Delta z_i F}{RT}\psi_i\right) \tag{3.3}$$

The excess surface charge is neutralized by the charge in the diffuse layer and the relationship between the charge and potential in the diffuse layer is given by the Grahame equation[120]. Because we assume that the shear plane is located at the OHP, the zeta potential coincides with the potential at the 2-plane. The main equations integrating the SCM have been summarized in Appendix A.2. For further details on the general mathematical implementation of SCMs, the reader is referred to, e.g., refs[64,79].

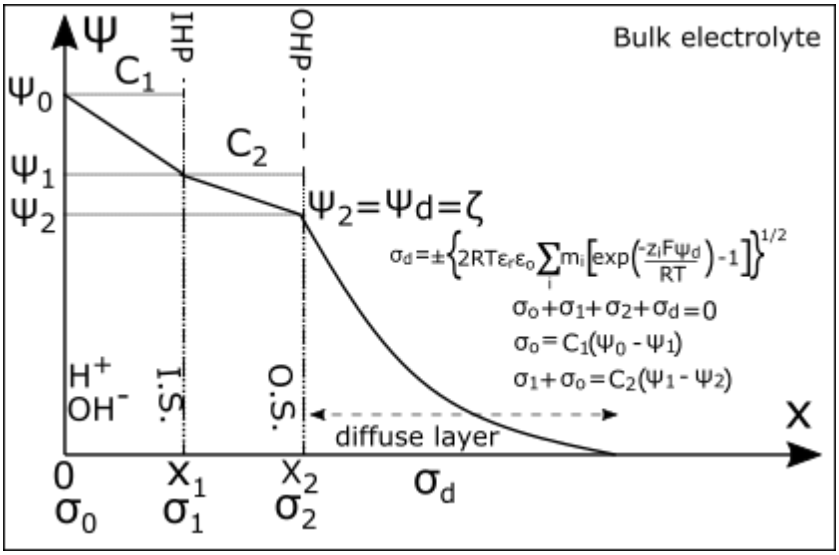

Figure 3.3. Schematic of the EDL description in the Phreeqc implementation of the CD-MUSIC model. Adapted from [64]. I.S. and O.S. represent inner- and outer-sphere complexes, respectively, and can be either cations or anions. In the figure, x [m] represents the interfacial region, ψ [V] is the potential, m_i is the concentration of ion i [mol/m^3], F [96485 C/mol] represents the Faraday constant, σ [C/m^2] is the charge density and C [F/m^2] is the capacitance. Here we assume that the shear plane is located at the OHP, thus ζ coincides with the potential at the OHP. From top to bottom, the first equation represents the Grahame equation, the second describes the electroneutrality, and the last two represent the charge-potential relationship. A summarized mathematical description of the model can be found in Appendix A.2.

Although the original work defines several types of surface sites (i.e., face, kink, and edges) depending on their position and coordination with the bulk, we considered only the calcium and carbonate face sites with a density of 4.95 #/nm^2 together with the capacitances values updated in the work of Sø et al.[89] (C_1=1.3 F/m^2, C_2=4.5 F/m^2). To customize the model for EOR applications, we defined additional reactions for Mg^{2+} and SO_4^{2-} (R3.8 and R3.5 in Figure 3.2, respectively), common ions in both seawater and formation water. We chose this model because it was shown to satisfactorily predict the zeta potential of calcite and chalk particles obtained at room temperature in low[67] and high[228] (≈0.5 M) electrolyte concentrations. The performance of the model against published zeta potential measurements carried out at ambient temperature in electrolyte systems containing divalent ions (i.e., Ca^{2+}, Mg^{2+}, SO_4^{2-}) is shown in Appendix A.2. Thus, we keep the log K values at 25ºC as shown in Figure

3.2 and we only optimize the enthalpies of the reactions by fitting the model to the streaming potential measurements up to 130ºC carried out by Mahrouqi et al.[184] using a least-squares optimization algorithm implemented in Python.

Because these measurements were carried out in a NaCl solution, we can only fit the enthalpies corresponding to the (de)protonation of the surface sites (R3.1, R3.2, and R3.6 in Figure 3.2) and interactions with (bi)carbonate and calcium (R3.3, R3.4, and R3.7 in Figure 3.2); the two latter species arise from the dissolution of the calcite in equilibrium with the brine. The remaining enthalpies for the surface reactions with magnesium and sulfate are obtained by adjusting the model to the effluent concentration from single-phase flooding tests. Lastly, the (predictive) performance of the model is assessed against additional flowthrough experiments and microcalorimetry measurements. The methodology is sketched in Figure 3.4.

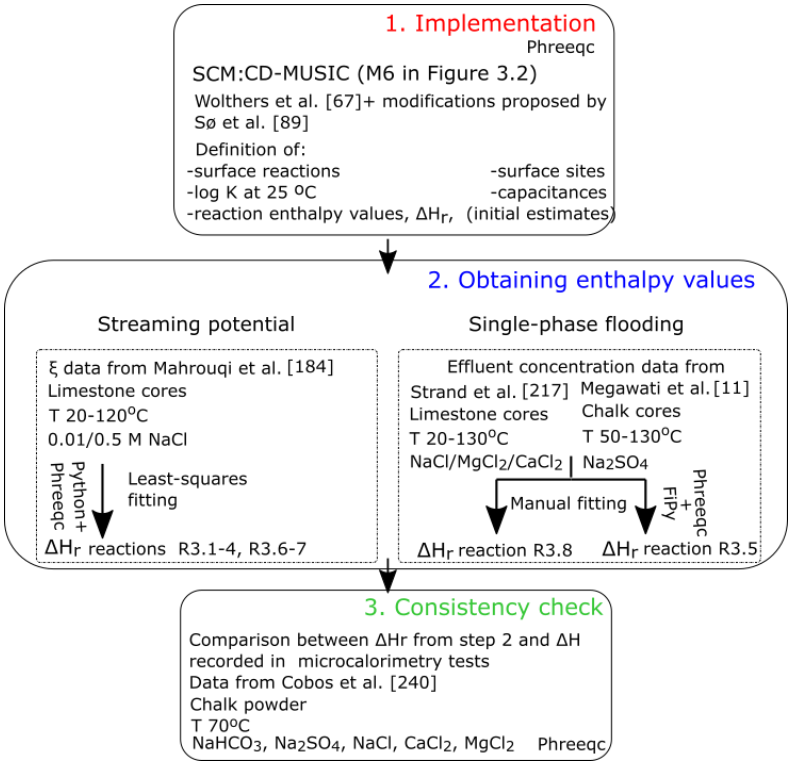

Figure 3.4. Description of the methodology. The reaction enthalpies (R3.1-R3.8 corresponding to model M6 in Figure 3.2) obtained by fitting the model to either electrokinetic data or effluent concentration from single-phase flooding tests are assumed general (not test-specific).

3.2.1 Selection and analysis of zeta potential data from streaming potential measurements

The zeta potential of natural intact rock samples is usually determined through streaming potential measurements. In this technique, when a pressure gradient (flow) is imposed on a saturated sample, the (mobile) ions in the diffuse layer are dragged downstream leading to a streaming current and, therefore, to a streaming potential. At the same time, the streaming potential causes a conduction current in the opposite direction. The streaming potential coupling coefficient is determined from the ratio of the potential difference and the pressure drop at steady-state when the conduction current is equivalent to the streaming current (e.g., references[161,242]). The ζ potential is inferred indirectly from the measured coupling coefficient through the Helmholtz-Smoluchowski (H-S) equation (eq. 3.4). This equation stems from equating the streaming and conduction current induced by fluid motion. For details on its derivation, the reader is referred to Hunter[161].

$$C = \frac{\Delta V}{\Delta P} = \frac{\varepsilon_0 \varepsilon_r \zeta}{\mu_f \sigma_f} \tag{3.4}$$

where C [V/Pa] is the streaming potential coupling coefficient, ΔV [V] is the streaming potential (potential difference between the two ends of the core sample), ΔP [Pa] is the pressure drop across the sample, ε_0 [$8.854 \cdot 10^{-12}$ F/m] is the vacuum permittivity, ε_r [-] is the fluid relative permittivity, μ_f [Pa·s] and σ_f [S/m] are the fluid viscosity and conductivity, respectively.

Eq. (3.4) assumes that only the flow of electrical charges through the fluid contributes to the conduction current. However, at low salinity, surface conductivity may become important and a modified H-S equation is commonly used (eq. 3.5); not considering surface conductivity effects was shown to have a considerable impact on the derived zeta potential at electrolyte concentrations lower than 0.05 M[93].

$$C = \frac{\Delta V}{\Delta P} = \frac{\varepsilon_0 \varepsilon_r \zeta}{\mu_f \sigma_r F} \tag{3.5}$$

where σ_r [S/m] is the conductivity of the fluid-saturated rock sample and F [-] is the formation factor given by eq. (3.6).

$$F = \frac{\sigma_f}{\sigma_r} \tag{3.6}$$

The formation factor should be obtained at relatively high salinity (>0.05-0.1 M), where surface conductivity effects become unimportant. When surface conductivity is not relevant, the product $\sigma_r F$ is equivalent to σ_f, thus, eqs. (3.4) and (3.5) are equivalent and should yield the same zeta potential.

The well-documented experimental results published in the work of Mahrouqi et al.[184] allow the analysis of the data and validating the conversion of the coupling coefficient to zeta potential. In that article, the authors report streaming potential measurements on three different limestone samples (i.e., Ketton, Estaillades, and Portland) in the presence of NaCl solutions (0.01 and 0.5 M) and at a temperature range between 20 and 120ºC. Since they included the raw data (i.e., C, σ_r, F) used to determine the zeta potential, we started by assessing the consistency between the reported conductivity of the aqueous fluids, saturated samples, and formation factor (Figure 3.5). The data at low salinity (Figure 3.5-a) shows that the surface conductivity of Ketton and Estaillades limestones is negligible as the product of the reported formation factor (13.87, 12.92, and 22.04 for the Ketton, Estaillades, and Portland limestones, respectively) and the saturated rock conductivity ($\sigma_r F$) is in agreement with the conductivity of the fluid saturating the sample. However, for the Portland limestone, the resulting conductivity exceeds that of the saturating fluid confirming the contribution of the surface conductivity, which can probably be ascribed to the 3% quartz content of this sample. Surprisingly, at high salinity conditions (Figure 3.5-b), which erase the importance and effects of surface conductivity, $\sigma_r F$ results in a (calculated) fluid conductivity significantly lower than expected at that concentration and temperature. This either suggests that gas entrapment led to a measured conductivity lower than the "true conductivity" of the saturated sample or that changes in petrophysical properties of the sample due to flow and pressure/temperature cycling may have resulted in a variation of the formation factor; however, the former explanation seems more likely, as the latter would have also affected the measurements at low salinity.

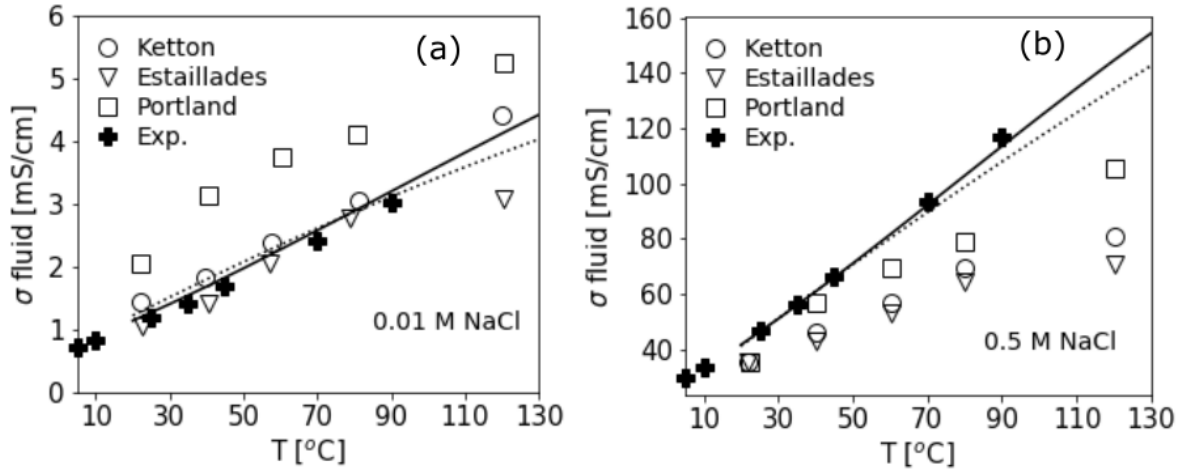

Figure 3.5. Analysis of the conductivity measurements of a core saturated with **(a)** 0.01 M and **(b)** 0.5 M reported by Al Mahrouqi et al.[184]. In the absence of surface conductivity, the product of the saturated core conductivity and the reported formation factor ($\sigma_r F$) should coincide with the conductivity of the fluid. The reported formation factor for Ketton, Estaillades, and Portland are 13.87, 12.92, and 22.04, respectively[184]. The markers pointing to rock samples correspond to the calculated fluid conductivity by considering the product of the formation factor and the conductivity of the saturated sample reported for each type of limestone. For comparison, we included the measured fluid conductivity by McCleskey[243]. The solid and dotted line corresponds to the conductivity predicted by PHREEQC and the correlations from Sen and Goode[244], respectively. At 0.5 M NaCl, replacing measured core conductivity and reported formation factor in eq. (3.6 yields a significantly lower fluid conductivity than expected at that specific salinity and temperature.

Considering the inconsistency shown in Figure 3.5-b, recalculating the zeta potential according to eq. (3.4) (using the fluid conductivity) features a different trend of the zeta potential with the temperature at high salinity compared to the reported measurements (Figure 3.6). Note that the viscosity and permittivity of the fluid were determined using the correlations from Kestin et al.[245] and Stogryn[246], akin to the original work.

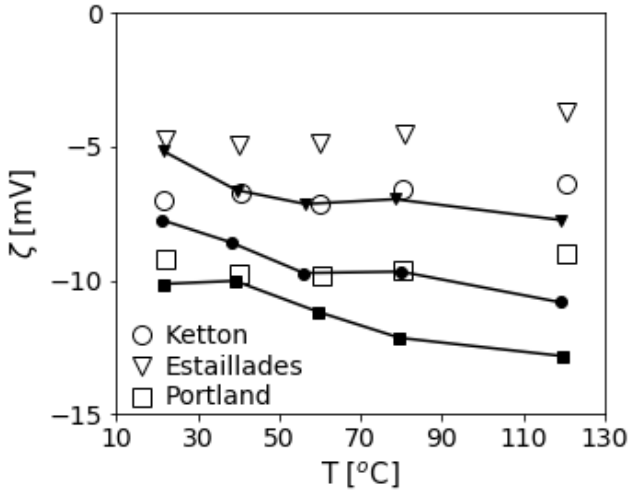

Figure 3.6. Discrepancy between the experimental reported zeta potential values (markers) for limestone samples in 0.5 M NaCl and the calculated zeta potential (lines) using the brine conductivity (eq. 3.4).

Thus, for the optimization of the enthalpies of the reactions we used the zeta potential values reported at 0.01 M and the calculated ones at 0.5 M. We only used the data from Ketton and Estaillades limestone as they share a similar mineralogical composition.

3.2.2 Single-phase core flooding experiments

The enthalpies obtained by fitting zeta potential measurements are used to replicate the effluent concentration from single-phase corefloods on limestone and chalk samples. However, since the lack

of calcite zeta potential measurements at high temperature and different electrolyte systems impedes obtaining enthalpies for all surface reactions, we also use these flow experiments to manually adjust the enthalpy of the surface interactions with Mg^{2+} and SO_4^{2-}. The species transport in porous media can be described according to eq. (3.7):

$$\frac{\partial}{\partial t}(\varphi c_i + (1-\varphi)\rho_s a_s q_i) + \nabla \cdot (\boldsymbol{u_w} c_i) + \nabla \cdot (-\varphi D_i \nabla c_i) = R_i \tag{3.7}$$

where t [s] is the time, φ [-] is the porosity, c_i [mol/m^3] is the concentration of species i, ρ_s [kg/m^3] is the mineral density, a_s [m^2/kg] is the specific surface area of the rock, q_i [mol/m^2] is the number of moles of species i adsorbed per unit surface area of rock, u_w [m/s] is the velocity of the water phase, D_i [m^2/s] is the diffusion coefficient of species i in the water phase and R_i is a source/sink term. Considering that in these experiments the Péclet number ($Pe = \frac{Lu_w}{D} \gg 1$, where L is a characteristic length scale) is high, i.e., the transport by advection dominates, the diffusion contribution in eq. (3.7) is assumed negligible.

To solve this equation in one dimension we coupled the geochemical reaction module PhreeqcRM[212] that solves the chemical equilibrium and updates the concentrations at each time-step, with FiPy[213], a finite volume partial differential equations solver developed for Python. For all cases, we set a uniform mesh of 50 cells along the 1D domain, which was considered equal to the length of the cores (between 5.0 and 7.0 cm depending on the publication).

3.2.3 Microcalorimetry

Lastly, we assessed the compatibility of the model with the enthalpy measurements from the microcalorimetry studies carried out by Cobos et al.[239]. These experiments consisted of recording enthalpy changes upon injecting 10 µL of several electrolyte solutions (e.g., NaCl, $CaCl_2$, $MgCl_2$, Na_2SO_4, and $NaHCO_3$) in a vial containing 100 mg of chalk. However, for the rock-brine system, the enthalpy change could not be measured directly as the heat of evaporation of the aqueous solutions masked the effect of any enthalpic effects stemming from the rock-brine interactions. The authors then determined separately the enthalpy change in the oil-brine-rock, oil-brine, and oil-rock systems and derived the contribution of the rock-brine interactions by subtracting from the former the two latter quantities. Thus, the enthalpies were considered to be additive and no isothermal heat of mixing was considered. Figure 3.7 shows the enthalpy change for ten injections performed every 10 minutes. As observed, the enthalpy change is more significant in the first injection compared to the remaining ones. We postulate that the response from the first injection is the most relevant for characterizing the effects originating from the surface reactions; with the first injection, the hydration and distribution of surface species occurs, whereas the introduction of the same fluid in the system can only lead to slight readjustments in the surface speciation.

To estimate the enthalpy change driven by the calcite surface reactivity, we predict with the SCM the surface speciation at the experimental conditions, and the number of moles of each surface species is multiplied by the corresponding reaction enthalpy. Note that we assume that the reaction enthalpy at 75ºC coincides with that defined at standard conditions as the specific heat of the surface species is unknown.

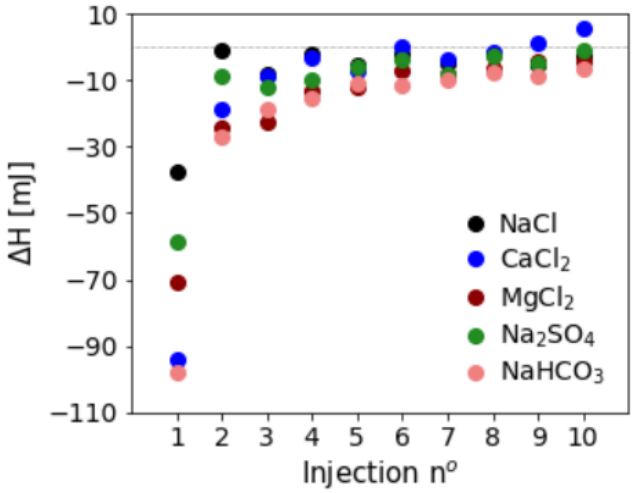

Figure 3.7. Enthalpy change associated with the interactions between chalk powder and different electrolytes. This enthalpy was inferred indirectly from isothermal titration calorimetry experiments of chalk with crude oil and brine, crude oil with brine, and chalk with crude oil. Data from ref[239]. Reproduced from[236]. Copyright 2021 EAGE.

3.3 Results and discussion

3.3.1 Zeta potential

To model the chemical system representative of the streaming potential measurements from the work of Mahrouqi et al.[184], we considered the NaCl solutions (0.01 and 0.5 M) in equilibrium with atmospheric CO_2 at room temperature and subsequent equilibration with calcite at the different experimental temperatures. It should be noted that we modeled a system containing only calcite and no other chemical impurities. The comparison between the experimental and modeled pH and pCa are shown in Figure 3.8 panels a and b, respectively. The predicted pH is slightly greater than the measured one; this difference may arise from the initial equilibration of the solution with the gas phase but also the presence of other mineral phases (e.g, quartz) in the limestone samples. The most surprising feature is that at the lowest NaCl concentration, the measured pCa decreases with increasing temperature, whereas an opposite trend is predicted in PHREEQC; the experimental trend is not consistent with the solubility behavior of calcite, i.e., greater solubility at a lower temperature.

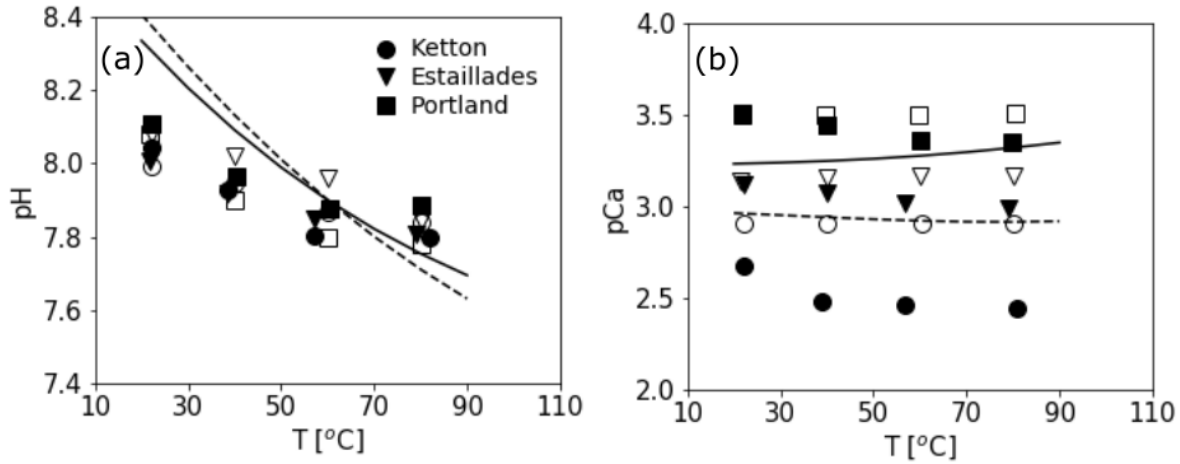

Figure 3.8. Comparison between the measured (markers) and predicted (lines) **(a)** pH and **(b)** pCa. The filled markers and solid lines correspond to the measurements in 0.01 M NaCl whereas the empty markers and dashed lines correspond to measurements in 0.5 M NaCl. Data from ref [184].

Figure 3.9 shows the experimental zeta potential data at different temperatures and the fitted SCM model to the same dataset. The fit is not ideal given the reduced number of data points corresponding to only two ionic strengths. Moreover, since the equilibrium constants at 25ºC are kept fixed, a discrepancy between the experimental data and the model is automatically induced. If more data were available at different temperatures, a better approach would be to obtain the equilibrium constant at each temperature separately. By representing ln K against 1/T, both the entropy and enthalpy shift associated with each surface reaction could be inferred. This preferred approach of obtaining the thermodynamic data of the calcite surface reactions would also allow assessing the plausibility of the assumption that the equilibrium constants follow a temperature dependence according to van't Hoff equation.

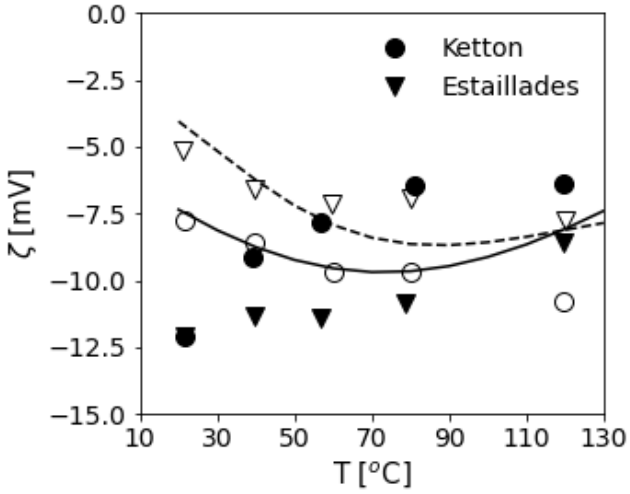

Figure 3.9. Experimental (markers)[184] and calculated (lines) zeta potential. Filled markers and solid lines correspond to measurements with 0.01 M NaCl and empty markers and dashed lines to 0.5 M NaCl. The fitted enthalpies for reactions R3.1, R3.3, R3.4, R3.6, and R3.7 in Figure 3.2 are -62.82, 20.68, 25.48, 1.80, 39.69 kJ/mol, respectively.

The results from the optimization suggest that the calcite protonation is more exothermic (ΔH_{prot}=-62.82 kJ/mol) compared to (hydrous) metal oxides[219,247–249] (ΔH_{prot}= -20 to -45 kJ/mol depending on the type) whereas the slightly endothermic deprotonation is in agreement with that found for hematite[250]. Through high-temperature electrophoresis measurements on different metal oxides, Rodríguez-Santiago et al.[248] showed that the magnitude of the protonation enthalpy of metal oxides increases with increasing isoelectric point/point of zero charge. Considering that calcite has a fairly high point of zero charge (between pH 8-9.5[37]), its higher protonation enthalpy is consistent with the previous observations[220].

3.3.2 Single-phase core flooding

To obtain also the enthalpies for the surface reactions with Mg^{2+} and SO_4^{2-}, we modelled the transport of ions through chalk and limestone core samples. In these experiments, the effluent concentration gives an indication of the retention of ions within the core. In the absence of precipitation, a retarded ion breakthrough suggests a stronger affinity for the surface. To quantify the missing enthalpies, we selected experiments performed at least at two different temperatures and with simple aqueous solutions to isolate the reactions of interest.

3.3.2.1 Interaction with sulfate

Megawati et al.[11] studied the adsorption of sulfate on natural calcite by performing flooding tests on Liège chalk (Belgium) at 50 and 130ºC. The core was initially saturated with 0.096 M NaCl and the tracer (thiocyanate) and sulfate concentration were monitored during the injection of 4 pore volumes (PV) of 0.024 M Na_2SO_4. As shown in Figure 3.10, the experiments reveal insignificant SO_4^{2-} retention at 50ºC but strong adsorption at 130ºC. The conditions of undersaturation with respect to anhydrite or

gypsum discard the possibility of sulfate retention due to precipitation. To describe the great adsorption difference between the two experimental conditions, a highly positive reaction enthalpy should be considered for the calcite interaction with sulfate that would strongly increase the equilibrium constant with temperature; a reaction enthalpy of 100 kJ/mol is required to adjust the model to the sulfate concentration in the effluent (Figure 3.10). Although the reaction enthalpy we inferred is close to that proposed in the work of Megawati et al. (84 kJ/mol)[11], it is rather high when compared with enthalpies reported for the adsorption of inorganic anions on mineral surfaces. Slightly negative enthalpies were found for the interaction of phosphate with calcite (-16.7±16.7 kJ/mol)[251] and aluminum hydroxide (-6.5±3 kJ/mol)[252] and marginally positive for the interaction of sulfate with aluminum hydroxide (2.9±1.4 kJ/mol)[252]; these enthalpies are also consistent with the observation from Machesky et al.[247] that anticipated decreased anion adsorption on hydrous metals at increasing temperature.

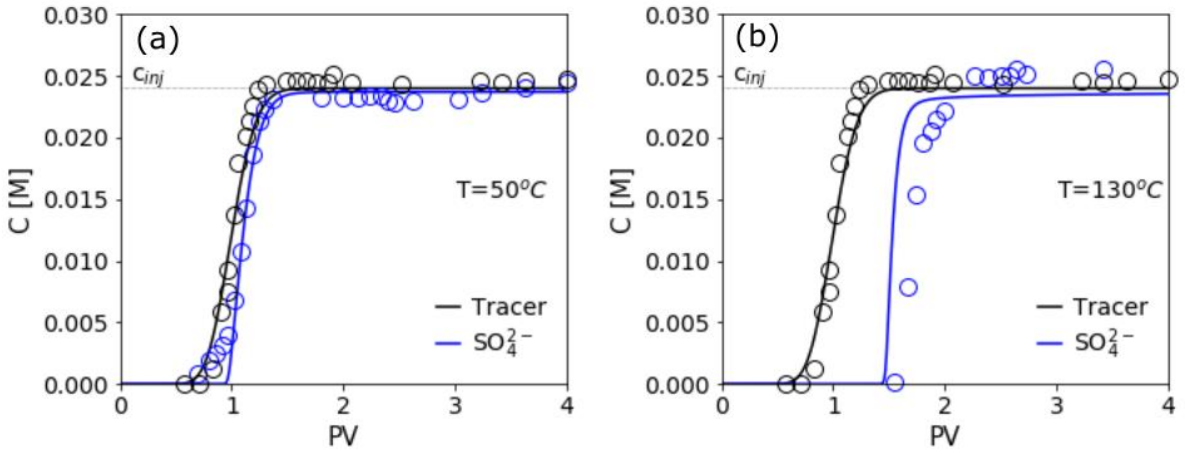

Figure 3.10. Effluent concentration during the injection (0.2 mL/min) of 0.024 M Na_2SO_4 aqueous solution into a Liège chalk core initially saturated with 0.096 M NaCl. Tests performed at **(a)** 50 ºC and **(b)** 130ºC. Experimental data from Megawati et al.[11].

Furthermore, the inferred enthalpy is not univocal as its value is constrained by the magnitude of the equilibrium constant at 25ºC and also by the competition between the SO_4^{2-} with other aqueous species for the surface sites. A log *K* of 0.35 was initially set because it resulted in a good agreement with the electrophoresis measurements performed on chalk particles in a NaCl/Na_2SO_4 aqueous solution. Higher log *K* at 25ºC decreases the enthalpy value required to fit the effluent concentration (e.g., with a log *K* at standard conditions of 1.0 or 2.0, the enthalpy of the reaction can be lowered to 80 and 60 kJ/mol, respectively) but increases the discrepancy between the model and electrokinetic data (Figure 3.11). Nonetheless, none of these log *K* values at standard conditions (i.e., 0.35, 1.0, 2.0) can explain the high sulfate retention (23 mg SO_4^{2-}/g limestone) measured at room temperature in a fixed bed with limestone particles[253]. Even if all calcium sites in a calcite sample with a specific surface area of 2 m^2/g were available for interaction with sulfate, the maximum possible retention would still be around 14.5 times lower than the intake capacity reported by Silva et al.[253]. This either means that sulfate adsorption in ref.[253] is controlled by the presence of chemical heterogeneities with a higher specific area and/or a greater number of reactive sites and/or that the retention does not proceed as envisioned in the SCM; supporting experimental data exists for both hypotheses. For instance, several publications[214,215] found that minute amounts of superficial nanoclays have a dramatic effect on the surface reactivity and adsorption behavior of biogenic calcite samples. Besides, multiple papers portray the retention of sulfate on calcite as a substitution reaction[150,254–256] that would require different treatment than an adsorption reaction; in this sense, the substitution of CO_3^{2-} by SO_4^{2-} would be better described through ion-exchange rather than surface complexation. However, since ion substitution is usually observed and reported from crystal growth experiments, its relevance in flow experiments such as those performed by Megawati et al.[11] is unclear; monitoring the carbonate content and pH of the effluent and also the carbonate core

after the flooding could be possible ways to resolve the extent of CO_3^{2-}/SO_4^{2-} substitution. Moreover, both the presence of nanoclays and the preferred substitution of CO_3^{2-} by SO_4^{2-} at kink sites[254,256] would introduce a surface charge heterogeneity that may considerably influence transport and adsorption properties[257,258] in carbonate environments. It is important to note that the real effect of the nanoclays and substitution reactions on the retention from solution cannot be inferred from electrophoretic mobility measurements because these give only an average zeta potential[207,259,260], whereas the transport and adsorption of ions may be governed by local surface charges. This may explain why the equilibrium constants inferred from zeta potential measurements obtained by electrophoresis cannot describe the concentration history of different ions from single-phase core floodings[69,240]. This is not a flaw in the electrophoretic mobility measurements as much as the utilization of an insufficient number of data points from poorly chosen brine-calcite mixtures for optimising the SCM model parameters.

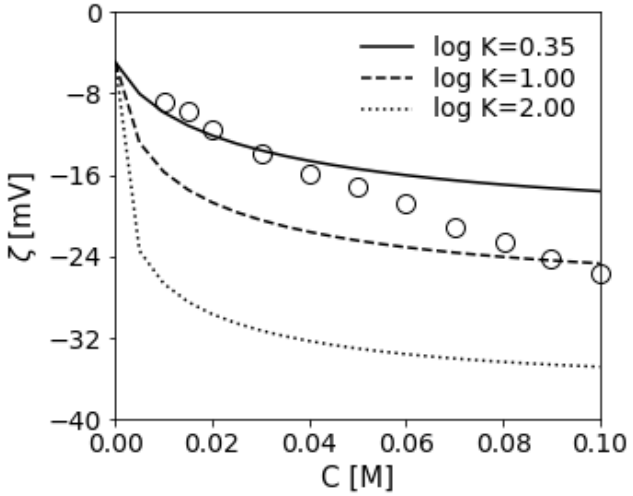

Figure 3.11. Predicted zeta potential of Stevns Klint chalk particles with increasing SO_4^{2-} concentration in 0.573 M NaCl background electrolyte concentration at pH=8.4 fixed by NaOH titrations at 25 °C. Experimental data (markers) from Zhang et al.[178]. At sulfate concentrations characteristic of seawater (≈0.024 M), the log *K* of 0.35 results in a better agreement with the experimental ζ-values.

Furthermore, obtaining binding constants exclusively relying on electrokinetic data has some implicit uncertainties; using zeta potential to calibrate/outline an SCM requires several assumptions regarding the capacitance values (both for the IHP and OHP) or the location of the shear plane. Here, for simplicity and to reduce the number of adjustable parameters, we considered constant capacitances and that the zeta potential coincides with the potential at the OHP. Yet, temperature, electrolyte type, or surface roughness may all have an impact and question these assumptions[126]. Characterizing the EDL properties and binding constants by combining electrokinetic measurements with potentiometric titrations or sorption data directly may help reduce/resolve the uncertainty[208,210,211].

3.3.2.2 Interaction with magnesium

To obtain the enthalpy of the Mg^{2+} reaction with the calcite surface, we used flooding tests on Middle Eastern limestone performed by Strand et al.[217] at four different temperatures (20, 70, 100, and 130°C). The cores, initially flushed and saturated with 0.571 M NaCl, were flooded with a brine of a similar background electrolyte concentration (≈0.5 M) supplemented with 0.013 M Mg^{2+}, Ca^{2+}, and a tracer (thiocyanate). To model these experiments, we considered that the limestone core was initially not in equilibrium with the NaCl solution as, if this was the case, we would expect Ca^{2+} to appear in the effluent right after the beginning of the experiment (even before the tracer) and the ratio between the outlet and injected calcium concentration to be always higher than zero due to the dissolution of calcite. A reaction enthalpy of around 50 kJ/mol is required to fit the magnesium concentration in the effluent at four different temperatures (Figure 3.12).

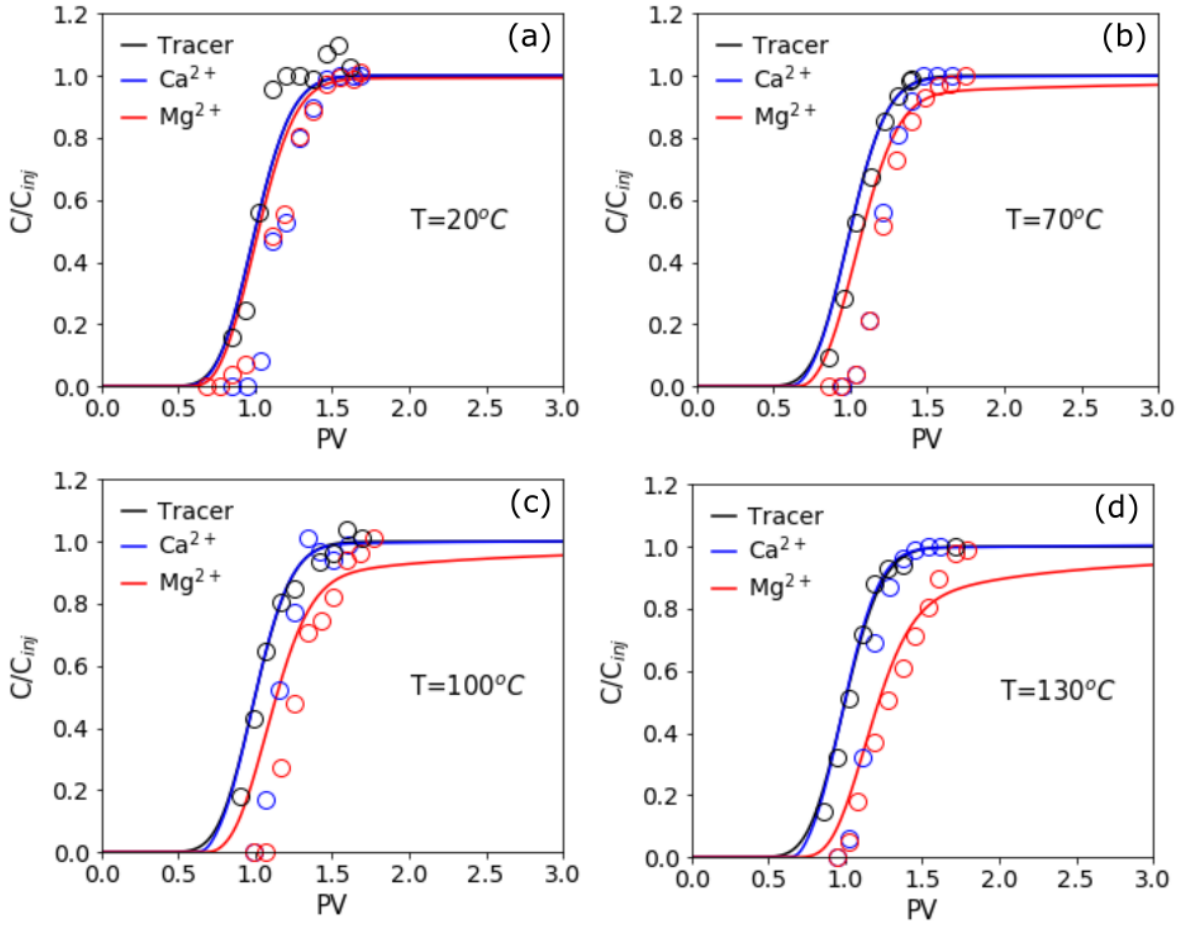

Figure 3.12. Effluent concentration during the injection (0.1 mL/min) of a brine mixture (0.571 M NaCl+0.013 M Ca^{2+}/Mg^{2+}) at four different temperatures: **(a)** 20ºC **(b)** 70ºC **(c)** 100ºC **(d)** 120ºC. The core was initially saturated and flushed with 0.571 M NaCl. Experimental data from Strand et al.[217].

To check the agreement of this enthalpy with other experimental datasets, we considered flooding tests with 0.219 M $MgCl_2$ solution performed on Kansas chalk at 130ºC and carried out by Sachdeva et al.[261] (Figure 3.13).

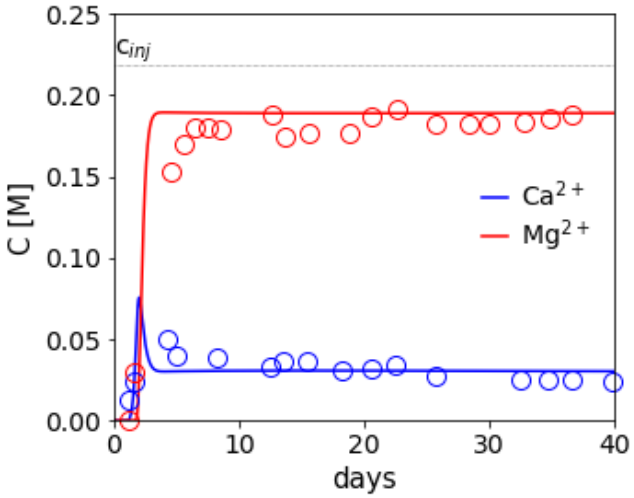

Figure 3.13. Effluent concentration during the injection (0.01 mL/min) of 0.219 M $MgCl_2$ aqueous solution into a Kansas chalk core initially saturated with 1.1 M NaCl. Data from Sachdeva et al.[261].

Given the high electrolyte concentration, supersaturation with respect to magnesium-bearing minerals is expected; the precipitation of newly formed Mg-minerals was disclosed through the core analysis after the flooding and also reported in other flowthrough experiments on chalk[262]. Contrary to the concentration profiles from Strand et al.[217], calcium was released from the core before magnesium, most probably due to calcite dissolution. To accommodate these experimental observations (i.e., precipitation of magnesium-containing minerals and calcite dissolution), we considered that in each reaction cell the solution is in equilibrium with dolomite, calcite, and magnesite; albeit suitable for calcite, this assumption carries more uncertainty when it comes to dolomite and magnesite dissolution/precipitation that are known for their slower kinetics compared to calcite. Although the model describes adequately the evolution of the effluent composition with time (Figure 3.13), the Mg^{2+} retention is not dictated by the adsorption at the calcite surface but by the precipitation of dolomite and magnesite.

The enthalpies we inferred for magnesium and calcium adsorption on limestone are greater than the enthalpies reported for cation adsorption on (hydrous) oxide metals[247,263] and calcite[264], considerably lower than those reported for magnesite (95±25 kJ/mol)[264], but in close agreement with those found for Zn^{2+} (which has an ionic radius in solution similar to Mg^{2+} [265]) adsorption on dolomite (34.35±10 kJ/mol)[264] or cation adsorption on hematite[247] (between 13 and 49 kJ/mol). The fact that both Ca^{2+} and Mg^{2+} adsorption are endothermic is compatible with their treatment as inner-sphere complexes. To adsorb, these cations need to lose their hydration sheath, which is a highly endothermic process. The lower hydration enthalpy of Ca^{2+} ($-\Delta H_{hyd}$=1602 kJ/mol) compared to Mg^{2+} ($-\Delta H_{hyd}$=1949 kJ/mol)[266] is also consistent with the higher adsorption enthalpy of the latter. Similar trends, e.g., increasing enthalpy of cation adsorption with decreasing hydration enthalpy, were also observed for silica surfaces[263,267–269]. The high positive enthalpies also imply that cation adsorption on the carbonate surface is accompanied by an important positive entropy shift. Besides the loss of water molecules experienced by the adsorbing ions, the entropy increase can also be justified by the disruption of the highly ordered water layers at the calcite surface[116] upon ion adsorption. The enthalpies of the calcite surface reactions inferred in this work are summarized in Table 3.1.

Table 3.1. Parameters of the SCM. The reaction enthalpies were optimized by fitting the model to high-temperature zeta potential measurements (marked with a) and single-phase flooding experiments (marked with b). Δz_0 and Δz_1 correspond to the net charge distributed at the surface (0-plane) and IHP (1-plane), respectively. Since no outer-sphere complexes were considered, there is no net charge placed at the OHP (2-plane), i.e., Δz_2 is 0 for all surface reactions. The capacitances relating charge and potential between the surface and the IHP and the IHP and OHP are C_1=1.3 and C_2=4.5 F/m^2, respectively. The specific surface area (ssa) of the different carbonate rock samples was defined in agreement with the values indicated in the original publication; when the ssa was not reported, we assumed a value of 2 m^2/g.

Reactions	log K [25°C]	ΔH_r [kJ/mol]	Δz_0	Δz_1
$\equiv CaOH^{-2/3}+H^+ \leftrightarrow \equiv CaOH_2^{+1/3}$	12.85	-62.82[a]	1	0
$\equiv CaOH^{-2/3} \leftrightarrow \equiv CaO^{-5/3}+H^+$	-24.73	0.0	-1	0
$\equiv CaOH^{-2/3}+CO_3^{2-} \leftrightarrow \equiv CaCO_3^{-5/3}+OH^-$	1.55	20.68[a]	0.6	-1.6
$\equiv CaOH^{-2/3}+CO_3^{2-}+H^+ \leftrightarrow \equiv CaHCO_3^{-2/3}+OH^-$	10.15	25.48[a]	0.6	-0.6
$\equiv CaOH^{-2/3}+SO_4^{2-} \leftrightarrow \equiv CaSO_4^{-5/3}+OH^-$	0.35	100.0[a]	0.6	-1.6
$\equiv CO_3H^{+2/3} \leftrightarrow \equiv CO_3^{-1/3}+H^+$	-3.58	1.80[a]	-1	0
$\equiv CO_3H^{+2/3}+Ca^{2+} \leftrightarrow \equiv CO_3Ca^{+5/3}+H^+$	-2.80	39.69[b]	-1	2
$\equiv CO_3H^{+2/3}+Mg^{2+} \leftrightarrow \equiv CO_3Mg^{+5/3}+H^+$	-2.20	50.0[b]	-1	2

3.3.3 Microcalorimetry

When calcite is contacted by the aqueous solution, an important contribution to the measured enthalpy is expected to arise from the surface hydration. Thus, the enthalpy change recorded in microcalorimetric measurements depends on the surface coverage. If a water molecule binds to each surface site, up to

10^{-5} mol of H_2O hydrate 100 mg of calcite (assuming a specific surface area of 2 m^2/g). Depending on the enthalpy value for the adsorption of water on calcite, 10^{-5} mol of adsorbed water would result in an enthalpy release between 56 to 96 mJ[270,271], which is within the same range as reported in the microcalorimetry measurements from Cobos et al.[239]. However, the fact that the enthalpy of the rock-fluid interactions was determined indirectly from the enthalpies measured for the crude oil-brine-rock, crude oil-rock, and oil-brine systems adds uncertainty to the reported values as the water coverage of the calcite particles in the crude oil-brine-rock system is unknown.

Figure 3.14 shows a comparison of the experimental enthalpies measured through calorimetry at 70°C in different electrolyte systems and those predicted with the SCM. Except for the NaCl system, the calculated enthalpies follow a trend similar to the experimental measurements, i.e, $\Delta H_{CaCl_2} \approx \Delta H_{NaHCO_3} < \Delta H_{MgCl_2} < \Delta H_{Na_2SO_4}$. Although experimental[137] and molecular dynamics[155,157] studies suggest that Na^+ may not be an indifferent ion for the calcite surface, we are not aware of any evidence showing that Na^+ interacts strongly with the calcite surface (or stronger than Ca^{2+} or Mg^{2+}) at high temperature to explain the less endothermic response observed in presence of NaCl. It is also possible that in presence of NaCl the surface was less water-wet, leading to higher surface coverage with oil and overall less exothermic response. Recording the enthalpy changes directly in the calcite-brine system would be more valuable for the thermodynamic analysis of the mineral surface reactions as it would allow eliminating the uncertainty related to the surface coverage. In this way, the enthalpic effects of different electrolytes could be assessed relative to pure water.

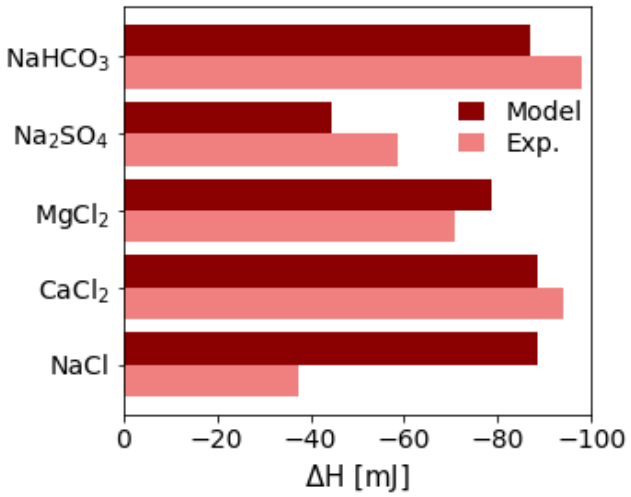

Figure 3.14. Comparison of measured and predicted enthalpy changes arising from the calcite interaction with different aqueous fluids at 75°C. Experimental data from Cobos et al.[239].

3.4 Conclusions

Isolating and quantifying the temperature effect on the contribution of simultaneous interactions exhibited at the calcite surface in aqueous environments is a challenging task. We derived reaction enthalpies for each interaction defined at the calcite surface by considering both zeta potential and flooding experiments. Our results indicate that calcite protonation is highly exothermic whereas the adsorption of Ca^{2+}, Mg^{2+}, and SO_4^{2-} are endothermic. We showed that these enthalpies are not univocal as they depend on the equilibrium constants at 25°C. For the specific case of sulfate adsorption, the equilibrium constant that satisfactorily described electrokinetic data at room temperature underestimated the sulfate retention measured in packed beds. Zeta potential may not be the best data to infer the effect of temperature on ion adsorption, as the transport of ions is influenced by local charges and not an average electrokinetic potential; this is even more relevant for natural samples that contain chemical heterogeneities that can strongly impact the reactivity at mineral surfaces. Moreover, although the calculated enthalpies were in agreement with the enthalpy changes indirectly inferred from

calorimetric titrations of calcite with crude oil and aqueous solutions, enthalpy data obtained directly when exposing calcite to different electrolytes would provide a more reliable characterization of the thermodynamics of ion adsorption. A wider experimental dataset is required to determine less uncertain enthalpy values, as well as to validate the assumption that the equilibrium constants show a temperature dependence consistent with van't Hoff equation.

4 An overview of the oil-brine interfacial behavior and a new surface complexation model

The few existing surface complexation models (SCM) for the brine-oil interface have important limitations: the chemistry of each crude oil is not considered, they cannot capture the water/non-polar hydrocarbons surface charge, the interactions between Na^+ and the acid sites are not included, and the equilibrium constants for the adsorption reactions are not validated against experimental data. We address the aforementioned constraints by proposing an improved diffuse-layer SCM for the oil-brine interface. The new model accounts for the chemistry of crude oil by considering surface sites linearly dependent on the TAN (total acid number) and TBN (total base number). We define weak sites to account for the negative surface charge observed for non-polar hydrocarbons in water. We optimize the parameters of our model by fitting the model to reported zeta potential measurements of oil in aqueous solutions. When we validate the optimized model against different experimental data sets, it generally shows a good performance for predicting the surface charge of oil in different brines with different pHs. We show that the acid and base numbers are only useful as a qualitative estimation of the distribution of polar groups at the oil surface, and a more sophisticated analysis is necessary to quantify the chemistry of the oil-brine interface.

This chapter is a revised layout of the article: M. Bonto, A.A. Eftekhari, H.M. Nick. An overview of the oil-brine interfacial behavior and a new surface complexation model. Scientific Reports, 2019.

4.1 Introduction

The increased oil recovery during low salinity waterflooding is a consequence of the interactions in the crude oil-brine-mineral system. While attempting to get more insight into this recovery method, most studies have focused on brine-mineral interactions. However, the idea that the increased oil recovery comes to a great extent from fluid-fluid interactions[162,272–274] has been recently gaining popularity. Several mechanisms related to the oil-brine system have been reported as responsible for the increased oil recovery: wettability alteration[162,275], viscoelasticity of the brine-oil interface[272,274,276,277], interfacial tension (IFT) alteration[278], emulsion formation[273,279], and viscosity decrease[273]. All these mechanisms, except wettability alteration, are linked exclusively to fluid-fluid interactions. In the following, we give an overview of previous studies on oil-brine interactions and their relevance to the mentioned mechanisms.

The wettability alteration relies on the stability of the water film found between the rock-brine and brine-oil interfaces; this stability is partially dictated by the surface charge at these interfaces. Comparable to the calcite surface, the interface between oil and water becomes charged due to the occurrence of acid/base interactions and adsorption reactions[280]. Ions present in the brine may be attracted to the water-oil interface, leading to an increase in their concentration at the interface and the development of a diffuse ionic layer. The thickness of the diffuse layer is related to the Debye length and therefore to the ionic strength. At lower ionic strength, the polar components of the oil may migrate and rearrange at the interface due to electrostatic attractions. However, when the salinity is increased, the Debye length is shorter, decreasing the attraction of the polar components[276]. The accumulation of active species at the interface will lower the IFT. The changes in the surface charge at the oil-water interface will also impact the interactions between oil droplets leading to changes in the rheological properties of the system[281,282]. The surface charge is indirectly estimated through electrophoretic mobility studies, which can be related to the zeta potential. The zeta potential measures the electrical potential at the surface of shear and indicates the adsorption and desorption of ions into the Stern layer[283]. To find the optimum concentration for the injection brine during modified salinity waterflooding, Jackson et al.[275] proposed to use zeta potential measurements at both brine-oil and mineral-brine interfaces. They correlated the cumulative increase in oil recovery with the cumulative normalized zeta potential, showing that a higher cumulative zeta potential leads to increased oil recovery. Through their integrated crude oil-brine-mineral zeta potential measurement, they showed that the oil-brine interface could be positively charged. Therefore, in such cases, the injected water composition should be selected in a way that also yields a positive zeta potential at the brine-mineral interface. Identical zeta potential polarity at both interfaces leads to repulsion and improves the stability of the water film, altering the wettability towards a more water-wet state. Sari et al.[284] highlighted the importance of the zeta potential at both oil-brine and mineral-brine interfaces and found a correlation between the absolute value of the sum of the zeta potential at the two interfaces and the contact angle; a higher modulus (i.e., identical polarity at the interfaces) corresponded to lower contact angles (a more water-wet state). Xie et al.[285] suggested studying the charges at both interfaces since the expansion of the double layer would be responsible for the wettability alteration. Alshakhs et al.[162] carried out zeta potential measurements at the rock-brine and brine-oil interfaces to discern which interface has a higher impact on the contact angle and disjoining pressure. They concluded that the wettability alteration is caused mostly by the brine-oil interactions. Contrastingly, Lu et al.[165] showed more skepticism regarding the relationship between the zeta potential and the contact angle. They explained that zeta potential measurements do not reflect the properties of the thin film interface, but rather the features of a region further away from this film. Therefore, the role of the thin water film properties on the wettability alteration might not be truly taken into account when a contact angle is inferred from these measurements.

The DLVO (Derjaguin-Landau-Verwey-Overbeek) theory has been widely used to explain the stability of emulsions, which are highly unstable colloidal systems. Higher electrostatic repulsive forces and,

therefore, higher zeta potentials theoretically increase the stability of these systems, while higher attractive van der Waals forces lead to instability[283]. García Olvera et al.[272] studied the changes in the viscoelasticity (a rheological property) and the emulsion stability of a sulfate-containing brine and different crude oil. A relationship between the asphaltene content and properties of the interface was observed: crude oil with higher asphaltene content showed higher elastic and viscous moduli and an increased IFT. The IFT decreased when sulfate was added to the brine. Additionally, they reported that naphtenic acids showed the opposite effect, destabilizing the emulsions. Contrary to this, Moradi et al.[286] found that both asphaltenes and naphtenic acids improve emulsion stability. They revealed that a higher ionic strength induces a better partitioning of the acids but inhibits asphaltene accumulation at the interface. Alvarado et al.[274] reported that the improved oil recovery is due to a combination of alteration of rock wettability and the development of interfacial viscoelasticity. Snap-off, which consists of the separation of the oil phase into a droplet or oil ganglion, might occur during secondary waterflooding. If an elastic interface is built up, the snap-off phenomenon can be reduced, which alters the residual oil saturation and possibly the relative permeabilities; consequently, this improves oil recovery. If the oil phase separation still occurs, some pore throats could be blocked due to the greater size of the droplets caused by the lower ionic strength, diverting the flow towards unswept zones. They attributed to this phenomenon the observed oscillations in the pressure drop during a tertiary waterflood. They also observed a higher oil recovery at low salinity compared to high salinity waterflooding, presumably caused by the higher elasticity between brine-crude oil in the presence of low salinity water. Chavez et al.[276] affirmed that injecting low salinity water allows the accumulation of amphiphilic components (i.e., components with both hydrophilic and hydrophobic parts) at the oil-brine interface, which increases the interface viscoelasticity and resulting in additional oil recovery. The higher interfacial elasticity prevents/reduces snap-off of the oil into small droplets, which leads to a more continuous interface that is easier to mobilize during waterflooding. By measuring elastic and viscous moduli of the interface, they studied the change in the viscoelasticity as a function of salinity, cation type, and the additional effect of a surfactant. They observed that the variation of viscoelasticity with salinity is nonmonotonic. A maximum in the viscoelasticity is observed at a specific salt concentration, beyond which the viscoelasticity decreases with increasing salt concentration. On the other hand, Ayirala et al.[287] reported that, even though the connectivity of the oil phase increases with increasing viscoelasticity of the interfacial film, very high viscoelasticity does not necessarily imply a higher oil recovery. Instead, they considered the coalescence time to contribute more to oil connectivity since this factor indicates the time that takes for the snapped-off droplets to reconnect. In the interfacial shear rheology experiments, the highest viscous and elastic moduli were obtained for the sulfate-containing brine. However, higher coalescence times were also obtained with this brine, indicating more isolation between the droplets. Thus, contrary to other publications[274,276], the authors conclude that ions that give rise to less rigid films and promote faster coalescence, reduce oil snap-off and increase the oil mobilization during waterflooding. All these seemingly contradictory observations can be better explained by a mechanistic model that describes the physicochemical interactions at the crude oil-brine interface and sheds light on the consistency of the reported data.

The role of IFT in low salinity waterflooding is a controversial topic. There is evidence that points to an increased oil recovery during low salinity waterflooding due to a decrease in the IFT[278]. However, the opposite is reported in other articles, which show a lower oil recovery factor due to IFT increase at lower salinities[288]. Lashkarbolooki and Ayatollahi[289] explain that the inconsistencies in the crude oil-brine IFT at different salinities arise from the different endogenous oil surface active components present in different oil samples; this requires further investigation. Zahid et al.[273] studied the formation of emulsions between three different crude oil types and seven brines. They observed emulsification between aqueous solutions and oil at room temperature, especially when distilled water or brine saturated in Mg^{2+} ions were used in the experiments. Although the ionic composition had an impact on the emulsification process, the authors could not establish any relationship between the salinity and the specific ion effect on the emulsion formation. Additionally, at high temperature and pressure, they

identified the formation of a possible microemulsion between one crude oil and an aqueous solution with increasing sulfate concentration, which could greatly influence oil recovery. The brine composition was also found to affect crude oil viscosity. The highest viscosity reduction was caused by sulfate ions, which were believed to promote a reorganization of the heavy components leading to a change in their shape ("coiling"). Gachuz-Muro et al.[290] also observed changes in the viscosity when placing different types of crude oil in contact with brine. They observed a higher viscosity alteration for very viscous oil. Chakravarti et al.[279] studied the effect of cation and anion types on emulsion formation between crude oil and brine. Emulsification, postulated to be triggered by heavier alkanes and acids, was observed in all cases. Therefore, emulsion formation depends on oil composition (especially the content of polar components) and salinity, reaching a maximum at a specific salt concentration. Sulfate and phosphate were identified as the most effective anions in promoting emulsification, while calcium and magnesium were the most effective cations. Perles et al.[291] reported that emulsions are stabilized through asphaltene adsorption at the oil-water interface and complexation of acidic groups with cations in the brine. They identified two basic steps in the stabilization process: first, accumulation of asphaltenes and resins at the oil-water interface, and second, a restructuring of the molecules at the interface, maximizing the intermolecular forces, through an "enthalpy-driven process"[292]. Although thicker and more rigid interfacial films were formed with saline solutions compared to distilled water, they found a specific salt concentration that resulted in maximum emulsion stability. Above this salt concentration, the excess of adsorbed molecules at the interface results possibly in greater compression of the interfacial film, hindering the stabilization mechanism; additionally, repulsion between adsorbed molecules can destroy the interfacial film, destabilizing the emulsions. The stability of emulsions is therefore related directly to the adsorption energy of the interfacially active molecules of the crude oil-water interface; increased energy of adsorption at the interface can enlarge the thickness of the interfacial film, decreasing the distance between the droplets and contributing to the steric stabilization of the emulsions. In a subsequent work[292], they highlighted the importance of temperature and aging time on the rheological properties of the crude oil-water interface, since these factors affect the diffusion of the surface-active molecules through the bulk phase and their reorganization at the interface. They also carried out interfacial rheological studies and measured higher elastic moduli (i.e., recoverable energy stored in the interface) and viscous moduli (i.e., dissipation of energy) in brine systems compared to deionized water. They indicated that the interfacial film provides more resistance to deformation and coalescence, which stabilizes the emulsions.

This work focuses on the interactions that occur at the crude oil-brine interface and attempts to find a mechanistic model that describes the physicochemical interactions at this interface. This model can serve as a foundation for explaining the role of oil and brine composition and their interactions on the interfacial properties of crude oil-brine systems, with several implications for the production and processing of crude oil. We first give a short overview of the existing models used to describe the electric properties of the oil-water interface. Then, we modify one of the models by including additional adsorption reactions and considering new types of surface sites. Finally, we test the accuracy of the optimized model by comparing its results with different zeta potential measurements available in the literature.

4.2 Previous models

Chow et al.[293] initially used the Ionizable Surface-Group model to predict the zeta potential of bitumen in brine solutions. This model assumes that the charge at the surface of bitumen comes from the dissociation of acid groups, which depends on pH and electrolyte concentration. To enable the prediction of the zeta potential using this method, the site density and the pK_a for the acid are required; these parameters were calculated by fitting the model to electrophoretic mobility measurements. In a later study[294], they also used this model to determine the surface charge of crude oil. Later, Buckley et al.[42] observed a positive charge on crude oil at low pH. They extended the Ionizable Surface-Group Model to account for both acid and base groups. All these studies assume that the zeta potential can be

calculated as the potential at an unknown and relatively short distance from the onset of the diffuse layer, taken as 0.5 or 0.6 nm. They obtained a different combination of parameters as a function of the slip plane distance. However, since the number of sites is part of the optimization process, no clear correlation is established between the content of active components in the crude oil and the surface site density. Therefore, this method would require an optimization procedure for each type of oil.

Das et al.[295] proposed a similar model for calculating the zeta potential of asphaltene in aqueous solutions. Their model considers the carboxylic and hydroxyl ionizable sites as proposed by Szymula et al.[296] and assumes that the zeta potential is equal to the surface potential. However, this method was not directly applied to oil-brine systems; the authors argued that crude oil might contain additional interfacially active material besides asphaltenes, which explains the lower zeta potential magnitudes for asphaltenes compared to crude oil. Brady et al.[94] proposed a surface complexation model to predict the zeta potential of oil in brine. They considered two surface sites: amine base sites and carboxylic acid sites. The basic sites only undergo protonation, yielding a positive surface charge at low pH. The acid sites can undergo dissociation and also react with divalent cations in the brine. No interaction with monovalent ions is considered. Furthermore, they assumed an equal number of base and acid sites. This model was also used in subsequent publications to reflect the chemical speciation with pH at the oil surface[297,298] and to show a correlation between the number of bonds between charged species on the oil and rock surfaces, and the contact angle[298]. However, the performance of the model to fit zeta potential experimental measurements was not demonstrated. Qiao et al.[96,97] also proposed a diffuse double layer model for the oil-brine interface. The model did not account for the contrasting chemistry of different crude oil types, assuming a constant number of carboxylic sites of 6 μmol/m^2. This surface complexation model was not tested against experimental data and while the equilibrium constants were reported as taken from Brady and Krumanshl[299], their values differed from those included in the aforementioned article. A common shortcoming of all these models is that they fail to reproduce the zeta potentials measured for hydrocarbons containing non-polar (ionizable) components (neither amine nor acid sites). Several publications[300–303] reported very negative zeta potentials for non-polar hydrocarbons (with no ionizable surface sites) in aqueous solutions. Most authors ascribe this observation to hydroxyl ion adsorption at the water-oil interface.

4.3 Surface complexation model

In the existing surface complexation models used to describe the electrical properties of the oil-brine interface, the number of sites is always taken as a constant, without accounting for the specific compositions of different crude oil[96,97]. The values of the equilibrium constants for the adsorption reactions of ionic species from the brine to the oil surface sites are often obtained from unspecified sources without proper validation. We address these issues by calculating the number of surface sites based on the measured concentrations of the acid and base groups. In addition, we validate the equilibrium constants by using oil in brine zeta potential measurements reported in the literature.

In this work, we consider a diffuse layer surface complexation model to estimate the surface potential, following the approach reported by Brady et al.[94]. In practice, the zeta potential is assumed to be equal to the surface potential[283]. Some other articles use the Debye Hückel approximation of the Gouy-Chapman theory to link the zeta potential to the surface potential[69,71]. However, this approximation should not be applied when the potentials are high (>25 mV); in such cases, the Poisson-Boltzmann equation needs to be solved. For systems containing 1:1 electrolytes, the Poisson-Boltzmann equation has an analytical solution known as the Gouy-Chapman equation[119].

The electrokinetic measurements rely on the assumption that the zeta potential is the potential at the boundary (shear plane) between the immobile and mobile phases. It is widely accepted that this plane lies close to the outer Helmholtz plane (OHP)[161,304]. Efforts have been made to provide methods to estimate the distance between these planes[305]. Different values for this distance can be found in various publications, i.e., 0.33 nm[71], 1-2 nm[304], 0.6 nm[42,294] and 2 nm[124]. Since there is no general agreement on

the location of the shear plane, we assume that the zeta potential is equal to the potential at the OHP (ζ=ψ_d) (see Figure 4.1), in agreement with many other publications, e.g., refs[67,93,306,307]. However, this assumption is not always valid; at high ionic strength, the exact location of the slip plane is required for the calculation of zeta potential (see e.g., chapter 1 of ref[305]).

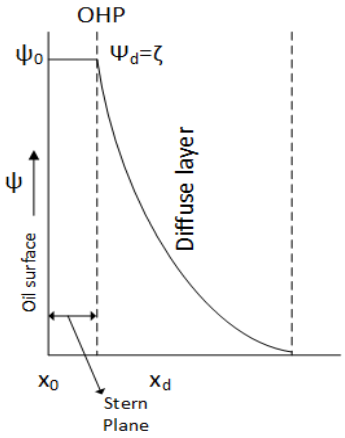

Figure 4.1. Schematic of the electrical double layer. The zeta potential is assumed to be equal to the potential at the d-plane (OHP).

The zeta potential, ζ, is then calculated in the speciation software PHREEQC[241] by explicitly defining "diffuse layer" calculations. The potential is computed by explicit integration of the Poisson-Boltzmann equation, following the procedure in Borkovec and Westall[308] (eq. 4.1):

$$\frac{d^2\psi(x)}{dx^2} = -\frac{F}{\varepsilon\varepsilon_0}\sum_{i=1}^{N} z_i(n_i(x) - {n_i}^0) \tag{4.1}$$

where the concentration $n_i(x)$ $[\frac{mol}{m^3}]$ at a distance x [m] follows a Boltzmann distribution (eq. 4.2):

$$n_i(x) = {n_i}^0 \exp\left(-\frac{z_i F\psi(x)}{RT}\right) \tag{4.2}$$

where F [C/mol] is the Faraday constant, ε_0 [8.85·10^{-12} F/m] is the vacuum permittivity, ε is the relative permittivity of water, z_i is the ionic valency, ${n_i}^0$ [mol/m^3] is the bulk concentration, R [8.314 J·mol^{-1}·K^{-1}] is the ideal gas constant, and T [K] is the temperature. Further details on the diffuse layer calculations may be found in refs[308,309].

It should be mentioned that the applicability of the Poisson-Boltzmann equation has limitations at higher ionic strength since it assumes that the ion density profile is only affected by the mean electrostatic potential[310,311]. As explained by Cavalli et al.[312], this equation only provides a good description of the system at low ionic strength where interactions between ions can be disregarded. However, Wang and Chen[313] showed that Poisson-Boltzmann provides a fairly good estimate of the ion density profile even at high concentrations, e.g., $1M$.

Another model uncertainty is the distribution of species around the oil-brine interface. The surface site density can only be defined when the interfacial region is exactly located[314]. Buckley et al.[42] highlighted that the oil-water interface is negatively charged due to the dissociation of carboxylic acids. However, at lower pH they observed a positive charge, indicating that base groups are also present at the oil-water interface. Among the acidic and basic functional groups, the naphtenic acids and the pyridinic nitrogen bases are considered the most interfacially active[315]. Naphtenic acids represent a mixture of cyclopentyl and cyclohexyl carboxylic acids mainly with molecular weight between 120-700 and a lower content

of other fractions (carboxyphenols, porphyrins, and asphaltene)[316]. Other researchers consider asphaltene content responsible for the charge development at the oil-brine interface[296,317]. Szymula et al.[296] reported that the surface charge of asphaltenes comes from the dissociation of carboxylic groups and the dissociation and protonation of hydroxyl groups, while Chaverot et al.[318] differentiate between the existence of either acidic (sulfuric or carboxylic) or basic (amine) groups. Generally, most authors accept that the charge at the oil-water interface comes from the ionization of base and acid surface groups. It is also widely agreed that the isoelectric point is not only affected by the base/acid ratio, but also by the absolute base number and the base and acid pK values[319].

The maximum number of acid and base sites can be calculated from the acid and base number (eqs. 4.3-4.4), respectively, as suggested in the work of Eftekhari et al.[69]:

$$N_{S,-COOH} = 0.602 \cdot 10^6 \cdot \frac{TAN}{1000 \cdot a_{oil} \cdot MW_{KOH}} \tag{4.3}$$

$$N_{S,-NH} = 0.602 \cdot 10^6 \cdot \frac{TBN}{1000 \cdot a_{oil} \cdot MW_{KOH}} \tag{4.4}$$

where $0.602 \cdot 10^6$ denotes the conversion factor from [mol/m^2] to [#/nm^2], $N_{S,-COOH}$ [#/nm^2] and $N_{S,-NH}$ [#/nm^2] denote the carboxylic and amine sites respectively, TAN [mg KOH/ g oil]$and\ TBN$ [mg KOH/g oil] denote total acid and basic number respectively, a_{oil} [m^2/g] denotes the specific area of oil, and MW_{KOH} represents the molecular weight of potassium hydroxide – 56.1 [g/mol].

The TBN is defined as the mass of KOH (in mg) equivalent to basic components per gram of oil, and the TAN represents the mass of KOH (in mg) required to neutralize acidic components in one gram of oil. For a crude oil with a high acid number (>1 mg/g KOH), most molecules at the oil-water interface would be carboxylic acids[320]. Due to their amphiphilicity, acids and bases can adsorb and desorb at the oil-water interface, ultimately reaching a new equilibrium[321]. Generally, the effect of the acid fraction on the oil-water interface has been more extensively studied than the basic fraction. Andersen et al.[322] showed through an infrared spectroscopic analysis of the crude oil-water interfacial film that the concentration of carboxylic acids is higher at the interface. When small amounts of acid were removed from the crude oil, increased IFT was observed. Through similar analysis, Guo et al.[323] also proved that active interfacial components, e.g., carboxylic and phenolic groups in the asphaltene fraction, are the main molecules present at the oil-water interface. Rønningsen et al.[324] emphasized the importance of the acid number as indicative of the tendency of crude oil to form stable emulsions with the water. Havre et al.[325] suggested that the amount of different acids in the bulk phase dictates the amount at the oil-water interface and that the dissociated acids are more interfacially active than the undissociated ones. Moradi et al.[286] reported competitive adsorption between asphaltenes and naphtenic acids at the oil-water interface. While asphaltenes adsorb at the interface forming a more rigid film structure, the dissociated naphtenic acids can also react with the cations in the brine, forming naphtenate salts. These salts can eventually accumulate at the water-oil interface decreasing the interfacial tension significantly.

The effect of bases on the oil-water interface has been studied less and is still not fully understood[322,326]. The structure of the basic components is derived mainly from pyrrolic and pyridinic groups, with the latter being the most interfacially active[321,327]. Saliu et al.[328] suggested that bases affect the oil-water emulsions only by stimulating other active fractions that are present in a latent state in the crude oil. Thus, bases are believed to interact with naphtenic acids from crude oil, eventually leading to emulsification. On the other hand, in IFT studies, Bertheussen et al.[321] observed no interactions between the acids and bases, inferring that they do not exist simultaneously in dissociated form due to similar pK_a values. Nenningsland et al.[326] studied the effect of basic molecules on the water-oil interface and observed changes in the IFT due to the bases protonation below a pH of 5, but no effect was observed on the surface pressure at a liquid/gas interface. However, the IFT decrease at low pH (where

protonation of bases occurs) was less than at high pH (where dissociation of carboxylic acids occurs), suggesting that bases have a lower surface affinity than naphtenic acids[321,326]. Hutin et al.[329] reported that higher TAN usually implies a lower IFT; even though basic components are expected to have a similar effect, the transfer of acid groups to the interface is much greater than the transfer of basic species, hence the predominant negative charge of crude oil[330].

Crude oil with the same base or acid number may develop a very different surface charge due to a contrasting surface species distribution. Conflicting views exist on the amount of active material in the bulk oil that can travel to the interface. Some authors argue that most bases and acids are thermodynamically favored to accumulate at the oil-water interface rather than staying in the bulk fluid[320]. Others suggest that the total acid/basic/asphaltene content should not be considered interfacially active and that the composition at the interface is very different from the composition in the bulk oil or brine[331]. In support of the latter group, Yang et al.[332] consider that only a fraction of the asphaltene content is responsible for emulsion stability. They proposed a method for separating the interfacially active asphaltene fraction and studied the emulsion stability. The interfacial film formed by this fraction, which represented only 2% of the total asphaltene content, was more rigid than the one generated by the remaining asphaltene fractions. In a later study[333], they showed that the interfacially active asphaltene fraction has a higher average molecular weight (1000-1200 g/mol) and a higher oxygen content than the remaining asphaltene fraction (700-750 g/mol), associated with sulfoxide groups. Furthermore, Chaverot et al.[318] reported that only 0.015% of the asphaltenes are surface-active, and at pH=2 the concentration of molecules adsorbed at the interface ranged from 1.9×10^{-7} to 2×10^{-6} mol/m^2.

In this work, besides the acid and base sites considered in the model proposed by Brady et al.[94], an additional type of weak site is included in the model. These weak sites account for the reported adsorption of hydroxyl ions at the non-polar hydrocarbon-brine interface. The performance of the model is assessed with and without these additional sites. While the amine and carboxylic site density ($N_{s,\,-NH}$ and $N_{s,\,-COOH}$, respectively) vary as a function of the AN and BN, the weak site density is constant at 0.3 #/nm^2, a value that was found to be almost independent of the type of oil[300]. Additionally, we constrain the range of oil site densities, based on experimental evidence that shows that only a fraction of the acid and bases will be present at the interface and that the acidic components are the most interfacially active[322–325]. Thus, we correlate the carboxylic sites linearly with the AN, by specifying a minimum $N_{s,\,>COOH}$ of 0.5 #/nm^2 (corresponding to AN=0.05) and a maximum $N_{s,\,>COOH}$ of 2.5 #/nm^2 (corresponding to AN=3). Analogously, the amine sites are correlated linearly with the BN, ranging from 0 (BN=0) to 2 (BN=3). However, if this approach yields $N_{s,\,-COOH} < N_{s,\,-NH}$, we set the amine site density equal to the carboxylic site density since we found no evidence in the available literature supporting the predominance of basic species over acid species at the brine-oil interface. Furthermore, the maximum value for the acid site density is chosen by analogy with the site density found for oil (benzene and decane) in the presence of surfactants[314]. These upper and lower limits for the AN and BN were used because the available experimental data falls within this range, although AN and BN can show larger values. Thus, in contrast to the Ionizable Surface-Group model used in refs[42,294], we do not include the number of sites in the optimization. Rather, we expect to provide a tool that can predict the isoelectric point and the zeta potential distribution relative to pH with reasonable accuracy, based on input parameters such as AN and BN. Moreover, if the surface site density is part of the optimization procedure, physically unrealistic values can be obtained, e.g., values that are higher than the maximum number of sites calculated from the total number of acid and basic molecules. For instance, in ref [42] a site density of 2 #/nm^2 is obtained in the optimization for a North Sea crude oil (ST-86-1) with a low acid number (0.15 mg/g KOH); however, if the site density is calculated from the actual number of molecules and specific surface area (calculated considering the crude oil density and assuming spherical droplets), a value around 0.6 #/nm^2 would be obtained. For the different experimental datasets considered in this work, the defined surface site densities obtained as a function of the crude oil base and acid number are shown in Table 4.1. We also consider additional complexation reactions between

the Na^+ and the carboxylic sites. The reactions included in the model and the initial equilibrium constants are shown in Table 4.2.

Table 4.1. Experimental acid and base number of the crude oils and defined surface site densities in the modeling for the utilized experimental data sets.

Ref	Type of oil	AN (mg/g KOH)	BN (mg/g KOH)	N_{-COOH} (#/nm^2)	N_{-NH} (#/nm^2)
Kolltveit[334]	Crude oil A	3	0.8	2.5	0.6
	Crude oil B	2	0.8	1.8	0.6
	Crude oil C	1	0.8	1.15	0.6
Buckley et al.[42]	Moutray	0.26	-	0.7	0.1
	Leduc	0.15	-	0.6	0.3
	ST-86-1	0.15	-	0.6	0.03
Chow et al.[294]	Moutray	0.26	-	0.7	0.1
	Bitumen	2	-	1.8	0.05
Alshakhs et al.[162]	Crude oil	1.15	1.25	1.2	0.8
Nasralla et al.[335]	Crude oil A	0.18	1.65	0.6	0.6
	Crude oil B	0.11	0.62	0.3	0.55
Ayirala et al.[287]	Crude oil	0.05	0.7	0.5	0.35
Takeya et al.[336]	Crude oil	0.39	1.86	0.75	0.75
Lu et al.[165]	Oil 1	0.21	5.6	0.6	0.6
	Oil 2	0.18	1.14	0.6	0.6

Table 4.2. Surface reactions and equilibrium constants before and after optimization. Column A refers to the log *K* values obtained when the optimization was performed considering weak sites (Model A); column B gathers the values in the absence of weak sites (model B); column C contains the log *K* values in the absence of weak sites and without considering the interaction between the surface of oil and Na^+ (model C).

Surface sites	Nº	Reactions	log *K*	A	B	C
Amine ≡NH	4.1	$\equiv NH+H^+ \leftrightarrow \equiv NH_2^+$	5.5	7.27	6.70	6.60
Carboxylic ≡COOH	4.2	$\equiv COOH \leftrightarrow \equiv COO^- + H^+$	-4.75	-4.62	-4.65	-4.80
	4.3	$\equiv COOH+Na^+ \leftrightarrow \equiv COO\text{-}Na+H^+$	-4.86	-3.40	-3.67	-
	4.4	$\equiv COOH+Ca^{2+} \leftrightarrow \equiv COO\text{-}Ca^+ + H^+$	-3.82	-3.30	-3.40	-3.4
	4.5	$\equiv COOH+Mg^{2+} \leftrightarrow \equiv COO\text{-}Mg^+ + H^+$	-3.47	-3.30	-3.40	-3.4
Weak ≡wOH	4.6	$\equiv wOH \leftrightarrow \equiv wO^- + H^+$	-8.93	-6.23	-	-
	4.7	$\equiv wOH+Na^+ \leftrightarrow \equiv wO\text{-}Na+H^+$	-8.93	-5.70	-	-
	4.8	$\equiv wOH+Ca^{2+} \leftrightarrow \equiv wO\text{-}Ca^+ + H^+$	-5.85	-4.6	-	-
	4.9	$\equiv wOH+Mg^{2+} \leftrightarrow \equiv wO\text{-}Mg^+ + H^+$	-5.85	-4.6	-	-

These initial intrinsic equilibrium constants are taken from the analogous aqueous reactions (of acetic acid and acetate) from the LLNL (Lawrence Livermore National Laboratory) database[241]. However, the actual occurrence of these adsorption reactions and the distribution of base and acid sites at the oil surface still needs to be experimentally investigated. The equilibrium constants for reactions 1-3 and 6-7 from Table 4.2 are optimized (with and without weak sites) by fitting the model to the experimental data from Buckley et al.[42] using a Julia[337] implementation of the Levenberg-Marquardt optimization algorithm[338,339]. The equilibrium constants for Ca^{2+} are further refined by fitting the model to the experimental data of Chow et al.[294], and the stability constant for the interaction of carboxylic sites with Mg^{2+} ions is considered to be the same as for Ca^{2+}. The optimized values are included in Table 4.2. In comparison with the calcite/brine system, the zeta potential measurements for the oil-brine interface are

relatively scarce and performed predominantly in 1:1 electrolyte systems. Moreover, the model is also optimized when no weak sites and no surface complexation between acid sites and Na^+ are considered (similar to the model of Brady et al.[94]).

4.4 Results and Discussion

The results of the optimized surface complexation model fitted to the experimental data from Buckley et al.[42] are shown in Figure 4.2. Since the base number was not reported in the cited work, we estimated the base site density from the relationship between acid/base site density ratio and the isoelectric point (IEP) inferred previously from Kolltveit's experimental data[334]. We are aware that this approach might be inaccurate, but IEP and BN/AN ratio were previously shown to be correlated[319]. The site densities are presented in Table 4.1. The low amine surface site density for the ST-86-1 crude oil is inferred because of the very low IEP (around 3). The solid lines correspond to the fitted model when weak sites and reaction with Na^+ are considered (Model A), the dashed lines represent the model in the absence of weak sites (Model B), and the dotted lines correspond to the model when no weak sites and no Na^+ interactions are considered (Model C). It is observed that the model that considers the interaction between sodium and carboxylic sites fits the data better compared to model C (which does not consider interaction with Na^+). The interaction between this monovalent ion and the carboxylic groups was already investigated and confirmed through molecular dynamic simulations in refs[340,341]. When this additional reaction was not considered (Model C), the model could not be successfully fitted to the experimental data set. It should be mentioned that the model proposed by Buckley et al.[42] fits satisfactorily to their experimental data by considering only de/protonation. However, they used the surface site density as an adjustable parameter, and they also defined a constant slip plane distance of 0.6 nm for the calculation of the zeta potential. Furthermore, since in the diffuse layer model all ions are assumed to be adsorbed as inner-sphere complexes in the d-plane, the IEP predicted by the models for the Leduc crude (Figure 4.2-b) changes with the NaCl concentration. However, this experimental data does not suggest changes in IEP with changes in the NaCl concentration, in contrast to the experimental data from Kolltveit[334].

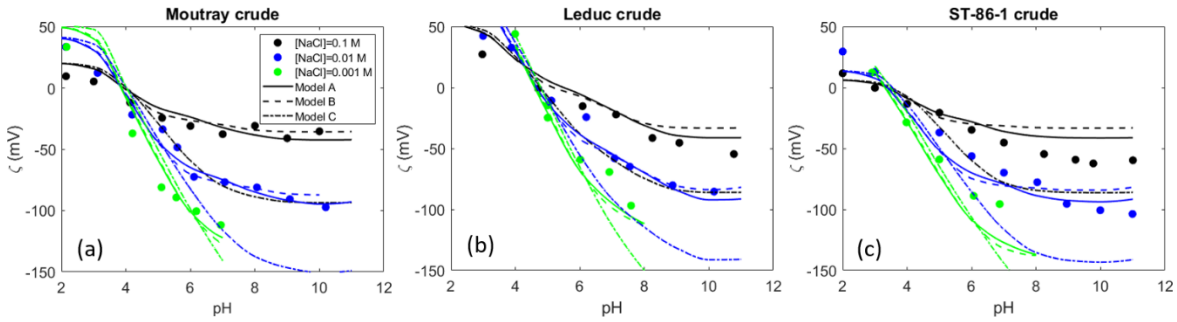

Figure 4.2. Zeta potential of three different crude oils in three different ionic strength NaCl solutions. The solid lines represent the prediction of the surface complexation model when considering weak sites, the dashed lines correspond to the case which does not consider weak sites (Model B), and the dotted lines represent the fit of the model when no weak sites and no Na^+ interaction with the crude oil are considered (Model C).

It can also be observed that model A fits the experimental data slightly better, especially for crude oil ST-86-1 (Figure 4.2-c). However, the base site density defined for the ST-86-1 crude is not sufficient to capture the positive zeta potential at lower pH values. Nevertheless, if the base site density is increased while keeping the same acid (or acid and weak) site density value, the IEP predicted by the model would be shifted to the right. The very low isoelectric point and the more positive zeta potential values might suggest a combination of a greater number of basic species at the surface at low pH with, probably, increased hydroxyl adsorption at the surface, a trend that could be predicted by increasing the number of weak sites. We must note that the acid site density cannot be increased more than the number of acid molecules indicated by the acid number of the oil, even though the AN is not a sufficient measure of the amount of active species at the interface. All in all, we postulate that defining higher surface site densities would not be reasonable since, according to the calculations (applying eq. 4.3), there would

not be enough acid molecules to yield a higher surface site density, even if all acid molecules accumulated at the interface. Therefore, it seems plausible that, in this case, the very negative zeta potential at high pH comes from the adsorption of hydroxyl ions at the interface. No major differences are observed between the goodness of fit of Model A and B since the combination of the equilibrium constants obtained through the optimization yields mostly the same results.

Similar experiments were carried out previously by Kolltveit[334]. The prediction of the models for this experimental data set is shown in Figure 4.3. Again, the model without Na^+ reaction (Model C) shows worse performance than the other two variants. Moreover, the models predict an IEP slightly shifted to the right for Crude Oil A (Figure 4.3-a) and Crude Oil C (Figure 4.3-c). Generally, in terms of zeta potential magnitudes, the experimental data is predicted better by Model A, though the performance of Model B is comparable and predicts the IEP slightly better. Furthermore, despite the lowest acid number of crude oil C, (see Table 4.1) at high pH, this crude oil shows comparable negative zeta potential values to crude oil A, which has three times higher AN. The very negative zeta potential values imply that, even though it has a lower acid number, this crude oil may have a higher number of active carboxylic acids at the surface than the other two, yielding the negative charge at high pH through the dissociation of the acids. Similarly, even though all crude oil types have the same base number, crude oil B shows considerably higher positive zeta potentials at low pH, especially at the lowest ionic strength. This indicates that TAN/TBN are not reliable indicators of the number of active molecules at the oil surface. This phenomenon complicates the development of consistent models for the oil surface charge prediction since there is no strong premise to support the surface site density definition.

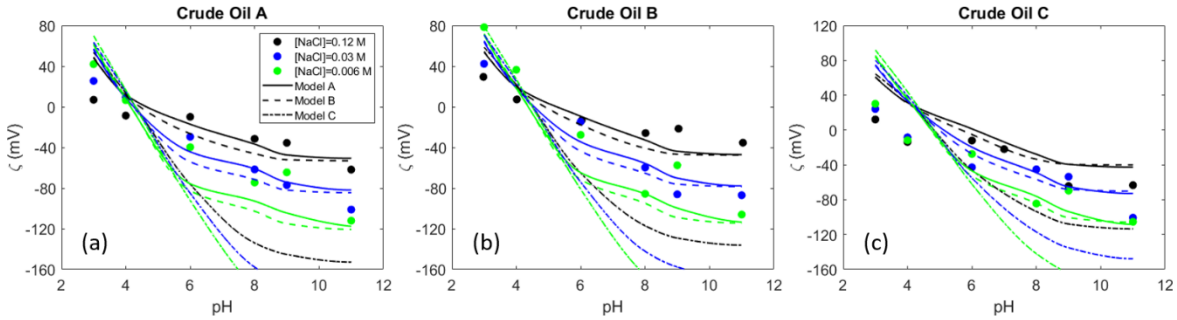

Figure 4.3. Zeta potential of three different crude oils in three different ionic strength NaCl brines.

Chow et al.[294] performed zeta potential measurements of bitumen and crude oil sample in NaCl brine. The acid number and the defined surface site densities of the samples are shown in Table 4.1. In this case, the base number was not reported. Therefore, it is estimated using the same procedure as for the experimental data of Buckley et al.[42]. The zeta potential prediction at two different ionic strength NaCl solutions is shown in Figure 4.4. Although the model accurately replicates the zeta potential trend, the experimental values are slightly lower than the model predictions. Model A provides a better prediction for the Moutray crude oil than model B. The prediction of model C deviates considerably at higher pHs, especially at lower ionic strength.

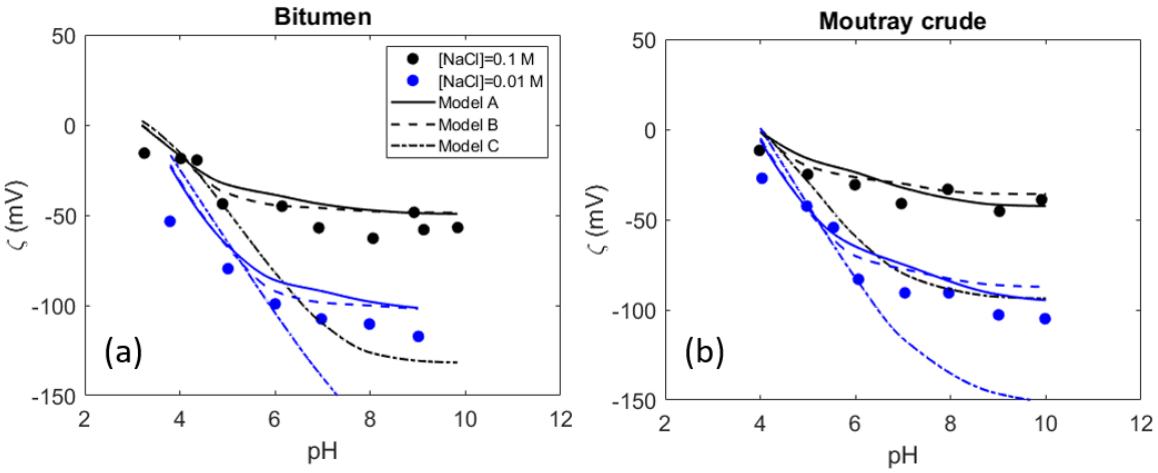

Figure 4.4. Zeta potential of **(a)** bitumen and **(b)** crude oil sample in two different ionic strength NaCl brines.

Chow et al.[294] also studied the effect of calcium ions by measuring the zeta potential in NaCl/$CaCl_2$ brine mixtures. The results of the model for this experimental data are shown in Figure 4.5. The model correctly predicts the decrease in the negative magnitude of the zeta potential with increasing Ca^{2+} concentration (Figure 4.5-a) and the fast decrease in the zeta potential with pH. At first, a higher number of carboxylic sites are available to form complexes with Na^+ and Ca^{2+} in the brine, increasing the surface charge. As soon as the surface sites are occupied, the zeta potential does not change further (Figure 4.5-b). The model satisfactorily predicts the diminished calcium effect observed at pH=4 due to reduced complexation between carboxylic acids and cations at lower pH compared to that at pH=10 (Figure 4.5-c). A similar fit is obtained when weak sites, no weak sites, or no Na^+ are considered, with the model that considers weak sites (model A) showing a slightly better performance.

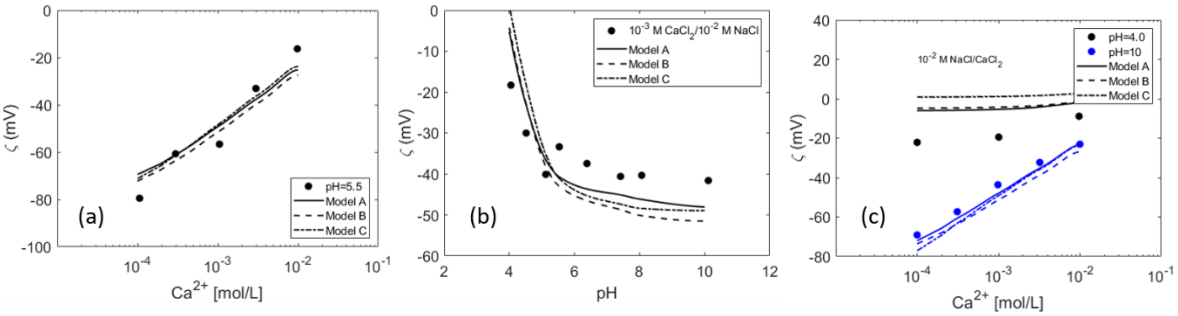

Figure 4.5. Zeta potential measurements of **(a)** bitumen at increasing Ca^{2+} concentration at a fixed pH=5.5; **(b)** crude oil sample in a $CaCl_2$/ NaCl brine mixture at different pHs **(c)** crude oil in a brine mixture with increasing $CaCl_2$ concentration at two different pH values. The equilibrium constant for the Ca^{2+} adsorption reaction was obtained by fitting the model to this experimental data.

Alshakhs et al.[162] measured the zeta potential of crude oil in different brine mixtures. They conducted the measurements at even lower ionic strength and also added Mg^{2+} and SO_4^{2-} to the brine. The results of the model are compared with this experimental data set in Figure 4.6.

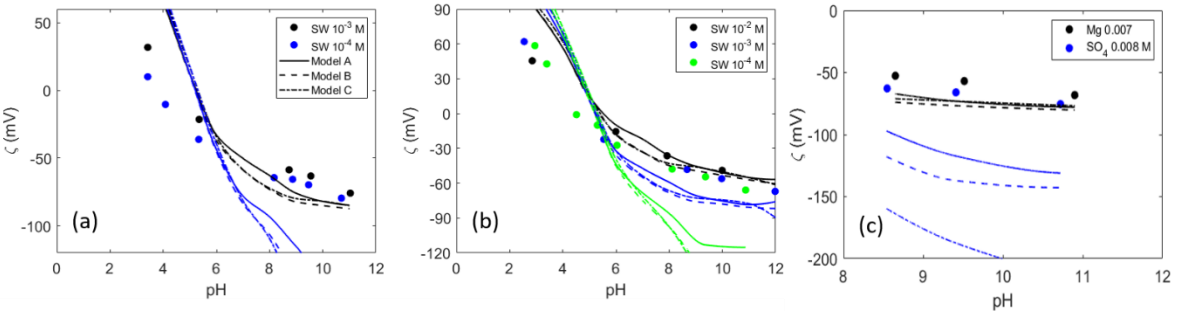

Figure 4.6. Zeta potential of crude oil in different brine compositions and ionic strength.

SW brine (Figure 4.6-a) is a combination of Na^+, Mg^{2+}, SO_4^{2-} and Cl^- ions. $MgSO_4$ brine (Figure 4.6-b) has the same ionic composition but is enriched in Mg^{2+} and SO_4^{2-}. Lastly, the Mg brine contains no SO_4^{2-} and the SO_4 brine contains no Mg^{2+} (Figure 4.6-c). The AN and BN of the crude oil are shown in Table 4.1. This crude oil had a significantly higher acid number than the samples studied by Chow et al.[294] and Buckley et al.[42]; but, surprisingly, the zeta potential values are less negative at high pH, even when measured at lower ionic strength. This could be a consequence of the Mg^{2+} which forms positive complexes with the carboxylic sites, making the zeta potential less negative. Moreover, this experimental data shows almost no variations in the zeta potential with ionic strength, in contrast to the other experimental data sets used in the present work. The measurements suggest that sulfate has a similar effect on the oil-brine zeta potential as Mg^{2+} (Figure 4.6-c), i.e., that of increasing the zeta potential. In contrast, other publications suggest that sulfate ions interact only with the mineral and not with the crude oil[94]. A higher contact angle was observed by Alshakhs and Kovscek[162] in the presence of sulfate ions, suggesting that sulfate does not increase the water wetness and that magnesium ions are more effective in altering the wettability toward water-wet conditions. Our models predict larger differences between the zeta potential at the three different ionic strengths compared to this experimental data set. Moreover, the base number reported for this crude oil is higher than the acid number and due to the combination of defined surface site densities, our models predict a higher isoelectric point, suggesting that the actual amine site density may be lower than the specified one. However, differences between the model and the experimental data could also arise because of incorrect equilibrium constants. In the model, all acid and base sites are considered to be identical; in reality, the AN and BN include acids and bases of different types which could certainly react differently with the ions in the brine.

Nasralla et al.[342] investigated the role of double layer expansion in the improved oil recovery during modified salinity waterflooding by measuring the zeta potential at both mineral-brine and brine-oil interfaces. Among multiple mechanisms for this recovery process, they considered the expansion of the double layer as the most dominant mechanism. They did not observe any increase in the oil recovery in tertiary mode (i.e., injecting low salinity brine into a core that is already flooded with the initial formation brine). This emphasizes the importance of the initial wetting state condition of the mineral in the success of smart waterflooding. To explain these observations, a later work studied the effect of the injection water salinity and cation type on the zeta potential[335]. They measured the zeta potential of two different crude oil in NaCl, $CaCl_2$, and $MgCl_2$ solutions at a pH value of around 4. The AN and BN of the oil samples are shown in Table 4.1. The performance of the models against the experimental data is assessed in Figure 4.7.

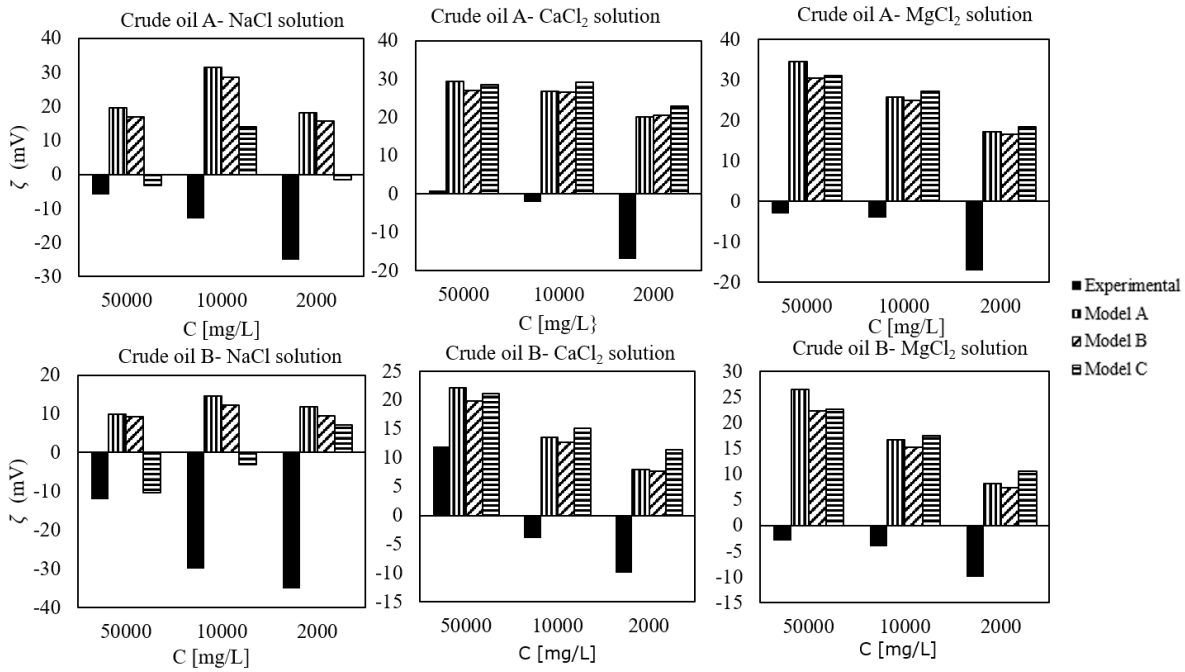

Figure 4.7. Zeta potential of two different crude oil in NaCl, $CaCl_2$, and $MgCl_2$ aqueous solutions at a pH ≈4. Data from ref[335].

These measurements are performed at a higher ionic strength than the previous data sets. This experimental data also shows that Mg^{2+} and Ca^{2+} interact mostly in the same way with the crude oil acid sites. This justifies the use of the same equilibrium constant for the adsorption of Ca^{2+} and Mg^{2+} on the carboxylic sites. It also questions the accuracy of the models that include the interaction of Mg^{2+} with the calcite surface sites but not with the oil[297]. Both crude oil types have a low acid number and a higher base number. Even though crude oil B has a lower AN, the experimental zeta potential values are more negative in the NaCl brine, while less negative values are obtained experimentally in the presence of $CaCl_2$ and $MgCl_2$. Our model cannot capture this trend because the surface site density is defined only by the AN and BN. It is possible to match the experimental data by including more types of surface sites and optimizing the equilibrium constants. However, the number of variables in the optimization becomes more than the number of data points, which makes the model overly complicated and impractical.

Overall, the prediction of the model for these experiments is not satisfactory, since in most cases the model does not even predict the correct polarity of the zeta potential. This indicates that the number of amine sites that are input to the model must be lowered for the model to be able to capture the IEP, which from these measurements appears to be somewhat lower than 4. The discrepancy between the model and the experimental evidence could be a consequence of the higher ionic strength of the brines in these experiments; note that the optimization of the model parameters was performed using zeta potentials obtained at lower ionic strength. Moreover, in this work a high oil/brine volume ratio is used in the electrophoretic measurements (20%), whereas much lower values (<1%) were reported in other publications[42,287,294,301]. The modeling of these data would benefit from more information on the experimental conditions (i.e., oil drop size, closed or open system, etc.). Ayirala et al.[287] performed zeta potential measurements on crude oil with very low AN and high BN (Table 4.1) in four different brines. Theoretically, a positive surface charge would be expected throughout the whole pH interval, since the fraction of acids undergoing dissociation is expected to be very low. As observed in Figure 4.8, if only acid and base sites are considered, the predicted zeta potential has a lower magnitude than measured. In this case, model C provides the best prediction for the systems that contain NaCl and Na_2SO_4. This shows that including a surface complexation reaction with Na^+ or defining weak sites improves the goodness of the fit. The fact that the pH of the oil-brine emulsions is not reported before the

electrophoretic measurements (the pH of the brines is reported instead) can also lead to differences between the predicted and the experimental zeta potential values. The authors mention that the negative surface charge of the oil can be explained by the brine pH of around 6. However, knowing the actual pH of the oil-brine system would facilitate the comparison between the results from the model and the experimental data.

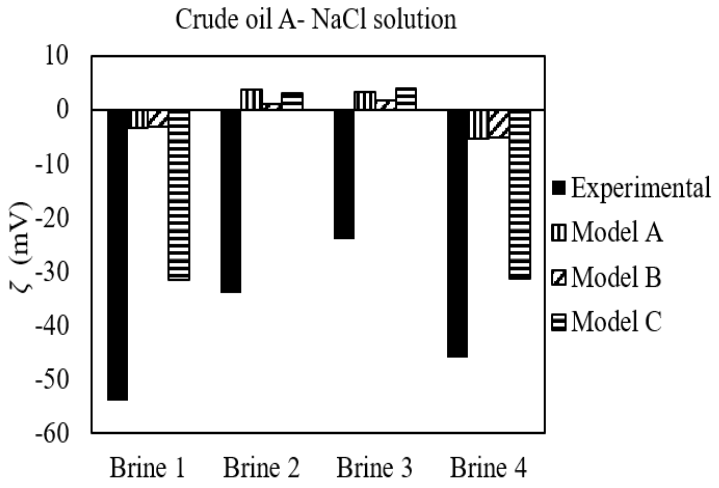

Figure 4.8. Zeta potential of crude oil in four different brines (measurements performed at pH≈6). Composition of the brines: brine 1- Na^+ and Cl^-; brine 2- Mg^{2+} and Cl^-; brine 3- $Ca^{2+}$and Cl^-; brine 4: Na^+ and SO_4^{2-}. All brines have similar ionic strength.

Takeya et al.[336] measured the oil-brine zeta potential in electrolyte solutions containing Na^+, Cl^-, Ca^{2+}, and Mg^{2+}. They performed these experiments at 50 ºC and only at pH values above 7. Based on these measurements, they proposed a CD-MUSIC model that represents the shift in the surface charge as a result of the deprotonation of carboxylic acid sites and their complexation with divalent cations in solution. Since no basic sites are considered, their model would not be able to capture the positive zeta potentials at low pHs. Figure 4.9 shows the experimental data at increasing calcium or magnesium concentration at a fixed pH. The three models correctly predict the shift in the zeta potential towards more positive values with increasing divalent cation concentrations. The model that does not consider weak sites (Model C) predicts more negative values since there are fewer sites available for interaction with Ca^{2+} and Mg^{2+}.

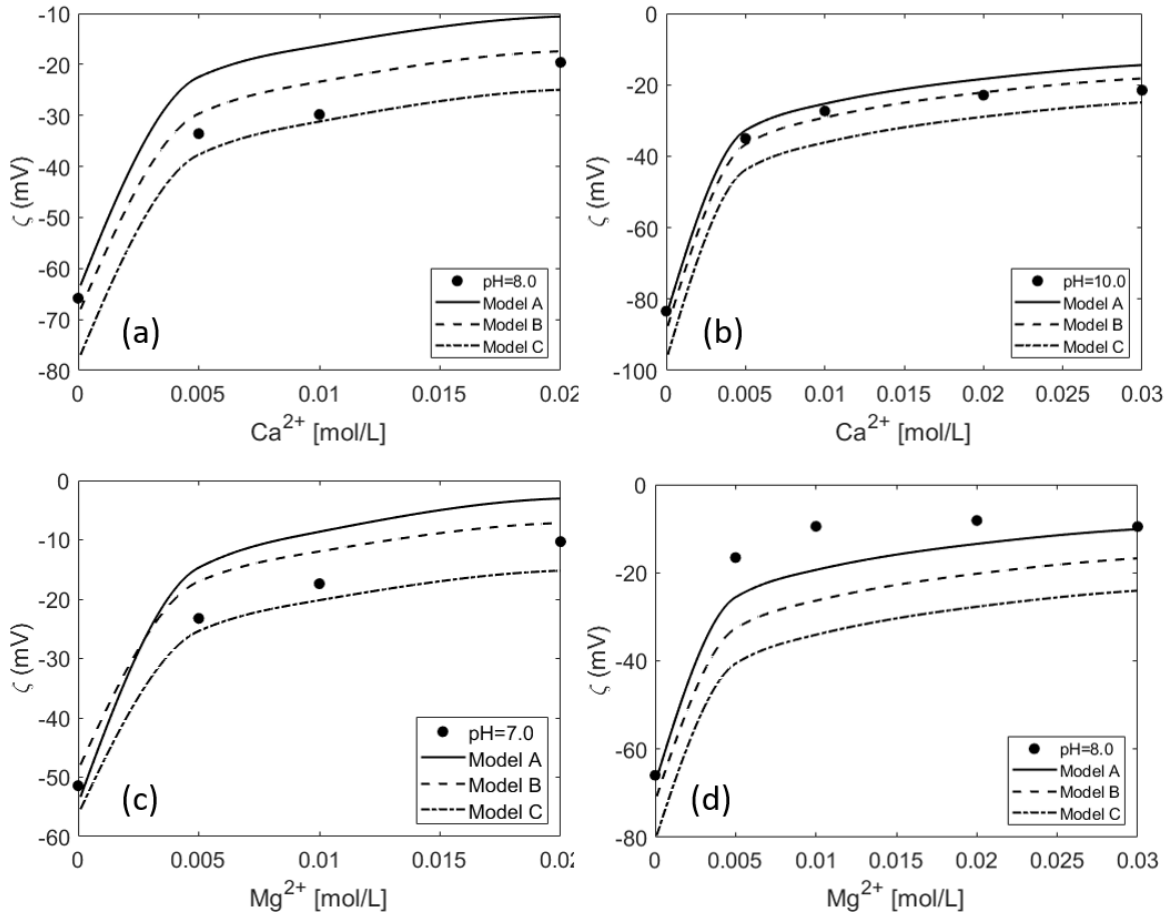

Figure 4.9. Experimental data from ref[336]: Measurements at varying **(a)** $CaCl_2$ concentration at a fixed pH=8 **(b)** $CaCl_2$ concentration at a fixed pH=10 **(c)** $MgCl_2$ at a fixed pH=7 **(d)** $MgCl_2$ at a fixed pH=8.

Figure 4.10 shows zeta potential measurements at a constant ionic strength of 0.02 M with increasing Ca^{2+} (Figure 4.10-a) and Mg^{2+} (Figure 4.10-b) concentrations. No pH values are reported for these measurements so they were modeled by assuming the equilibrium pH predicted by PHREEQC. As observed in Figure 4.10-a and -b, the model does not predict the jump in the zeta potential between 0-0.002 M Ca^{2+}. More measurements would be needed at intermediate Ca^{2+} values to see the actual trend of the data between these two points. Moreover, comparing Figure 4.10-a and the changes in the zeta potential with pH at constant ionic strength (Figure 4.10-c) shows that the value of 120 mV in 0.02 M NaCl corresponds to approximately a pH=10. This means that the first measurement in Figure 4.10-a would correspond to a very high pH (≈10). However, the equilibrium pH predicted by PHREEQC for that system is around 6.6, which could explain the differences in the prediction of the model and the experimental zeta potential. This demonstrates the importance of monitoring the pH during the zeta potential measurements. Having the pH as an input to the model would add more consistency to the comparison between the model and experimental data. Finally, differences in the predicted and measured values may also arise due to the higher temperature of the oil-brine system. In this study, the standard enthalpy of the surface complexation reactions (see Table 4.2) were taken from the LLNL database for the analog aqueous phase reactions, and the equilibrium constants were then calculated at the specified temperature from the van't Hoff equation within PHREEQC.

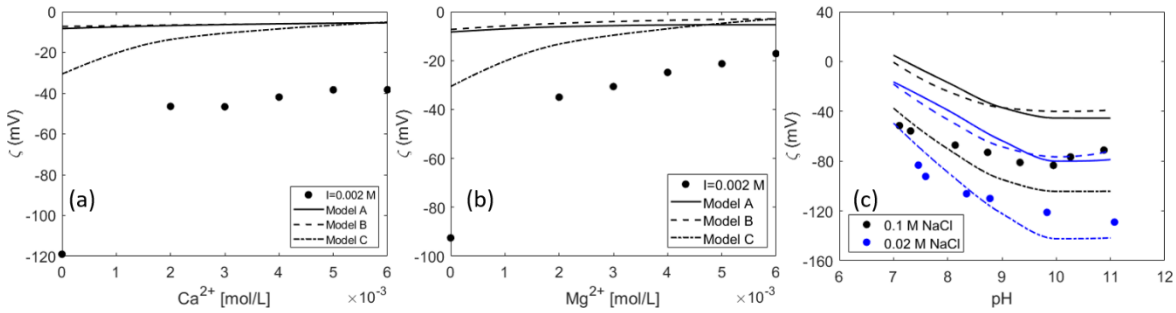

Figure 4.10. Experimental data from ref [336]: Measurements at a constant ionic strength (fixed with NaCl solution) at increasing: **(a)** $CaCl_2$ concentration **(b)** $MgCl_2$ concentration **(c)** 0.1 and 0.02 M varying pH.

Lu et al.[165] studied the temperature effect on the interactions at the calcite-brine and oil-brine interfaces. They measured the zeta potential at the oil-brine interface for two different types of oil in NaCl and $MgCl_2$ from low (10^{-5} M) to very high (3 M) concentrations. Only the experimental data up to 0.1 M is modeled here. Following the procedure used to link the surface sites to the TAN and TBN, we used the same amine and carboxylic sites for both crude oil samples. This is also in fair agreement with the experimental data, which shows no major differences between the zeta potential measurements for the two crude oil types. Since no information on the equilibrium pH is provided, the data is modeled assuming the equilibrium pH predicted by PHREEQC. However, as explained earlier, this might be very different from the actual pH of the system, resulting in discrepancies between the modelled and measured zeta potential. Generally, the model prediction for the NaCl system (Figure 4.11-a) is not as good as for the system with Mg^{2+} (Figure 4.11-b). A nonmonotonic behavior of the zeta potential is observed experimentally in the presence of monovalent electrolytes, which cannot be captured by the models if the equilibrium pH is assumed. Specifying the measured pH would make the predictions of the model and the interpretation of the experimental data more reliable.

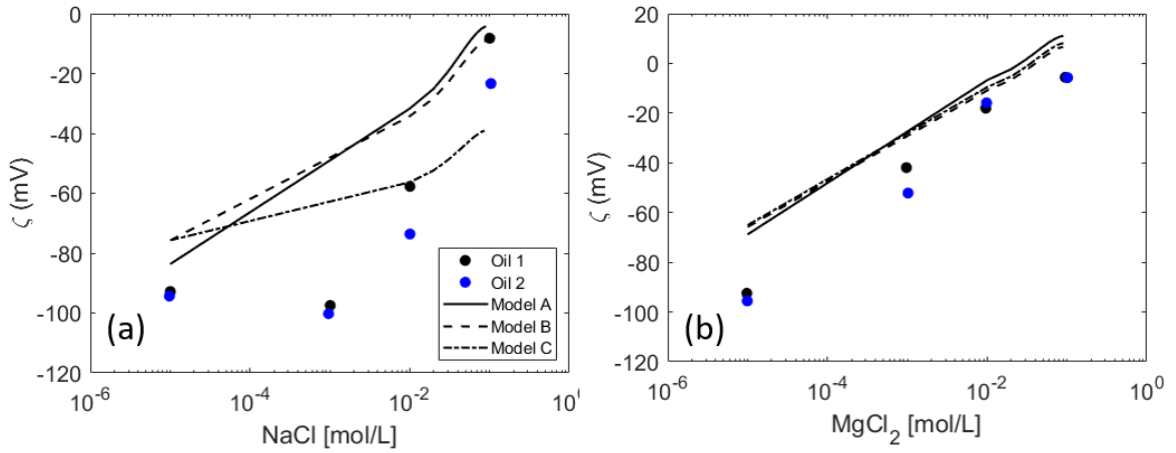

Figure 4.11. Zeta potential measurements for two different crude oils at increasing **(a)** NaCl concentration **(b)** $MgCl_2$ concentration. Data from ref[165].

Lastly, model A is tested against zeta potential measurements of non-polar hydrocarbons (with no ionizable components) in aqueous solutions (Figure 4.12). The predicted zeta potential follows the general trend of the experimental measurements. It is observed that the values reported in ref [301] (Figure 4.12-a) are higher than the ones in ref[302] (Figure 4.12-b) at similar experimental conditions. Therefore, the accumulation of hydroxyls at the surface might not be the only mechanism responsible for the surface charge developed at the non-polar hydrocarbon-water interface. The physical properties of each non-polar oil, and possibly the presence of impurities, might also lead to differences in the surface charge. Differences in the measured zeta potential could also arise due to variations in the oil specific area (different oil drop sizes in the preparation of the emulsions) or from a different oil/water volumetric fraction used in the experiments (0.05% in ref [301] and 0.5% in ref [302]). The uncertainty in predicting the

zeta potential is also made obvious in the work of Marinova et al.[301], where it was shown that the error associated with the measurements in Figure 4.12-a reaches ±15 mV. Additionally, the equation used to relate electrophoretic mobility and zeta potential can also lead to different estimations of the electrokinetic potential. While Smoluchowski's equation was used in ref [301] to estimate the zeta potential from the electrophoretic mobility, no information on this aspect is provided in ref [302]. Moreover, the agreement between the model and the experimental data in Figure 4.12-d is fairly good, considering that no information on the pH was reported and that the calculation is based on the equilibrium pH predicted by PHREEQC, which, as discussed before, may be different to the pH in the experimental system.

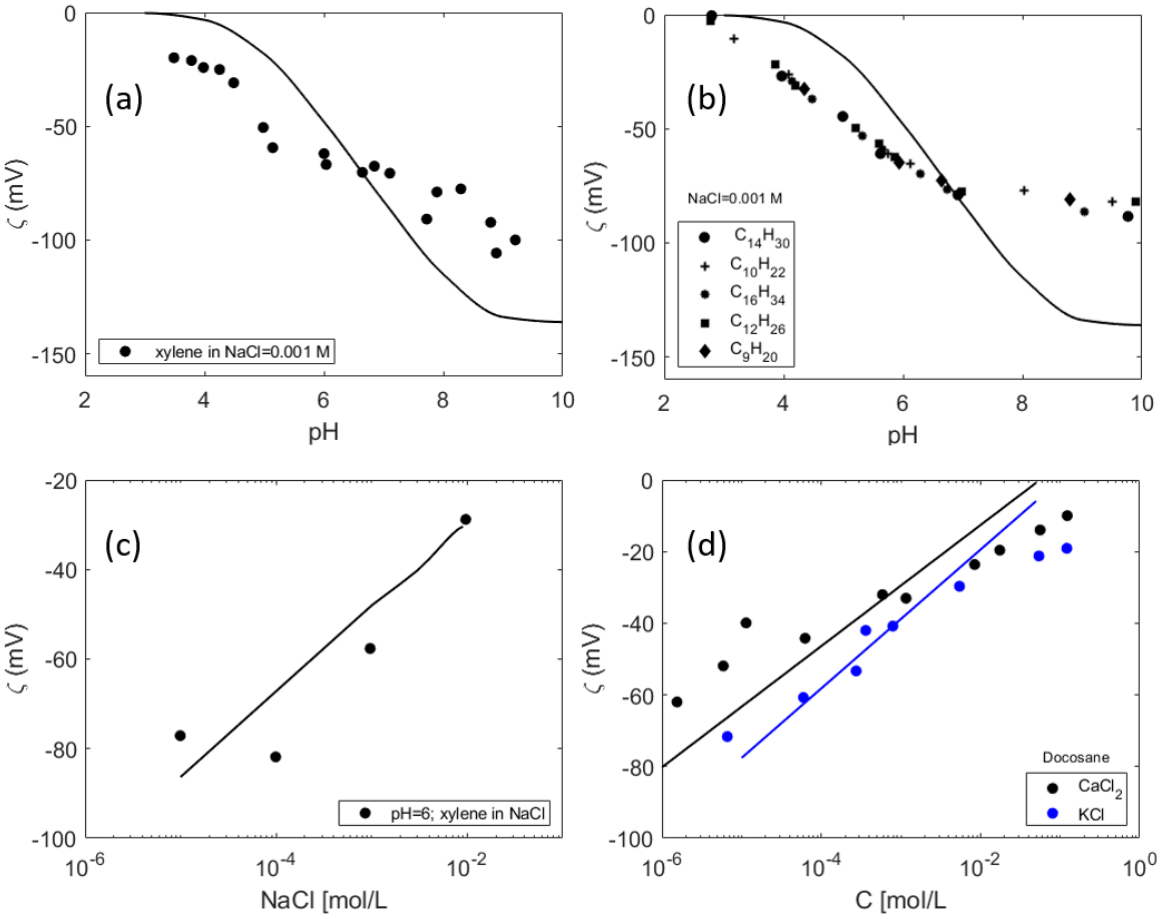

Figure 4.12. Prediction of the model with weak sites for **(a)** experimental data from ref [301]: zeta potential measurements of xylene in NaCl solution [0.001 M] at different pH; **(b)** experimental data from ref [302]: zeta potential measurements with pH of different alkanes in [0.001 M NaCl solution] **(c)** experimental data from ref [301]: zeta potential measurements of xylene in different NaCl concentrations at a fixed pH=6 **(d)** experimental data from ref [303]: zeta potential measurements of docosane in $CaCl_2$/KCl solutions; no pH measurements are reported, and the predicted zeta potential is at the equilibrium pH predicted by PHREEQC.

4.5 Conclusions

In this work, we propose a diffuse layer surface complexation model to predict the zeta potential at the oil-aqueous solution interface, assuming that the presence of carboxylic and amine sites at the oil surface is linearly dependent on the TAN and TBN. A third type of weak site is included to account for the reported adsorption of hydroxyls at the interface. This model is a useful tool to determine the changes in the wettability, assess the optimum water composition during low salinity waterflooding, and provide insight into emulsion stability. The key findings extracted from this study are summarized as follows:

- The success of the model's predictions relies heavily on the definition of active sites at the oil surface. Currently, the acid and basic number are the main parameters used to estimate the amount of surface-active material in the crude oil. However, these do not give an exact indication of the extent of active species that actually 'travel' to the interface. Therefore, the AN and BN do not display a clear picture of the type and distribution of reactive sites at the oil surface.
- The addition of a complexation reaction between the carboxylic sites and Na^+ was necessary to provide a satisfactory zeta potential prediction.
- Including weak surface sites improved the prediction of the model, especially for crude oil with very low AN, which still shows a very negative zeta potential. Under these circumstances, the negative zeta potential is probably a consequence of the adsorption of hydroxyl ions at the interface, which is described by the addition of weak surface sites.
- The performance of the model was generally satisfactory at low ionic strength (up to 0.1 M) while higher deviations were observed at higher ionic strength (1.5 M). The lack of consistent experimental evidence and the inherent limitations of the Poisson-Boltzmann equation at high salinity increased the discrepancy between the model and the measured zeta potential.
- Generally, the model performed worse at reproducing experimental data sets that do not report the pH. From the analyzed experimental data, it could be inferred that the pH of the oil-brine system predicted by PHREEQC is different from the one in the experiments. More insight can be obtained from the modeling of the data if the experimental conditions are properly described.

5 A wettability indicator parameter based on the thermodynamic modelling of chalk-oil-brine systems

The complex physicochemical interactions in the calcite-brine-crude oil system, triggered by the injection of modified salinity water (MSW) into the reservoir, are modelled by several researchers. However, the proposed models are either not consistent with a wettability alteration mechanism or cannot explain the observed improved oil recovery in chalk. We propose a new methodology denominated "Available Adsorption Sites" (AAS) that assesses the wettability alteration as a combined effect of a chemical and electrostatic contribution. Thus, we describe mathematically the interactions between the polar groups in the oil phase and the chalk by considering analogy with the thermodynamics of adsorption of an ion on a charged surface. The chalk wetting properties depend on the number of sites available for the adsorption of oleic polar groups at the mineral surface and the electrical potential at the rock-brine and brine-oil interfaces. We evaluate how the AAS parameter correlates with the remaining oil saturation from spontaneous imbibition tests on chalk samples. This approach is not only useful for the predictive evaluation of the outcome of MSW in chalk reservoirs but can also be integrated into reactive transport models and assess the flow of organic contaminants (e.g., naphtenic acids) in chalk aquifers. The model can potentially be applied to other carbonates.

This chapter is a revised layout of the article: M. Bonto, A.A. Eftekhari, H.M. Nick. A wettability indicator parameter based on the thermodynamic modelling of chalk-oil-brine systems. Energy & Fuels, 2020.

5.1 Introduction

Modifying the injecting water composition or lowering its ionic strength has received a distinguished status among other enhanced oil recovery (EOR) techniques because of its feasibility and benign impact on the environment[343]; its implementation is similar to a normal waterflooding[224] and usually, no chemicals are used in the injected water. However, differences in the performance of this recovery method were observed depending on the constituent reservoir rock. In sandstone formations, its effectiveness relies on reducing the water salinity, whereas the success in carbonates was highly dependent on the presence of certain ions[344]. Many mechanisms are held responsible for the modified-salinity waterflooding (MSW) effect in sandstones, viz., fines migration, double layer expansion, or ion exchange. The level of disagreement among researchers on the prevailing mechanisms for carbonates is even higher; fines migration, emulsification, dissolution, wettability alteration, water weakening (for chalk) are some of the proposed mechanisms. Several recent publications reviewed extensively these mechanisms[19,344–346]. Although the debate on the performance of modified salinity water in carbonates within the scientific community is still open, wettability alteration seems to be the most appealing mechanism for both experimental[7,61,347–349] and modelling[96,100,350–352] studies.

5.1.1 Experimental studies on wettability

The wettability of a carbonate reservoir in the presence of oil and water varies depending on the preference of the rock surface to be covered by one of the fluid phases. This property controls the distribution of oil and water within the reservoir, having an impact on hydrocarbon production[353]. Wettability is most commonly quantified by contact angle measurements, Amott[354], and USBM (United States Bureau of Mines)[355] methods.

The extensive number of studies that report contact angle measurements in the context of modified salinity waterflooding[170,284,285,356–359] show that, probably, this is the most used method for assessing the wettability of a surface[360]. However, this approach is often criticized because the contact angle is determined for a system that may not represent the real reservoir conditions[353]. These measurements provide an incomplete description of wettability, being unable to account for changes in pore geometry, initial water saturation, and (chemical) heterogeneities[361,362]. These limitations may be partially the cause of the large variability associated with the contact angle measurements reported in the literature.

On the other hand, the Amott and USBM methods indicate the average wettability of a core[363]. In the Amott test, the wettability is assessed as a function of the ratio of oil recovered by spontaneous imbibition to that from forced imbibition without accounting for the imbibition rate[364]. In the USBM method, the wettability number is defined by the ratio of the area under the capillary pressure curve for secondary water drainage to that under the imbibition curve[360]. The main problem with both the Amott and USBM wettability tests is that they are insensitive near the range of neutral wettability[365,366]. Some years ago, Strand et al.[153] proposed a new method for quantifying the wettability of chalk, especially near neutral-wet conditions. This test is based on the chromatographic separation between a tracer and a potential determining ion for the calcite surface.

In many cases, however, the wettability is assessed only qualitatively through spontaneous imbibition tests. Thus, a core is considered more or less water wet depending on the imbibed volumes of brine and the imbibition rate[363], which are eventually indicators of the surface energy[367]. However, the rate and amount of water imbibed are governed by the imbibition capillary pressure curve[368], thus, by factors like viscosity, oil-brine interfacial tension, pore structure, and initial saturation of the core[363]. Some publications proposed ways of characterizing the wettability based on these tests[366,369].

Many authors performed spontaneous imbibition tests with different brine compositions on chalk and limestone samples. These studies were primarily carried out to show qualitatively that the end-point recovery by spontaneous imbibition, thus the system wettability, may be shifted by changing the ionic

concentration of the imbibing fluid. These spontaneous imbibition tests were performed in one or several stages. The first imbibition stage is usually carried out with formation water. When no more oil is recovered, the temperature is increased or the imbibing brine is switched to compositions consisting of seawater dilutions/modifications. Ideally, these spontaneous imbibition tests should be implemented with native state cores (cores from the subsurface with preserved wettability conditions)[353,370,371], as the cores with restored wettability may sometimes be not representative of the in-situ reservoir wetting conditions. However, the use of native cores can also be problematic. For instance, factors like interactions with drilling fluids, and changes in the pressure and temperature as the core is brought to surface can alter the in-situ wettability conditions of the native cores, questioning whether these cores reflect the true subsurface wettability conditions[353]. Even though extreme precautions were taken for preservation and packaging, native cores may result in very poor reproducibility; passing from anaerobic to aerobic conditions can affect the behavior of a core during spontaneous imbibition or core flooding experiments[372]. The displacement experiments on cores from different parts of the same reservoir can yield different results not only because of different wetting conditions but also because of heterogeneity in the mineralogy or other properties[373]. Because of the difficulties associated with preserving the wettability of the native cores, these are usually cleaned with solvents when brought to surface; then the wettability is artificially restored to have a core as representative as possible to that found in the reservoir[365]. The wettability restoration consists of initially flushing formation water through the core. Then, oil is injected into the sample, simulating the primary drainage of oil into the reservoir, and setting an initial water saturation (S_{wi})[353]. After this step, the sample is aged by maintaining the rock in contact with the oil at a high temperature either statically (keeping the sample in a volume of oil) or dynamically (continuously flushing the sample with oil throughout the aging time)[368]. Many of the spontaneous imbibition tests were performed on outcrop chalk. The wettability restoration is applied in the same way to these outcrop samples so they can be used as reservoir analogues. These cores have not been in contact with oil so they do not undergo the solvent cleaning procedure. In some cases (e.g., ref[374]), deionized water is used initially to remove any salts that might be present because of a prior contact of the rock with seawater. If these salts are not removed, the core surface properties can be significantly different because of the initial presence of potential determining ions on the chalk surface, e.g., SO_4^{2-} [374]. As we show later in this paper, the core preparation, and the aging procedure strongly influence the final oil recovery from displacement experiments. We gather the experimental conditions of several spontaneous imbibition tests performed on carbonate samples (mostly chalk and limestone) in Table 5.1. Different procedures for performing the saturation and the aging are used. We group the methods used to establish the initial water saturation in the following:

a) cores evacuated and saturated with initial water under vacuum followed by flooding with several pore volumes (PV) of oil (usually between 1.5-2.0 PV) in each direction
b) cores are first saturated with the initial brine and placed on a porous plate where they are drained with water-saturated nitrogen gas until the desired brine saturation is obtained; this is followed by oil flooding in each direction
c) the crude oil used in the dynamic aging was replaced by injection of 5 PV of decahydronaphtalene which was afterward displaced by 5 PV of decane to reach S_{wi}
d) saturation by centrifugation or evaporation to reach a target value; afterward, the samples were placed in a container with dead crude oil to bring them to initial oil saturation

For the aging, we identify two main procedures:

a) static aging in a closed container, usually, for at least 4 weeks at high temperature (70-90 ^{o}C) in the same oil that was used to achieve the initial water saturation
b) dynamic aging: continuous oil injection during 4-8 days at high temperature (90 ^{o}C)

Table 5.1. Summary of spontaneous imbibition tests performed in the context of modified salinity waterflooding for carbonate reservoirs. All the experiments included are performed on cores with a specific formation water and saturated with oil with a specific acid and base number (AN and BN). "DIW" stands for deionized water. The letters in the "S_{wi}" and "Aging" fields correspond to the procedures described in the "Experimental studies on wettability" section. The samples with an asterisk correspond to reservoir samples while the others to outcrop samples.

Ref	Core material	Oil properties AN/BN [mg KOH/g oil]	Cleaning/ Pre-conditioning	S_{wi}-aging	T_{imb} [°C]	Objective of the study
6	Stevns Klint chalk	Crude oil diluted with n-heptane and filtered AN: 2.07; 0.17; 0.55	No	(a)-(e)	70-130	Effect of sulfate and calcium on the improved oil recovery from chalk
348	Stevns Klint chalk	Filtered crude oils mixed and diluted → different AN/BN ratio by adding benzyl amine; AN=0.5	No	(a),(b)-(e)	50-110	Study the effect of bases on the wettability of a crude oil/brine /chalk system
178	Stevns Klint chalk	Filtered crude oil: Oil A: AN=2.07; BN=0.50 Oil B: AN=0.55; BN=0.13	No	(a)-(e)	70-130	Effect of Ca^{2+}, SO_4^{2-}, and temperature on the wettability and oil recovery from chalk
60	Stevns Klint chalk	Filtered crude oil: Oil A: AN=2.07; BN=0.50 Oil B: AN=0.55; BN=0.13	No	(a)-(e)	40-130	Study the impact of Mg^{2+} on spontaneous imbibition into moderate water-wet chalk
30	Stevns Klint chalk	Filtered and diluted in n-heptane crude oil: AN=1.9	Pre-flushing (DIW - 250 mL).	(b)-(e)	100-120	Study the effect of salinity, ionic composition, and temperature on the wettability of chalk
375	Stevns Klint chalk	Filtered diluted crude oil: Oil A: AN=2.0 BN=0.5 Oil B: AN=0.5 BN=0.3 Oil C: AN≈0 BN≈0	Pre-flushing (DIW - 250 mL)	(b)-(e)	70-120	Optimize the concentration of the active ions, i.e., Ca^{2+} and SO_4^{2-} in seawater depleted in NaCl
349	Stevns Klint chalk	Filtrated centrifuged crude oil: Oil A: AN=0.5 BN=0.32	Pre-flushing (DIW - 4 PV)	(b)-(e)	90	Find optimum NaCl and SO_4^{2-} concentration for modified seawater in chalk reservoirs
376	Stevns Klint chalk	Filtered, diluted crude oil with different AN: 2.07, 0.76, 0.49, 0.31, 0.17	No	(a)-(e)	70	Study the effect of AN and temperature on the wetting conditions for carbonates
377	Stevns Klint chalk	Filtered and diluted North Sea crude oil and 40% heptane: AN=2.07, BN=0.47	No	(a)-(e)	40-130	Evaluate the effect of various ratios of Ca^{2+} and SO_4^{2-} on wettability alteration and spontaneous imbibition at various temperatures
378	Stevns Klint Niobrara Rørdal chalks	Crude oil: AN=0.41 BN=1.4;Asphaltenes: 0.59%	No	(c)-(f)	130	Use of SO_4^{2-} for enhanced oil recovery during SI at elevated temperatures in different types of chalk at various wettability conditions
225	Stevns Klint chalk	Crude oil from three oil reservoirs was used for the experiments	No	(d)-(e)	60-85	Effect of different brine composition on the wettability and oil recovery from carbonates with different pore properties
	Limestone*		Yes (procedure not mentioned)			
379	Stevns Klint chalk	Crude oil diluted and filtrated; Res40: AN=1.7 Toil: AN=0.05 BN=0.44	No	(a)-(e)	70-130	Effect of SO_4^{2-} and temperature on the spontaneous imbibition into preferential oil-wet carbonate during a wettability alteration process
	Middle East Limestone*		Not mentioned			
380	Carbonate (Oman)*	Filtered dead crude oil from a carbonate reservoir from Oman. AN/BN not mentioned.	Soxhlet extractor (1 month) + methanol flushing	(a)-(e)	70	Test the potential of modified salinity water on reservoir cores by carrying out SI tests with different ionic strength
381	Carbonate*	Filtered dead crude oil AN=2.45	Not mentioned	(a)-(e)	120	Test different brines to improve the oil recovery at high temperature in limestone formations
382	Indiana limestone	Filtered crude oil from an Omani carbonate reservoir AN=0.37	No	(a)-(e)	75	Test different brine recipes to observe their effect on the wettability of an oil-wet limestone core sample through SI tests and contact angle measurements

Although different types of experiments may give insights into the effect of a particular brine on diverse properties (e.g., wettability, interfacial tension) known to affect the oil recovery, the eventual response to modified salinity is best assessed through spontaneous imbibition or core flooding experiments[383]. These experiments provide the capillary pressure-saturation functions and the relative permeability curves at different brine salinity[384]. The information obtained from displacement tests can further benefit from the progress in pore-scale imaging techniques that reveal unique features of multiphase flow, e.g.,

interfacial areas, menisci curvature, in-situ contact angles, which may be relevant for designing improved oil recovery strategies[385].

However, resources and time constraints associated with spontaneous and forced imbibition experiments promoted an increasing effort to seek faster alternatives that would help to efficiently select candidates for field applications. For instance, flotation tests[386] were proposed as a quick tool for determining which brine composition would result in more water-wet conditions given certain mineral and crude oil properties. Moreover, predictive models and correlations could speed up the screening process even further. Some authors focused on the statistical analysis of a large database of experiments carried out in the context of MSW on sandstones[387] and carbonates[388]. Both publications report the difficulty of performing such analysis because of the great amount of underreported experimental conditions. Additionally, Bartels et al.[383] emphasize the lack of standardization of the protocols used in the experiments, which complicates the comparison of different experimental studies. Apart from the statistical approach, mechanistic models for the wettability alteration that could explain the extra oil recovery at the core scale have also been a target of intense investigation. These models are important because, although they may not provide information on the additional amount of recovered oil[383], they can reveal which combination of crude oil, formation water, and injection brine is susceptible to IOR during MSW. Some of these mechanistic models are briefly introduced below.

5.1.2 Multiphase flow models and surface complexation modelling

Most mechanistic multiphase flow models proposed for the MSW in carbonate reservoirs have focused so far on modelling the wettability alteration. Wettability itself does not appear as an independent equation when we deal with solving the two-phase flow in porous media. However, this property strongly affects the relative permeability and the capillary pressure, governing the success of a waterflooding process[353,370,371]. Thus, the few mathematical models for MSW focus on capturing the wettability alteration by implementing an interpolation of the relative permeability curves and capillary pressure between the wettability states for the rock in equilibrium with the initial water and the new equilibrium after MSW injection.

Yu et al.[350] developed a numerical two-phase 1D model which describes the wettability alteration as a function of the adsorption of a wettability agent (salt, a single component in the water phase) on the calcite surface. The adsorption of salt was quantified by using a Langmuir isotherm and the amount of adsorbed salt was used as interpolant for the relative permeability curves. Since the ionic composition of the aqueous phase is not considered, the constants of the adsorption isotherm are not based on the physicochemical conditions of the system but represent simple fitting parameters. In a later work[389], they compared the output from their model with the oil recovery they obtained from spontaneous imbibition tests. This model was further developed by Evje and Hiorth[351] by including specific mineral-brine interactions. They considered the wettability alteration to be a function of calcite dissolution. For the water-rock interactions, the transport model included three mineral phases ($CaCO_3$, $CaSO_4$, and $MgCO_3$) undergoing dissolution/precipitation and three aqueous species (Ca^{2+}, SO_4^{2-}, and Mg^{2+}). An equilibrium condition is considered for the ionic interactions in the aqueous phase. The interpolant, in this case, is dependent on the amount of dissolved calcite, which is consequently linked to the wettability alteration. This model was not validated against any experimental data. Later, Andersen and Evje[352] coupled a geochemical model including ion exchange to the flow equations, trying to reproduce spontaneous imbibition tests. The relative permeability curves are shifted in several ways by testing several base cases, i.e., sulfate adsorption, anhydrite precipitation, or calcite dissolution.

Brady et al.[94] introduced two diffuse layer (DL) surface complexation models (SCM) for describing the interactions occurring at the calcite-water and water-oil interfaces. They also introduced the concept of the "bond product sum", *BPS*, that represents the sum of oppositely charged pair products at the mineral-brine and brine-oil interfaces (eq. 5.1).

$$BPS = \sum [\equiv \text{Calcite}^-][\equiv \text{Oil}^+] + [\equiv \text{Calcite}^+][\equiv \text{Oil}^-] \quad (5.1)$$

where $[\equiv \text{Calcite}^-]$ and $[\equiv \text{Calcite}^+]$ stand for the concentration of negative and positive species at the calcite surface, respectively, $[\equiv \text{Oil}^-]$ and $[\equiv \text{Oil}^+]$ represent the negative and positive species at the oil surface.

This parameter depicts in a very elementary way the electrostatic pair abundance. A higher bond product sum would reflect stronger attraction between the two interfaces, i.e., more oil-wet conditions, whereas lower BPS represents a greater separation between the interfaces (more water-wet conditions). Later, this concept gained popularity and was further used in many subsequent publications that showed that BPS was consistent with the improved oil recovery from spontaneous imbibition tests[357] from Austad et al.[7], contact angle measurements[298,358], and core floods[95] performed by Yousef et al.[224].

Qiao et al.[96] implemented a multiphase flow reactive transport model using a finite-difference numerical approximation. This work includes the surface complexation models for the mineral-brine and brine-oil interfaces as proposed by Brady et al.[94] and interaction between the carboxylic acids in the oil phase with the positive surface sites at the calcite surface. The number of calcium carboxylates bonds was used as an interpolation factor for the relative permeability curves. This model was validated against spontaneous imbibition tests from ref [30]. In a later publication[97], they used this model to reproduce effluent concentrations from chromatographic wettability tests and core flooding experiments from refs [7,30,217,224]. The proposed model has many adjustable parameters and a lack of consistency in the modelling of the data is observed, i.e., an electrical double layer (EDL) is considered in some cases, whereas for other similar experimental conditions the EDL is ignored. A different approach was adopted just to ensure a better fit to the experimental data. Other inaccuracies of this model were previously reported by Korrani and Jerauld[100]. Eftekhari et al.[69] developed a reactive transport single-phase flow model based on a finite volume approximation coupled to an SCM for the chalk-brine interface. They first optimized the equilibrium constants for the surface reactions by fitting the model to the zeta potential reported for pulverized Stevns Klint chalk[178]. Afterward, they used the optimized parameters to predict the breakthrough composition of different ions in chromatographic experiments on the Stevns Klint chalk cores[60], which resulted in a poor fit. Therefore, they suggested a new optimization procedure to fit the SCM model to both chromatographic (single-phase core flooding) and zeta potential experimental data. Then they used the optimized SCM for the chalk-brine interface together with an SCM for the oil-brine interface and estimated the number of bonds between the calcite positive surface sites and the carboxylic acids. They correlated the residual oil saturation from spontaneous imbibition tests reported in the literature[30,60] with the number of bonds predicted with the models. They observed a rough correlation between the number of bonds between the calcium sites and the carboxylic acids. Sanaei and Sepehrnoori[390] developed an in-house simulator coupled to a surface complexation model in IPhreeqc. They first estimated the zeta potential at the rock-brine and brine-oil interfaces; then they calculated the disjoining pressure in the water film by considering electrostatic, van der Waals, and structural forces. From the disjoining pressure, they inferred a microscopic contact angle and this angle was the interpolation factor for modelling the wettability alteration effect on the relative permeability curves. Although the authors emphasize the need for predictive models, they show mostly fitted trends of their proposed surface complexation model. For each modelled data set, they adjust either the number of surface sites or the equilibrium constants. They used this model to match oil recovery curves and effluent concentrations from the MSW flooding experiments performed by Chandrasekhar et al.[391] by considering, additionally, the relative permeability curves and the minerals saturation index as fitting parameters. Erzuah et al.[103] used a DLM surface complexation model for the brine-oil and rock-brine interfaces. They compared the wettability obtained in flotation tests with the total bond product concept earlier introduced by Brady et al.[94] and the number of calcium complexes. They observed a correlation between the number of oil-wet particles in the flotation tests and the calculated amount of Ca^{2+} adsorbed

on the calcite surface. Korrani and Jerauld[100] suggested a multicomponent reactive transport model implemented in UTCOMP-IPhreeqc to depict displacement processes in sandstone and carbonate reservoirs. The interactions at the calcite-brine and the brine-oil interfaces are accounted for by two surface complexation models adopting the procedure from Brady et al.[94]. To describe mathematically the wettability alteration they proposed an interpolant between water-wet and oil-wet conditions, which they called "wetting film stability number" (SN) (eq. 5.2).

$$SN = 0.09\varepsilon_r^{1.5}\psi_{o/b}\psi_{r/b}\sqrt{\frac{T}{I}} \tag{5.2}$$

where ε_r [78.5 - at 25ºC] is the water relative permittivity, $\psi_{o/b}$ [V] and $\psi_{r/b}$ [V] are the surface potentials at the oil/brine and brine/rock, respectively, T [K] is the temperature and I [mol/m^3] is the ionic strength.

The stability number is a concept that stems from the stability condition of the wetting-water layer formulated by Hirasaki[43] based on the calculations proposed by Usui[392] for calculating the energy of interaction between dissimilar double layers at constant surface charge by use of the linear Debye-Hückel approximation. The stability number is proportional to the ratio of electrostatic and van der Waals forces and reflects the minimum stable electrical potential. Korrani and Jerauld make simplifications to the original equation by assuming no changes in some of the parameters in the original equation, i.e., value for the Hamaker constant. They also impose restrictions on the minimum and maximum stability number (between 0.1 and 2). They use this approach to explain the low salinity effect observed for both sandstones and carbonates. For the case of carbonates, they model core flooding experiments from Shehata et al.[393] and Yousef et al.[394]. However, the authors pointed out that this wettability interpolant does not explain the improved oil recovery observed by Zhang and Austad[178] and Fathi et al.[30] in spontaneous imbibition tests on chalk.

In a consistent and coherent model that addresses the effect of wettability on the relative permeability and capillary pressure by interpolation between two wetting states, the chosen interpolant should correlate, at least qualitatively, with a parameter that gives an experimental or theoretical indication of the wetting state. When a core becomes water-wet, more water can be imbibed and replace oil. A rock, i.e., a mineral is water-wet by nature and becomes "oil-wet" when covered by an organic compound. As more polar organic material adsorbs on the surface, the more oil-wet the rock turns into, and the higher the remaining oil saturation (at P_c=0) in an imbibition test is expected. From this brief review on the geochemical and transport modeling work for wettability alteration in the context of the MSW in carbonates, we observe that some of these interpolants (e.g., adsorption of salt, dissolution/precipitation of salts) were in most cases included in the flow equations without checking previously their relationship with the wettability. The two interpolants that are linked to the DLVO theory, therefore to the wettability alteration, are the "stability number"[100] and the "bond product sum"[94]. However, generally, we observe a lack of systematic studies showing the capabilities or the extent to which these interpolators can explain the wettability alteration of carbonates, specifically for chalk. Since the wettability is a property dependent on both mineral-water and water-oil interfaces, the shift in the wetting condition during MSW may take place differently depending on the rock type. Therefore, there may not exist a unique model consistent with the modified salinity water recovery observed in all types of formations. In this work, we attempt to describe the wettability alteration of chalk during MSW flooding. However, before including a parameter in the flow equations for the modelling of different aspects of forced and spontaneous displacement experiments, we first need to systematically test the interpolating parameters. Thus, in this work, we first assess the relationship between the "BPS" and "SN" and the remaining oil saturation from spontaneous imbibition tests performed on chalk at different temperatures, formation and imbibing water compositions, and oil acid and base numbers. We assume that at the end of these tests, the capillary pressure is zero and no more water can be imbibed into the system, thus a constant remaining oil saturation is reached. Later, we propose a new wettability

interpolator to describe the wettability alteration during MSW in chalk. We also assess the consistency between these wettability interpolators and the water-wet fraction of chalk particles from flotation tests. These results are included in Appendix A.3.

5.2 Methodology

In the spontaneous imbibition tests, the core is first in equilibrium with an initial formation brine. At the end of the experiment, the core is either in equilibrium with the imbibing brine or with a mixture of the imbibing and formation brine, depending on whether the imbibing fluid is continuously refreshed or not. Here, we assume the imbibing water fully replaces the formation water at the end of the experiment. We define a set of dimensionless parameters that reflect the relative increase/decrease of bonds/stability of the final oil-brine-rock equilibrium state with respect to the initial state. We assess the SN/BPS at initial conditions by considering equilibrium between the mineral-formation brine-crude oil, whereas for the final condition we consider the equilibrium established in the mineral-imbibing brine-crude oil system. Thus, we define the ratios $\frac{SN_{final\ brine}}{SN_{initial\ brine}}$ and $\frac{BPS_{final\ brine}}{BPS_{initial\ brine}}$ and we check their correlation with the remaining oil saturation from the spontaneous imbibition tests (mostly on chalk) included in Table 5.1 performed at several temperatures with different brine composition and crude oil properties.

As observed from the definition of the BPS and SN in eqs. (5.1) and (5.2), respectively, quantifying these two parameters requires the use of two thermodynamic models to simulate the speciation (bonds) and the charge at these two interfaces (zeta potential). Several SCMs[67,68,104,175,358] were shown to successfully fit zeta potential measurements performed on diverse electrolyte-calcite systems. Here, we obtain the concentration of species and the zeta potential at the rock-brine interface by considering a Charge Distribution MultiSite Complexation (CD-MUSIC) SCM[67], which was shown to predict satisfactorily the electrokinetic potential of chalk particles in aqueous solutions[395], without the need of further refining the values of the equilibrium constants. This model allows placing the charge of the ions in three different adsorption planes, depending on their affinity for the surface. These planes are the surface plane (or 0-plane), inner Helmholtz plane (IHP or 1-plane), and Outer Helmholtz plane (OHP or 2-plane). To describe the charge development at the oil-brine interface, we used a diffuse layer model[227], which considers a variable number of ionizable carboxylic and amine sites at the oil surface linearly dependent on the acid and base numbers (AN and BN). However, we set a physical limitation of a maximum 2.5 #/nm^2 (value inferred experimentally for the decane-water interface in the presence of surfactants[396]) for both surface sites. We also restrict the maximum ratio of amine to carboxylic sites to one, consistent with the experimental evidence that shows a higher affinity of acidic groups for the oil-water interface[321,329,397]. The detailed procedure for the definition of the oil surface groups based on the AN and BN can be found in our previous publication[227]. Moreover, given the high temperatures and high ionic strength of the formation and imbibing fluids, we used Pitzer database from PHREEQC[398] for the surface complexation modelling of the two interfaces. Table 5.2 includes the relevant parameters of both models. For the rock-brine SCM, we only consider the predominant face sites of the $\{10\bar{1}4\}$ calcite cleavage plane[89], resulting in the definition of two hydrated surface sites, i.e., $CaOH^{-2/3}$ and $CO_3H^{+2/3}$. The fractional charge of the surface sites comes from the lower coordination number (CN) of Ca at the surface with respect to the bulk. Within the bulk, Ca has a coordination number of six, i.e., each calcium is bonded to six oxygens from six different CO_3. According to Pauling's rule of electroneutrality [399], the positive charge of the Ca (z=2) is distributed uniformly among the different oxygens so that the charge per bond corresponds to +1/3 (z/CN)[85]. Thus, at the surface, where calcium has a coordination number of 5, Ca holds a positive charge of +1/3 and the CO_3 a negative charge of -1/3. Moreover, in the presence of water, the calcite surface is hydrated[33]. Assuming dissociative adsorption of water, the surface sites become $CaOH^{-2/3}$ and $CO_3H^{+2/3}$. Note however that considering a 1:1 stoichiometry for the Ca:CO_3 sites, the defined charge at the surface sites does not affect the calculated zeta potential because there is an equal number of surface sites with an opposite charge but

the same magnitude. The equilibrium constants for calcite interaction with Na^+, Cl^- and SO_4^{2-} are taken as for solution complexation from Lawrence Livermore National Laboratory (LLNL) database for PHREEQC[241]. The enthalpies of the calcite surface reactions are taken from the work of Eftekhari et al. [69], inferred from the equilibrium constants proposed at different temperatures in ref [5]. For the enthalpies of the complexation reactions at the oil surface, we consider those of acetate from LLNL database. The dashes correspond to values that were not found; a value of 0 kJ/mol was used in these cases. For all mineral-water interactions, a specific surface area of 2 m^2/g was considered[30]. The values of Δz_0 and Δz_1 represent the net charge transfer in the different planes upon adsorption of an ionic specie on the calcite surface. As observed in Table 5.2, the charge of the oxyanions (e.g., HCO_3^-, CO_3^{2-},SO_4^{2-}) is partially shared with the oxygen at the surface. Thus, a fraction of the central atom of the oxyanion is assigned to the surface plane (0-plane) and the remaining charge to the corresponding adsorption plane (1- and 2-plane in case of inner and outer-sphere complexation, respectively). For instance, considering the CO_3 ion and that 0.4 of the charge of C is assigned to the surface plane, the net surface charge in the 0-plane, Δz_0, is [+1-2+0.4·4] (where the first term corresponds to the dihydroxylation, the second to the charge of the oxygen at the surface, and the third term to the fractional charge of the carbon assigned to the surface). In the same way, the net charge in the 1-plane, Δz_1, is [2·(-2)+0.6·4], corresponding to the charge of the two O oriented towards the solution and the remaining charge assigned to the 1-plane. The fractions of sorbed ions could be used as adjustable parameters. However, we kept the charge distribution and log *K* values proposed in the original work [67] without further modification.

Table 5.2. Primary parameters of the surface complexation models for the calcite/brine and brine/oil interfaces.

		Surface reactions	Log *K*	ΔH [kJ/mol]	Δz_0	Δz_1
Calcite-brine CD-MUSIC C_1=1.3 F/m² C_2=4.5 F/m²	Calcium sites 4.95 #/nm²	$\equiv CaOH^{-2/3}+H^+ \leftrightarrow \equiv CaOH_2^{+1/3}$	12.85	-82.71	1	0
		$\equiv CaOH^{-2/3} \leftrightarrow \equiv CaO^{-5/3}+H^+$	-24.73	-	-1	0
		$\equiv CaOH^{-2/3}+CO_3^{2-} \leftrightarrow \equiv CaCO_3^{-5/3}+OH^-$	1.55	14.91	0.6	-1.6
		$\equiv CaOH^{-2/3}+CO_3^{2-}+H^+ \leftrightarrow \equiv CaHCO_3^{-2/3}+OH$	10.15	13.51	0.6	-0.6
		$\equiv CaOH^{-2/3}+SO_4^{2-} \leftrightarrow \equiv CaSO_4^{-5/3}+OH^-$	0.35	14.44	0.6	-1.6
		$\equiv CaOH^{-2/3}+Cl^- \leftrightarrow \equiv CaCl^{-2/3}+OH^-$	-9.98	-	1	-1
	Carbonate sites 4.95 #/nm²	$\equiv CO_3H^{+2/3}+Ca^{2+} \leftrightarrow \equiv CO_3Ca^{+5/3}+H^+$	-2.8	15.67	-1	2
		$\equiv CO_3H^{+2/3} \leftrightarrow \equiv CO_3^{-1/3}+H^+$	-3.58	8.70	-1	0
		$\equiv CO_3H^{+2/3}+Mg^{2+} \leftrightarrow \equiv CO_3Mg^{+5/3}+H^+$	-2.2	17.41	-1	2
		$\equiv CO_3H^{+2/3}+Na^+ \leftrightarrow \equiv CO_3Na^{+2/3}+H^+$	-12.27	-	-1	1
Oil-brine DLM	Amine sites	$\equiv NH+H^+ \leftrightarrow \equiv NH_2^+$	5.5	30	Sites linearly dependent on TAN and TBN	
	Carboxylic sites	$\equiv COOH \leftrightarrow \equiv COO^-+H^+$	-4.75	0.0		
		$\equiv COOH+Na^+ \leftrightarrow \equiv COO\text{-}Na+H^+$	-4.86	-0.03		
		$\equiv COOH+Ca^{2+} \leftrightarrow \equiv COO\text{-}Ca^++H^+$	-3.82	1.17		
		$\equiv COOH+Mg^{2+} \leftrightarrow \equiv COO\text{-}Mg^++H^+$	-3.47	-8.42		
	Weak sites	$\equiv wOH \leftrightarrow \equiv wO^-+H^+$	-8.93	-		
		$\equiv wOH+Na^+ \leftrightarrow \equiv wO\text{-}Na+H^+$	-8.93	-		
		$\equiv wOH+Ca^{2+} \leftrightarrow \equiv wO\text{-}Ca^++H^+$	-5.85	-		
		$\equiv wOH+Mg^{2+} \leftrightarrow \equiv wO\text{-}Mg^++H^+$	-5.85	-		

Next, we propose a novel model (see Figure 5.1) to describe the shift in the wetting conditions of chalk. We compare the results of this new methodology with the relationship between the parameters proposed by Korrani and Jerauld[100] and Brady et al.[94] and the wettability alteration of chalk cores. Figure 5.1 also

shows the consistency between the calcite-brine and brine-oil SCMs and reported zeta potential measurements. The performance of the model for the oil-brine interface for different zeta potential datasets was assessed elsewhere [227]. Since we expect predictive capabilities from these models, we do not use any adjustable parameters to show the correlation of the BPS/SN with the remaining oil saturation from spontaneous imbibition tests.

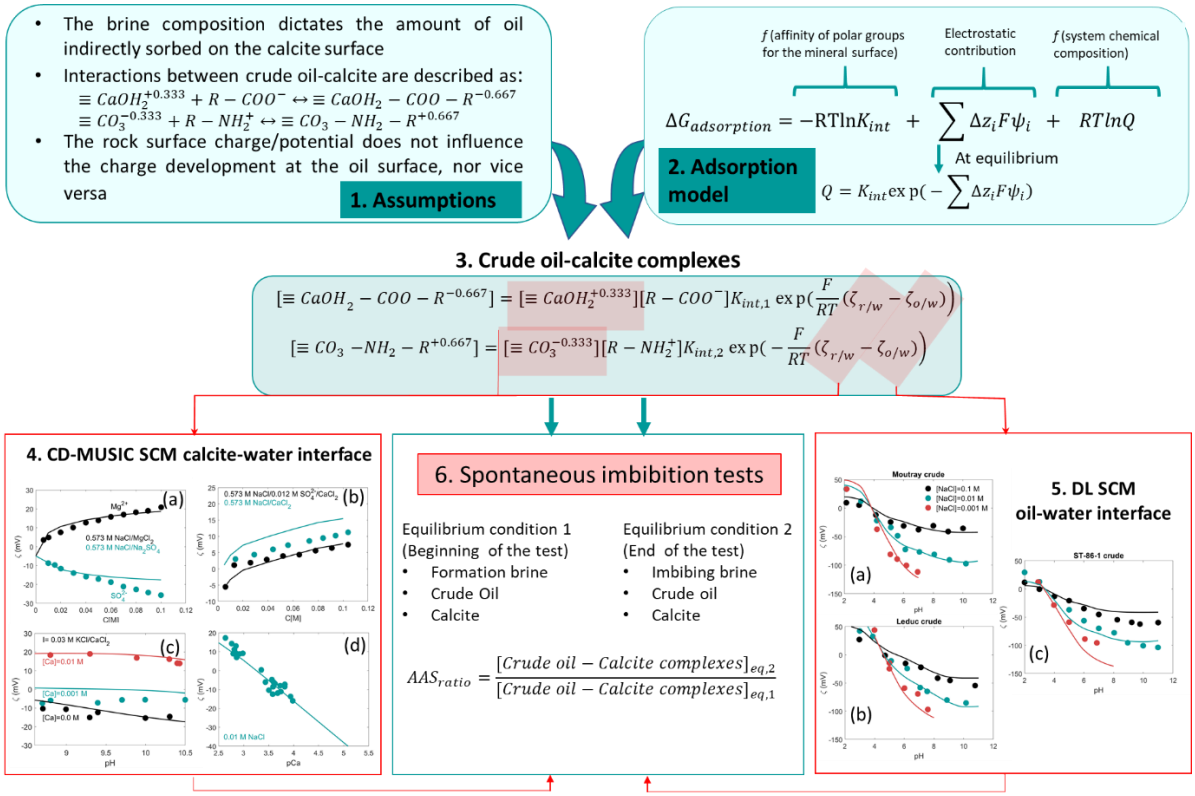

Figure 5.1. Description of the methodology followed in this study. Based on the proposed model for the adsorption of polar groups on the calcite surface, we estimate the ratio of complexes between the calcite and amine and carboxylic groups from the oil phase at two different equilibrium conditions, i.e., with imbibing and formation brine. This ratio depends on the speciation at the calcite surface and the zeta potential at the calcite-brine and brine-oil interfaces. This approach contrasts the BPS and SN parameters, which take into account either the speciation (BPS) or the zeta potentials (SN). The potential at the calcite-brine and brine-oil interfaces is estimated through a CD-MUSIC model and DLM, respectively. In step 4 we show the performance of the calcite-brine SCM for predicting (no fitting parameters were used) zeta potential measurements reported by **(a)** Zhang et al.[400,401], **(b)** Zhang et al.[401], **(c)** Cicerone et al.[402], **(d)** Pierre et al.[403]. In step 5 we show the DLM for the oil-brine interface fitted to the experimental data from Buckley et al.[42].

5.2.1 Mechanism for the wettability alteration in chalk: "Available Adsorption Sites (AAS)"

Different brine compositions may lead to additional oil recovery by influencing the oil adsorbed indirectly (through a thin water layer) on the mineral surface[95]. Thus, we attempt to explain the wettability change as a function of the adsorption of polar components from the crude oil on the rock surface. The polar groups we consider are molecules with ionizable amine and carboxylic groups. The approach we follow to describe the adsorption of these groups is analogous to that described by Hiemstra et al.[85] and later by Tadanier and Eick[73] for ion adsorption on a charged mineral surface.

The change in the free energy associated with the adsorption ($\Delta G_{adsorption}$) of a polar group on a charged surface comes from the change in chemical energy and an electrostatic term as given by eq. (5.3):

$$\Delta G_{adsorption} = \Delta G_{intrinsic} + \Delta G_{electrostatic} + RTlnQ \tag{5.3}$$

Where $\Delta G_{intrinsic}$ [J/mol] represents the Gibbs energy change caused by the adsorption reaction, $\Delta G_{electrostatic}$ [J/mol] represents the energy required to bring a charged species from the oil-water interface to the rock surface, and the third term represents the dependence of the free energy of adsorption on the system composition; R [J mol^{-1} K^{-1}] denotes the ideal gas constant, T [K] is the temperature and Q is the quotient of the reaction.

The intrinsic term can be expressed as shown in eq. (5.4):

$$\Delta G_{intrinsic} = -RTlnK_{int} \tag{5.4}$$

where K_{int} is the intrinsic surface adsorption equilibrium constant.

The electrostatic contribution to the Gibbs energy of adsorption (eq. 5.5) represents the work that needs to be done or released to cause a net charge change Δz_i at plane/position *i (0-, 1- or 2-)* with potential ψ_i[V] with respect to the bulk:

$$\Delta G_{electrostatic} = \sum \Delta z_i F \psi_i \tag{5.5}$$

where F [96485.33 C/mol] denotes Faraday's constant.

However, in this case, the polar species do not adsorb from the electroneutral bulk solution but another charged surface (oil-water interface). Thus, considering that the potential at the oil-brine interface is equivalent to the zeta potential, $\zeta_{o/b}$, we express the electrostatic term as:

$$\Delta Gelectrostatic = \Delta z_i F(\psi_i - \zeta_{o/b}) \tag{5.6}$$

At equilibrium, the change in Gibbs energy is zero ($\Delta G_{adsorption}$=0) and from eqs. (5.3) to (5.6), we obtain:

$$Q = K_{int} exp\left(-\sum \Delta z_i F(\psi_i - \zeta_{o/b})\right) \tag{5.7}$$

This approach represents a simplified description of the overall adsorption process. We assume here that the rock electrical double layer does not overlap with that of oil. In other words, we consider that the two interfaces are far enough, such that the potential at the rock surface does not affect the charge development at the oil-water interface, nor vice versa. This assumption allows treating the speciation and charge development at the two interfaces separately. If the interaction between the two interfaces was considered, then the charge development at the two interfaces could not be solved independently through two different SCMs. In that case, the charging behavior at the two interfaces should be treated simultaneously resulting in a strongly coupled system where the potential/charge at one interface affects the charge/potential at the other interface.

We define the following descriptive reactions of adsorption of polar components from the crude oil on the calcite surface:

R5.1 – Adsorption of carboxylic groups: $\equiv CaOH_2^{+1/3} + R\text{-}COO^- \leftrightarrow \equiv CaOH_2\text{-}COO\text{-}R^{-2/3}$

R5.2 – Adsorption of amine groups: $\equiv CO_3^{-1/3} + R\text{-}NH_2^+ \leftrightarrow \equiv CO_3\text{-}NH_2\text{-}R^{+2/3}$

Since these reactions do not involve any de/protonation and assuming that the polar groups adsorb at the OHP, the net charge change in the different planes is $\Delta z_0 = \Delta z_1 = 0$ and $\Delta z_2 = -1$ for reaction R5.1 and $\Delta z_2 = 1$ for reaction R5.2. Considering that the calcite potential at the OHP (2-plane) coincides with the zeta potential, $\zeta_{r/b}$, eq. (5.7) becomes:

$$Q = K_{int} \exp\left(-\Delta z_2 F(\zeta_{r/b} - \zeta_{o/b})\right) \tag{5.8}$$

From eq. (5.8) we define the concentration of complexes between the polar groups and the calcite surface:

$$[\equiv \mathrm{CaOH_2\text{-}COO\text{-}R^{-2/3}}]=[\equiv \mathrm{CaOH_2^{+1/3}}][\mathrm{R\text{-}COO^-}]K_{int,1}\exp\left(\frac{F}{RT}(\zeta_{r/b}-\zeta_{o/b})\right) \quad (5.9)$$

$$[\equiv \mathrm{CO_3\text{-}NH_2\text{-}R^{+2/3}}]=[\equiv \mathrm{CO_3^{-1/3}}][\mathrm{R\text{-}NH_2^+}]K_{int,2}\exp\left(-\frac{F}{RT}(\zeta_{r/b}-\zeta_{o/b})\right) \quad (5.10)$$

where the square brackets denote concentrations (the activity coefficient of the surface species is assumed as 1). We have only included the interactions with de/protonated calcite sites since these are by far the most numerous (observed from speciation results).

Then, we define the total available adsorption sites ratio (eq. 5.11) as the relative increase/decrease of calcite-crude oil interactions at the final (end of imbibition) conditions with respect to the initial (beginning of imbibition) conditions:

$$AAS_{ratio}=\frac{[\equiv \mathrm{CaOH_2^{+1/3}}][\mathrm{R\text{-}COO^-}]K_{int,1}\exp\left(\frac{F}{RT}(\zeta_{r/b}-\zeta_{o/b})\right)\Big|_2+[\equiv \mathrm{CO_3^{-1/3}}][\mathrm{R\text{-}NH_2^+}]K_{int,2}\exp\left(-\frac{F}{RT}(\zeta_{r/b}-\zeta_{o/b})\right)\Big|_2}{[\equiv \mathrm{CaOH_2^{+1/3}}][\mathrm{R\text{-}COO^-}]K_{int,1}\exp\left(\frac{F}{RT}(\zeta_{r/b}-\zeta_{o/b})\right)\Big|_1+[\equiv \mathrm{CO_3^{-1/3}}][\mathrm{R\text{-}NH_2^+}]K_{int,2}\exp\left(-\frac{F}{RT}(\zeta_{r/b}-\zeta_{o/b})\right)\Big|_1} \quad (5.11)$$

where subscripts 1 and 2 refer to the initial and final/current conditions, respectively.

Considering the continuous flow of oil in a reservoir, we assume there is an unceasing source of polar components in the system. Although this assumption may be less plausible for crude oils with very low content of polar groups, it implies that the available de/protonated calcite sites represent the limiting factor that governs the amount of carboxylic or amine complexes with the rock surface. Hence, considering that the concentration of de/protonated polar groups is comparable at initial and final conditions, i.e., $[\mathrm{R\text{-}COO^-}]|_2 \approx [\mathrm{R\text{-}COO^-}]|_1$ and $[\mathrm{R\text{-}NH^+}]|_2 \approx [\mathrm{R\text{-}NH^+}]|_1$ and dividing both numerator and denominator by $K_{int,1}[\mathrm{R\text{-}COO^-}]$, eq. (5.11) is rewritten as:

$$AAS_{ratio}=\frac{[\equiv \mathrm{CaOH_2^{+1/3}}]\exp\left(\frac{F}{RT}(\zeta_{r/b}-\zeta_{o/b})\right)\Big|_2+A\,[\equiv \mathrm{CO_3^{-1/3}}]\exp\left(-\frac{F}{RT}(\zeta_{r/b}-\zeta_{o/b})\right)\Big|_2}{[\equiv \mathrm{CaOH_2^{+1/3}}]\exp\left(\frac{F}{RT}(\zeta_{r/b}-\zeta_{o/b})\right)\Big|_1+A\,[\equiv \mathrm{CO_3^{-1/3}}]\exp\left(-\frac{F}{RT}(\zeta_{r/b}-\zeta_{o/b})\right)\Big|_1} \quad (5.12)$$

where $A=\frac{[\mathrm{R\text{-}NH^+}]K_{2,int}}{[\mathrm{R\text{-}COO^-}]K_{1,int}}$. Constant A depends on the composition of the crude oil and the relative intrinsic affinity of the amine groups for the calcite surface with respect to that of the acidic components. We expect the defined ratio (A parameter) to have a value within the range [0,1] since most density functional theory (DFT) studies report higher energy of adsorption of carboxylic groups compared to nitrogen-containing molecules[404,405]. However, interpreting the affinity of carboxylic and amine-containing molecules for the calcite surface from published DFT studies can be challenging. First, the reported values in the literature differ significantly. Chun et al.[406] report a Gibbs energy of -122 kJ/ mol for benzoate and -292.6 kJ/mol for stearate. Values around -100 kJ/mol were reported by Ataman et al.[407] for several molecules containing carboxylic groups, whereas much larger values were reported by Ghatee et al.[408] (-28867 kJ/mol for hexanoic acid). The contrast in the reported values may be caused by the use of different computational methods in the DFT simulations but also by the presence of different side groups or the considered coverage[405,407]. While some authors[405,407] report the Gibbs energy of adsorption at a fixed coverage (0.13 ML), other publications[406] compute the profile of the adsorption energy with coverage and report the minimum value as the Gibbs energy of adsorption. The discrepancy between the published values for the adsorption energy is also a consequence of the chemical conditions of the system considered in the simulations. Most DFT studies perform calculations at 0 K in vacuum conditions without including a solvent[409]. However, the presence of water in the system may have an

important impact on the adsorption of organic molecules on the calcite surface[49,404]. Freeman et al.[404] investigated the adsorption of methanoic acid and methylamine adsorption on the calcite surface. Although they observed the same trend as observed in the studies in vacuum, i.e., stronger adsorption of methanoic acid compared to methylamine, they obtained lower adsorption energies on the calcite $\{10\bar{1}4\}$ surface in presence of water, i.e., (-39.3 kJ/mol for methylamine and -64.1 kJ/mol for methanoic acid). On the other hand, Budi et al.[409] only observed adsorption of carboxylic acids and methanol in aqueous conditions at 25ºC, whereas nitrogen-containing molecules showed positive Gibbs energy of adsorption.

With the definition of the interactions between the basic and acidic polar groups in the oil and the calcite surface as given by R5.1 and R5.2, we seek a simple quantitative description of the reactions and not necessarily a true representation of the chemical bonding. While in the model we simply consider that the carboxylic groups interact with the calcium sites, Freeman et al.[404] showed that the methanoic acid binds to the surface in a more complex way; the alcohol hydrogen of the acid interacts with the carbonate oxygen through a hydrogen bond, whereas the carbonyl oxygen of the acid group interacts with the calcium sites. Thus, one carboxylic group could interact with both the calcium and carbonate sites. Moreover, the orientation of the molecules towards the surface can also affect the adsorption process[410]. However, naphtenic acids in the crude oil or even asphaltenes that contain carboxylic or amine groups are usually part of large molecules that have multiple functional groups and where multiple mechanisms can occur simultaneously. Breaking down the interactions of these large molecules into more basic units is challenging.

5.3 Results and Discussion

5.3.1 "SN_{ratio}" and "BPS_{ratio}" versus the remaining oil saturation from spontaneous imbibition tests

Figure 5.2 shows scatter plots of the SN and BPS ratios with the remaining oil saturation from several imbibition tests performed at different conditions (summarized in Table 5.1). We calculate these ratios by considering the output from the SCMs. We show separately the data obtained by using oils with different properties (acid and base numbers), as shown in the title of each plot. We tested the relationship between SN and BPS ratios with the remaining oil by calculating Pearson's correlation coefficient, r, and the p-value to assess whether r is significant. We included both parameters in the figure caption for each dataset. If the p-value is smaller than a certain significance level (usually taken as 0.05) then the correlation coefficient is considered significant. We observe that the BPS ratio does not show a correlation with the remaining oil saturation and in many cases shows values greater than one. This means that the number of bonds at the end of the imbibition is greater than the number of bonds in presence of the formation brine, suggesting more oil-wet conditions with the modified-salinity imbibing brine, which is in contrast with the imbibition experiments. On the other hand, the increase in the stability number ratio shows in some cases an increasing remaining oil saturation, which contradicts the physical significance of this parameter. Moreover, as observed in the expression for this interpolator, the stability number can display positive and negative values, depending on the potential exhibited at the rock-brine and brine-oil interfaces. Despite this, Korrani and Jerauld[100] had restricted its value in their calculation to a positive range, implying that the zeta potentials at the rock-brine and oil-brine have the same polarity. Our calculations suggest, however, that this parameter can be negative in many cases. This is consistent with the experimental evidence included in Figure 5.1 which shows that the zeta potential of the calcite-brine interface in presence of divalent cations is positive, whereas the reported zeta potential of the oil-brine interface[227] is mostly negative at the slightly basic pH (7-8) of carbonate reservoirs. Thus, the interpolators proposed in the literature fail to explain the wettability alteration observed in the spontaneous imbibition tests on outcrop chalk samples.

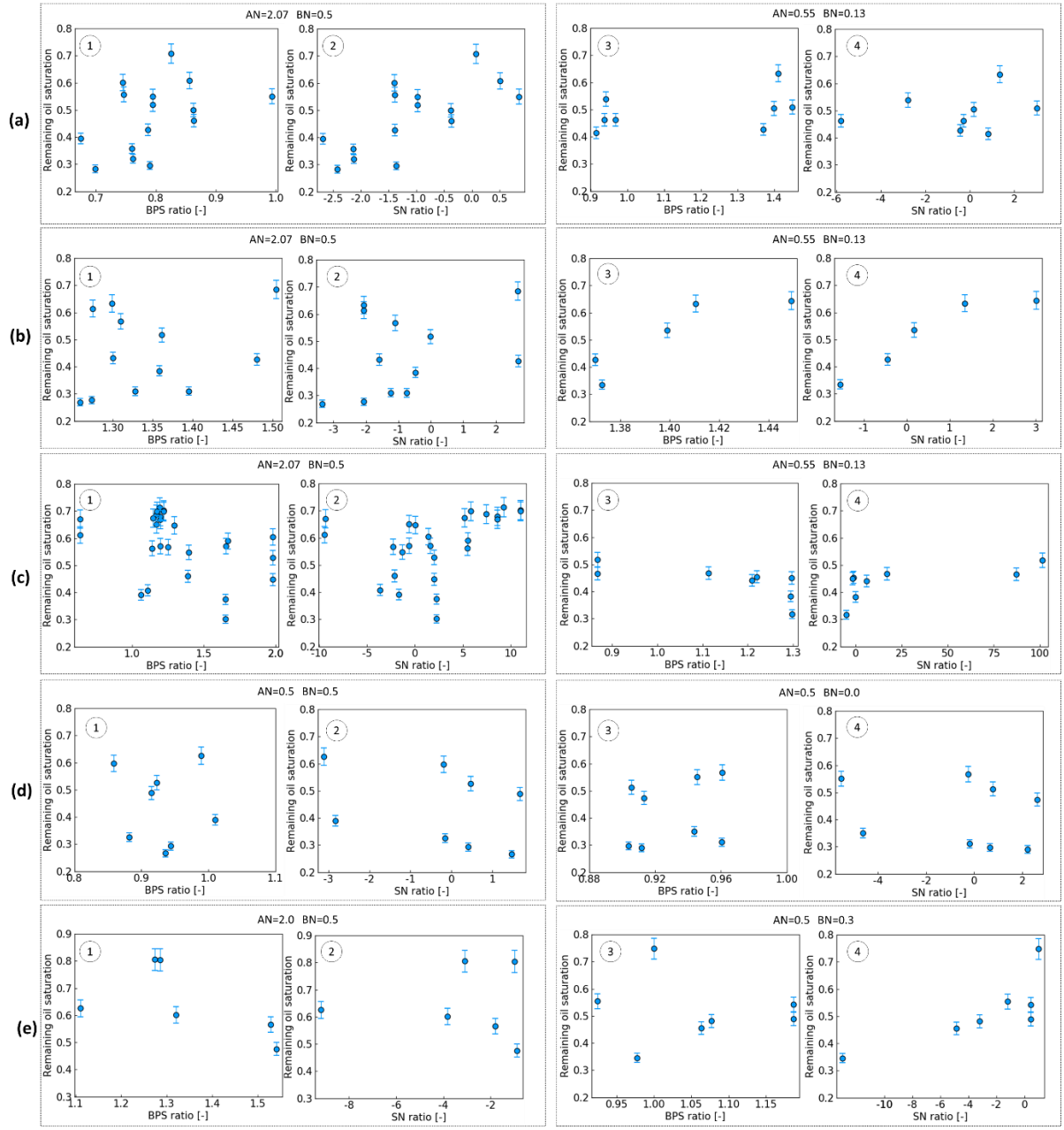

Figure 5.2. Correlation of BPS and SN with the remaining oil saturation at the end of spontaneous imbibition tests ($P_c \approx 0$). The error bars correspond to ±5% experimental error associated with Amott tests [411]. Data from: **(a)** Zhang et al., 2006 [6] 1) r=0.428, p=0.11 2) r=0.705, p=0.003 3) r=0.409, p=0.313 4) r=0.2, p=0.634 **(b)** Zhang and Austad, 2006 [178] 1) r=0.269, p=0.397 2) r=0.348, p=0.266 3) r=0.876, p=0.051 4) r=0.932, p=0.022 **(c)** Zhang et al., 2007 [60] 1) r=-0.389, p=0.0493, 2) r=0.388, 0.049 , 3) r=-0.693, p=0.056 4) r=0.637, p=0.089 **(d)** Puntervold et al., 2007, [348] 1) r=-0.061, p=0.88 2) r=-0.368, p= 0.368, 3) r=0.233, p= 0.578, 4) r=-0.229, p=0.584 **(e)** Fathi et al., 2011, [375] 1) r=-0.573, p=0.233 2) r=0.005, p=0.991, 3) r=-0.080, p=0.864, 4) r=-0.77, p=0.041. Each dataset contains data from experiments performed with two different oils. The AN and BN [mg KOH/g oil) of the oil used for the aging are included in the figures. The circled numbers in the plots enumerate the panels of each figure.

5.3.2 AAS_{ratio} versus the remaining oil saturation from SI tests

Following the same procedure as for the SN and BPS ratio, we calculate the AAS ratio at equilibrium conditions with the formation brine (initial condition) and with the imbibing brine (final condition) used in several spontaneous imbibition tests. Figure 5.3 shows the scatter plot of the AAS ratio with the remaining oil saturation from spontaneous imbibition tests carried out on outcrop Stevns Klint chalk (Figure 5.3-a to -i) and limestone samples (Figure 5.3-j and -k). The correlation coefficient and the p-value are included in the figure caption for the different datasets. The AAS_{ratio} was generated assuming

that the *A* parameter in eq. (5.12) is one. As we have previously discussed in the *methodology* section, inferring experimentally this value is not currently possible. Most crude oils have a larger content of bases compared to acids[319] but the affinity of the bases for the calcite surface is lower than that of carboxylic acids. Thus, we can expect that the numerator and denominator of the term *A* have the same weight. Moreover, we performed the calculations with other values of *A* and, generally, we observed that the *AAS ratio* correlation with the remaining oil saturation was not sensitive to the value of *A* above 0.5. Further analysis of experimental data is needed to tackle the value of A, which is outside the scope of this paper.

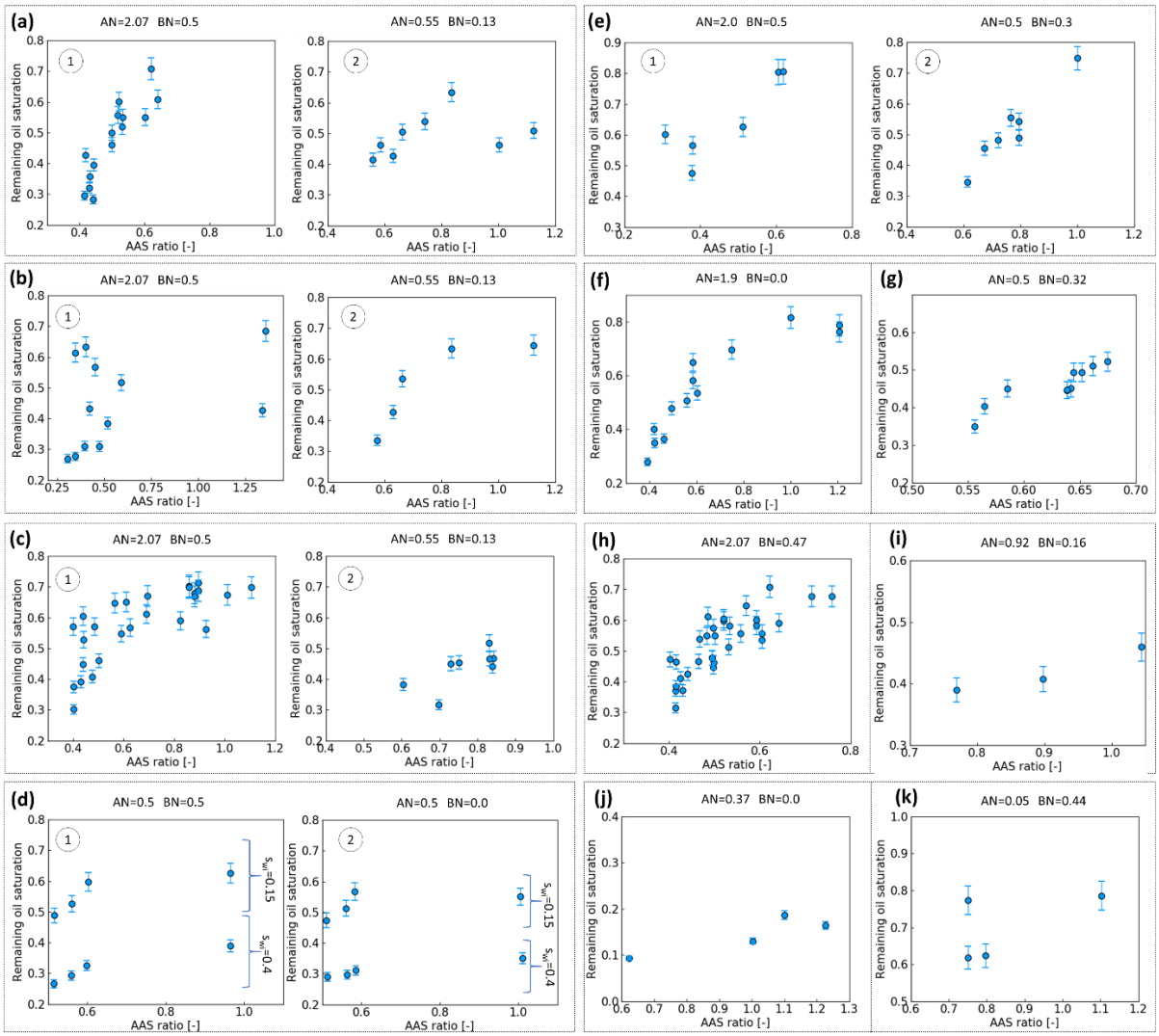

Figure 5.3. Correlation of AAS with the remaining oil saturation at the end of spontaneous imbibition tests ($P_c \approx 0$) for chalk (a to i) and limestone (j and k). The error bars correspond to ±5% experimental error associated with Amott tests [411]. Data from: **(a)** Zhang et al., 2006 [6] 1) r=0.880, p<0.0001; 2) r=0.362, p=0.377 **(b)** Zhang and Austad, 2006 1) r=0.365, p=0.243, 2) r=0.830, p=0.08] [178]; **(c)** Zhang et al., 2007 [60] , 1) r=0.753, p<0.0001; 2) r=0.703, p=0.515 **(d)** Puntervold et al., 2007, 1) r=0.341, p=0.407 2) r=0.233, p= 0.584 [348]; **(e)** Fathi et al., 2011 1) r= 0.859, p=0.028, 2) r= 0.966, p=0.0003 [375]; **(f)** Fathi et al., 2010, r=0.890, p<0.0001[30]; **(g)** Puntervold et al., 2015 [349], r=0.945, p<0.0001; **(h)** Tweheyo et al., 2006 [377], r=0.803, p<0.0001; **(i)** Romanuka et al., 2012 [225], e=0.972, p=0.15; **(j)** Karimi et al., 2016 [382], r=0.877, p=0.12; **(k)** Høgnesen et al., 2005 [379], r=0.568, p=0.431. The circled numbers in the plots enumerate the panels of each figure. In all cases, the AAS ratio was calculated using a constant A=1.

For the spontaneous imbibition tests on chalk, shown in Figure 5.3-a to -i, we observe that the measured remaining oil saturation increases with the calculated AAS ratio. An increase in the available adsorption sites, i.e., more interactions between the oil polar groups and the mineral surface sites, leads to higher remaining oil saturation. Generally, the AAS ratio shows a value below one, meaning that there are

fewer interactions with the polar groups in the presence of the imbibing brine compared to the formation brine. However, for several cases, i.e., Figure 5.3-a (right), -b, -c (left), -d (left), and -f, we note data points showing values greater than one. These correspond to imbibition experiments carried out with seawater without sulfate. In most cases, the use of this brine results in the lowest oil recovery, i.e., higher remaining oil saturation. Considering equilibrium with this brine, the model anticipates more oil-wet conditions than with the formation brine. For the estimation of the BPS, SN, and AAS ratios of different experimental datasets, we separated the measurements based on the crude oil properties. The type of oil affects the initial wetting conditions, hence, the recovery by spontaneous imbibition. We analyze the results from spontaneous imbibition tests carried out by different authors in similar conditions, i.e., same rock type, temperature, initial formation water, and imbibing brine. The only difference in these experiments is the acid and base number of crude oil. Figure 5.4-a shows that crude oil with lower content of polar groups generally shows a higher oil recovery. However, the data in Figure 5.4 (panels b and c), which shows data from cores prepared with different initial water saturation, suggests that the interpretation of the results is more complicated. There seems to be a combined effect of the initial water saturation and the properties of the crude oil on the final oil recovery. At lower initial water saturation S_{wi} (Figure 5.4-b), the recovery is higher for the cores aged in the oil with a lower polar group content (same acid number and no base groups). However, at higher initial water saturation (Figure 5.4-c) no trend can be established. This could also suggest that at higher S_{wi} the contact between the polar groups and the rock surface is hindered and the change of the wettability during the aging procedure is less effective. Rücker et al. [412] showed through μCT images that similar saturations can correspond to very different oil coverage of the rock surface, resulting in contrasting wetting conditions. They suggest that the wettability of a system should preferably be assessed by the relationship between the capillary pressure and the contact area between the oil and the rock. Thus, different methods used to establish S_{wi} may result in different capillary pressure and eventually different wetting conditions.

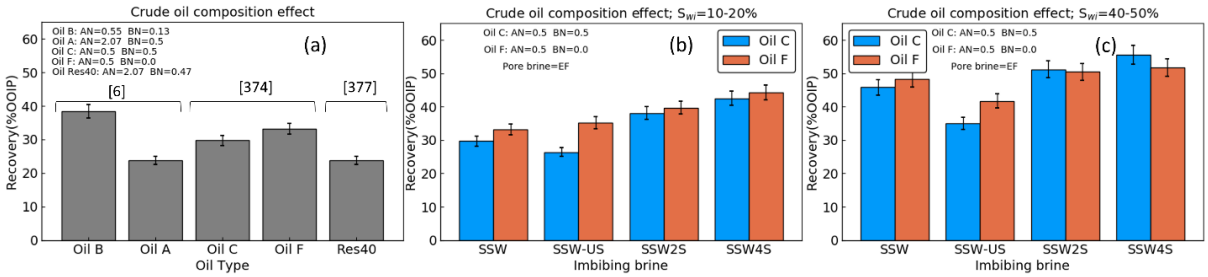

Figure 5.4. Effect of crude oil properties on the final oil recovery from spontaneous imbibition tests with different imbibing brine compositions. **(a)** Imbibition tests performed at 70 0C with different AN/BN crude oils; initial pore water: Ekofisk brine; imbibition brine: seawater; data from [6,374,377]; The numbers in the square brackets correspond to the reference number where the experimental data is taken from**. (b)** Imbibition tests performed at 70 °C with two different types of oil on cores with low initial water saturation; pore brine: Ekofisk brine; data from[348]. **(c)** Imbibition tests performed at 70 °C with two different types of oil on cores with high initial water saturation; pore brine: Ekofisk brine; data from[348]. In panels (b) and (c) SSW stands for synthetic seawater, SSW-US is SSW without sulfate, SSW2S is SSW with twice the concentration of sulfate, and SSW4S is SSW with four times the concentration of sulfate. The error bars correspond to ±5% experimental error associated with Amott tests [411].

In our adsorption model, we partially account for the crude oil composition. We consider the ionizable groups, which govern the electrokinetic properties at the oil-water interface. For the bulk oil, we make important simplifications considering that the concentration of the polar groups is maintained constant throughout the test, i.e., the adsorption of polar groups on the surface does not alter their concentration significantly. We consider that this assumption is especially valid at the reservoir scale, where the adsorbed polar groups can be replaced due to the diffusion of the polar groups over the millions of years that oil resides in the reservoir. We are aware, however, that describing the complex crude oil composition in terms of two main polar groups with similar affinity for the surface may represent an overly simplified picture of the true adsorption processes taking place in the crude oil-brine-rock system.

Although the data from the work of Puntervold et al.[348] shows an evident trend of increasing oil recovery with increasing S_{wi} (Figure 5.4, panels b and c), this pattern may not always be so obvious. Viksund et al.[413] studied the effect of the initial water saturation on the final oil recovery for chalk. For Stevns Klint chalk they observed that higher initial water saturation resulted in higher final oil recovery. The opposite effect was observed for Rørdal chalk, which showed a lower oil recovery for higher initial water saturation. Figure 5.5 shows the oil recovery from spontaneous imbibition tests carried out by Fernø et al.[378] on outcrop chalk from different locations with different initial water saturation. No relationship between S_{wi} and the recovery factor is observed from these data.

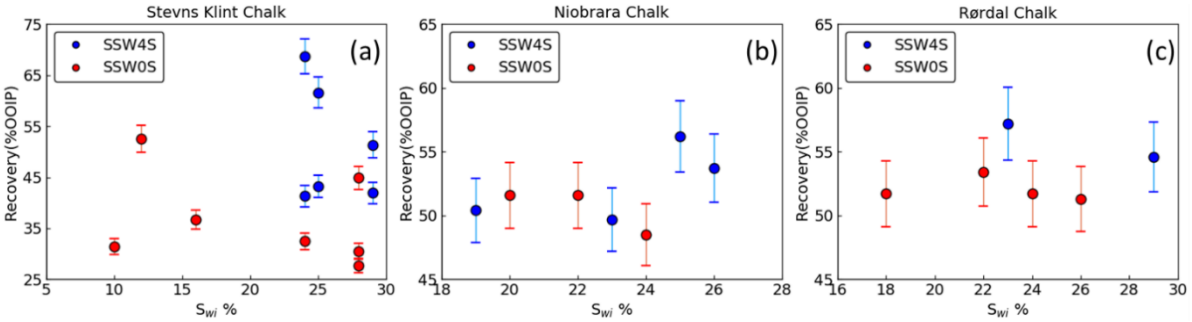

Figure 5.5. Effect of initial water saturation on the final oil recovery from spontaneous imbibition tests performed with two different imbibing brines carried out on different outcrop chalk types: **(a)** Stevns Klint chalk **(b)** Niobrara chalk **(c)** Rørdal chalk. Data from[378]. The spontaneous imbibition tests were performed at 130 ºC and all the cores were initially saturated with the same brine. SSW0S corresponds to synthetic seawater without any sulfate and SSW4S corresponds to synthetic seawater with four times sulfate concentration. The error bars correspond to ±5% experimental error associated with Amott tests[411].

The effect of S_{wi} on oil recovery is one of the limitations of our model. In the proposed thermodynamic formulation, we do not include a dependency on the initial water saturation nor the thickness of the water film. Therefore, for an imbibition test performed at different initial water saturation with all the other conditions kept constant, our model shows that AAS versus oil recovery correlates well *only* for experiments with the same S_{wi}. For different S_{wi} values, however, the model fails to show a relationship with the experimental data (Figure 5.3-d). For the data from Puntervold et al.[348] shown in Figure 5.3-d we observe two identical trends for contrasting remaining oil saturations. This behavior is caused by the different initial water saturation used in the cores. The data points associated with the higher remaining oil saturation correspond to cores that were initially set to lower water saturation, i.e., 10-20%, and the ones associated with the lower remaining oil saturations correspond to cores with S_{wi} around 30-50%. In our calculations, we used values of 15% and 40% for the cores with low and high initial water saturation, respectively. The data from Fernø et al.[378] shows also that different types of chalk can have different recovery behavior during displacement tests. Our model cannot reflect these differences because we consider a homogeneous calcite surface at the brine-rock interface. Thus, we do not account directly for any heterogeneities, organic, or siliceous surface coating which may affect the wetting properties of the rocks[413].

Among all the experiments used for testing the wettability parameters, the remaining oil saturation from spontaneous imbibition tests with one of the crude oils from Zhang and Austad[178] (Figure 5.3-b left) shows the poorest relation with the available adsorption sites ratio. A closer look into these data reveals that for some of the cores a different aging time was applied during the establishment of the initial wettability condition. All the cores equilibrated with the less acidic crude oil (AN=0.55 and BN=0.13) were aged for 30 days and the data obtained from these cores correlate with AAS (Figure 5.3-b right). However, some of the cores saturated with the higher acidic oil were aged for 28 days, whereas others for 57 days. Figure 5.6 shows the data from Zhang and Austad corresponding to the cores saturated in the acidic oil (AN=2.07 and BN=0.5) and aged for 57 days. Disregarding the point that shows a much higher residual oil saturation, we observe an increasing trend in the AAS ratio with increasing oil saturation after the imbibition. It should be noted that the test with seawater with twice-enriched sulfate

(SSW×2S) was performed twice (the arrows in Figure 5.6 indicate the repeated mentioned test), resulting in very different oil recovery.

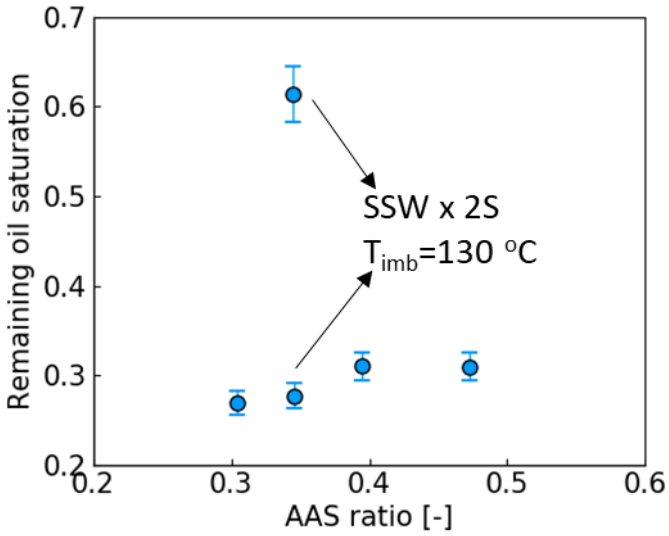

Figure 5.6. Correlation between the remaining oil saturation from the spontaneous imbibition tests performed on cores saturated with oil with AN=2.07 and BN=0.5 and aged for 57 days. SSW×2S corresponds to synthetic seawater with twice the sulfate concentration. Data from Zhang and Austad[178]. The error bars correspond to ±5% experimental error associated with Amott tests[411].

This analysis of published experimental data shows the importance of the core preparation on the obtained experimental results, but also exposes another constraint of the idea behind AAS. The parameter defined in this work is based solely on thermodynamic considerations and accounts for neither the initial water saturation nor the aging time. Although being irrelevant at the reservoir scale, the aging time has an important impact on the experimental results. Figure 5.7 shows the aging effect on the final oil recovery from spontaneous imbibition tests. Although variable optimum aging times are reported in the literature, the time required to achieve uniform initial wetting conditions upon contact with the crude oil is most likely unique to each core sample and experimental conditions[414].

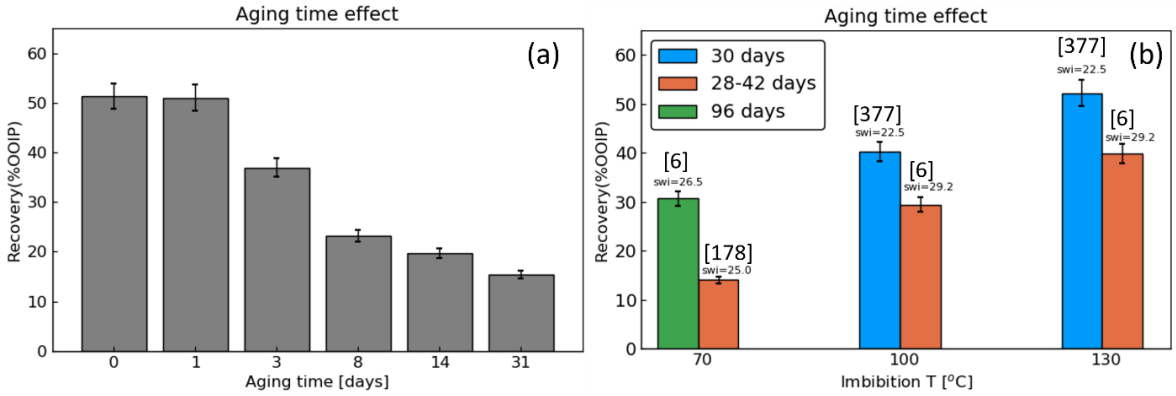

Figure 5.7. Effect of aging time on the final oil recovery from spontaneous imbibition tests: **(a)** Data from ref [365] **(b)** Data from refs[6,178,377]. The numbers in the brackets correspond to the references where the experimental data was taken from. The error bars correspond to ±5% experimental error associated with Amott tests[411].

The purpose of the aging time is to ensure equilibrium between the rock-brine-crude oil. The fact that the recovery changes depending on the aging time (Figure 5.7-b) indicates that the core had not reached equilibrium with the oil and the water during the aging procedure and the cores most likely have different initial wetting conditions. Thus, non-equilibrium conditions can also be responsible for the scattering in the correlation between the AAS ratio and the oil recovery.

Increasing the temperature during the aging stage plays also an important role in the core wetting condition, turning the wettability towards more oil-wet. The aging temperature in the spontaneous imbibition tests was shown to have a higher influence on the oil production than the ionic composition of the imbibing brine[376]. Figure 5.8 shows the effect of the aging temperature and crude oil properties on the final oil recovery.

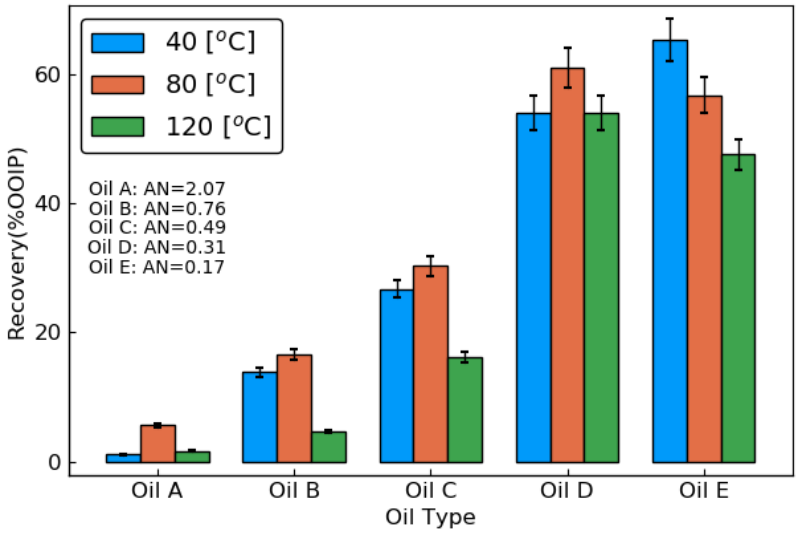

Figure 5.8. Effect of aging temperature and crude oil properties on the oil recovery from spontaneous imbibition tests carried out at 70 °C. Initial water saturation of the cores was between 24-34%. The pore brine composition corresponds to Ekofisk formation water and the imbibing fluid is seawater. Data from ref[376]. The error bars correspond to ±5% experimental error associated with Amott tests[411].

Comparable to the other parameters involved in the aging procedure, our model cannot account for the differences in the aging temperature if this is different from the temperature fixed in the imbibition test. Most considered datasets include cores aged at 90 °C. If the imbibition temperature is the same as the aging temperature, the model can account for the differences in the recovery because the initial equilibrium would be calculated at the aging temperature. The AAS value at initial conditions could also be calculated at the aging temperature. However, the effect of temperature on the surface speciation and the charge development, thus on the AAS, although currently included in the model mostly based on analogous aqueous phase speciation reactions, requires further separate investigation.

We also investigated the correlation of the AAS with the results from spontaneous imbibition tests on limestone (Figure 5.3-j and -k). We found these experiments to be less numerous than on chalk. Some of the reported data sets were also lacking parameters we use in the modelling (i.e., crude oil properties[380]). Given the reduced number of data points that we have considered, we cannot observe a statistically significant correlation between AAS and the remaining oil saturation for limestone. For some brine compositions, the calculated AAS ratio is larger than one. We postulate that two main factors are responsible for this behavior. First, the formation water used in the experiments with limestone has a much higher ionic strength (>3 M) than that used for chalk (≈1.5 M). Generally, the applications of surface complexation models and the underlying equations become limited at high ionic strength[312,313]. Secondly, the electrokinetic properties of the limestone/water interface were shown to be different from those at the chalk/water interface[24]. Thus, the equilibrium constants we used for the CD-MUSIC model for the calcite-water interface, which showed a good prediction of the chalk electrokinetic behavior, may not be representative of the electrical properties at the limestone-water interface. Because we use a unique set of equilibrium constants for the calcite surface speciation, our model cannot capture the different imbibition behavior of different types of chalks or different types of carbonates. However, the different oil recovery is not necessarily an effect of chemical heterogeneities but of different pore shapes. Romanuka et al.[225] reported different imbibition behavior for three different kinds of limestone with similar mineralogy. Thus, an important limitation of our model is that it does not account for the

pore shape, which may play an important role in understanding how the wettability is established at the pore level[415].

The way the aging procedure is conducted is associated with other challenges. Several authors consider dynamic aging as more appropriate for establishing initial wetting conditions because it requires a shorter aging time and achieves more homogeneous wettability conditions[368,416]. However, factors like the injection rate [368], the length of the cores, and the direction of injection of the oil[416] have also an impact on the dynamic aging procedure, thus, on the initial wettability conditions.

The discussion above shows that the remaining oil saturation from these experiments is tightly linked to the core preparation procedure. Initial water saturation, crude oil properties, aging time, and temperature dictate the final oil recovery from these experiments. If the cores do not have the same initial wettability, not only the interpretation of the experimental results but also the modelling of the data becomes more difficult. Even minor changes in the core preparation procedure can affect the initial wetting conditions, thus the final oil recovery. The tremendous impact of the protocol of spontaneous imbibition tests on the produced oil was also demonstrated by Bartels et al.[417]. However, in the calculation of the AAS for the different imbibition tests, the input variables in our model are the formation and imbibing brine compositions, crude oil properties, and the imbibition temperature. Thus, the proposed model cannot account for any non-equilibrium conditions that may arise during the core preparation procedure. Note that even though we attempted to include the effect of all the aspects from the core preparation procedure on the AAS parameters, their contribution to the wettability cannot be easily isolated because these factors are usually interdependent[373]. Moreover, the scope of this paper is not to provide an empirical formulation with many adjustable parameters just to reach better correlations at the core scale. Our model attempts to explain the wettability alteration that occurs at the reservoir scale, where the effects of the core preparation procedure are no longer relevant. Standardized experimental procedures and the progress in imaging of core-scale flow experiments[385,417] may provide further insight into the wettability alteration during MSW. However, even the strictest core preparation protocols may not be enough for setting analogous wetting conditions for chalk samples, whose surface was shown to be covered by organic coatings[214,418] resulting in heterogeneous surface properties[419]. A remaining challenge of the AAS formulation is that it does not account for the mineralogical heterogeneity nor the pore shape. However, we postulate that we could somehow account for the specific mineralogy indirectly through the electrostatic term, which is proportional to the potential difference between the rock-water and oil-water interfaces. In this work, for the calcite/water SCM, we used equilibrium constants that resulted in a good prediction of the electrokinetic potential of Stevns Klint chalk. These equilibrium constants could be adjusted to make the model suitable for other types of carbonates by fitting the model to the, e.g., measured zeta potential of the rock samples in different brine compositions and temperatures. The application of the AAS parameter is not limited to the mechanistic modelling of MSW in chalk but it can also be integrated into reactive transport models to assess the flow of organic contaminants, e.g., naphtenic acids, in the subsurface[420].

5.4 Conclusions

The experimental research performed in the context of modified salinity waterflooding of chalk cores needs to be closely complemented by modelling work to eventually assess and predict the behavior of this improved oil recovery method at a larger scale. The parameter used in the interpolation between water-wet and oil-wet conditions should correlate with the wettability of chalk. The main key findings of this study can be summarized as follows:

- We could not find correlations between the previously suggested interpolants for carbonates (“bond product sum” and “stability number”) and the remaining oil saturation from spontaneous imbibition tests on chalk. These parameters cannot explain the wettability alteration nor the improved oil recovery observed in chalk when injecting brines with different compositions.

- We proposed a new wettability interpolant called “Available Adsorption Sites” as a function of the interactions of polar molecules from the oil phase with the chalk surface. We described these interactions in analogy with the thermodynamics of adsorption of ions on charged surfaces. This parameter correlates almost linearly with the remaining oil saturation from most spontaneous imbibition tests for chalk.
- The factors involved in the core preparation procedure (e.g., initial water saturation, aging temperature, aging time, etc.) influence the initial wetting conditions and the final oil recovery in the lab. Because of this, imbibition tests performed with the same oil, formation water, and imbibing brine may yield different oil recovery. Non-equilibrium conditions, the intrinsic heterogeneous chalk surface properties, or differences in the core preparation procedure can introduce scattering in the correlation between AAS and the remaining oil saturation.
- This model can potentially apply to other carbonates. However, further investigation is needed to address the correlation between the AAS ratio and the remaining oil saturation from spontaneous imbibition tests on rocks with different mineralogy, e.g., limestone.

6 Adsorption of carboxylates on calcite: coupled effect of calcite-brine and brine-oil interactions

The adsorption of polar organic molecules on the surface of brine saturated carbonate rocks alters the relative mobility of oil and water, with important implications for oil production and groundwater remediation. We propose a mathematical model for the adsorption of polar organic acid groups (initially contained in an oil phase) on calcite in the presence of brine. We reduce the problem into smaller subsystems and characterize them by identifying the key interactions. The oil-brine equilibrium is dictated by the partitioning of acidic components between the two phases. The dissolved acids ionize to carboxylate species in the water phase, which may either form complexes with the calcite surface or precipitate as calcium carboxylate salts by binding calcium ions from the solution. All these interactions are implemented into a Phreeqc model as equilibrium and kinetic processes. To obtain the main parameters (e.g., partition, ionization, or adsorption constants) governing the behavior of the different subsystems at different chemical conditions, we tune the sub-models to relevant experimental data (e.g., partitioning, precipitation, adsorption, and electrokinetic measurements). We then assess the performance of the model by coupling the reaction network to the transport equations and simulating the crude oil injection within a chalk core to predict effluent acid concentration history. By defining the total acidity of crude oil as a mixture of several carboxylic acids, our model satisfactorily fits the experimental data. The total acid number that is commonly reported as the sole indicator for the concentration of organic acids in oil does not allow distinguishing between different types of organic acids nor their affinity towards the calcite surface. More sophisticated analytical methods for quantifying the acid species in the crude oil are required for a more accurate description of the adsorption process using our model.

This chapter is a revised layout of the article: M. Bonto, A.A. Eftekhari, H.M. Nick Adsorption of carboxylates on calcite: coupled effect of calcite-brine and brine-oil interactions. Submitted.

6.1 Introduction

The hydrophilic nature of the pristine calcite surface may be drastically impacted by exposure to certain impurities[33]. The adsorption of organic entities may change the surface wettability, growth, and dissolution, affecting the reactive transport of species through carbonate porous media and separation processes[53,421–424]. Research in the field of oil recovery has made an important contribution to the existing knowledge on the interactions between calcite and organic molecules. Within this field, scientists have tried for many years to unravel why, opposite to sandstones, many carbonate reservoirs are mixed/oil-wet[425]. Understanding the development of the initial wetting condition is also crucial for deducing how the wettability can be reversed towards a more water-wet state through enhanced oil recovery (EOR) techniques such as modified salinity waterflooding (MSW). The popular disagreement on the recovery mechanisms in carbonate reservoirs upon MSW is most likely caused by (i) the vague understanding of the hydrocarbon phase and its particularities in terms of crude oil components, and (ii) the strong segregation of the research on either calcite-brine or oil-brine interactions, hence the lack of a holistic approach; these are the two main aspects addressed and discussed in this work.

Although different organic molecules may lead to divergent effects on the calcite surface reactivity[426], the interfacially active polar components in the oil phase are still treated as agglutinates in terms of the total acid and base numbers (TAN and TBN, respectively). The TAN and TBN are determined through potentiometric titrations and expressed in mg KOH/g oil; they merely indicate the total acidic or basic material within the bulk oil, without accounting for any other properties, e.g., size/chain length or aromaticity, that eventually determine the partitioning of these acid/base groups between the oil/water phases[427] or their activity at interfaces[428]. The shortcomings of characterizing the oil in terms of the TAN/TBN are extensively documented. Neither the electrokinetic behavior at the crude-oil water interface[227], oil-wet fraction from flotation tests[103], oil-recovery in microfluidic devices[429] nor contact angles[430] showed any correlation with TAN/TBN. This was somehow expected as some acids/bases preferably stay in the bulk fluid (either oil or water depending on the solubility) rather than traveling and adsorbing at interfaces[431]. Compared to acids, bases are less likely to travel to the oil-water interface or to interact with the calcite surface[321,326]. Acids, on the other side, may bind to the calcite surface to different extents depending on their molecular structure[432]. However, even once adsorbed on the mineral, carboxylates may not necessarily decrease the calcite affinity for the water phase as the carboxylates themselves may be hydrophilic enough to bind water molecules[433]. Thus, different acids in the oil phase may have contrasting effects on calcite wettability. Fathi et al.[434] showed that cores aged with crude oil containing acidic components that are "water-extractable" lead to lower oil recovery in spontaneous imbibition tests; this implies that those acids that partition into the brine phase are more efficient in shifting the calcite wettability towards oil-wet conditions. Contrastingly, Madsen and Lind[435] suggest that acids readily soluble in water (i.e., benzoic acid) cannot adsorb on calcite from an aqueous phase; their observations are consistent with many other publications (e.g., refs [421,436]) that advocate only for the adsorption of long-chain fatty acids, which are less soluble in water. Despite the low solubility, long-chain fatty acids (C10-C20) often populate the oil/brine interface[428] because of their amphiphilic structure.

The coupled nature of the interactions between crude oil, brine, and rock hampers appraising the weight that each of these interactions plays on the overall system behavior. In other words, although the different interplaying parts are identified, their contribution cannot be easily assessed. To address this challenge, many experiments were designed to separately study the interactions in the brine-rock[137,170,181] or oil-brine[15,16,287] systems. The knowledge coming from these experiments is extremely valuable and essential for the development of surface complexation models (SCMs) for both the calcite-brine (e.g., refs [67,69,104]) and oil-brine interfaces[227]. These SCMs, which describe and quantify the adsorption and charge development at both interfaces based on the brine and crude oil composition, are often used to assess the wetting conditions. For instance, previous publications have reported a

correlation between the surface speciation and electrokinetic potential at the oil-brine and rock-brine interfaces and the residual oil saturation from spontaneous imbibition tests on chalk[101] and contact angle of calcite[298]. Others[102] have shown that contact angles can be estimated based on the DLVO[39] (Derjaguin-Landau-Verwey-Overbeek) extended theory. However, none of these approaches considers an explicit interaction between the crude oil components and the calcite, making it impossible to quantify the polar components adsorbed on the mineral, which eventually governs the wettability condition. Moreover, in the previous models the two interfaces are assumed to be independent (e.g., refs [95,100,101]) as these models do not consider that some oil components partition between the oil and water phases, leading to changes not only in the pH but also calcite reactivity.

To overcome the limitations of the existing models, we propose a unifying method to describe the overall crude oil-brine-calcite interactions by specifically accounting for the oil-brine equilibria and the adsorption of polar acid groups at the calcite surface. To validate the model, we considered several types of batch experimental data: (i) partitioning of carboxylic acids between the oil and water phases, (ii) adsorption of carboxylic acids on the calcite surface, and (iii) electrokinetic measurements of calcite suspensions containing fatty acids. Then, we check the consistency of the model against dynamic adsorption experiments that report the TAN of the effluent during the injection of a specific crude oil within a chalk core. We also assess whether describing the crude oil in terms of only TAN is reasonable and sufficient to appraise the adsorption of crude oil components on the calcite surface and the associated shift in the wetting conditions.

6.2 Methodology

To describe the adsorption of polar groups at the calcite surface, we considered the coupled equilibria between the oil-brine and calcite-brine systems. We first propose a model for the interactions between the oil and brine phases. This model is then coupled to an SCM that explicitly accounts for the adsorption of the polar groups transferred to the brine onto calcite. A complete description of the models is provided hereafter.

6.2.1 Oil-brine equilibria

In presence of an aqueous solution and oil, carboxylic acids (represented by R-COOH) may partition between the two phases. Note that with the term carboxylic acid we also include naphtenic acids, not only saturated acids. The acids partitioned in the water phase may dissociate depending on the pH. Once dissociated, carboxylates ($R\text{-}COO^-$) may bind (especially) calcium ions from the solution leading to the formation of calcium carboxylate precipitates, $Ca\text{-}(RCOO)_2$. Other equilibrium reactions such as dimerization may also take place[321] but these have not been included here. The partitioning, dissociation, and precipitation may be represented by the equilibrium reactions (R6.1) to (R6.3), respectively.

$$R\text{-}COOH_{(o)} \overset{K_{wo}}{\longleftrightarrow} R\text{-}COOH_{(w)} \quad \text{(R6.1)}$$

$$R\text{-}COOH_{(w)} \overset{K_a}{\leftrightarrow} R\text{-}COO^- + H^+ \quad \text{(R6.2)}$$

$$Ca\text{-}(RCOO)_2 \overset{K_{Ca}}{\longleftrightarrow} 2RCOO^- + Ca^{2+} \quad \text{(R6.3)}$$

where K_{wo} [-] is the oil-water partition constant, K_a [-] is the dissociation constant, K_{Ca} [-] is the solubility product of the calcium carboxylate precipitate, R-COOH represents the carboxylic acid formed by a radical R of variable chain length/structure with a carboxylic group -COOH, and the subscripts “o” and “w” refer to the oil and water phase, respectively.

We formulate this equilibrium model within the geochemistry software Phreeqc[241] by explicitly defining the carboxylic acid and the pertinent undergone equilibrium reactions (R6.1 to R6.3). When the oil/organic phase contains a mixture of unknown carboxylic acids, the defined carboxylic acid is

rather a pseudocomponent mimicking the overall behavior of the acid mixture. For crude oil, the total number of acid moles included in the equilibrium calculations are calculated from its TAN. We obtain plausible values for the constants involved in the defined equilibria by fitting the model to experimental data obtained from oil-water partitioning experiments[321,329].

6.2.2 Calcite-brine-oil equilibria

To quantify the adsorption of aqueous species on the calcite surface we implement in Phreeqc the Charge Distribution Multi-SIte complexation (CD-MUSIC) model proposed for calcite by Wolthers et al.[67]. According to this model, the calcite-water interface consists of three different electrostatic adsorption planes, e.g., the surface, inner Helmholtz plane (IHP), and Outer Helmholtz plane (OHP), where different ions/aqueous species bind depending on their affinity for the surface. The net charge change, Δz, experienced by each of these planes upon ion adsorption depends on the structure of the surface complex. Here we consider that the adsorption of ions takes place essentially on the predominant $\{10\bar{1}4\}$ calcite cleavage plane, characterized by an equal number of hydrated calcium and carbonates sites (4.95 #/nm^2)[89]. Besides the surface reactions included in our previous publications[101,221], i.e., de(protonation) and the adsorption of calcite lattice ions (i.e., Ca^{2+} and CO_3^{2-}) or ions commonly present in seawater (e.g., Mg^{2+} and SO_4^{2-}), we define an explicit interaction between the calcite and carboxylate ion. Since we presume that the calcite surface is hydrated, only the carboxylates partitioned in the water phase can adsorb on the calcite surface; this is consistent with the observations from the work of Fathi et al.[434]. Moreover, as previously indicated by several experimental studies[437–439], we postulate that carboxylates interact with the calcite calcium sites leading to the removal of the hydroxyl group upon adsorption. Thus, the adsorption of carboxylates on the calcite surface is represented by reaction (R6.4):

$$\equiv CaOH^{-2/3} + R\text{-}COO^- \overset{K_{ads}}{\longleftrightarrow} \equiv CaOOC\text{-}R^{-2/3} + OH^- \qquad \text{(R6.4)}$$

where K_{ads} [-] represents the intrinsic equilibrium constant of the adsorption reactions.

According to the theory behind surface complexation modelling, the total energy of adsorption of a species on a charged surface is given by a chemical contribution proportional to the intrinsic equilibrium constant, K_{ads}, and an electrostatic term proportional to the product of the net charge change in the adsorption plane and the potential difference between the adsorption plane with respect to the bulk[73,101]. Thus, the extent of the surface reaction does not depend only on the intrinsic equilibrium constant but also on the electrostatic contribution. An apparent equilibrium constant, K_{app}, that takes into account both contributions, is given by eq. (6.1).

$$K_{app} = K_{ads} \exp\left(-\sum \Delta z_i F \psi_i\right) \qquad (6.1)$$

where F [96485.33 C/mol] is the Faraday's constant, Δz_i is the net charge change at plane i caused by the adsorption reaction, and ψ_i [V] is the potential at plane i with respect to the bulk.

Depending on the type/structure of the adsorbing acid, the adsorption constant, K_{ads}, may take values within a range of several orders of magnitude. Thus, the adsorption of carboxylic acids at the calcite surface from the crude oil cannot be accurately modelled unless the identity of the acids in the crude oil is resolved. Despite the existing evidence on the adsorption of asphaltenes and resins on the calcite (e.g., refs [440,441]), their molecular weight (MW) and charge in water are highly unknown, which impedes any attempt of obtaining the equilibrium constant based on these data. Since we are not interested in all organic acids that adsorb on the calcite surface but rather in those that have an impact on its wetting characteristics, to constrain our model, we need to select a well-known molecule that is representative of the acidic components in the crude oil that affect the calcite wettability. Long-chain carboxylic acids with carbon numbers between 10 and 25 are known to be the most interfacially active acids[428] and have an important effect on calcite wettability[421,436,442]; because of this and the fairly large amount of

experimental data available in the literature, we chose oleate to tune the surface reaction between the carboxylate ion and calcite (R6.4).

To include reaction (R6.4) within our SCM implemented in Phreeqc, we need to define both the intrinsic equilibrium constant, $K_{ads,}$ and the net charge change in each adsorption plane (see eq. 6.1). However, abstracting a reasonable charge distribution considering the unknown structure of the surface complex formed by these large organic molecules seems rather ambitious. In analogy with the adsorption of oxyanions (e.g., CO_3^{2-}), we assumed that when carboxylates adsorb, a fraction of the charge of the carbon in the carboxylic group is neutralized by the surface oxygen, whereas the remaining charge is assigned to the IHP. Thus, if we consider that half of the carbon charge is assigned to the 0-plane, the net charge change at the surface (Δz_0) is [+1-2+0.5·4], where the first term corresponds to the loss of the hydroxyl ion upon the adsorption reaction, the second represents the charge of the surface oxygen and the third term represents the fraction of charge of the carbon ion. The remaining fraction of the carbon charge [0.5·4] and the charge of the second oxygen [-2] are placed in the IHP; if this was the only charge contribution to this plane, the net charge change at the IHP (Δz_1) would amount to 0. Nonetheless, the remaining radical, R-, may also contribute to the net charge of both the IHP and OHP. Since we do not have any information on the contribution of the radical to the net charge change at neither the IHP nor OHP, we define only the net charge change at the surface (Δz_0=1) and leave Δz_1 and Δz_2 as adjustable parameters. Thus, we obtain the intrinsic equilibrium adsorption constant, K_{ads}, Δz_1, and Δz_2 by considering both the adsorption experiments reported by Young and Miller[443] and electrokinetic measurements performed by Rao et al.[172]. The inferred parameters are further validated against additional adsorption and electrokinetic datasets.

6.2.3 Flowthrough (dynamic) retention tests

Although batch experiments are valuable for characterizing the interactions between calcite, brine, and oil, our final goal is to use the reaction network to describe reactive transport processes in porous media. Under flow conditions, some of these interactions will be influenced by the residence time of the fluids, the specific surface area (ssa) of the solid, or the interfacial contact area between the fluids. Thus, we assess whether the model can explain the dynamic retention of polar groups measured during the flooding of crude oil within a calcite core. The transport of acid species through porous media can be described according to eq. (6.2):

$$\frac{\partial}{\partial t}(\varphi c_i + (1-\varphi)\rho_s a_s q_i + \varphi s_i) + \nabla \cdot (\boldsymbol{u_o} c_i) + \nabla \cdot (-\varphi D_i \nabla c_i) = R_i \qquad (6.2)$$

where t [s] is the time, φ [-] is the porosity, c_i [mol/m^3] is the concentration of acid i, ρ_s [kg/m^3] is the mineral density, a_s [m^2/kg] is the specific surface area of the rock, q_i [mol/m^2] is the number of moles of acid species i adsorbed per unit surface area of rock, s_i [mol/m^3] is the number of moles of acid i precipitated per unit volume of solution, u_o [m/s] is the velocity of the oil phase, D_i [m^2/s] is the diffusion coefficient of acid i in the oil phase and R_i is a source/sink term.

We solve the transport of acid species in one dimension by using FiPy[213], a finite volume tool for solving partial differential equations developed for Python. This solver is coupled to the PhreeqcRM[212] reaction module, which at each time-step solves for the chemical interactions in the calcite-brine-oil system. We assess the consistency between this transport model and the flowthrough tests with crude oil on cores at irreducible water saturations published recently by Puntervold et al.[424]. Thus, for the size of the 1D domain, we consider the length of the core (L=6.4 cm) and a uniform mesh of 50 cells. For all Phreeqc calculations, we use the Lawrence Livermore National Laboratory database ("llnl.dat").

6.3 Results and Discussion

6.3.1 Oil-brine equilibria

We obtained the constants of reactions (R6.1) to (R6.3) by fitting the equilibrium model described in section 6.2.1 to the experimental data from Bertheussen et al.[321] (Figure 6.1). In the experiments considered, the authors determined the amount of naphtenic acid partitioned at different pHs between an oil phase (heptane) and an aqueous solution containing 3.5 wt % NaCl. To observe the effect of calcium on the partitioning, they also carried out experiments in 3.5 wt % NaCl containing 10 mM $CaCl_2$. The experiments were performed with two naphtenic acids of different MW. We chose this dataset because compared to other partitioning experiments available in the literature (e.g. refs [427,444]), in this publication, the experimental protocols and the ratio of aqueous solutions/oil phases are clearly outlined.

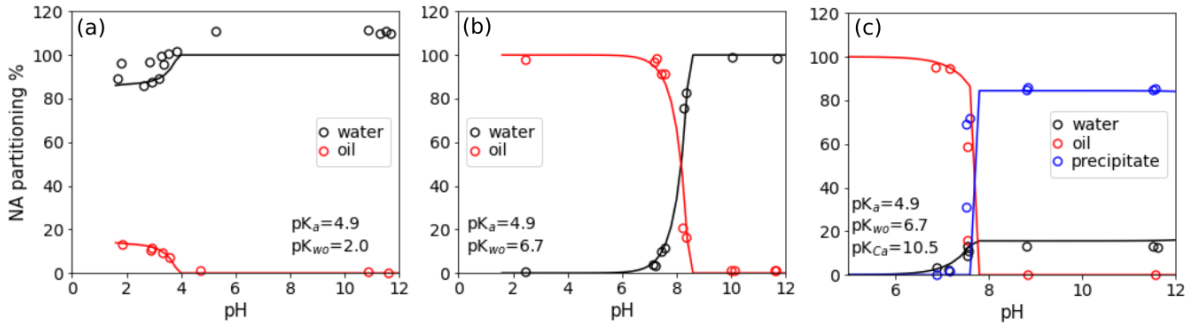

Figure 6.1. Naphtenic acid partitioning between heptane and 3.5 wt % NaCl aqueous solution at different pHs: **(a)**10 mM low MW naphtenic acid (phenylacetic acid); **(b)** 1 mM high MW naphtenic acid (4-heptylbenzoic acid); **(c)** 1 mM high MW naphtenic acid (4-heptylbenzoic acid) in the presence of 10 mM $CaCl_2$. The lines show the model fitted to the experimental data (markers) from Bertheussen et al.[321].

The structure and MW of the naphtenic acids have a great impact on their partition between the oil and the water phase. The lower MW naphtenic acid (Figure 6.1-a) has a partition constant within 4 orders of magnitude higher than the high MW acid (Figure 6.1-b) and will stay predominantly in the water phase along the entire pH range studied (2-12). This is consistent with previous publications that have shown that the acid partition coefficient linearly decreases as its MW increases[427]. Moreover, with the same ionization constant, pK_a=4.9, we described well both equilibria. While adding calcium to the aqueous solution showed no impact on the partitioning of the lower MW acid, a significant amount of acid was lost near neutral and basic pH conditions for the system containing the high MW acid (Figure 6.1-c). This loss was attributed to the formation of a calcium carboxylate precipitate. We found that the solubility product that fits the acid distribution between the different phases (pK_{Ca}=10.6) is slightly higher than that inferred for naphtenic acids extracted from a North Sea crude oil[444] (e.g., pK_{Ca} between 11-14). However, the solubility product depends greatly on the structure of the naphtenic acid (e.g., number of C=C unsaturations and length of alkyl chain). This explains the wide range of solubility products (pK_{Ca} between 9.9 and 14.8) reported for fatty acids calcium precipitates[445]. Other factors such as the background electrolyte concentration may also lead to changes in the onset of precipitation and measured solubility products. It is important to note that the parameters inferred in this work are not directly comparable with those obtained by Bertheussen et al.[321] as we do not include dimerization and the equilibrium calculations consider activities, not concentrations.

Besides partitioning experiments performed at pH values fixed by acid/base titrations, the evolution of the pH upon the mass transfer of acids from an oil phase to the water phase or oil-water interface provides important insights into the oil-brine equilibria. To determine the impact of acid partitioning on the pH of an aqueous solution, Hutin et al.[329] prepared oil in water emulsions at an initial fixed pH. These oil in water emulsions were prepared either with crude oil, diluted crude oil, or xylene containing

dissolved carboxylic acids. After mixing the emulsions for at least 2 h, they recorded the final pH. Since the temporal evolution of the pH is not reported, we assume that this is the equilibrium pH. Considering the same dissociation constant as for the experiments included in Figure 6.1 (pK_a=4.9), the performance of the model for different partition constant values against the experimental data from Hutin et al.[329] is shown in Figure 6.2. The experimental data shows that the $pH_{initial}$-pH_{final} trends for the crude oil and the diluted crude oil (data sets 2 and 4) are very similar, independently of the TAN. This was expected as, despite the different acid numbers caused by dilution, both crude oil samples contain the same type of acids, hence, with a very similar partitioning behavior. The greater importance of the type of acid compared to the TAN is also substantiated by the experiments performed with xylene containing two different acids, which show a clear distinct behavior despite having the same TAN. Moreover, compared with the model oil systems (xylene+carboxylic acids), the partition coefficient matching the experimental data for the crude oil is up to two orders of magnitude lower than that for xylene with dodecanoic acid (data set 1) or mixture of naphtenic acids (data set 3). Besides the different acids contained in the crude oil, the organic phase (solvent) in which the acids are dissolved may also explain the different partitioning behavior for systems containing xylene compared to crude oil.

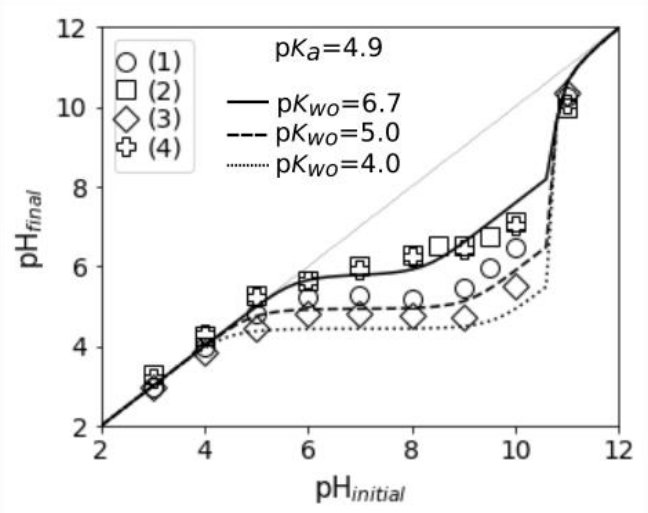

Figure 6.2. Final vs initial pH upon mixing crude/model oil containing carboxylic acids with 0.085 M NaCl solution with different pHs (adjusted by 0.1 M HCl/NaOH titrations). The markers correspond to experimental measurements with different oil phases reported by Hutin et al.[329]: (1) xylene + dodecanoic acid (TAN=1.25); (2) crude oil with TAN=4.2; (3) xylene + mixture of naphtenic acids (TAN=1.25); (4) diluted oil with TAN=1.25. The lines correspond to the calculated final pH considering that 15 wt % in the overall oil-aqueous solution mixture corresponds to the oil phase (density 0.864 g/L) with an acid content that results in a TAN of 1.25 mg KOH/g oil. The partition constant represents the only adjustable parameter, as the ionization constant was kept fixed in analogy with the results from Figure 6.1 (pK_a=4.9).

6.3.2 Calcite-brine-oil equilibria

The adsorption of oleate on calcite is usually quantified through static batch experiments. In these experiments, oleate salts are dissolved in aqueous solutions of known concentration, and the adsorbed amount is determined by mass balance (e.g., refs [172,443,446]). To obtain the equilibrium constant of the surface reaction between oleate and calcite (R6.4) we considered the work of Young and Miller[443] who measured the adsorption of oleate from an aqueous solution with an initial pH of 9.2. Equilibrium oleate concentrations above 1×10^{-5} M triggered a great loss of oleate from the solution; this loss was pinpointed as precipitation of calcium oleate at the calcite surface. To model these data, we first implemented in Phreeqc the model for the speciation of oleate proposed by Kulkarni and Somasundaran[447]. However, to simplify the model and to limit the oleate species that interact with calcite to only carboxylate, we did not include the dimerization reaction (as this would require defining an additional reaction between the calcite and the dimers and not only the carboxylates) nor the formation of acid soaps from these dimers. Besides, the activity of the dimer is expected to be at least an order of magnitude lower than that of the monomer[447]. Thus, we represented the speciation of oleic

acid in aqueous solutions by considering only the partitioning and dissociation of oleic acid considering the equilibrium constants (pK_{wo}=7.6 and pK_a=4.95) reported by Kulkarni and Somasundaran[447]. Since sodium oleate salt is soluble in water, we assumed it to be completely dissociated. Moreover, to mirror the experimental observations, we considered that oleate is depleted from the solution through both surface complexation with the calcite (R6.4) and calcium oleate precipitation (R6.3). Note that although the initial aqueous phase does not contain calcium ions, the equilibration of the solution with the calcite provides a source of calcium ions. By adjusting the adsorption constant for the surface complexation reaction (R6.4) and the calcium oleate solubility product (pK_{ads}=-3.45 and pK_{Ca}=13.5, respectively) we fitted the model to the experimental data from Young and Miller[443] (Figure 6.3-a). The calcium solubility product is consistent with values reported in previous publications[172,448]. In our calculations, we assume that calcite is in equilibrium with the solution. Then, an increase in the oleate concentration leads to calcite dissolution and a rise in the calcium concentration in the solution. This continuous source of calcium ions causes the discrepancy between model and data at high oleate equilibrium concentrations (≈10^{-4} M). The coating of the surface by oleate, which may hamper the dissolution of the calcite, may explain the recorded plateau; this behavior cannot be captured by our model. Along with the data from Young and Miller[443] we also included other datasets that have not been used in the optimization. Since some of the publications report the adsorption per unit mass, we obtain the adsorption density (mol/m^2) by considering the ssa of the calcite sample used in the experiments. For the cases that the ssa is not reported (e.g., data sets 2 and 4 in Figure 6.3-a) we assume that the ssa is 0.5 m^2/g. The net charge change at the IHP and OHP was adjusted to 0.2 and -0.2, respectively, so that the model is consistent with the electrokinetic measurements carried out by Rao et al.[172] (Figure 6.3-b). In these experiments, the zeta potential of calcite in 0.002 M $NaClO_4$, and different pHs (adjusted by HCl/NaOH additions) was measured through electrophoresis in the presence and absence of oleate. Note that we did not fit the zeta potential values but rather defined the charge distribution so that the model shows a similar relative decrease in the zeta potential upon the addition of oleate.

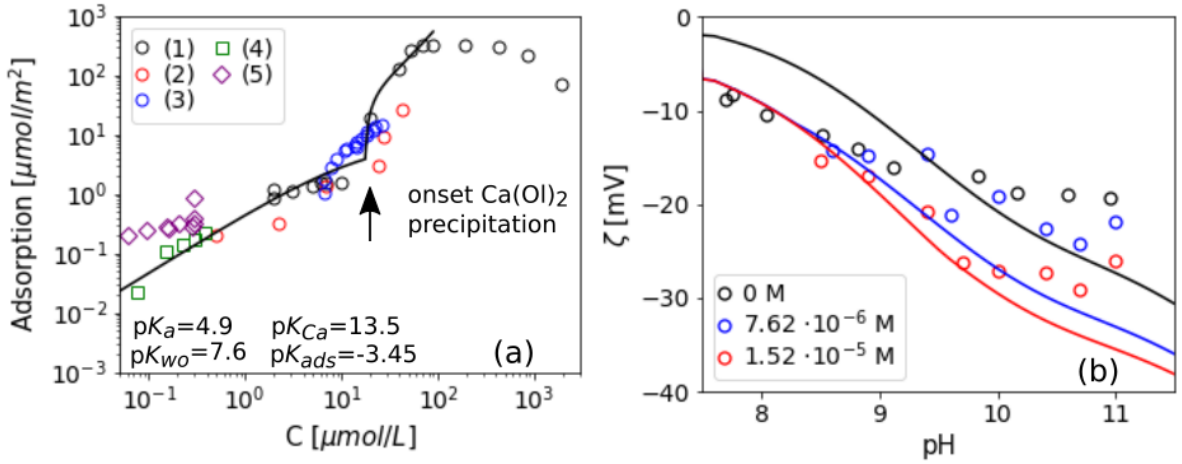

Figure 6.3. **(a)** Adsorption of long-chain fatty acids on calcite. The datasets represent: (1) oleate adsorption measured with FT-IR at 20 ºC and pH=9.2 (data from Young and Miller[443]) (2) oleate adsorption from aqueous solution at a pH of 9.6 fixed by HCl/NaOH titrations-data from [446] (3) oleate adsorption on calcite from water solutions at pH of 10 fixed by HCl/NaOH titrations – data from Rao et al.[172] (4) adsorption of heptadecanoic acid on calcite -data from Meyers and Quinn [449] (5) stearic acid adsorption on calcite data from Suess [450]. Data sets (2) and (4) report the adsorption per gram of calcite and the specific surface area (ssa) was not reported. We converted the adsorption data per m^2 by assuming a ssa of 0.5 m^2/g. The model (line) was fitted to dataset (1) by adjusting the equilibrium constant pK_{ads} of oleate adsorption (R6.4) to -3.45 and calcium carboxylate solubility product to pK_{Ca}=13.5. For the modeling, we initially fixed the pH of the solution to 9.2 by adding NaOH, followed by equilibration of the solution with the calcite. **(b)** Zeta potential of calcite in aqueous solutions with and without oleate at different pHs adjusted by HCl/NaOH titrations. Experimental data from Rao et al. [172]. The lines represent the results generated with the model by considering equilibration with the calcite (ssa=9.5 m^2/g) in the absence of a gas phase and pH fixed by adding HCl/NaOH. The net charge change at the surface plane was set to 1 (see Methodology section for details), whereas that at the IHP and OHP was adjusted (Δz_1=0.2, Δz_2=-0.2) so that the modeled relative decrease of the calcite zeta potential upon increasing the oleate concentration was consistent with the experimental observations.

To test the validity of the inferred parameters at different chemical conditions, we assessed the equilibrium concentration of oleate and calcium predicted by the model in a calcite-aqueous solution-oleate system against the measured values by Rao et al.[172] (Figure 6.4-a). While the model shows a good agreement with the equilibrium calcium concentration, it tends to overestimate the oleate concentration in solution at equilibrium conditions, especially at low initial oleate concentrations; this eventually implies that the model slightly underestimates the overall adsorption of oleate and this underestimation is higher at low initial oleate concentrations. Moreover, the model predicts satisfactorily the zeta potential of calcite at increasing oleate concentration measured by Mishra et al.[451] (Figure 6.4-b).

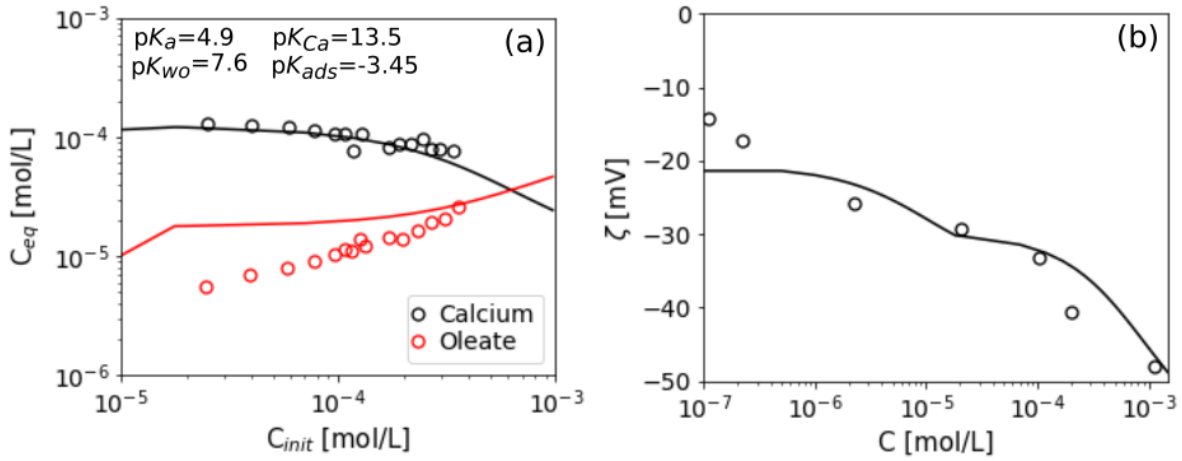

Figure 6.4. **(a)** Calcium and oleate concentration in the supernatant at different initial oleate concentrations. The markers represent the data from the experiments on oleate adsorption on calcite (ssa=9.5 m^2/g) performed by Rao et al.[172] at a pH of 10 fixed by NaOH titrations. The lines represent the prediction (no adjustable parameters) of the model considering that the oleate solution is in equilibrium with the calcite in the absence of a gas phase (no CO_2). **(b)** Zeta potential at increasing oleate concentration. Markers correspond to the zeta potential of calcite in an aqueous solution with a background electrolyte of 2×10^{-3} M $NaClO_4$ (pH of 10 adjusted by NaOH titrations) and increasing oleate concentration; experimental data from Mishra et al.[451]. The lines represent the prediction (no adjustable parameters) of the model considering equilibration of the solution with the calcite in the absence of a gas phase. Since the ssa of the calcite sample is not mentioned, we used the same ssa from the tests of Rao et al.[172] (ssa=9.5 m^2/g).

6.3.3 Dynamic retention tests

Puntervold et al.[424] have recently carried out flooding tests with crude oil to assess the retention of polar groups in chalk core samples. Before the flooding, the cores were initialized to 10% irreducible water saturation through evaporation, with the remaining pore space being occupied by air. When oil is initially injected into the sample it saturates the sample by displacing the air. Then, the effluent was periodically sampled for TAN measurements. A decrease in the effluent TAN compared to the initial injection value is interpreted as a loss of acidic compounds from the crude oil stream by adsorption on the rock surface. To reduce this system to a single-phase problem, here we assume no air trapping and that the oil pushes out the air following a piston-like displacement. To account for the retention of acid components contained in crude oil on calcite, we consider that the adsorption is analogous to that of oleate and the loss of acid from the crude oil occurs through both precipitation and surface complexation. The performance of the transport model against the experimental data from Puntervold et al.[424] is shown in Figure 6.5; this figure shows the sensitivity of the acid retention to its partition constant (panel a) and calcium carboxylate solubility product (panel b) and the effect of dispersion (panel c). For all scenarios, we considered the same ionization constant (pK_a=4.9) that described well the oil-brine equilibria in the experiments of Hutin et al.[329] and Bertheussen et al.[321] and the constant we inferred for the adsorption of oleate on calcite (pK_{ads}=-3.45). These results show that the partitioning constant is the parameter that has the highest impact on the acid retention within the core. Nonetheless, the model (both with and without dispersion), independently of the value of the parameters, cannot portray the slanting profiles for the effluent TAN observed experimentally.

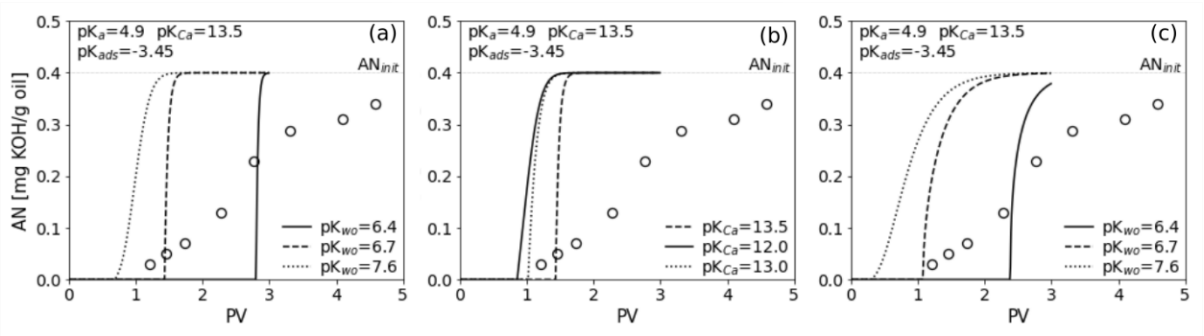

Figure 6.5. Evolution of the acid number in the crude oil effluent during the injection of crude oil in a Stevns Klint chalk sample (q=0.1 ml/min) at 50 ºC. The lines and markers represent the prediction of the model and the experimental data from ref.[424], respectively. The panels show the sensitivity of the acid retention to **(a)** brine-oil acid partitioning constant, K_{wo} **(b)** solubility product, K_{Ca} of the calcium salt, **(c)** same as (a) but including the effect of dispersion (D_L=1e-8 m^2/s).

We postulate that this mismatch may be explained by the fact that some of the interactions we include in the model cannot occur instantly (equilibrium) but are rather dictated by kinetics. For instance, the partitioning of the acid species between the oil and water phase, which has a great effect on the transport of these polar groups through a calcite core, is usually determined via experiments where the contact between the two phases is promoted through continuous mixing for a relatively substantial time (e.g., 24 h[321,452,453]). The residence time, contact area, and mixing of the crude oil and water phase within a porous media may be insufficient to achieve equilibrium conditions. Yet, since we did not come across any experimental data showing the development of the partitioning with time, we lack the basis for introducing a time-dependent acid transfer within our reactive transport model. A kinetic approach can, however, be adopted for the formation of calcium carboxylate salts/soaps considering the precipitation of calcium myristate experiments reported by Sarac et al.[454]. The kinetic precipitation of calcium carboxylate salts is addressed hereafter.

Following an analogy with water-mineral interactions, calcium carboxylate may undergo either precipitation or dissolution depending on its saturation ratio. Considering the stoichiometry of the calcium carboxylate formation (R6.3), the saturation ratio (Ω) at different chemical conditions is calculated from the ion activation product (IAP) and the solubility product (K_{Ca}) as given by eq. (6.3)

$$\Omega = \frac{\{\mathrm{Ca^{+2}}\}\{\mathrm{R\text{-}COO^{-}}\}^2}{\{\mathrm{Ca^{+2}}\}\{\mathrm{R\text{-}COO^{-}}\}^2|_{eq.}} = \frac{IAP}{K_{Ca}} \tag{6.3}$$

where {} denote activities.

To describe the kinetics of calcium carboxylate precipitation-dissolution per volume of solution, V [m^3], we consider the general expression for the rate[455] (eq. 6.4):

$$\frac{dn_{\mathrm{Ca\text{-}(RCOO)_2}}}{Vdt} = -kf(a_i)g(\Delta G_r) \tag{6.4}$$

where $n_{\mathrm{Ca\text{-}(RCOO)_2}}$ are the moles of calcium carboxylate, k is the kinetic constant, $f(a_i)$ denotes the dependence of the rate on the activity of the species involved in the reaction, and $g(\Delta G_r)$ is related to the driving force for the precipitation/dissolution. The rate often includes a term dependent on the surface area. However, since in this case we deal with a poorly soluble salt that does not exist in the system initially (the initial surface area is zero), we do not include any dependence on the surface area.

The function $f(a_i)$ is commonly expressed as the product of species activities (eq. 6.5):

$$f(a_i) = \prod_i a_i^{n_i} \tag{6.5}$$

where n_i gives the reaction order with respect to the activities of species involved in the reaction, a_i.

The rate given by eq. (6.3) represents either dissolution or precipitation reaction depending on the sign of the dimensionless term $g(\Delta G_r)$. We express this term as a function of the saturation ratio, Ω, and an adjustable parameter, p (eq. 6.6):

$$g(\Delta G_r) = (1 - \Omega^p) \tag{6.6}$$

Replacing eqs. (6.5)-(6.6) in equation (6.4) and assuming a zero-order reaction (simplest mechanism) with respect to the species involved in the reaction, the dissolution/precipitation rate of calcium carboxylate is given by eq. (6.7):

$$-\frac{dn_{\text{Ca-(RCOO)}_2}}{Vdt} = k(1 - \Omega^p) \tag{6.7}$$

with the kinetic constant, k, having units of [mol·m^{-3}·s^{-1}].

Note that when the saturation ratio is higher than 1, the solution is oversaturated with respect to the organic calcium salt and the kinetic rate denotes precipitation whereas if the saturation ratio is smaller than 1, the rate denotes dissolution. Thus, we consider that oil-brine interactions are represented by the equilibrium reactions (R6.1) and (R6.2), whereas reaction (R6.3) is governed by the rate given by eq. (6.7). To obtain the kinetic parameters k and p, we fit the oil-brine model to the experimental data from Sarac et al. [454]; in these experiments, the authors mixed $CaCl_2$ (1 wt % Ca^{2+}) brines of different initial pHs (fixed by NaOH titrations) with an equal volume of model oil (1 wt % myristic acid in toluene) and filtered out and measured the fatty acid calcium precipitates formed at different times throughout the experiment. To limit the number of adjustable parameters, we assumed that the ionization constant of the myristic acid is equivalent to that of oleic acid and that found for naphtenic acids (pK_a=4.9).

Figure 6.6 shows the fit of the model to the experimental data obtained at different pHs for two optimization scenarios. In the first scenario (solid lines) we manually adjusted the kinetic parameters, k and p; the remaining parameters, i.e., partitioning constant and solubility product, were considered analogous to those we found by fitting the experimental data from Hutin et al.[329] for crude oil and calcium oleate precipitate, respectively (pK_{wo}=6.7, pK_{Ca}=13.5). In the second scenario (dashed lines), we used a least-squares optimization algorithm implemented in Python to fit the model to the experimental data measured at the lower pH (pH=8) by optimizing not only the kinetic parameters k and p but also the solubility product and partition constant, K_{Ca} and K_{wo}, respectively. Note that we used only the experimental data at the lower pH because our equilibrium model is not consistent with the equilibrium precipitation reached at high pHs where the equilibria may be dictated by additional competing interactions (e.g., acid association or micellization[427]) not captured by our formulation. A significantly lower solubility product would be required to match the experimental observations at the higher pHs. Nonetheless, this would introduce a mismatch in the predicted equilibrium solubility at lower pHs. Since we are interested in the behavior of the calcium carboxylates at pH conditions closer to those observed of carbonate reservoir (pHs somewhere between 6-8 depending on the brine composition[99]), we find the experiments at the lower pH (pH=8) the most relevant ones. The solubility product obtained through the optimization is slightly lower than that found to match the calcium oleate precipitation. This is unexpected as myristic acid has a shorter chain length (C14), which should, a priori, render this molecule less hydrophobic compared to oleate (C18), and the solubility product would be expected to be higher (solubility product depends on chain length). This could be explained by the fact that oleic acid has one unsaturation in its chain which could increase the solubility of the calcium oleate with respect to calcium myristate[456]. The slightly higher partition coefficient obtained for myristate is consistent with its shorter chain length compared to oleate[427].

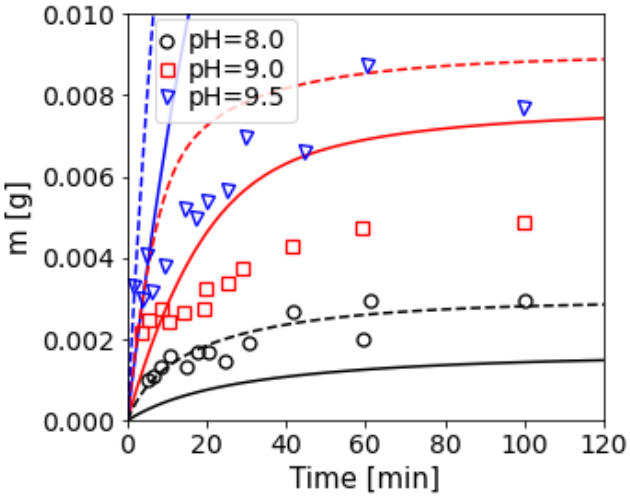

Figure 6.6. Evolution of calcium myristate precipitation with time. The markers correspond to the experimental data from Sarac et al. 454. The solid lines represent the fit of the model considering pK_{wo}=6.7, pK_{Ca}=13.5 and manually adjusting the kinetic parameters (k=1e-9 mol·m^{3}·s^{-1}, p=0.35), whereas the dashed lines were obtained by fitting the model to the experimental data obtained at pH=8 with four adjustable parameters (pK_{wo}=6.5, pK_{Ca}=13.76, k=3.82e-9 mol·m^{3}·s^{-1}, p=0.28).

The results of the transport model for different pK_{wo} and pK_{Ca} while considering that the precipitation of the calcium carboxylate is driven by kinetics are shown in Figure 6.7 together with the experimental data from Puntervold et al.[424]

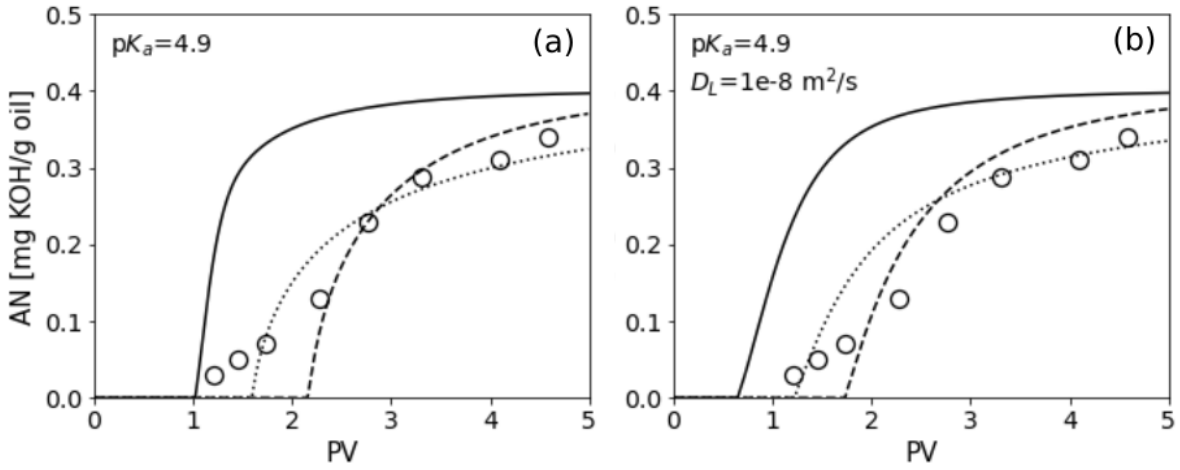

Figure 6.7. Retention of polar groups during the injection of crude oil in a chalk core (ssa=2 m^2/g, φ=44.8%) with 10% irreducible water saturation. The lines represent the prediction of the model whereas the markers correspond to the experimental data from Puntervold et al.[424] The line style represents different model parameters: solid lines – pK_{wo}=6.7, pK_{Ca}=13.5 mol·m^{-3}·s^{-1}, k =1e-9, p=0.35, dashed lines – pK_{wo}=6.5, pK_{Ca}=13.76, k =3.82e-9 mol·m^{-3}·s^{-1}, p =0.28, dotted lines – pK_{wo}=6.3, pK_{Ca}=13.5, k=1e-9, p=0.35. Panel **(a)** considers the transport of polar groups only by advection whereas in panel **(b)** we include a dispersion coefficient, D_L, of 1e-8 m^2/s.

Including kinetics for the precipitation of calcium carboxylates within our transport model can still not explain the slanting AN profile observed experimentally. Compared to the transport of polar groups by advection only (Figure 6.7-a), including a dispersion coefficient (Figure 6.7-b) slightly improves the performance of the model. Since no tracer is used in these experiments, we cannot support with experimental evidence the relevance of dispersion in these experiments. Yet, the homogeneity of Stevns Klint chalk and our previous modelling studies[69,221] of brine injection in chalk, where we successfully reproduced the tracer concentration history by considering only advection, rather suggest that dispersion should not be significant.

Despite its complexity, up to this point, we considered that crude oil polar content is represented by a single acid pseudocomponent. This was a necessary assumption that allowed us to constrain the adsorption model and the kinetics. However, this simple representation of the crude oil phase may eventually cause a discrepancy between the model and the experimental data. The limitations of modeling the equilibria between brine and oil containing a mixture of naphtenic acids using a single pseudocomponent have been previously addressed by Bertheussen et al.[452,453]. They showed that considering just one pseudocomponent, characterized by a certain pK_{wo}, could not explain the partitioning of an acid mixture between an oil and water phases. Then, they split the acid mixture into different MW fractions and performed separate equilibrium partitioning experiments with each of these fractions. They showed that the pK_{wo} increased linearly with the average molecular weight of the acid fraction used in the experiments and that the partitioning of a mixture of acids between oil and water phases can be described by considering their additive contribution. They proposed a linear relationship between the partition coefficient and the average molecular weight. Since the oil-brine equilibria are modelled differently in this work, we cannot directly use their proposed relationship. Thus, by fitting our model to the equilibrium partitioning data reported for different molecular weight acid fractions, we obtain a relationship between the average molecular weight and the partition constant. The relationship between the pK_{wo} and average MW is inferred in Appendix A.4 by considering the partitioning of a naphtenic acid commercial mixture between toluene and 3.5 wt % NaCl measured by Bertheussen et al.[453]. We use this relationship to calculate the pK_a for the different MW acid fractions integrated into a naphtenic acid mixture extracted from a North Sea crude oil. The difference between modelling the oil-brine equilibria using a single pseudocomponent compared to multiple ones is shown in Figure 6.8.

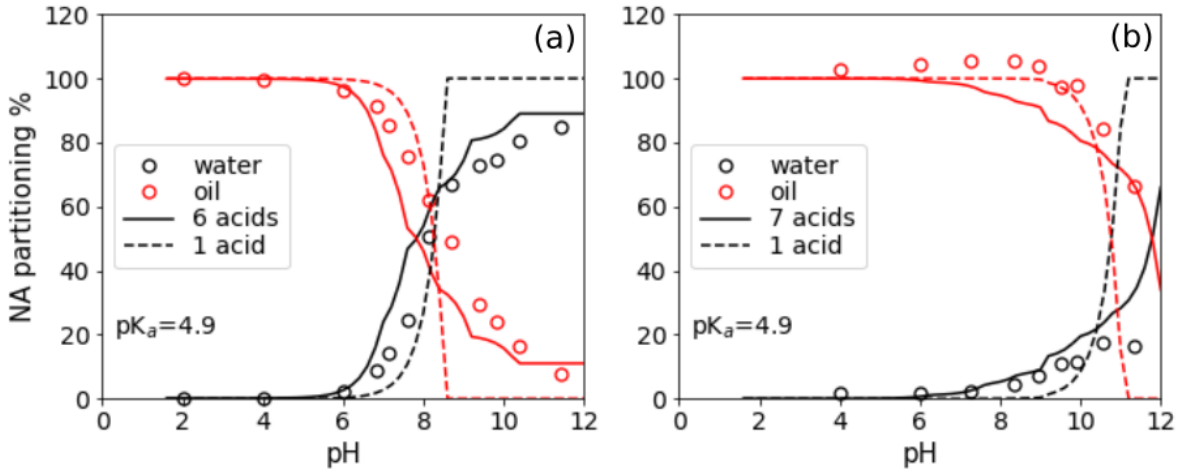

Figure 6.8. Equilibrium partitioning data of (a) naphtenic acid commercial mixture (split into 6 different MW fractions) and (b) naphtenic acid mixture extracted from a North Sea crude oil (split into 7 different MW fractions) between toluene and 3.5 wt % NaCl. The markers show experimental data whereas the lines indicate the modelled behavior. The model that considers only one acid (dashed lines) was fitted using **(a)** pK_{wo}=5.8 and **(b)** pK_{wo}=8.7. The solid lines show the prediction of the model when different MW acid fractions (outlined in the original work) are considered; for each of these fractions, we calculated its partitioning constant based on the pK_{wo}-MW relationship inferred in Appendix A.4. For details on the different MW acid fractions, the reader is referred to the original publications, i.e., ref [453] (experimental data in panel a) and ref [452] (experimental data in panel b).

While it may seem that at pHs below 8.5 (pH conditions of carbonate reservoirs), the single pseudocomponent model behaves better than the model that includes the contribution of 6-7 acid fractions, this will not necessarily be the case for aqueous solutions containing calcium. Lower MW acid fractions do not bind calcium ions whereas heavier fractions do[321]. Describing the acid mixture as multiple pseudocomponents would allow differentiating between the fractions that bind calcium and those that do not. On the other hand, considering several acids will increase the complexity of the model

as it does not only increase the number of reactions for the oil-brine equilibria but it would also require defining additional surface reactions characterized by an unknown equilibrium constant.

We compare again our transport model to the experimental data from Puntervold et al.[424] by considering a second pseudocomponent to describe the acid content of the crude oil. Thus, we define a "low" and "high" MW acid, with the latter undergoing all the interactions discussed previously (e.g., partitioning, complexation, and precipitation), whereas the former can partition into the water but does not bind calcium ions nor adsorbs on the calcite surface. The consistency between the model (lines) and experimental data is shown in Figure 6.9. During the experiment, the effluent is not sampled nor analyzed continuously; at any sampling time, samples of 6 ml are taken, thus the measured TAN is an average of the sampled 6 ml. To account for this effect on the experimental data, we average our modelled results (dashed lines). Including a second pseudocomponent improves the agreement between model and experimental data. Nonetheless, since in these experiments the TAN is the only variable reported, the values of the partitioning constants of the two acid pseudocomponents used to describe the acidic content of the crude oil cannot be critically evaluated. The progress in analytical tools/protocols for identifying and quantifying the acid polar content in crude oil may help resolve whether the partition constant needed to fit dynamic retention tests is consistent with the identity of the acids present in the crude oil.

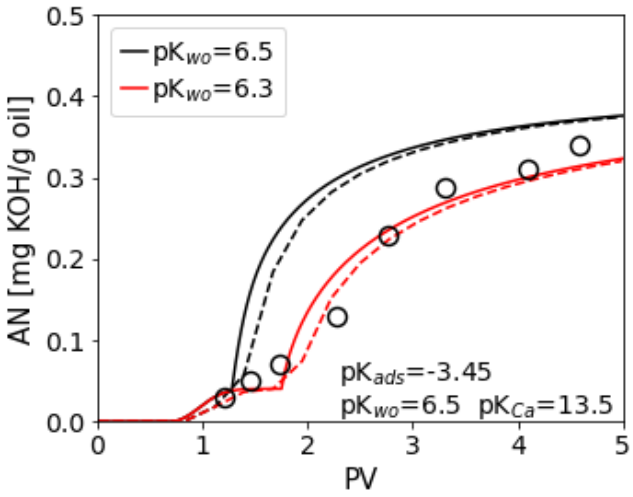

Figure 6.9. Performance of the reactive transport model using two pseudocomponents for the description of the acidic content of the crude oil. The markers correspond to the experimental data from Puntervold et al. [424]. For the modelling, we considered that the acid content in the crude oil can be described by a molar fraction of 90% "heavier" fraction with pK_{wo}=6.5 (solid black line) or pK_{wo}=6.3 (solid red line) and 10% "lower fraction" with pK_{wo}=-5.8. Both pseudocomponents are assumed to have the same ionization constant (pK_a=4.9) but only the heavier fraction adsorbs on the calcite surface (pK_{ads}=-3.45) and binds calcium ions from solution leading to the formation of calcium carboxylates (pK_{Ca}=13.5, k=1e-9 mol·m^{-3}·s^{-1}, p=0.35). To account for the effect of sampling volume on the experimental results, we also replot the averaged results (dashed lines).

The proposed model could be further refined provided additional experimental data become available. For instance, although basic components are considered to affect less the calcite wettability, some bases may still partition into the water up to neutral pH conditions. Even if these bases were not to adsorb on the calcite, they may stimulate the transfer of acidic components and lead to a different equilibrium partitioning[328]. The presence of different types of acids or other types of functional groups in the crude oil may promote the coadsorption of these acids[421,446]; this type of phenomenon or interactions between the acids once adsorbed on the calcite surface (e.g., "tail-to-tail arrangement"[457]) cannot be represented by our model. Additionally, similar to calcium, other types of divalent ions (e.g., magnesium) may also affect the partitioning or the precipitation of carboxylate salts. Lastly, the effect of temperature on oil-brine equilibria and interactions of carboxylate with calcite is yet to be resolved.

6.4 Conclusions

Predicting and quantifying the adsorption of acid polar groups from the crude oil on the calcite surface cannot be achieved unless these groups are identified and their interactions with both oil and brine are thoroughly characterized. In this work, we proposed a reaction network that accounts for the acid partitioning, carboxylate complexation with calcite, and precipitation of calcium carboxylate salts to be used for modelling the reactive transport of acid species through calcite-containing carbonate formations. The reaction network, once constrained and tuned to batch experimental data obtained with model oil, was coupled to the advection-diffusion equation. This reactive transport model could not explain the effluent TAN profiles recorded during the single-phase flooding tests with crude oil through chalk samples. Considering dispersion or a kinetic control on the formation of carboxylate precipitates only partially aligned the model and the experimental observations. Representing the crude oil acid content in terms of two pseudocomponents instead of one, improved the agreement between model and experimental data. However, reporting only the TAN leads to a heavily undetermined system as the parameters describing the calcite-brine-oil interactions range over several orders of magnitude depending on the nature/identity of the acid. Crude oil types with the same TAN can interact with the brine and the mineral in a completely different manner whereas oil with different TAN may lead to equivalent interactions if the acids contained are very similar. Therefore, the TAN describes only qualitatively the acid content in the crude oil and cannot be used to accurately quantify the interactions between calcite and acid polar species. The model proposed in this work can be used to predict the adsorption of polar groups on the calcite surface and the flow of carboxylic contaminants in the subsurface provided their structure is known.

7 Conclusions and Outlook

7.1 Conclusions

The additional oil recovery during MSW in carbonate reservoirs is governed primarily by the interactions between the calcite, brine, and crude oil. The present thesis provides an improved description of these interactions, supporting the development of advanced reactive transport models that could help design the implementation of MSW at the field scale and predict the oil mobilization under diverse conditions.

The adsorption of ions and charge development at the calcite-water interface is assessed predominantly (and indirectly) through electrokinetic measurements. These measurements are often used to tune the SCMs that describe the reactivity of calcite in presence of aqueous solutions. Yet, the contrast between published zeta potential measurements challenges the definition of a univocal set of parameters for each model. The discrepancies between the reported zeta potential may be explained by different non-equilibrium conditions, sample preparation, or impurities. Chapter 2 highlights the importance of experimental protocols during the electrokinetic measurements on calcite-aqueous solution systems; the equilibration procedure (e.g., pCO_2, equilibration times), solution composition, and pH at equilibrium are necessary to ensure that the modelled system is representative of the experimental conditions. Moreover, different SCMs, independently of their electrostatic description of the interface, may fit equally well the zeta potential of calcite in aqueous solutions. Yet, the main assumptions behind the models (e.g., the definition of surface reactions) affect considerably their prediction performance; in some cases, a model, once tuned to a particular dataset, cannot be extrapolated/used to predict the trends under significantly different chemical conditions (e.g., different ionic strength). Because of the uncertainties in the electrokinetic data and the fact that it cannot characterize the rigid part of the electrical double layer, considering additional types of data (e.g., proton charge and adsorption) to tune the models is highly recommended.

Besides chemical conditions, rock-fluid interactions are also governed by temperature. In Chapter 3, both electrokinetic and single-phase flooding tests were used to obtain the effect of temperature on calcite surface reactivity. The reaction enthalpies, inferred by assuming that the equilibrium constants follow a temperature dependency according to the van't Hoff equation, show that calcite protonation is highly exothermic whereas the adsorption of divalent ions (e.g., Ca^{2+}, Mg^{2+}, and SO_4^{2-}) is endothermic. The obtained enthalpies are consistent with the enthalpy changes recorded through microcalorimetry measurements on chalk powders.

SCMs may also be used to interpret and quantify fluid-fluid interactions. Chapter 4 proposes an SCM to describe the electrokinetic behavior of crude oil in the presence of aqueous solutions. Representing the oil surface as an array of base and acid groups linearly dependent on the crude oil TBN and TAN, respectively, results, in many cases, in a fair prediction of the zeta potential of the crude oil. Including a reaction between the acid sites and Na^+, usually considered indifferent ion, improved the performance of the model. Considering a third type of adsorption sites, denominated weak sites, is deemed necessary to account for the negative zeta potential exhibited by non-polar oils. Additional insight on the

distribution of bases and acids at the oil-brine interface and the effect of salinity on this distribution is necessary to refine the model and provide better predictions.

In carbonate formations, the oil mobility and the additional oil recovery are not related to the ionic strength. Mechanistic models proposed in the literature for the wettability alteration, which consider either the surface speciation or the zeta potential at the calcite-brine and brine-oil interface, cannot explain the experimental observations obtained on chalk cores. The parameter formulated in Chapter 5, which depends on both the zeta potential and surface speciation, shows a relationship with the remaining oil saturation from spontaneous imbibition tests on chalk cores and could be used to assess the shift in the wetting conditions when switching brines.

Many of the models developed within the context of MSW consider two segregated and non-coupled calcite-brine and brine-oil systems. To overcome this, Chapter 6 provides a coupled formulation of these systems to allow quantifying the retention of polar acid groups on the chalk surface. The model, initially tuned and validated to experimental data obtained on systems with model oil spiked with a specific carboxylic acid, could not fully describe the recorded profile of the total acid content in the effluent during the injection of crude oil through a chalk core. Representing the crude oil mixture as two pseudocomponents instead of one improved the agreement between the model and experimental data.

7.2 Outlook

This thesis represents an important step towards the development of advanced models for subsurface applications. Nonetheless, to further consolidate the models proposed herein, several aspects and limitations should be addressed in the future.

The effect of chemical heterogeneity on calcite-fluid interactions, not addressed in this thesis, is of utmost importance for natural systems, where carbonates, besides the main $CaCO_3$ constituent, are sprinkled with other secondary mineral phases or organic impurities. Chemical impurities may introduce a surface charge heterogeneity which may challenge the application of traditional electrokinetic theory, which relies on the assumption that particles are uniformly charged. At the same time, the presence of surface charge heterogeneity questions the significance of the average calcite zeta potential measured in the presence of impurities for transport processes. The presence of chemical impurities may explain why the SCM, once tuned to zeta potential data, could not explain the ion retention in limestone or chalk samples during single-phase flooding tests with brine. To corroborate this hypothesis and isolate the effect of impurities on the aqueous species transport, single-phase flooding tests on cores consisting of pure calcite aggregates are highly encouraged. At the same time, experiments to assess the effect of impurities and models that can describe chemically heterogeneous systems are required. Preferably, an initial baseline model for synthetic calcite should be further extended or refined to describe the behavior of natural samples.

Zeta potential measurements of calcite in the presence of aqueous solutions performed at temperatures higher than ambient conditions are still relatively scarce. The existing data at high temperatures concerns mostly diverse natural calcite samples. Thus, the enthalpies reported in Chapter 3 were inferred by combining several types of experimental data (e.g., streaming potential, single-phase flooding tests) obtained on different natural calcite samples and by various research groups. While the effect of chemical impurities is not elucidated, the found enthalpies should be further refined using data strictly obtained on synthetic samples to isolate the response from calcite minerals. Furthermore, the effect of temperature on model parameters such as capacitance should also be investigated.

A more accurate description of calcite-brine-oil interactions is only possible provided that the active polar groups from the crude oil are identified. TAN/TBN are not good indicators of the potential of acids/bases in the crude oil to partition into the water, or attach to the calcite surface and shift its wetting conditions. Thus, further work on analyzing the polar components present in the crude oil is

recommended. This analysis could also bring more insights for modelling the electrokinetic behavior of crude oil in aqueous solutions. In Chapter 4, the oil surface was represented as an array of base and acid groups following a linear relationship with the TAN/TBN. To refine this representation, the species that have a particular affinity for the oil-brine interface need to be isolated and their significance/fraction within the total TAN/TBN needs to be assessed. The distribution of polar species at the oil-brine interface at different salinities and temperatures is still uncertain. Experimental work tackling the effect of temperature on the zeta potential at the oil-water interface is required before this can be integrated into the model. Moreover, as discussed in Chapter 6, some acids in the oil may partition in the water and ionize changing the pH; coupling the equilibrium partitioning to the oil-brine SCM may result in a better representation of the real chemical system.

The thesis has addressed predominantly the calcite-brine-oil interactions and their relevance to wettability alteration. Yet, other mechanisms leading to EOR during MSW can be formulated based on some of the models proposed in this work. For instance, fines migration and chalk weakening are tightly linked to the electrokinetics at the calcite-water interface. The reactive network proposed in Chapter 6 could be further coupled to the two-phase flow equations and assessed against core flooding experiments or used to describe the flow of naphtenic acid contaminants.

In this thesis, the interactions taking place at the pore scale have only been upscaled to the core scale. Because of the small scale considered, priority was given to developing rigorous models consistent with experimental observations, without taking into consideration aspects such as computational efficiency. However, using these models for describing larger scales may be computationally prohibitive. Thus, future research should address the upscaling of the interactions modelled here to field scale.

A Appendix

A.1 Supplementary material for Chapter 2

The models fitted to the experimental data from Song et al.[175] displaying the confidence interval are shown in Figure A.1.

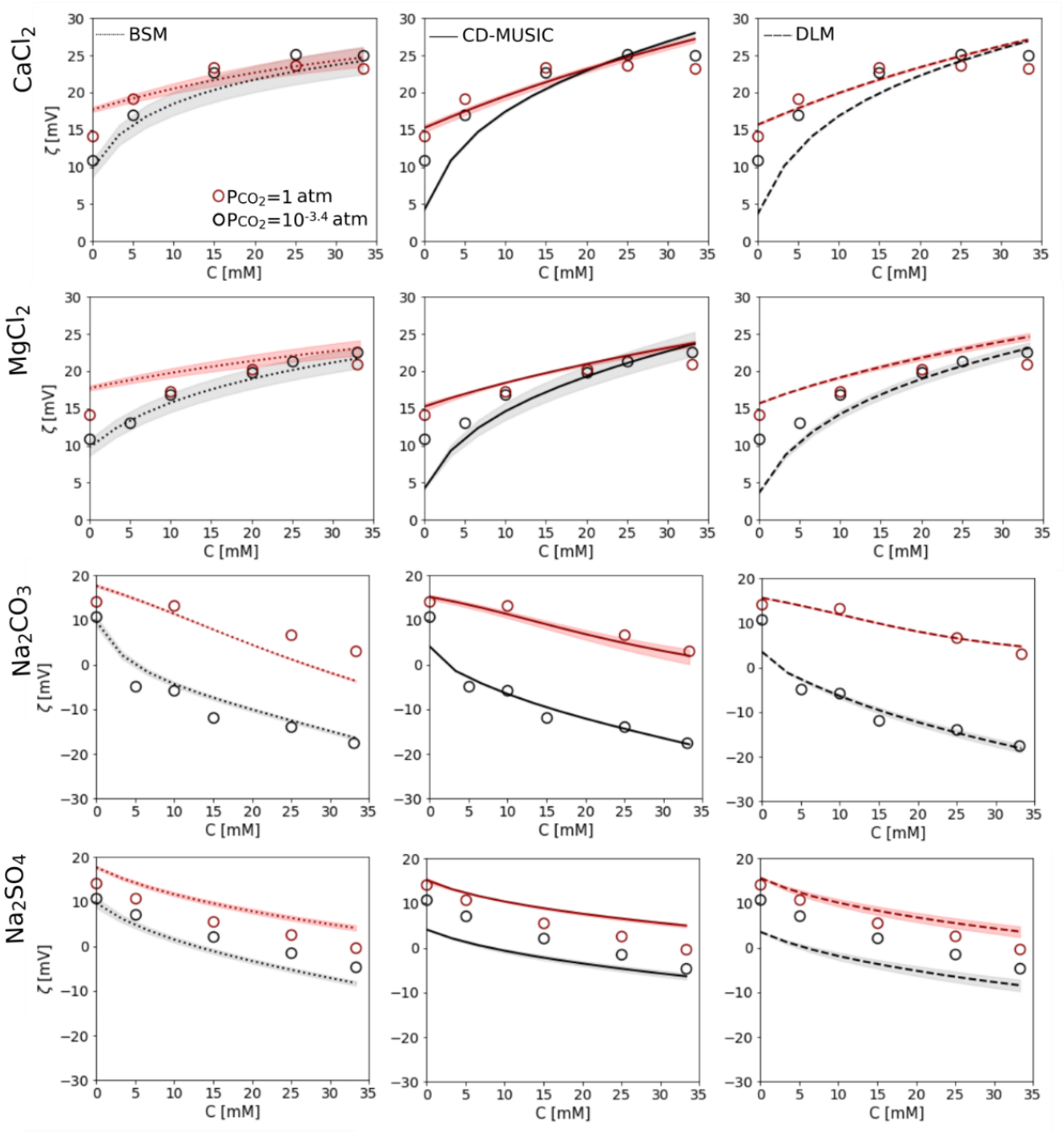

Figure A.1. Models fitted to the experimental data of Song et al.[175] The shaded area next to each line accounts for the uncertainty of the model parameters.

A.2 Supplementary material for Chapter 3

SCMs describe the binding of ions at mineral-water interfaces through equilibrium reactions between the surface sites and aqueous species. The change in the free energy associated with the adsorption of an ion on a charged surface, ΔG_{ads} [J/mol], comes from the change in chemical energy, ΔG_{int} [J/mol], and an electrostatic term, ΔG_{el} [J/mol][73] (eq. A.1):

$$\Delta G_{adsorption} = \Delta G_{intrinsic} + \Delta G_{el} + RTlnQ \tag{A.1}$$

where R [J mol^{-1} K^{-1}] denotes the ideal gas constant, T [K] is the temperature, and Q is the quotient of the reaction.

The change in chemical energy is proportional to the intrinsic equilibrium constant, K, of the adsorption reaction (eq. A.2):

$$\Delta G_{intrinsic} = -RTlnK \tag{A.2}$$

The intrinsic equilibrium constant is assumed to follow a temperature dependence according to van't Hoff equation (eq. 3.1). Considering a constant enthalpy of reaction, ΔH_r [J/mol], the definite integral of eq. (3.1) between 25ºC and any temperature, T, yields:

$$ln\frac{K_{@T}}{K_{@298\,K}} = -\frac{\Delta H_r}{R}\left(\frac{1}{T} - \frac{1}{298}\right) \tag{A.3}$$

Thus, the equilibrium constant at any temperature can be calculated provided that the equilibrium constant at 25ºC and the enthalpy of reactions are known.

The electrical contribution to the total energy of adsorption can be calculated as:

$$\Delta G_{el} = \sum \Delta z_i F \psi_i \tag{A.4}$$

where Δz_i and ψ_i [V] are the net charge change and potential at plane i, respectively, and F [96485 C/mol] is the Faraday constant.

At equilibrium, $\Delta G_{adsorption} = 0$ and combining eqs. (A.1), (A.2), and (A.4), the reaction quotient and the intrinsic equilibrium constant are related as:

$$Q = K\exp\left(-\sum \frac{\Delta z_i F}{RT}\psi_i\right) \tag{A.5}$$

For instance, considering the adsorption of a cation, C^{m+}, on a mineral with hydrated surface sites, ≡SOH yields the surface specie $\equiv SOC^{m-1}$ (RA.1):

$$\equiv SOH + C^{m+} \leftrightarrow \equiv SOC^{m-1} + H^+ \tag{RA.1}$$

Thus, eq. (A.5) can be rewritten as:

$$\frac{[SOC^{m-1}][H^+]}{[SOH][C^{m+}]} = K\exp\left(-\sum \frac{\Delta z_i F}{RT}\psi_i\right) \tag{A.6}$$

Considering inner-sphere complexation and that the charge of the cation is placed entirely at the IHP (1-plane), the net charge change at the IHP is $\Delta z_1 = +m$. Since according to reaction (RA.1) the adsorption promotes the deprotonation of the surface sites, the net charge change at the surface (0-plane) is $\Delta z_0 = -1$. This particular adsorption reaction does not affect the net charge at the OHP ($\Delta z_2 = 0$). Thus, eq. (A.6) becomes:

$$K = \frac{[SOC^{m-1}][H^+]}{[SOH][C^{m+}]}\exp\left(\frac{F}{RT}(m\psi_1 - \psi_0)\right) \tag{A.7}$$

The surface charge density at the different planes can be calculated from the surface speciation. If reaction (RA.1) is the only one taking place, the surface charge density at the surface and IHP, σ_0 *and* σ_1 [C/m^2], respectively, is given by eqs. (A.8)-(A.9):

$$\sigma_0 = -\frac{F}{ssa * a}[\mathrm{SOC}^{m\text{-}1}] \quad \text{(A.8)}$$

$$\sigma_1 = m\frac{F}{ssa * a}[\mathrm{SOC}^{m\text{-}1}] \quad \text{(A.9)}$$

where *ssa* [m^2/g] is the specific surface area of the mineral and *a* [g/L] is the concentration of solids in solution. When several surface reactions are defined, the charge density in each plane is calculated by considering all surface species that affect that particular plane. The sum of all surface species is equivalent to the total number of available sites defined at the mineral surface (mass balance equation).

In the CD-MUSIC model, the charge and the potential at each plane are related through two capacitances:

$$\sigma_o = C_1(\psi_o - \psi_1) \quad \text{(A.10)}$$

$$\sigma_1 + \sigma_o = C_2(\psi_1 - \psi_2) \quad \text{(A.11)}$$

where C_1 and C_2 (F/m^2) are the capacitances of the IHP and OHP, respectively.

The charge and potential in the diffuse layer are related through the Grahame equation[120]:

$$\sigma_d = \pm\left\{2RT\varepsilon_r\varepsilon_o\sum_j m_j\left[\exp\left(\frac{-z_iF\psi_d}{RT}\right)-1\right]\right\}^{1/2} \quad \text{(A.12)}$$

where ε_0 [8.854·10^{-12} F/m] is the vacuum permittivity, ε_r [-] is the fluid relative permittivity, and m_j is the concentration of ion *j* [mol/m^3].

Since the interface is overall electroneutral, the excess surface charge is neutralized by the charge in the diffuse layer:

$$\sigma_o + \sigma_1 + \sigma_2 + \sigma_d = 0 \quad \text{(A.13)}$$

These equations are available and solved within Phreeqc by simply defining relevant surface reactions and specifying the equilibrium constants at 25ºC, enthalpies of the reactions, capacitances values, surface site density, specific surface area, and physicochemical conditions (e.g., solution composition, temperature, solid-liquid ratio). The enthalpies of the reactions are optimized by fitting the model to zeta potential data obtained at different temperatures.

The CD-MUSIC model implemented in this work uses the equilibrium constants at 25ºC proposed in the work of Wolthers et al.[67]. Figure A.2 shows the performance of the SCM for predicting the electrokinetic potential of calcite in different electrolyte systems at room temperature.

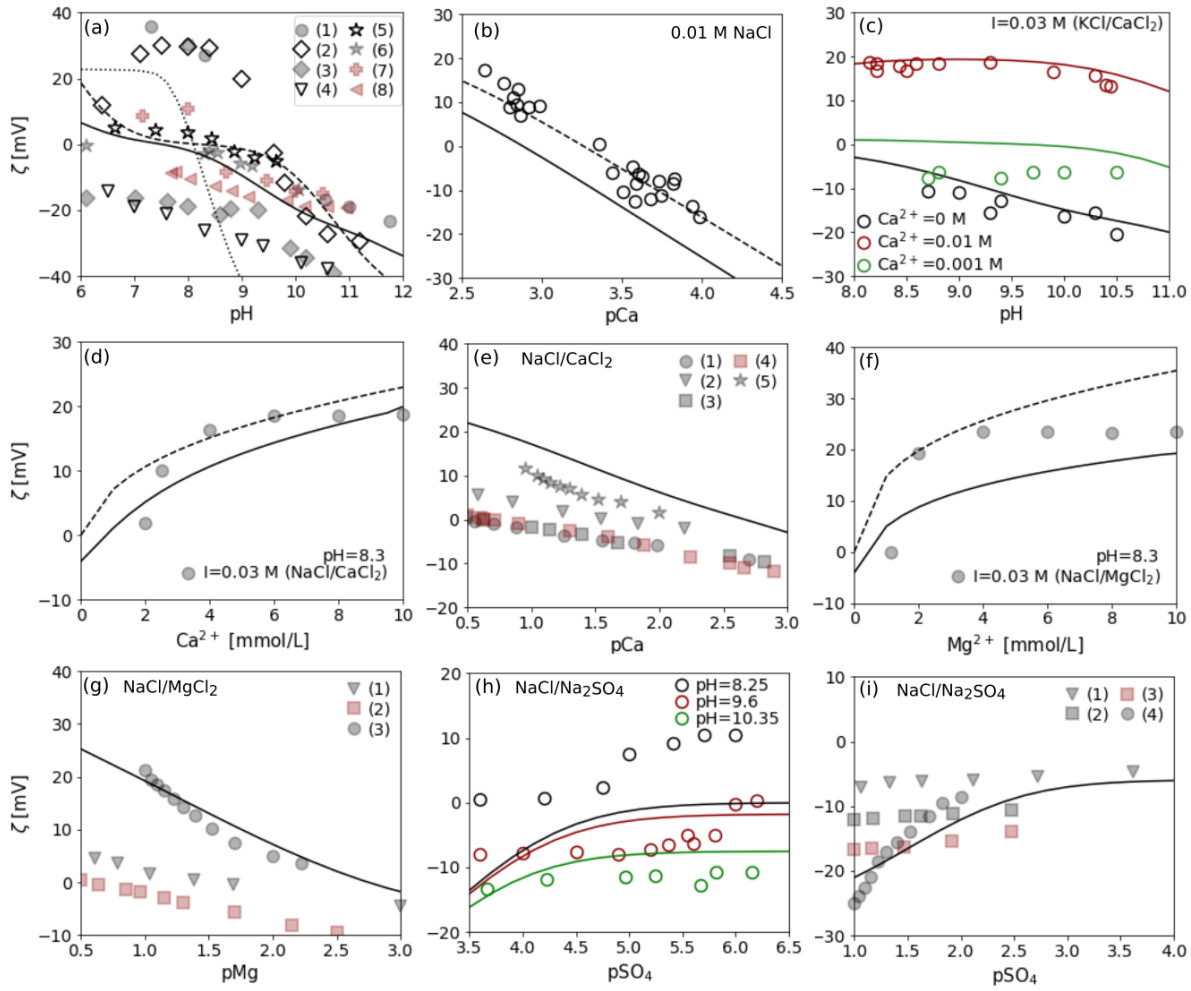

Figure A.2. Predicted zeta potential (no fitting parameters) against experimental data reported in the literature. In all panels, empty markers correspond to measurements performed on synthetic calcite whereas filled markers show measurements carried out on natural samples. **(a)** ζ measurements on calcite in monovalent electrolytes at different pHs. The datasets represent measurements on (1) 0.001 M NaCl/natural calcite suspensions – data from [139]; (2), (3) suspensions consisting of synthetic and natural calcite in 0.001 M NaCl, respectively – data from [176]; (4) 0.001 M NaCl/synthetic calcite suspensions – data from [177]; (5), (6) synthetic calcite and chalk in 0.001 M NaCl, respectively – data from [179]; (7) natural calcite particles in 0.002 M $NaClO_4$ – data from [171]; (8) natural calcite particles in 0.002 M $NaClO_4$ – data from [172]. The dotted lines correspond to the prediction of the model considering equilibrium conditions between the calcite particles (4% wt. solids and ssa of 7.1 m^2/g), solution, and atmospheric CO_2 (equilibrium reached between pHs 7-10). The solid lines correspond to equilibrium in a closed system (no CO_2). The dashed lines correspond to non-equilibrium conditions with respect to both CO_2 and calcite. **(b)** ζ of synthetic calcite particles (4% wt. solids, ssa=22.3 m^2/g) in 0.01 M NaCl against the equilibrium calcium concentration at different pHs (adjusted with HCl/NaOH titrations) – data from [139]. The solid line shows the predicted ζ against the theoretical calcium concentration in solution assuming equilibrium with respect to calcite and atmospheric CO_2. The dashed line shows the predicted ζ considering equilibrium with respect to calcite in a closed system (no CO_2) and $CaCl_2$ titrations. **(c)** ζ measurements of calcite suspensions (assumed 1% wt. solids and ssa= 2 m^2/g) in $CaCl_2$/KCl mixtures at constant ionic strength (0.03 M) and different pHs (adjusted with NaOH/HCl titrations). The lines correspond to the prediction of the model considering equilibrium with respect to calcite in a closed system. **(d)** ζ of natural calcite particles (4% wt. solids, ssa=7.1 m^2/g) at increasing $CaCl_2$ concentration, ionic strength fixed to 0.03 M with NaCl, and pH adjusted to 8.3 by HCl/NaOH titrations – data from [139]. The lines represent the prediction of the model considering either equilibrium with respect to calcite (solid lines) or non-equilibrium (dashed lines) in a closed system (no CO_2). **(e)** ζ variation with the equilibrium calcium concentration (natural calcite samples). The datasets represent measurements on (1), (2), (3) Ketton, Estaillades, and Portland limestone samples, respectively, in 0.5 M NaCl and variable $CaCl_2$ concentration – data from [137]; (4) Portland limestone in 0.05 M NaCl and variable $CaCl_2$ concentration – data from [156]; (5) chalk in 0.573 M and variable $CaCl_2$ concentration at pH=8.4 (fixed by HCl/NaOH titrations) – data from [178]; The lines represent the prediction of the model considering that the electrolyte solution is in equilibrium with the calcite particles (1% wt., ssa=2 m^2/g) in the absence of CO_2; **(f)** ζ of natural calcite particles (4% wt., ssa=7.1 m^2/g) at increasing $MgCl_2$ concentration, ionic strength fixed to 0.03 M with NaCl, and pH adjusted to 8.3 by HCl/NaOH titrations. – data from [139]. The lines represent the prediction of the model assuming either equilibrium with respect to calcite (solid lines) or non-equilibrium (dashed lines) in a closed system (no CO_2). **(g)** ζ of carbonate rock samples in NaCl/$MgCl_2$ electrolyte mixtures. The datasets represent measurements on (1) Estailades limestone sample in

0.5 M NaCl and increasing $MgCl_2$ concentration. – data from [137]; (2) Portland limestone sample in 0.05 M NaCl and increasing $MgCl_2$ concentration – data from [156]; (3) chalk powder in 0.573 M NaCl and varying $MgCl_2$ concentration and a pH fixed to 8.4 by HCl/NaOH additions – data from [60]. The lines represent the prediction of the models considering equilibrium between the calcite suspension (assumed 1% wt. solids, ssa=2 m^2/g) (no CO_2). **(h)** ζ of synthetic calcite particles (4% wt. solids, ssa=22.3 m^2/g) in 0.01 M NaCl, variable sulfate concentration and fixed pH (adjusted with HCl/NaOH titrations)– data from [139]. The lines represent the prediction of the model considering non-equilibrium with respect to both atmospheric CO_2 and calcite. **(i)** ζ of carbonate rock samples in NaCl/Na_2SO_4 electrolyte mixtures. Measurements on (1), (2) Estailades and Portland limestone samples, respectively, in 0.5 M NaCl and increasing Na_2SO_4 concentration. – data from [137]; (3) Portland limestone sample in 0.05 M NaCl and increasing $MgCl_2$ concentration – data from [156]; (4) chalk powder in 0.573 M NaCl and variable Na_2SO_4 concentration and pH fixed to 8.4 by HCl/NaOH titrations – data from [60]. The lines represent the prediction of the model considering equilibrium with respect to calcite (assumed 1% wt. solids, ssa=2 m^2/g) in the absence of a gas phase (no CO_2).

A.3 Supplementary material for Chapter 5

Flotation tests were proposed as a fast and reliable method to quantify the water-wet and oil-wet fraction of a given rock[386]. Although they cannot replace imbibition tests, they can be convenient for designing, for instance, the brine recipe used in displacement experiments. In this section, we test the consistency of BPS, AAS, and SN with the results from the flotations tests performed by Sohal et al.[386] on chalk. In these experiments, the rock is first crushed, wetted, and aged with a brine of specific composition. Then, the brine is decanted and the wetted particles are aged in oil. The decanted effluent is placed again together with the aged chalk particles for the flotation tests, which consist of first shaking the system and then allowing the particles to settle. The water-wet particles will sink, whereas the oil-wet particles will float. For a given mineral and crude oil properties, the water and oil-wet fractions will vary depending on the brine composition. This experimental procedure has a major difference compared to spontaneous imbibition and core flooding tests. In imbibition experiments, the cores are saturated with a formation brine and then aged in oil. The effect of the modified salinity brine is assessed relative to the formation brine. In these flotation tests, the modified brine is also the initial brine. Since the chalk particles were wetted with a different initial water composition, their initial wetting condition may not be the same, which may hamper the comparison of the different brine chemistry effect on the chalk wettability.

We perform the geochemical modelling of this system by considering that the initial brine is in equilibrium with atmospheric CO_2. During the wetting stage of the experiment, we assume equilibrium between the previous solution with the mass of calcite used in the experiments. We first validate these assumptions by comparing the reported pH of the decanted effluent and the predicted one by Phreeqc using Pitzer database (Figure A.3). Considering no gas phase resulted in a larger disagreement between the calculated and predicted pH (Figure A.3-b). Thus, we calculate BPS, AAS, and SN considering a CO_2 gas phase in contact with the solutions during the preparation procedure. Note that we also include anhydrite in our calculations (can precipitate but not dissolve) since we observed that the saturation index for anhydrite was 0.15 and 0.42 for seawater with no NaCl (SW0NaCl), and seawater enriched with sulfate (SWNaCl4S), respectively.

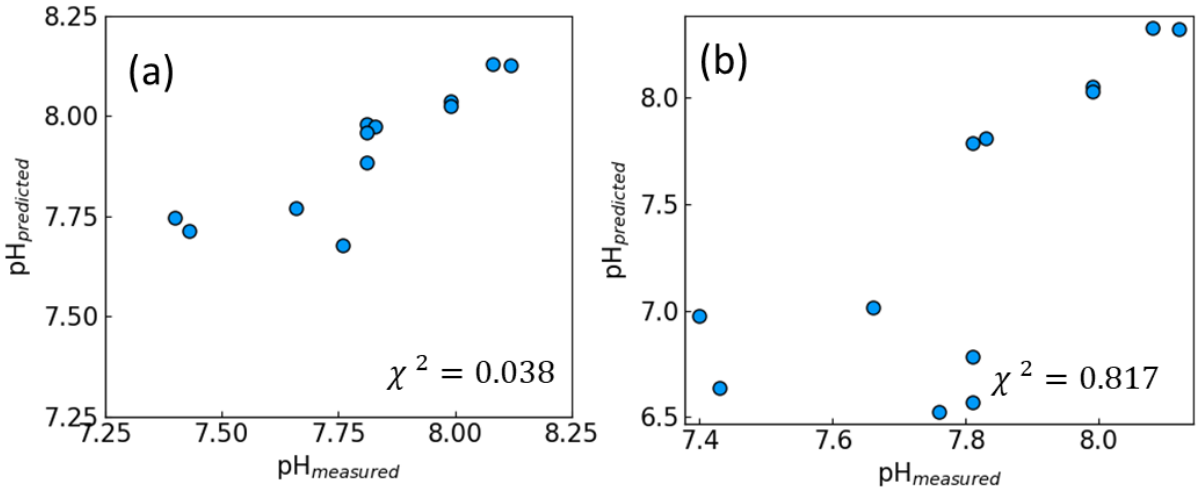

Figure A.3. Measured pH of decanted effluent from flotation tests and the PHREEQC predicted pH considering (a) equilibrium between atmospheric CO_2 with the aqueous solutions; (b) no gas phase.

Two measurements were reported from these flotation tests, i.e., the fraction of water-wet particles and the amount of oil retained on the water-wet particles. Since in these tests the wetting brine before the aging is the same as the modified brine in the flotation test, we cannot define the ratios of the parameters corresponding to two different equilibrium conditions with two different brines as we did for the spontaneous imbibition tests. Thus, we show the scatter plots of BPS, AAS, and SN against the fraction

of water wet particles (Figure A.4) and the remaining oil saturation on the water-wet particles (Figure A.5).

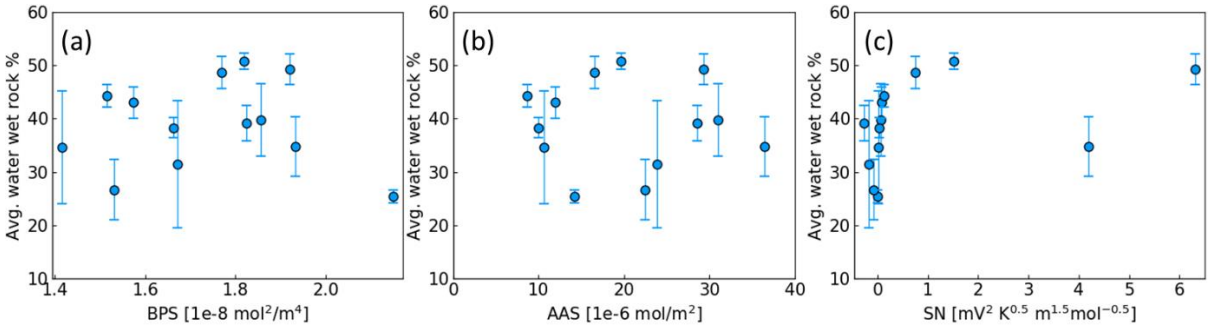

Figure A.4. Average fraction of chalk water-wet particles from flotation tests performed at 100 ºC vs **(a)** BPS; **(b)** AAS; **(c)** SN. Data from [386]. The error bars correspond to the 95% confidence interval estimated from the data in figures 9 and 10 in the original paper that show results from repeated experiments.

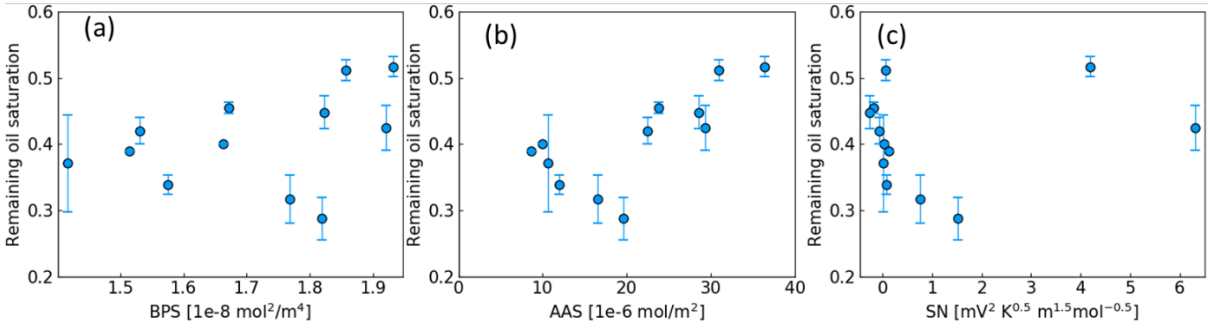

Figure A.5. Average remaining oil saturation on the water-wet chalk fraction from flotation tests performed at 100 ºC vs **(a)** BPS, **(b)** AAS, **(c)** SN. Data from [386]. The error bars correspond to the 95% confidence interval estimated from the data in figures 9 and 10 in the original paper that show results from repeated experiments.

Among the three parameters, SN seems to apriori show a trend with the experimental data. However, some brine compositions that experimentally were shown to result in higher water-wet fractions correspond to negative values of this parameter. A negative SN, by definition, points to an unstable water film, thus oil-wet conditions. Generally, the three interpolants seem to be more related to the attached oil on the water-wet particles rather than with the amount of water-wet particles. Sohal et al.[386] also pointed out that they did not see any relation between the amount of water-wet particles and the amount of oil attached to these but they did see that this residual oil saturation was brine-dependent. We consider that the parameter we propose, $AAS_{ratio,}$ is not consistent with these flotation tests because in these experiments the conditions we assumed for deriving this parameter do not hold (e.g., same brine used in the aging as in the flotation tests). AAS_{ratio} is a tool that provides a relative measure of the altered wettability conditions of a system due to the change of the brine composition and/or the temperature from an initial state to a new one.

A.4 Supplementary material for Chapter 6

Bertheussen et al.[453] separated a commercial mixture of naphtenic acids into different molecular weights fractions. They prepared 4-10 mM mixtures by dissolving the different acid fractions into toluene. This organic phase was then added to 3.5 wt % NaCl solutions and shaken together for 24 h. The two phases were then separated and the amount of acid in each phase (i.e., toluene and brine) was determined. Analogous to the experiments modeled in section 3, we fit the toluene (oil)-brine equilibria model to the experimental data obtained for the different fractions. The only fitting parameter was the partition constant as the acid ionization constant was kept constant for all MW fractions (pK_a=4.9). The model fitted to the experimental data is shown in Figure A.6.

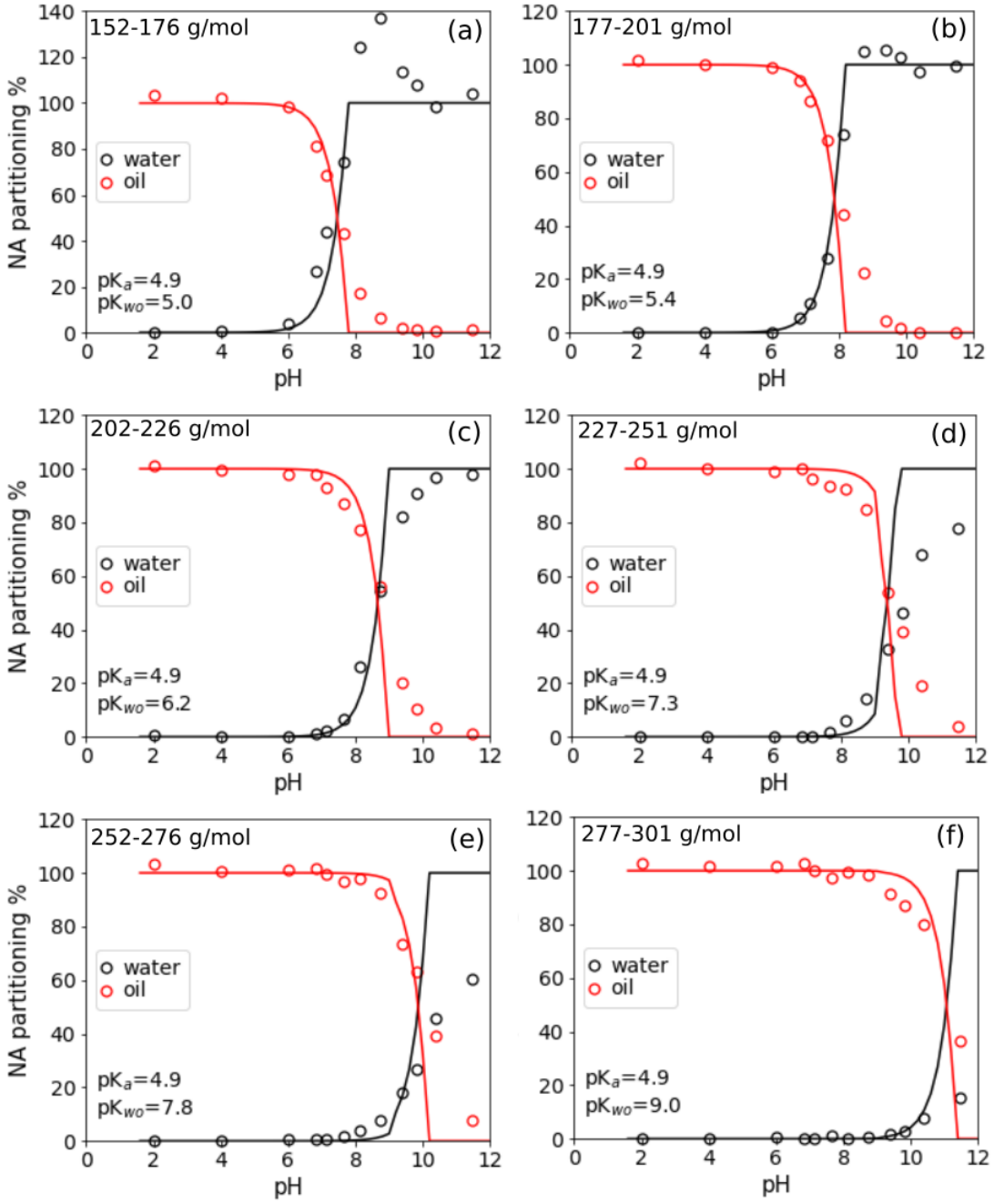

Figure A.6. Equilibrium partitioning of different MW acid fractions between a NaCl aqueous solution and toluene (represented by oil in the legend). The markers represent the experimental data from Bertheussen et al.[453] whereas the lines represent the oil-brine model that we implemented in Phreeqc. The value of the partition constant used to fit the model is included in each panel. Each panel shows the partitioning data of acids within an MW range. The value of this range is shown in the panels.

Based on the average MW of these fractions and the partition constant needed to fit these data, the pK_{wo}-MW relationship is shown in Figure A.7.

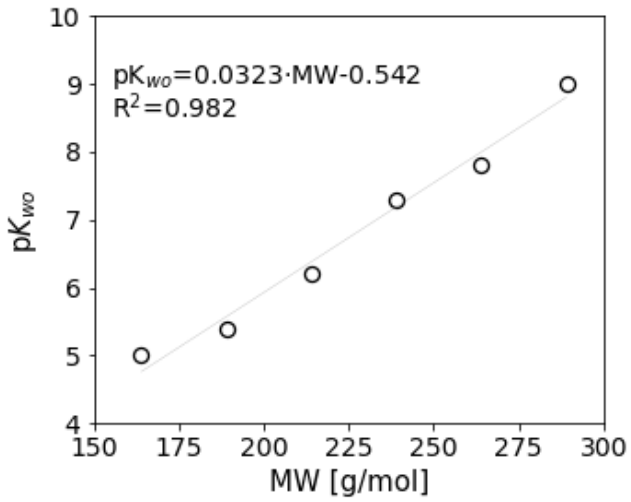

Figure A.7. Acid partitioning constant as a function of the acid average molecular weight.

Bibliography

(1) Danish Energy Agency. *Resource Assessment and Production Forecasts*; 2018.

(2) Hjuler, M. L.; Fabricius, I. L. Engineering Properties of Chalk Related to Diagenetic Variations of Upper Cretaceous Onshore and Offshore Chalk in the North Sea Area. *Journal of Petroleum Science and Engineering* **2009**, *68* (3–4), 151–170. https://doi.org/10.1016/j.petrol.2009.06.005.

(3) Hao, J.; Feilberg, K. L.; Shapiro, A. Kinetics of Calcite Dissolution and Ca–Mg Ion Exchange on the Surfaces of North Sea Chalk Powders. *ACS Omega* **2020**, *5* (28), 17506–17520. https://doi.org/10.1021/acsomega.0c02000.

(4) Bonto, M.; Welch, M. J.; Lüthje, M.; Andersen, S. I.; Veshareh, M. J.; Amour, F.; Afrough, A.; Mokhtari, R.; Hajiabadi, M. R.; Alizadeh, M. R.; Larsen, C. N.; Nick, H. M. Challenges and Enablers for Large-Scale CO2 Storage in Chalk Formations. *Earth-Science Reviews* **2021**, *222*, 103826. https://doi.org/10.1016/j.earscirev.2021.103826.

(5) Hiorth, A.; Cathles, L. M.; Madland, M. V. The Impact of Pore Water Chemistry on Carbonate Surface Charge and Oil Wettability. *Transport in Porous Media* **2010**, *85* (1), 1–21. https://doi.org/10.1007/s11242-010-9543-6.

(6) Zhang, P.; Tweheyo, M. T.; Austad, T. Wettability Alteration and Improved Oil Recovery in Chalk: The Effect of Calcium in the Presence of Sulfate. *Energy & Fuels* **2006**, *20* (5), 2056–2062. https://doi.org/10.1021/ef0600816.

(7) Austad, T.; Shariatpanahi, S. F.; Strand, S.; Black, C. J. J.; Webb, K. J. Conditions for a Low-Salinity Enhanced Oil Recovery (EOR) Effect in Carbonate Oil Reservoirs. *Energy & Fuels* **2012**, *26* (1), 569–575. https://doi.org/10.1021/ef201435g.

(8) Heggheim, T.; Madland, M. V.; Risnes, R.; Austad, T. A Chemical Induced Enhanced Weakening of Chalk by Seawater. *Journal of Petroleum Science and Engineering* **2005**, *46* (3), 171–184. https://doi.org/10.1016/j.petrol.2004.12.001.

(9) Katika, K.; Alam, M. M.; Alexeev, A.; Chakravarty, K. H.; Fosbøl, P. L.; Revil, A.; Stenby, E.; Xiarchos, I.; Yousefi, A.; Fabricius, I. L. Elasticity and Electrical Resistivity of Chalk and Greensand during Water Flooding with Selective Ions. *Journal of Petroleum Science and Engineering* **2018**, *161*, 204–218. https://doi.org/10.1016/j.petrol.2017.11.045.

(10) Madland, M. V.; Hiorth, A.; Omdal, E.; Megawati, M.; Hildebrand-Habel, T.; Korsnes, R. I.; Evje, S.; Cathles, L. M. Chemical Alterations Induced by Rock–Fluid Interactions When Injecting Brines in High Porosity Chalks. *Transport in Porous Media* **2011**, *87* (3), 679–702. https://doi.org/10.1007/s11242-010-9708-3.

(11) Megawati, M.; Hiorth, A.; Madland, M. V. The Impact of Surface Charge on the Mechanical Behavior of High-Porosity Chalk. *Rock Mechanics and Rock Engineering* **2013**, *46* (5), 1073–1090. https://doi.org/10.1007/s00603-012-0317-z.

(12) Amour, F.; Bonto, M.; Hajiabadi, M. R.; Nick, H. M. Sensitivity Study of Chemical Effects on the Compaction Behavior of Reservoir Chalk (Dan Field, Danish North Sea); OnePetro, 2021.

(13) Bonto, M.; Eftekhari, A. A.; Nick, H. A Mechanistic Model for the Fines-Migration During the Modified-Salinity Waterflooding in Carbonate Reservoirs; European Association of Geoscientists & Engineers, 2019; Vol. 2019, pp 1–18. https://doi.org/10.3997/2214-4609.201900077.

(14) Sharma, M. M.; Yortsos, Y. C. Fines Migration in Porous Media. *AIChE Journal* **1987**, *33* (10), 1654–1662. https://doi.org/10.1002/aic.690331009.

(15) Garcia-Olvera, G.; Alvarado, V. Interfacial Rheological Insights of Sulfate-Enriched Smart-Water at Low and High-Salinity in Carbonates. *Fuel* **2017**, *207*, 402–412. https://doi.org/10.1016/j.fuel.2017.06.094.

(16) Lashkarbolooki, M.; Riazi, M.; Ayatollahi, S.; Zeinolabedini Hezave, A. Synergy Effects of Ions, Resin, and Asphaltene on Interfacial Tension of Acidic Crude Oil and Low–High Salinity Brines. *Fuel* **2016**, *165*, 75–85. https://doi.org/10.1016/j.fuel.2015.10.030.

(17) Mahzari, P.; Sohrabi, M. Crude Oil/Brine Interactions and Spontaneous Formation of Micro-Dispersions in Low Salinity Water Injection. In *All Days*; SPE: Tulsa, Oklahoma, USA, 2014; p SPE-169081-MS. https://doi.org/10.2118/169081-MS.
(18) Aldousary, S.; Kovscek, A. R. The Diffusion of Water through Oil Contributes to Spontaneous Emulsification during Low Salinity Waterflooding. *Journal of Petroleum Science and Engineering* **2019**, *179*, 606–614. https://doi.org/10.1016/j.petrol.2019.04.041.
(19) Hao, J.; Mohammadkhani, S.; Shahverdi, H.; Esfahany, M. N.; Shapiro, A. Mechanisms of Smart Waterflooding in Carbonate Oil Reservoirs - A Review. *Journal of Petroleum Science and Engineering* **2019**, *179*, 276–291. https://doi.org/10.1016/j.petrol.2019.04.049.
(20) Tetteh, J. T.; Brady, P. V.; Barati Ghahfarokhi, R. Review of Low Salinity Waterflooding in Carbonate Rocks: Mechanisms, Investigation Techniques, and Future Directions. *Advances in Colloid and Interface Science* **2020**, *284*, 102253. https://doi.org/10.1016/j.cis.2020.102253.
(21) Mohammadkhani, S.; Anabaraonye, B. U.; Afrough, A.; Mokhtari, R.; Feilberg, K. L. Crude Oil–Brine–Rock Interactions in Tight Chalk Reservoirs: An Experimental Study. *Energies* **2021**, *14* (17), 5360. https://doi.org/10.3390/en14175360.
(22) Mohammadi, M.; Mahani, H. Direct Insights into the Pore-Scale Mechanism of Low-Salinity Waterflooding in Carbonates Using a Novel Calcite Microfluidic Chip. *Fuel* **2020**, *260*, 116374. https://doi.org/10.1016/j.fuel.2019.116374.
(23) Selem, A. M.; Agenet, N.; Gao, Y.; Raeini, A. Q.; Blunt, M. J.; Bijeljic, B. Pore-Scale Imaging and Analysis of Low Salinity Waterflooding in a Heterogeneous Carbonate Rock at Reservoir Conditions. *Sci Rep* **2021**, *11* (1), 15063. https://doi.org/10.1038/s41598-021-94103-w.
(24) Mahani, H.; Keya, A. L.; Berg, S.; Nasralla, R. Electrokinetics of Carbonate/Brine Interface in Low-Salinity Waterflooding: Effect of Brine Salinity, Composition, Rock Type, and PH on ζ-Potential and a Surface-Complexation Model. *SPE Journal* **2017**, *22* (01), 053–068. https://doi.org/10.2118/181745-PA.
(25) Lashkarbolooki, M.; Riazi, M.; Hajibagheri, F.; Ayatollahi, S. Low Salinity Injection into Asphaltenic-Carbonate Oil Reservoir, Mechanistical Study. *Journal of Molecular Liquids* **2016**, *216*, 377–386. https://doi.org/10.1016/j.molliq.2016.01.051.
(26) Guo, H.; Kovscek, A. R. Investigation of the Effects of Ions on Short-Range Non-DLVO Forces at the Calcite/Brine Interface and Implications for Low Salinity Oil-Recovery Processes. *Journal of Colloid and Interface Science* **2019**, *552*, 295–311. https://doi.org/10.1016/j.jcis.2019.05.049.
(27) Taheriotaghsara, M.; Bonto, M.; Eftekhari, A. A.; Nick, H. M. Prediction of Oil Breakthrough Time in Modified Salinity Water Flooding in Carbonate Cores. *Fuel* **2020**, *274*, 117806. https://doi.org/10.1016/j.fuel.2020.117806.
(28) Taheriotaghsara, M.; Eftekhari, A. A.; Nick, H. M. Adsorption- and Diffusion-Controlled Wettability Change in Modified Salinity Water Flooding. *Energy Fuels* **2020**, *34* (11), 13767–13781. https://doi.org/10.1021/acs.energyfuels.0c02493.
(29) Jerauld, G. R.; Lin, C. Y.; Webb, K. J.; Seccombe, J. C. Modeling Low-Salinity Waterflooding. **2008**, 13.
(30) Fathi, S. J.; Austad, T.; Strand, S. "Smart Water" as a Wettability Modifier in Chalk: The Effect of Salinity and Ionic Composition. *Energy & Fuels* **2010**, *24* (4), 2514–2519. https://doi.org/10.1021/ef901304m.
(31) Downing, R. A.; Price, M.; Jones, J. P. *The Hydrogeology of the Chalk of North-West Europe*; Oxford University Press, 2005.
(32) Ballesteros, D.; Farrant, A.; Nehme, C.; Woods, M.; Todisco, D.; Mouralis, D. Stratigraphical Influence on Chalk Cave Development in Upper Normandy, France: Implications for Chalk Hydrogeology. *International Journal of Speleology* **2020**, *49* (3), 187–208.
(33) Stipp, S. L.; Hochella, M. F. Structure and Bonding Environments at the Calcite Surface as Observed with X-Ray Photoelectron Spectroscopy (XPS) and Low Energy Electron Diffraction (LEED). *Geochimica et Cosmochimica Acta* **1991**, *55* (6), 1723–1736. https://doi.org/10.1016/0016-7037(91)90142-R.

(34) Wolthers, M.; Tommaso, D. D.; Du, Z.; Leeuw, N. H. de. Calcite Surface Structure and Reactivity: Molecular Dynamics Simulations and Macroscopic Surface Modelling of the Calcite – Water Interface. *Physical Chemistry Chemical Physics* **2012**, *14* (43), 15145–15157. https://doi.org/10.1039/C2CP42290E.
(35) Geissbühler, P.; Fenter, P.; DiMasi, E.; Srajer, G.; Sorensen, L. B.; Sturchio, N. C. Three-Dimensional Structure of the Calcite–Water Interface by Surface X-Ray Scattering. *Surface Science* **2004**, *573* (2), 191–203. https://doi.org/10.1016/j.susc.2004.09.036.
(36) Fenter, P.; Kerisit, S.; Raiteri, P.; Gale, J. D. Is the Calcite–Water Interface Understood? Direct Comparisons of Molecular Dynamics Simulations with Specular X-Ray Reflectivity Data. *The Journal of Physical Chemistry C* **2013**, *117* (10), 5028–5042. https://doi.org/10.1021/jp310943s.
(37) Somasundaran, P.; Agar, G. E. The Zero Point of Charge of Calcite. *Journal of Colloid and Interface Science* **1967**, *24* (4), 433–440. https://doi.org/10.1016/0021-9797(67)90241-X.
(38) Villegas-Jiménez, A.; Mucci, A.; Paquette, J. Proton/Calcium Ion Exchange Behavior of Calcite. *Physical Chemistry Chemical Physics* **2009**, *11* (39), 8895. https://doi.org/10.1039/b815198a.
(39) Derjaguin, B.; Landau, L. Theory of the Stability of Strongly Charged Lyophobic Sols and of the Adhesion of Strongly Charged Particles in Solutions of Electrolytes. *Progress in Surface Science* **1993**, *43* (1), 30–59. https://doi.org/10.1016/0079-6816(93)90013-L.
(40) Verwey, E. J. W. Theory of the Stability of Lyophobic Colloids. *J. Phys. Chem.* **1947**, *51* (3), 631–636. https://doi.org/10.1021/j150453a001.
(41) Plank, J.; Bassioni, G. Adsorption of Carboxylate Anions on a CaCO3 Surface. *Zeitschrift für Naturforschung B* **2007**, *62* (10), 1277–1284. https://doi.org/10.1515/znb-2007-1008.
(42) Buckley, J. S.; Takamura, K.; Morrow, N. R. Influence of Electrical Surface Charges on the Wetting Properties of Crude Oils. *SPE Reservoir Engineering* **1989**, *4* (03), 332–340. https://doi.org/10.2118/16964-PA.
(43) Hirasaki, G. J. Wettability: Fundamentals and Surface Forces - SPE Formation Evaluation, 6(2) https://www.onepetro.org/journal-paper/SPE-17367-PA (accessed 2019 -01 -02).
(44) Kühnle, A. Self-Assembly of Organic Molecules at Metal Surfaces. *Current Opinion in Colloid & Interface Science* **2009**, *14* (2), 157–168. https://doi.org/10.1016/j.cocis.2008.01.001.
(45) Hauke, C. M.; Bechstein, R.; Kittelmann, M.; Storz, C.; Kilbinger, A. F. M.; Rahe, P.; Kühnle, A. Controlling Molecular Self-Assembly on an Insulating Surface by Rationally Designing an Efficient Anchor Functionality That Maintains Structural Flexibility. *ACS Nano* **2013**, *7* (6), 5491–5498. https://doi.org/10.1021/nn401589u.
(46) Rahe, P.; Schütte, J.; Kühnle, A. NC-AFM Contrast Formation on the Calcite ($10\bar {1}4$) Surface. *Journal of Physics: Condensed Matter* **2012**, *24* (8), 084006. https://doi.org/10.1088/0953-8984/24/8/084006.
(47) Rahe, P. From Dewetting to Wetting Molecular Layers: C 60 on CaCO 3(1014) as a Case Study. *Physical Chemistry Chemical Physics* **2012**, *14* (18), 6544–6548. https://doi.org/10.1039/c2cp40172j.
(48) Marutschke, C.; Walters, D.; Cleveland, J.; Hermes, I.; Bechstein, R.; Kühnle, A. Three-Dimensional Hydration Layer Mapping on the (10.4) Surface of Calcite Using Amplitude Modulation Atomic Force Microscopy. *Nanotechnology* **2014**, *25* (33), 335703. https://doi.org/10.1088/0957-4484/25/33/335703.
(49) Nalbach, M.; Raiteri, P.; Klassen, S.; Schäfer, S.; Gale, J. D.; Bechstein, R.; Kühnle, A. Where Is the Most Hydrophobic Region? Benzopurpurine Self-Assembly at the Calcite–Water Interface. *The Journal of Physical Chemistry C* **2017**, *121* (43), 24144–24151. https://doi.org/10.1021/acs.jpcc.7b09825.
(50) Nalbach, M. Structure-Dependent Dissolution and Restructuring of Calcite Surfaces by Organophosphonates. *Crystal Growth and Design* **2017**, *17* (11), 5867–5874. https://doi.org/10.1021/acs.cgd.7b00959.
(51) Lindner, R.; Kühnle, A. On-Surface Reactions. *ChemPhysChem* **2015**, *16* (8), 1582–1592. https://doi.org/10.1002/cphc.201500161.

(52) Kittelmann, M. Molecular Self-Assembly on an Insulating Surface: Interplay between Substrate Templating and Intermolecular Interactions. *Journal of Physics Condensed Matter* **2012**, *24* (35), 354007. https://doi.org/10.1088/0953-8984/24/35/354007.
(53) Zhang, C.; Wei, S.; Hu, Y.; Tang, H.; Gao, J.; Yin, Z.; Guan, Q. Selective Adsorption of Tannic Acid on Calcite and Implications for Separation of Fluorite Minerals. *Journal of Colloid and Interface Science* **2018**, *512*, 55–63. https://doi.org/10.1016/j.jcis.2017.10.043.
(54) Yang, Q.; Liu, Y.; Gu, A.; Ding, J.; Shen, Z. Investigation of Calcium Carbonate Scaling Inhibition and Scale Morphology by AFM. *Journal of Colloid and Interface Science* **2001**, *240* (2), 608–621. https://doi.org/10.1006/jcis.2001.7669.
(55) Westin, K.-J.; Rasmuson, Å. C. Crystal Growth of Aragonite and Calcite in Presence of Citric Acid, DTPA, EDTA and Pyromellitic Acid. *Journal of Colloid and Interface Science* **2005**, *282* (2), 359–369. https://doi.org/10.1016/j.jcis.2004.03.029.
(56) Laumann, S.; Micić, V.; Lowry, G. V.; Hofmann, T. Carbonate Minerals in Porous Media Decrease Mobility of Polyacrylic Acid Modified Zero-Valent Iron Nanoparticles Used for Groundwater Remediation. *Environmental Pollution* **2013**, *179*, 53–60. https://doi.org/10.1016/j.envpol.2013.04.004.
(57) Eriksson, R.; Merta, J.; Rosenholm, J. B. The Calcite/Water Interface: I. Surface Charge in Indifferent Electrolyte Media and the Influence of Low-Molecular-Weight Polyelectrolyte. *Journal of Colloid and Interface Science* **2007**, *313* (1), 184–193. https://doi.org/10.1016/j.jcis.2007.04.034.
(58) Suh, S.; Choi, K.-O.; Yang, S.-C.; Kim, Y. E.; Ko, S. Adsorption Mechanism of Alkyl Polyglucoside (APG) on Calcite Nanoparticles in Aqueous Medium at Varying PH. *Journal of Solid State Chemistry* **2017**, *251*, 122–130. https://doi.org/10.1016/j.jssc.2017.04.020.
(59) Wang, S.; Edwards, I. M.; Clarens, A. F. Wettability Phenomena at the CO_2–Brine–Mineral Interface: Implications for Geologic Carbon Sequestration. *Environmental Science & Technology* **2013**, *47* (1), 234–241. https://doi.org/10.1021/es301297z.
(60) Zhang, P.; Tweheyo, M. T.; Austad, T. Wettability Alteration and Improved Oil Recovery by Spontaneous Imbibition of Seawater into Chalk: Impact of the Potential Determining Ions Ca2+, Mg2+, and SO42−. *Colloids and Surfaces A: Physicochemical and Engineering Aspects* **2007**, *301* (1–3), 199–208. https://doi.org/10.1016/j.colsurfa.2006.12.058.
(61) Strand, S.; Høgnesen, E. J.; Austad, T. Wettability Alteration of Carbonates—Effects of Potential Determining Ions (Ca2+ and SO42−) and Temperature. *Colloids and Surfaces A: Physicochemical and Engineering Aspects* **2006**, *275* (1–3), 1–10. https://doi.org/10.1016/j.colsurfa.2005.10.061.
(62) Tang, G.-Q.; Morrow, N. R. Influence of Brine Composition and Fines Migration on Crude Oilrbrinerrock Interactions and Oil Recovery. **1999**, 13.
(63) Risnes, R.; Madland, M. V.; Hole, M.; Kwabiah, N. K. Water Weakening of Chalk—Mechanical Effects of Water–Glycol Mixtures. *Journal of Petroleum Science and Engineering* **2005**, *48* (1–2), 21–36. https://doi.org/10.1016/j.petrol.2005.04.004.
(64) Lützenkirchen, J. *Surface complexation models of adsorption: A critical survey in the context of experimental data . Adsorption: Theory, Modeling, and Analysis*; Marcel Dekker, Inc, 270 Madison Avenue, New York, USA, 631-710, 2002.
(65) Delgado, A. V.; Arroyo, F. J.; Arroyo, F. J. *Electrokinetic Phenomena and Their Experimental Determination: An Overview*, 1st Edition.; CRC Press: Boca Raton, 2001. https://doi.org/10.1201/9781482294668-3.
(66) Stumm, W.; Morgan, J. J. *Aquatic Chemistry: Chemical Equilibria and Rates in Natural Waters*; Wiley, 1996.
(67) Wolthers, M.; Charlet, L.; Van Cappellen, P. The Surface Chemistry of Divalent Metal Carbonate Minerals; a Critical Assessment of Surface Charge and Potential Data Using the Charge Distribution Multi-Site Ion Complexation Model. *American Journal of Science* **2008**, *308* (8), 905–941. https://doi.org/10.2475/08.2008.02.

(68) Heberling, F.; Trainor, T. P.; Lützenkirchen, J.; Eng, P.; Denecke, M. A.; Bosbach, D. Structure and Reactivity of the Calcite–Water Interface. *Journal of Colloid and Interface Science* **2011**, *354* (2), 843–857. https://doi.org/10.1016/j.jcis.2010.10.047.
(69) Eftekhari, A. A.; Thomsen, K.; Stenby, E. H.; Nick, H. M. Thermodynamic Analysis of Chalk–Brine–Oil Interactions. *Energy & Fuels* **2017**, *31* (11), 11773–11782. https://doi.org/10.1021/acs.energyfuels.7b02019.
(70) Van Cappellen, P.; Charlet, L.; Stumm, W.; Wersin, P. A Surface Complexation Model of the Carbonate Mineral-Aqueous Solution Interface. *Geochimica et Cosmochimica Acta* **1993**, *57* (15), 3505–3518. https://doi.org/10.1016/0016-7037(93)90135-J.
(71) Song et al.; Zeng, Y.; Wang, L.; Duan, X.; Maura, P. Surface Complexation Modeling of Calcite Zeta Potential Measurements in Brines with Mixed Potential Determining Ions (Ca2+, CO32-, Mg2+, SO42-) for Characterizing Carbonate Wettability. *Journal of Colloid and Interface Science* **2017**, *506*, 169–179. https://doi.org/10.1016/j.jcis.2017.06.096.
(72) Song, J.; Rezaee, S.; Zhang, L.; Zhang, Z.; Puerto, M.; Wani, O. B.; Vargas, F.; Alhassan, S.; Biswal, S. L.; Hirasaki, G. J. Characterizing the Influence of Organic Carboxylic Acids and Inorganic Silica Impurities on the Surface Charge of Natural Carbonates Using an Extended Surface Complexation Model. *Energy Fuels* **2019**, *33* (2), 957–967. https://doi.org/10.1021/acs.energyfuels.8b03896.
(73) Tadanier, C. J.; Eick, M. J. Formulating the Charge-Distribution Multisite Surface Complexation Model Using FITEQL. *Soil Science Society of America Journal* **2002**, *66* (5), 1505–1517. https://doi.org/10.2136/sssaj2002.1505.
(74) Sverjensky, D. A.; Sahai, N. Theoretical Prediction of Single-Site Surface-Protonation Equilibrium Constants for Oxides and Silicates in Water. *Geochimica et Cosmochimica Acta* **1996**, *60* (20), 3773–3797. https://doi.org/10.1016/0016-7037(96)00207-4.
(75) Sposito, G. On the Surface Complexation Model of the Oxide-Aqueous Solution Interface. *Journal of Colloid and Interface Science* **1983**, *91* (2), 329–340. https://doi.org/10.1016/0021-9797(83)90345-4.
(76) Sahai, N.; Sverjensky, D. A. Evaluation of Internally Consistent Parameters for the Triple-Layer Model by the Systematic Analysis of Oxide Surface Titration Data. *Geochimica et Cosmochimica Acta* **1997**, *61* (14), 2801–2826. https://doi.org/10.1016/S0016-7037(97)00128-2.
(77) Davis, J. A.; Leckie, J. O. Surface Ionization and Complexation at the Oxide/Water Interface. 3. Adsorption of Anions. *Journal of Colloid and Interface Science* **1980**, *74* (1), 32–43. https://doi.org/10.1016/0021-9797(80)90168-X.
(78) Westall, J.; Hohl, H. A Comparison of Electrostatic Models for the Oxide/Solution Interface. *Advances in Colloid and Interface Science* **1980**, *12* (4), 265–294. https://doi.org/10.1016/0001-8686(80)80012-1.
(79) Goldberg, S. Use of Surface Complexation Models in Soil Chemical Systems. *Advances in Agronomy* **1992**, *47*, 233–329.
(80) Goldberg, S. Surface Complexation Modeling. Reference Module in Earth Systems and Environmental Sciences. **2013**.
(81) Loeppert, R. H.; Schwab, A. P.; Goldberg, S.; Goldberg, S. Adsorption Models Incorporated into Chemical Equilibrium Models. In *SSSA Special Publication*; Soil Science Society of America and American Society of Agronomy, 1995. https://doi.org/10.2136/sssaspecpub42.c5.
(82) Sahai, N.; Sverjensky, D. A. Solvation and Electrostatic Model for Specific Electrolyte Adsorption. *Geochimica et Cosmochimica Acta* **1997**, *61* (14), 2827–2848. https://doi.org/10.1016/S0016-7037(97)00127-0.
(83) Pokrovsky, O. S.; Mielczarski, J. A.; Barres, O.; Schott, J. Surface Speciation Models of Calcite and Dolomite/Aqueous Solution Interfaces and Their Spectroscopic Evaluation. *Langmuir* **2000**, *16* (6), 2677–2688. https://doi.org/10.1021/la980905e.

(84) Pokrovsky, O. S.; Schott, J. Surface Chemistry and Dissolution Kinetics of Divalent Metal Carbonates. *Environmental Science & Technology* **2002**, *36* (3), 426–432. https://doi.org/10.1021/es010925u.
(85) Hiemstra, T.; Van Riemsdijk, W. H. A Surface Structural Approach to Ion Adsorption: The Charge Distribution (CD) Model. *Journal of Colloid and Interface Science* **1996**, *179* (2), 488–508. https://doi.org/10.1006/jcis.1996.0242.
(86) Hiemstra, T.; Venema, P.; Riemsdijk, W. H. V. Intrinsic Proton Affinity of Reactive Surface Groups of Metal (Hydr)Oxides: The Bond Valence Principle. *Journal of Colloid and Interface Science* **1996**, *184* (2), 680–692. https://doi.org/10.1006/jcis.1996.0666.
(87) Heberling, F.; Bosbach, D.; Eckhardt, J.-D.; Fischer, U.; Glowacky, J.; Haist, M.; Kramar, U.; Loos, S.; Müller, H. S.; Neumann, T.; Pust, C.; Schäfer, T.; Stelling, J.; Ukrainczyk, M.; Vinograd, V.; Vučak, M.; Winkler, B. Reactivity of the Calcite–Water-Interface, from Molecular Scale Processes to Geochemical Engineering. *Applied Geochemistry* **2014**, *45*, 158–190. https://doi.org/10.1016/j.apgeochem.2014.03.006.
(88) Sø, H. U.; Postma, D.; Jakobsen, R.; Larsen, F. Competitive Adsorption of Arsenate and Phosphate onto Calcite; Experimental Results and Modeling with CCM and CD-MUSIC. *Geochimica et Cosmochimica Acta* **2012**, *93*, 1–13. https://doi.org/10.1016/j.gca.2012.06.021.
(89) Sø, H. U.; Postma, D.; Jakobsen, R.; Larsen, F. Sorption of Phosphate onto Calcite; Results from Batch Experiments and Surface Complexation Modeling. *Geochimica et Cosmochimica Acta* **2011**, *75* (10), 2911–2923. https://doi.org/10.1016/j.gca.2011.02.031.
(90) Lakshtanov, L. Z.; Stipp, S. L. S. Experimental Study of Nickel(II) Interaction with Calcite: Adsorption and Coprecipitation. *Geochimica et Cosmochimica Acta* **2007**, *71* (15), 3686–3697. https://doi.org/10.1016/j.gca.2007.04.006.
(91) Mettler, S.; Wolthers, M.; Charlet, L.; Gunten, U. von. Sorption and Catalytic Oxidation of Fe(II) at the Surface of Calcite. *Geochimica et Cosmochimica Acta* **2009**, *73* (7), 1826–1840. https://doi.org/10.1016/j.gca.2009.01.003.
(92) Martin-Garin, A.; Van Cappellen, † P.; Charlet, L. Aqueous Cadmium Uptake by Calcite: A Stirred Flow-through Reactor Study. *Geochimica et Cosmochimica Acta* **2003**, *67* (15), 2763–2774. https://doi.org/10.1016/S0016-7037(03)00091-7.
(93) Li, S.; Leroy, P.; Heberling, F.; Devau, N.; Jougnot, D.; Chiaberge, C. Influence of Surface Conductivity on the Apparent Zeta Potential of Calcite. *Journal of Colloid and Interface Science* **2016**, *468*, 262–275. https://doi.org/10.1016/j.jcis.2016.01.075.
(94) Brady, P. V.; Krumhansl, J. L.; Mariner, P. E. Surface Complexation Modeling for Improved Oil Recovery. In *SPE Improved Oil Recovery Symposium*; Society of Petroleum Engineers: Tulsa, Oklahoma, USA, 2012. https://doi.org/10.2118/153744-MS.
(95) Brady, P. V.; Thyne, G. Functional Wettability in Carbonate Reservoirs. *Energy Fuels* **2016**, *30* (11), 9217–9225. https://doi.org/10.1021/acs.energyfuels.6b01895.
(96) Qiao, C.; Li, L.; Johns, R. T.; Xu, J. A Mechanistic Model for Wettability Alteration by Chemically Tuned Waterflooding in Carbonate Reservoirs. *SPE Journal* **2015**, *20* (04), 767–783. https://doi.org/10.2118/170966-PA.
(97) Qiao, C.; Johns, R.; Li, L. Modeling Low-Salinity Waterflooding in Chalk and Limestone Reservoirs. *Energy & Fuels* **2016**. https://doi.org/10.1021/acs.energyfuels.5b02456.
(98) Tetteh, J. T.; Alimoradi, S.; Brady, P. V.; Barati Ghahfarokhi, R. Electrokinetics at Calcite-Rich Limestone Surface: Understanding the Role of Ions in Modified Salinity Waterflooding. *Journal of Molecular Liquids* **2020**, *297*, 111868. https://doi.org/10.1016/j.molliq.2019.111868.
(99) Tetteh, J. T.; Veisi, M.; Brady, P. V.; Barati Ghahfarokhi, R. Surface Reactivity Analysis of the Crude Oil–Brine–Limestone Interface for a Comprehensive Understanding of the Low-Salinity Waterflooding Mechanism. *Energy Fuels* **2020**, *34* (3), 2739–2756. https://doi.org/10.1021/acs.energyfuels.9b03664.

(100) Korrani, A. K. N.; Jerauld, G. R. Modeling Wettability Change in Sandstones and Carbonates Using a Surface-Complexation-Based Method. *Journal of Petroleum Science and Engineering* **2019**, *174*, 1093–1112. https://doi.org/10.1016/j.petrol.2018.12.016.
(101) Bonto, M.; Eftekhari, A. A.; M. Nick, H. Wettability Indicator Parameter Based on the Thermodynamic Modeling of Chalk-Oil-Brine Systems. *Energy Fuels* **2020**, *34* (7), 8018–8036. https://doi.org/10.1021/acs.energyfuels.0c00716.
(102) Taheriotaghsara, M.; Bonto, M.; Nick, H. M.; Eftekhari, A. A. Estimation of Calcite Wettability Using Surface Forces. *Journal of Industrial and Engineering Chemistry* **2021**, *98*, 444–457. https://doi.org/10.1016/j.jiec.2021.03.019.
(103) Erzuah, S.; Fjelde, I.; Omekeh, A. V. Wettability Estimation Using Surface-Complexation Simulations. *SPE Reservoir Evaluation & Engineering* **2018**. https://doi.org/10.2118/185767-PA.
(104) Yutkin, M. P.; Mishra, H.; Patzek, T. W.; Lee, J.; Radke, C. J. Bulk and Surface Aqueous Speciation of Calcite: Implications for Low-Salinity Waterflooding of Carbonate Reservoirs. *SPE Journal* **2018**, *23* (01), 84–101. https://doi.org/10.2118/182829-PA.
(105) Bordeaux-Rego, F.; Mehrabi, M.; Sanaei, A.; Sepehrnoori, K. Improvements on Modelling Wettability Alteration by Engineered Water Injection: Surface Complexation at the Oil/Brine/Rock Contact. *Fuel* **2021**, *284*, 118991. https://doi.org/10.1016/j.fuel.2020.118991.
(106) Sanaei, A.; Tavassoli, S.; Sepehrnoori, K. Investigation of Modified Water Chemistry for Improved Oil Recovery: Application of DLVO Theory and Surface Complexation Model. *Colloids and Surfaces A: Physicochemical and Engineering Aspects* **2019**, *574*, 131–145. https://doi.org/10.1016/j.colsurfa.2019.04.075.
(107) Fenter, P.; Lee, S. S. Hydration Layer Structure at Solid–Water Interfaces. *MRS Bulletin* **2014**, *39* (12), 1056–1061. https://doi.org/10.1557/mrs.2014.252.
(108) Fenter, P.; Geissbühler, P.; DiMasi, E.; Srajer, G.; Sorensen, L. B.; Sturchio, N. C. Surface Speciation of Calcite Observed in Situ by High-Resolution X-Ray Reflectivity. *Geochimica et Cosmochimica Acta* **2000**, *64* (7), 1221–1228. https://doi.org/10.1016/S0016-7037(99)00403-2.
(109) Fenter, P.; Sturchio, N. C. Mineral-Water Interfacial Structures Revealed by Synchrotron X-Ray Scattering. *Progress in Surface Science* **2004**, *77* (5–8), 171–258. https://doi.org/10.1016/j.progsurf.2004.12.001.
(110) Raiteri, P.; Gale, J. D.; Quigley, D.; Rodger, P. M. Derivation of an Accurate Force-Field for Simulating the Growth of Calcium Carbonate from Aqueous Solution: A New Model for the Calcite−Water Interface. *The Journal of Physical Chemistry C* **2010**, *114* (13), 5997–6010. https://doi.org/10.1021/jp910977a.
(111) de Leeuw, N. H.; Parker, S. C. Surface Structure and Morphology of Calcium Carbonate Polymorphs Calcite, Aragonite, and Vaterite: An Atomistic Approach. *J. Phys. Chem. B* **1998**, *102* (16), 2914–2922. https://doi.org/10.1021/jp973210f.
(112) Leeuw, N. H. de; Parker, S. C. Atomistic Simulation of the Effect of Molecular Adsorption Ofwater on the Surface Structure and Energies of Calcitesurfaces. *J. Chem. Soc., Faraday Trans.* **1997**, *93* (3), 467–475. https://doi.org/10.1039/A606573B.
(113) Andersson, M. P.; Stipp, S. L. S. How Acidic Is Water on Calcite? *J. Phys. Chem. C* **2012**, *116* (35), 18779–18787. https://doi.org/10.1021/jp304671k.
(114) Lardge, J. S.; Duffy, D. M.; Gillan, M. J. Investigation of the Interaction of Water with the Calcite (10.4) Surface Using Ab Initio Simulation. *The Journal of Physical Chemistry C* **2009**, *113* (17), 7207–7212. https://doi.org/10.1021/jp806109y.
(115) Kerisit, S.; Parker, S. C.; Harding, J. H. Atomistic Simulation of the Dissociative Adsorption of Water on Calcite Surfaces. *The Journal of Physical Chemistry B* **2003**, *107* (31), 7676–7682. https://doi.org/10.1021/jp034201b.
(116) Kerisit, S.; Parker, S. C. Free Energy of Adsorption of Water and Metal Ions on the {10$\bar{1}$4} Calcite Surface. *J. Am. Chem. Soc.* **2004**, *126* (32), 10152–10161. https://doi.org/10.1021/ja0487776.

(117) Mahani, H.; Keya, A. L.; Berg, S.; Nasralla, R. The Effect of Salinity, Rock Type and PH on the Electrokinetics of Carbonate-Brine Interface and Surface Complexation Modeling; Society of Petroleum Engineers, 2015. https://doi.org/10.2118/175568-MS.
(118) Stipp, S. L. S. Toward a Conceptual Model of the Calcite Surface: Hydration, Hydrolysis, and Surface Potential. *Geochimica et Cosmochimica Acta* **1999**, *63* (19–20), 3121–3131. https://doi.org/10.1016/S0016-7037(99)00239-2.
(119) Israelachvili, J. N. *Intermolecular and Surface Forces*, Third Edition.; Elsevier, 2011. https://doi.org/10.1016/C2011-0-05119-0.
(120) Grahame, D. C. The Electrical Double Layer and the Theory of Electrocapillarity. *Chem. Rev.* **1947**, *41* (3), 441–501. https://doi.org/10.1021/cr60130a002.
(121) Appelo, C. A. J.; Postma, D. *Geochemistry, Groundwater and Pollution*, 2nd Edition.; CRC Press.
(122) Lützenkirchen, J.; Marsac, R.; Kulik, D. A.; Payne, T. E.; Xue, Z.; Orsetti, S.; Haderlein, S. B. Treatment of Multi-Dentate Surface Complexes and Diffuse Layer Implementation in Various Speciation Codes. *Applied Geochemistry* **2015**, *55*, 128–137. https://doi.org/10.1016/j.apgeochem.2014.07.006.
(123) Goldberg, S.; Criscenti, L. J.; Turner, D. R.; Davis, J. A.; Cantrell, K. J. Adsorption–Desorption Processes in Subsurface Reactive Transport Modeling. *Vadose Zone Journal* **2007**, *6* (3), 407. https://doi.org/10.2136/vzj2006.0085.
(124) Harding, I. H.; Healy, T. W. Electrical Double Layer Properties of Amphoteric Polymer Latex Colloids. *Journal of Colloid and Interface Science* **1985**, *107* (2), 382–397. https://doi.org/10.1016/0021-9797(85)90191-2.
(125) Hiemstra, T.; Yong, H.; Van Riemsdijk, W. H. Interfacial Charging Phenomena of Aluminum (Hydr)Oxides. *Langmuir* **1999**, *15* (18), 5942–5955. https://doi.org/10.1021/la981301d.
(126) Zembala, M. Electrokinetics of Heterogeneous Interfaces. *Advances in Colloid and Interface Science* **2004**, *112* (1), 59–92. https://doi.org/10.1016/j.cis.2004.08.001.
(127) Zhang, C. Communication: Computing the Helmholtz Capacitance of Charged Insulator-Electrolyte Interfaces from the Supercell Polarization. *J. Chem. Phys.* **2018**, *149* (3), 031103. https://doi.org/10.1063/1.5038639.
(128) Bockris, J. *Modern Electrochemistry 1, 2A, and 2B.*, 2nd ed.; Springer US, 2007.
(129) Cheng, J.; Sprik, M. The Electric Double Layer at a Rutile TiO_2 Water Interface Modelled Using Density Functional Theory Based Molecular Dynamics Simulation. *Journal of Physics: Condensed Matter* **2014**, *26* (24), 244108. https://doi.org/10.1088/0953-8984/26/24/244108.
(130) Ardizzone, S.; Trasatti, S. Interfacial Properties of Oxides with Technological Impact in Electrochemistry. *Advances in Colloid and Interface Science* **1996**, *64*, 173–251. https://doi.org/10.1016/0001-8686(95)00286-3.
(131) Bonthuis, D. J.; Gekle, S.; Netz, R. R. Profile of the Static Permittivity Tensor of Water at Interfaces: Consequences for Capacitance, Hydration Interaction and Ion Adsorption. *Langmuir* **2012**, *28* (20), 7679–7694. https://doi.org/10.1021/la2051564.
(132) Hiemstra, T.; Van Riemsdijk, W. H. On the Relationship between Charge Distribution, Surface Hydration, and the Structure of the Interface of Metal Hydroxides. *Journal of Colloid and Interface Science* **2006**, *301* (1), 1–18. https://doi.org/10.1016/j.jcis.2006.05.008.
(133) Ballenegger, V.; Hansen, J.-P. Dielectric Permittivity Profiles of Confined Polar Fluids. *The Journal of Chemical Physics* **2005**, *122* (11), 114711. https://doi.org/10.1063/1.1845431.
(134) Hiemstra, T.; Van Riemsdijk, W. H. Physical Chemical Interpretation of Primary Charging Behaviour of Metal (Hydr) Oxides. *Colloids and Surfaces* **1991**, *59*, 7–25. https://doi.org/10.1016/0166-6622(91)80233-E.
(135) Sverjensky, D. A. Prediction of Surface Charge on Oxides in Salt Solutions: Revisions for 1:1 (M+L−) Electrolytes. *Geochimica et Cosmochimica Acta* **2005**, *69* (2), 225–257. https://doi.org/10.1016/j.gca.2004.05.040.

(136) Takeya, M.; Shimokawara, M.; Elakneswaran, Y.; Nawa, T.; Takahashi, S. Predicting the Electrokinetic Properties of the Crude Oil/Brine Interface for Enhanced Oil Recovery in Low Salinity Water Flooding. *Fuel* **2019**, *235*, 822–831. https://doi.org/10.1016/j.fuel.2018.08.079.
(137) Al Mahrouqi, D.; Vinogradov, J.; Jackson, M. D. Zeta Potential of Artificial and Natural Calcite in Aqueous Solution. *Advances in Colloid and Interface Science* **2017**, *240*, 60–76. https://doi.org/10.1016/j.cis.2016.12.006.
(138) Thompson, D. W.; Pownall, P. G. Surface Electrical Properties of Calcite. *Journal of Colloid and Interface Science* **1989**, *131* (1), 74–82. https://doi.org/10.1016/0021-9797(89)90147-1.
(139) Pierre, A.; Lamarche, J. M.; Mercier, R.; Foissy, A.; Persello, J. Calcium as Potential Determining Ion in Aqueous Calcite Suspensions. *Journal of Dispersion Science and Technology* **1990**, *11* (6), 611–635. https://doi.org/10.1080/01932699008943286.
(140) Zachara, J. M.; Cowan, C. E.; Resch, C. T. Sorption of Divalent Metals on Calcite. *Geochimica et Cosmochimica Acta* **1991**, *55* (6), 1549–1562. https://doi.org/10.1016/0016-7037(91)90127-Q.
(141) Sø, H. U.; Postma, D.; Jakobsen, R.; Larsen, F. Sorption and Desorption of Arsenate and Arsenite on Calcite. *Geochimica et Cosmochimica Acta* **2008**, *72* (24), 5871–5884. https://doi.org/10.1016/j.gca.2008.09.023.
(142) Comans, R. N. J.; Middelburg, J. J. Sorption of trace metals on calcite: Applicability of the surface precipitation model http://dspace.library.uu.nl/handle/1874/16798 (accessed 2018 -12 -23).
(143) Kaushansky, P.; Yariv, S. The Interactions between Calcite Particles and Aqueous Solutions of Magnesium, Barium or Zinc Chlorides. *Applied Geochemistry* **1986**, *1* (5), 607–618. https://doi.org/10.1016/0883-2927(86)90068-5.
(144) Mucci, A.; Canuel, R.; Zhong, S. The Solubility of Calcite and Aragonite in Sulfate-Free Seawater and the Seeded Growth Kinetics and Composition of the Precipitates at 25°C. *Chemical Geology* **1989**, *74* (3), 309–320. https://doi.org/10.1016/0009-2541(89)90040-5.
(145) Flaathen, T. K.; Oelkers, E. H.; Gislason, S. R.; Aagaard, P. The Effect of Dissolved Sulphate on Calcite Precipitation Kinetics and Consequences for Subsurface CO2 Storage. *Energy Procedia* **2011**, *4*, 5037–5043. https://doi.org/10.1016/j.egypro.2011.02.476.
(146) Ruiz-Agudo, E.; Putnis, C. V.; Jiménez-López, C.; Rodriguez-Navarro, C. An Atomic Force Microscopy Study of Calcite Dissolution in Saline Solutions: The Role of Magnesium Ions. *Geochimica et Cosmochimica Acta* **2009**, *73* (11), 3201–3217. https://doi.org/10.1016/j.gca.2009.03.016.
(147) Liu, Y.; Sheng, X.; Dong, Y.; Ma, Y. Removal of High-Concentration Phosphate by Calcite: Effect of Sulfate and PH. *Desalination* **2012**, *289*, 66–71. https://doi.org/10.1016/j.desal.2012.01.011.
(148) Sakuma, H.; Andersson, M. P.; Bechgaard, K.; Stipp, S. L. S. Surface Tension Alteration on Calcite, Induced by Ion Substitution. *J. Phys. Chem. C* **2014**, *118* (6), 3078–3087. https://doi.org/10.1021/jp411151u.
(149) Andersson, M. P.; Dideriksen, K.; Sakuma, H.; Stipp, S. L. S. Modelling How Incorporation of Divalent Cations Affects Calcite Wettability–Implications for Biomineralisation and Oil Recovery. *Scientific Reports* **2016**, *6* (1). https://doi.org/10.1038/srep28854.
(150) Takano, B. Geochemical Implications of Sulfate in Sedimentary Carbonates. *Chemical Geology* **1985**, *49* (4), 393–403. https://doi.org/10.1016/0009-2541(85)90001-4.
(151) Nielsen, M. R.; Sand, K. K.; Rodriguez-Blanco, J. D.; Bovet, N.; Generosi, J.; Dalby, K. N.; Stipp, S. L. S. Inhibition of Calcite Growth: Combined Effects of Mg2+ and SO42–. *Crystal Growth & Design* **2016**, *16* (11), 6199–6207. https://doi.org/10.1021/acs.cgd.6b00536.
(152) Tang, Y.; Zhang, F.; Cao, Z.; Jing, W.; Chen, Y. Crystallization of CaCO3 in the Presence of Sulfate and Additives: Experimental and Molecular Dynamics Simulation Studies. *Journal of Colloid and Interface Science* **2012**, *377* (1), 430–437. https://doi.org/10.1016/j.jcis.2012.02.069.
(153) Strand, S.; Standnes, D. C.; Austad, T. New Wettability Test for Chalk Based on Chromatographic Separation of SCN− and SO42−. *Journal of Petroleum Science and Engineering* **2006**, *52* (1), 187–197. https://doi.org/10.1016/j.petrol.2006.03.021.

(154) de Leeuw, N. H.; Parker, S. C. Modeling Absorption and Segregation of Magnesium and Cadmium Ions to Calcite Surfaces: Introducing MgCO3 and CdCO3 Potential Models. *J. Chem. Phys.* **2000**, *112* (9), 9.
(155) Liu, J.; Wani, O. B.; Alhassan, S. M.; Pantelides, S. T. Wettability Alteration and Enhanced Oil Recovery Induced by Proximal Adsorption of Na+, Cl-, Ca2+, Mg2+, and SO42- Ions on Calcite. *Phys. Rev. Applied* **2018**, *10* (3), 034064. https://doi.org/10.1103/PhysRevApplied.10.034064.
(156) Alroudhan, A.; Vinogradov, J.; Jackson, M. D. Zeta Potential of Intact Natural Limestone: Impact of Potential-Determining Ions Ca, Mg and SO4. *Colloids and Surfaces A: Physicochemical and Engineering Aspects* **2016**, *493*, 83–98. https://doi.org/10.1016/j.colsurfa.2015.11.068.
(157) Ricci, M.; Spijker, P.; Stellacci, F.; Molinari, J.-F.; Voïtchovsky, K. Direct Visualization of Single Ions in the Stern Layer of Calcite. *Langmuir* **2013**, *29* (7), 2207–2216. https://doi.org/10.1021/la3044736.
(158) Hofmann, S.; Voïtchovsky, K.; Spijker, P.; Schmidt, M.; Stumpf, T. Visualising the Molecular Alteration of the Calcite (104) – Water Interface by Sodium Nitrate. *Scientific Reports* **2016**, *6* (1). https://doi.org/10.1038/srep21576.
(159) Delgado, A. V.; González-Caballero, F.; Hunter, R. J.; Koopal, L. K.; Lyklema, J. Measurement and Interpretation of Electrokinetic Phenomena. *Journal of Colloid and Interface Science* **2007**, *309* (2), 194–224. https://doi.org/10.1016/j.jcis.2006.12.075.
(160) O'Brien, R. W.; Cannon, D. W.; Rowlands, W. N. Electroacoustic Determination of Particle Size and Zeta Potential. *Journal of Colloid and Interface Science* **1995**, *173* (2), 406–418. https://doi.org/10.1006/jcis.1995.1341.
(161) Hunter, R. J. *Zeta Potential in Colloid Science: Principles and Applications*; Academic Press, 1981.
(162) Alshakhs, M. J.; Kovscek, A. R. Understanding the Role of Brine Ionic Composition on Oil Recovery by Assessment of Wettability from Colloidal Forces. *Advances in Colloid and Interface Science* **2016**, *233*, 126–138. https://doi.org/10.1016/j.cis.2015.08.004.
(163) Ahmadi, P.; Asaadian, H.; Khadivi, A.; Kord, S. A New Approach for Determination of Carbonate Rock Electrostatic Double Layer Variation towards Wettability Alteration. *Journal of Molecular Liquids* **2019**, *275*, 682–698. https://doi.org/10.1016/j.molliq.2018.11.106.
(164) Cicerone, D. S.; Regazzoni, A. E.; Blesa, M. A. Electrokinetic Properties of the Calcite/Water Interface in the Presence of Magnesium and Organic Matter. *Journal of Colloid and Interface Science* **1992**, *154* (2), 423–433. https://doi.org/10.1016/0021-9797(92)90158-I.
(165) Yingda Lu; Najafabadi, N. F.; Firoozabadi, A. Effect of Temperature on Wettability of Oil/Brine/Rock Systems. *Energy & Fuels* **2017**, *31* (5), 4989–4995. https://doi.org/10.1021/acs.energyfuels.7b00370.
(166) Foxall, T.; Peterson, G. C.; Rendall, H. M.; Smith, A. L. Charge Determination at Calcium Salt/Aqueous Solution Interface. *Journal of the Chemical Society, Faraday Transactions 1: Physical Chemistry in Condensed Phases* **1979**, *75* (0), 1034. https://doi.org/10.1039/f19797501034.
(167) Huang, Y. C.; Fowkes, F. M.; Lloyd, T. B.; Sanders, N. D. Adsorption of Calcium Ions from Calcium Chloride Solutions onto Calcium Carbonate Particles. *Langmuir* **1991**, *7* (8), 1742–1748. https://doi.org/10.1021/la00056a028.
(168) Li, S.; Jackson, M. D.; Agenet, N. Role of the Calcite-Water Interface in Wettability Alteration during Low Salinity Waterflooding. *Fuel* **2020**, *276*, 118097. https://doi.org/10.1016/j.fuel.2020.118097.
(169) Chen, L.; Zhang, G.; Wang, L.; Wu, W.; Ge, J. Zeta Potential of Limestone in a Large Range of Salinity. *Colloids and Surfaces A: Physicochemical and Engineering Aspects* **2014**, *450*, 1–8. https://doi.org/10.1016/j.colsurfa.2014.03.006.
(170) Mahani, H.; Keya, A. L.; Berg, S.; Bartels, W.-B.; Nasralla, R.; Rossen, W. R. Insights into the Mechanism of Wettability Alteration by Low-Salinity Flooding (LSF) in Carbonates. *Energy & Fuels* **2015**, *29* (3), 1352–1367. https://doi.org/10.1021/ef5023847.

(171) Mishra, S. K. The Electrokinetics of Apatite and Calcite in Inorganic Electrolyte Environment. *International Journal of Mineral Processing* **1978**, *5* (1), 69–83. https://doi.org/10.1016/0301-7516(78)90006-6.
(172) Rao, K. H.; Antti, B.-M.; Forssberg, E. Mechanism of Oleate Interaction on Salt-Type Minerals Part I. Adsorption and Electrokinetic Studies of Calcite in the Presence of Sodium Oleate and Sodium Metasilicate. *Colloids and Surfaces* **1988**, *34* (3), 227–239. https://doi.org/10.1016/0166-6622(88)80101-X.
(173) Siffert, D.; Fimbel, P. Parameters Affecting the Sign and Magnitude of the Eletrokinetic Potential of Calcite. *Colloids and Surfaces* **1984**, *11* (3), 377–389. https://doi.org/10.1016/0166-6622(84)80291-7.
(174) Smallwood, P. V. Some Aspects of the Surface Chemistry of Calcite and Aragonite Part I: An Electrokinetic Study. *Colloid and Polymer Science* **1977**, *255* (9), 881–886. https://doi.org/10.1007/BF01617095.
(175) Song, J.; Zeng, Y.; Wang, L.; Duan, X.; Puerto, M.; Chapman, W. G.; Biswal, S. L.; Hirasaki, G. J. Surface Complexation Modeling of Calcite Zeta Potential Measurements in Brines with Mixed Potential Determining Ions (Ca2+, CO32−, Mg2+, SO42−) for Characterizing Carbonate Wettability. *Journal of Colloid and Interface Science* **2017**, *506*, 169–179. https://doi.org/10.1016/j.jcis.2017.06.096.
(176) Vdović, N.; Bišćan, J. Electrokinetics of Natural and Synthetic Calcite Suspensions. *Colloids and Surfaces A: Physicochemical and Engineering Aspects* **1998**, *137* (1), 7–14. https://doi.org/10.1016/S0927-7757(97)00179-9.
(177) Sondi, I.; Bišćan, J.; Vdović, N.; Škapin, S. D. The Electrokinetic Properties of Carbonates in Aqueous Media Revisited. *Colloids and Surfaces A: Physicochemical and Engineering Aspects* **2009**, *342* (1), 84–91. https://doi.org/10.1016/j.colsurfa.2009.04.012.
(178) Zhang, P.; Austad, T. Wettability and Oil Recovery from Carbonates: Effects of Temperature and Potential Determining Ions. *Colloids and Surfaces A: Physicochemical and Engineering Aspects* **2006**, *279* (1), 179–187. https://doi.org/10.1016/j.colsurfa.2006.01.009.
(179) Lakshtanov, L. Z.; Okhrimenko, D. V.; Karaseva, O. N.; Stipp, S. L. S. Limits on Calcite and Chalk Recrystallization. *Crystal Growth & Design* **2018**, *18* (8), 4536–4543. https://doi.org/10.1021/acs.cgd.8b00537.
(180) Alotaibi, M. B.; Nasr-El-Din, H. A.; Fletcher, J. J. Electrokinetics of Limestone and Dolomite Rock Particles. *SPE Reservoir Evaluation & Engineering* **2011**, *14* (05), 594–603. https://doi.org/10.2118/148701-PA.
(181) Ayirala, S. C.; Saleh, S. H.; Enezi, S. M.; Al-Yousef, A. A. Effect of Salinity and Water Ions on Electrokinetic Interactions in Carbonate Reservoir Cores at Elevated Temperatures. *SPE Reservoir Evaluation & Engineering* **2018**, *21* (03), 733–746. https://doi.org/10.2118/189444-PA.
(182) Alotaibi, M. B.; Yousef, A. The Role of Individual and Combined Ions in Waterflooding Carbonate Reservoirs: Electrokinetic Study. *SPE Reservoir Evaluation & Engineering* **2017**, *20* (01), 077–086. https://doi.org/10.2118/177983-PA.
(183) Collini, H.; Li, S.; Jackson, M. D.; Agenet, N.; Rashid, B.; Couves, J. Zeta Potential in Intact Carbonates at Reservoir Conditions and Its Impact on Oil Recovery during Controlled Salinity Waterflooding. *Fuel* **2020**, *266*, 116927. https://doi.org/10.1016/j.fuel.2019.116927.
(184) Mahrouqi, D. A.; Vinogradov, J.; Jackson, M. D. Temperature Dependence of the Zeta Potential in Intact Natural Carbonates. *Geophysical Research Letters* **2016**, *43* (22), 11,578-11,587. https://doi.org/10.1002/2016GL071151.
(185) Al-Hashim, H.; Kasha, A.; Abdallah, W.; Sauerer, B. Impact of Modified Seawater on Zeta Potential and Morphology of Calcite and Dolomite Aged with Stearic Acid. *Energy Fuels* **2018**, *32* (2), 1644–1656. https://doi.org/10.1021/acs.energyfuels.7b03753.
(186) Kasha, A.; Al-Hashim, H.; Abdallah, W.; Taherian, R.; Sauerer, B. Effect of Ca2+, Mg2+ and SO42− Ions on the Zeta Potential of Calcite and Dolomite Particles Aged with Stearic Acid. *Colloids*

and Surfaces A: Physicochemical and Engineering Aspects **2015**, *482*, 290–299. https://doi.org/10.1016/j.colsurfa.2015.05.043.
(187) Pourchet, S.; Pochard, I.; Brunel, F.; Perrey, D. Chemistry of the Calcite/Water Interface: Influence of Sulfate Ions and Consequences in Terms of Cohesion Forces. *Cement and Concrete Research* **2013**, *52*, 22–30. https://doi.org/10.1016/j.cemconres.2013.04.002.
(188) Newville, M.; Stensitzki, T.; Allen, D. B.; Ingargiola, A. *LMFIT: Non-Linear Least-Square Minimization and Curve-Fitting for Python*; Zenodo, 2014. https://doi.org/10.5281/zenodo.11813.
(189) Uygur, V.; Rimmer, D. L. Reactions of Zinc with Iron-Oxide Coated Calcite Surfaces at Alkaline PH. *European Journal of Soil Science* **2000**, *51* (3), 511–516. https://doi.org/10.1046/j.1365-2389.2000.00318.x.
(190) Kaufmann, G.; Dreybrodt, W. Calcite Dissolution Kinetics in the System CaCO3–H2O–CO2 at High Undersaturation. *Geochimica et Cosmochimica Acta* **2007**, *71* (6), 1398–1410. https://doi.org/10.1016/j.gca.2006.10.024.
(191) Ruiz-Agudo, E.; Kowacz, M.; Putnis, C. V.; Putnis, A. The Role of Background Electrolytes on the Kinetics and Mechanism of Calcite Dissolution. *Geochimica et Cosmochimica Acta* **2010**, *74* (4), 1256–1267. https://doi.org/10.1016/j.gca.2009.11.004.
(192) Eisenlohr, L.; Meteva, K.; Gabrovšek, F.; Dreybrodt, W. The Inhibiting Action of Intrinsic Impurities in Natural Calcium Carbonate Minerals to Their Dissolution Kinetics in Aqueous H2O–CO2 Solutions. *Geochimica et Cosmochimica Acta* **1999**, *63* (7), 989–1001. https://doi.org/10.1016/S0016-7037(98)00301-9.
(193) Berner, R. A. The Role of Magnesium in the Crystal Growth of Calcite and Aragonite from Sea Water. *Geochimica et Cosmochimica Acta* **1975**, *39* (4), 489–504. https://doi.org/10.1016/0016-7037(75)90102-7.
(194) Sun, W.; Jayaraman, S.; Chen, W.; Persson, K. A.; Ceder, G. Nucleation of Metastable Aragonite CaCO3 in Seawater. *PNAS* **2015**, *112* (11), 3199–3204.
(195) Sand, K. K.; Pedersen, C. S.; Sjöberg, S.; Nielsen, J. W.; Makovicky, E.; Stipp, S. L. S. Biomineralization: Long-Term Effectiveness of Polysaccharides on the Growth and Dissolution of Calcite. *Crystal Growth & Design* **2014**, *14* (11), 5486–5494. https://doi.org/10.1021/cg5006743.
(196) Belova, D. A.; Johnsson, A.; Bovet, N.; Lakshtanov, L. Z.; Stipp, S. L. S. The Effect on Chalk Recrystallization after Treatment with Oxidizing Agents. *Chemical Geology* **2012**, *291*, 217–223. https://doi.org/10.1016/j.chemgeo.2011.10.025.
(197) Kaszuba, M.; Corbett, J.; Watson, F. M.; Jones, A. High-Concentration Zeta Potential Measurements Using Light-Scattering Techniques. *Philos Trans A Math Phys Eng Sci* **2010**, *368* (1927), 4439–4451. https://doi.org/10.1098/rsta.2010.0175.
(198) Dong, W.; Wan, J. Additive Surface Complexation Modeling of Uranium(VI) Adsorption onto Quartz-Sand Dominated Sediments. *Environ. Sci. Technol.* **2014**, *48* (12), 6569–6577. https://doi.org/10.1021/es501782g.
(199) Anderson, P. R.; Benjamin, M. M. Modeling Adsorption in Aluminum-Iron Binary Oxide Suspensions. *Environmental Science & Technology* **1990**, *24* (10), 1586–1592. https://doi.org/10.1021/es00080a020.
(200) Anderson, P. R.; Benjamin, M. M. Surface and Bulk Characteristics of Binary Oxide Suspensions. *Environ. Sci. Technol.* **1990**, *24* (5), 692–698. https://doi.org/10.1021/es00075a013.
(201) Meng, X.; Letterman, R. D. Effect of Component Oxide Interaction on the Adsorption Properties of Mixed Oxides. *Environ. Sci. Technol.* **1993**, *27* (5), 970–975. https://doi.org/10.1021/es00042a021.
(202) Lützenkirchen, J.; Behra, Ph. A New Approach for Modelling Potential Effects in Cation Adsorption onto Binary (Hydr) Oxides. *Journal of Contaminant Hydrology* **1997**, *26* (1), 257–268. https://doi.org/10.1016/S0169-7722(96)00073-3.
(203) Meng, X.; Letterman, R. D. Modeling Ion Adsorption on Aluminum Hydroxide-Modified Silica. *Environ. Sci. Technol.* **1993**, *27* (9), 1924–1929. https://doi.org/10.1021/es00046a023.

(204) Koopal, L. K.; van Riemsdijk, W. H. Electrosorption on Random and Patchwise Heterogeneous Surfaces: Electrical Double-Layer Effects. *Journal of Colloid and Interface Science* **1989**, *128* (1), 188–200. https://doi.org/10.1016/0021-9797(89)90397-4.
(205) Williams, D. J. A.; Williams, K. P. Electrophoresis and Zeta Potential of Kaolinite. *Journal of Colloid and Interface Science* **1978**, *65* (1), 79–87. https://doi.org/10.1016/0021-9797(78)90260-6.
(206) Feick, J. D.; Chukwumah, N.; Noel, A. E.; Velegol, D. Altering Surface Charge Nonuniformity on Individual Colloidal Particles. *Langmuir* **2004**, *20* (8), 3090–3095. https://doi.org/10.1021/la0355545.
(207) Drelich, J.; Wang, Y. U. Charge Heterogeneity of Surfaces: Mapping and Effects on Surface Forces. *Advances in Colloid and Interface Science* **2011**, *165* (2), 91–101. https://doi.org/10.1016/j.cis.2010.12.009.
(208) Penners, N. H. G.; Koopal, L. K.; Lyklema, J. Interfacial Electrochemistry of Haematite (α-Fe2O3): Homodisperse and Heterodisperse Sols. *Colloids and Surfaces* **1986**, *21*, 457–468. https://doi.org/10.1016/0166-6622(86)80109-3.
(209) Sprycha, R.; Szczypa, J. Some Supplementary Considerations on the Estimation of Surface Ionization Constants from Electrokinetic Data. *Journal of Colloid and Interface Science* **1987**, *115* (2), 590–592. https://doi.org/10.1016/0021-9797(87)90084-1.
(210) Sprycha, R.; Szczypa, J. Estimation of Surface Ionization Constants from Electrokinetic Data. *Journal of Colloid and Interface Science* **1984**, *102* (1), 288–291. https://doi.org/10.1016/0021-9797(84)90221-2.
(211) Sprycha, R. Electrical Double Layer at Alumina/Electrolyte Interface: I. Surface Charge and Zeta Potential. *Journal of Colloid and Interface Science* **1989**, *127* (1), 1–11. https://doi.org/10.1016/0021-9797(89)90002-7.
(212) Parkhurst, D. L.; Wissmeier, L. PhreeqcRM: A Reaction Module for Transport Simulators Based on the Geochemical Model PHREEQC. *Advances in Water Resources* **2015**, *83*, 176–189. https://doi.org/10.1016/j.advwatres.2015.06.001.
(213) Guyer, J. E.; Wheeler, D.; Warren, J. A. FiPy: Partial Differential Equations with Python. *Computing in Science Engineering* **2009**, *11* (3), 6–15. https://doi.org/10.1109/MCSE.2009.52.
(214) Okhrimenko, D. V.; Dalby, K. N.; Skovbjerg, L. L.; Bovet, N.; Christensen, J. H.; Stipp, S. L. S. The Surface Reactivity of Chalk (Biogenic Calcite) with Hydrophilic and Hydrophobic Functional Groups. *Geochimica et Cosmochimica Acta* **2014**, *128*, 212–224. https://doi.org/10.1016/j.gca.2013.12.011.
(215) Skovbjerg, L. L.; Hassenkam, T.; Makovicky, E.; Hem, C. P.; Yang, M.; Bovet, N.; Stipp, S. L. S. Nano Sized Clay Detected on Chalk Particle Surfaces. *Geochimica et Cosmochimica Acta* **2012**, *99*, 57–70. https://doi.org/10.1016/j.gca.2012.05.037.
(216) Chen, J. Y.; Ko, C.-H.; Bhattacharjee, S.; Elimelech, M. Role of Spatial Distribution of Porous Medium Surface Charge Heterogeneity in Colloid Transport. *Colloids and Surfaces A: Physicochemical and Engineering Aspects* **2001**, *191* (1), 3–15. https://doi.org/10.1016/S0927-7757(01)00759-2.
(217) Strand, S.; Austad, T.; Puntervold, T.; Høgnesen, E. J.; Olsen, M.; Barstad, S. M. F. "Smart Water" for Oil Recovery from Fractured Limestone: A Preliminary Study. *Energy & Fuels* **2008**, *22* (5), 3126–3133. https://doi.org/10.1021/ef800062n.
(218) Machesky, M. L.; Wesolowski, D. J.; Palmer, D. A.; Ridley, M. K. On the Temperature Dependence of Intrinsic Surface Protonation Equilibrium Constants: An Extension of the Revised MUSIC Model. *Journal of Colloid and Interface Science* **2001**, *239* (2), 314–327. https://doi.org/10.1006/jcis.2001.7584.
(219) Kulik, D. A. Thermodynamic Properties of Surface Species at the Mineral–Water Interface under Hydrothermal Conditions: A Gibbs Energy Minimization Single-Site 2pKA Triple-Layer Model of Rutile in NaCl Electrolyte to 250°C. *Geochimica et Cosmochimica Acta* **2000**, *64* (18), 3161–3179. https://doi.org/10.1016/S0016-7037(00)00413-0.
(220) Kulik, D. A. Chapter 7 - Standard Molar Gibbs Energies and Activity Coefficients of Surface Complexes on Mineral-Water Interfaces (Thermodynamic Insights). In *Interface Science and*

Technology; Lützenkirchen, J., Ed.; Surface Complexation Modelling; Elsevier, 2006; Vol. 11, pp 171–250. https://doi.org/10.1016/S1573-4285(06)80051-7.
(221) Bonto, M.; Nick, H. M.; Eftekhari, A. A. Thermodynamic Analysis of the Temperature Effect on Calcite Surface Reactions in Aqueous Environments. *Energy Fuels* **2021**. https://doi.org/10.1021/acs.energyfuels.1c01652.
(222) Gupta, R.; Smith, G. G.; Hu, L.; Willingham, T.; Lo Cascio, M.; Shyeh, J. J.; Harris, C. R. Enhanced Waterflood for Carbonate Reservoirs - Impact of Injection Water Composition; Society of Petroleum Engineers, 2011. https://doi.org/10.2118/142668-MS.
(223) Nasralla, R. A.; Mahani, H.; van der Linde, H. A.; Marcelis, F. H. M.; Masalmeh, S. K.; Sergienko, E.; Brussee, N. J.; Pieterse, S. G. J.; Basu, S. Low Salinity Waterflooding for a Carbonate Reservoir: Experimental Evaluation and Numerical Interpretation. *Journal of Petroleum Science and Engineering* **2018**, *164*, 640–654. https://doi.org/10.1016/j.petrol.2018.01.028.
(224) Yousef, A. A.; Al-Saleh, S. H.; Al-Kaabi, A.; Al-Jawfi, M. S. Laboratory Investigation of the Impact of Injection-Water Salinity and Ionic Content on Oil Recovery From Carbonate Reservoirs. *SPE Reservoir Evaluation & Engineering* **2011**, *14* (05), 578–593. https://doi.org/10.2118/137634-PA.
(225) Romanuka, J.; Hofman, J.; Ligthelm, D. J.; Suijkerbuijk, B.; Marcelis, F.; Oedai, S.; Brussee, N.; van der Linde, H.; Aksulu, H.; Austad, T. Low Salinity EOR in Carbonates. In *SPE Improved Oil Recovery Symposium*; Society of Petroleum Engineers: Tulsa, Oklahoma, USA, 2012. https://doi.org/10.2118/153869-MS.
(226) Kallesten, E. I.; Zimmermann, U.; Madland, M. V.; Bertolino, S.; Omdal, E.; Andersen, P. Ø. Mineralogy and Geochemistry of Reservoir and Non-Reservoir Chalk from the Norwegian Continental Shelf. *Journal of Petroleum Science and Engineering* **2021**, *205*, 108914. https://doi.org/10.1016/j.petrol.2021.108914.
(227) Bonto, M.; Eftekhari, A. A.; Nick, H. M. An Overview of the Oil-Brine Interfacial Behavior and a New Surface Complexation Model. *Scientific Reports* **2019**, *9* (1), 1–16. https://doi.org/10.1038/s41598-019-42505-2.
(228) Eftekhari, A. A.; Nick, H.; Bonto, M. An Overview of the Thermodynamic Models for the Chalk Surface Reactions with Brine; European Association of Geoscientists & Engineers, 2018; Vol. 2018, pp 1–5. https://doi.org/10.3997/2214-4609.201800760.
(229) Bonto; Eftekhari, A. A.; Nick, H. A Calibrated Model for the Carbonate-Brine-Crude Oil Surface Chemistry and Its Effect on the Rock Wettability, Dissolution, and Mechanical Properties. In *SPE Reservoir Simulation Conference*; Society of Petroleum Engineers: Galveston, Texas, USA, 2019. https://doi.org/10.2118/193865-MS.
(230) Yutkin, M. P.; Radke, C. J.; Patzek, T. W. Chemical Compositions in Salinity Waterflooding of Carbonate Reservoirs: Theory. *Transport in Porous Media* **2021**, *136*, 411–429. https://doi.org/10.1007/s11242-020-01517-7.
(231) Brady, P. V. Silica Surface Chemistry at Elevated Temperatures. *Geochimica et Cosmochimica Acta* **1992**, *56*, 2941–2946. https://doi.org/10.1016/0016-7037(92)90371-O.
(232) Johnson, B. B. Effect of PH, Temperature, and Concentration on the Adsorption of Cadmium on Goethite. *Environmental Science & Technology* **1990**, *24* (1), 112–118. https://doi.org/10.1021/es00071a014.
(233) Atkins, P.; de Paula, J. *Physical Chemistry*, 8th ed.; Oxford, 2006.
(234) Alotaibi, M. B.; Nasr-El-Din, H. A.; Fletcher, J. J. Electrokinetics of Limestone and Dolomite Rock Particles. *SPE Reservoir Evaluation & Engineering* **2011**, *14* (05), 594–603. https://doi.org/10.2118/148701-PA.
(235) Rodríguez, K.; Araujo, M. Temperature and Pressure Effects on Zeta Potential Values of Reservoir Minerals. *Journal of Colloid and Interface Science* **2006**, *300* (2), 788–794. https://doi.org/10.1016/j.jcis.2006.04.030.
(236) Bonto, M.; Eftekhari, A. A.; Nick, H. Analysis of the Temperature Impact on the Calcite Surface Reactivity in Modified Salinity Water Applications; European Association of Geoscientists & Engineers, 2021; Vol. 2021, pp 1–12. https://doi.org/10.3997/2214-4609.202133082.

(237) Morel, J.-P.; Marmier, N.; Hurel, C.; Morel-Desrosiers, N. Thermodynamics of Selenium Sorption on Alumina and Montmorillonite. *Cogent Chemistry* **2015**, *1* (1), 1070943. https://doi.org/10.1080/23312009.2015.1070943.
(238) Cobos, J. E.; Westh, P.; Søgaard, E. G. Isothermal Titration Calorimetry Study of Brine–Oil–Rock Interactions. *Energy Fuels* **2018**, *32* (7), 7338–7346. https://doi.org/10.1021/acs.energyfuels.8b00512.
(239) Cobos, J. E.; Søgaard, E. G. Effect of Individual Ions on Rock-Brine-Oil Interactions: A Microcalorimetric Approach. *Fuel* **2021**, *290*, 119955. https://doi.org/10.1016/j.fuel.2020.119955.
(240) Awolayo, A. N.; Sarma, H. K.; Nghiem, L. X. Numerical Modeling of Fluid-Rock Interactions During Low-Salinity-Brine-CO Flooding in Carbonate Reservoirs. In *SPE Reservoir Simulation Conference*; Society of Petroleum Engineers: Galveston, Texas, USA, 2019. https://doi.org/10.2118/193815-MS.
(241) Parkhurst, D. L.; Appelo, C. *Description of Input and Examples for PHREEQC Version 3—A Computer Program for Speciation, Batch-Reaction, One-Dimensional Transport, and Inverse Geochemical Calculations*; US Geol. Surv. Tech. Methods Book 6, 497, 2013.
(242) Vinogradov, J.; Jaafar, M. Z.; Jackson, M. D. Measurement of Streaming Potential Coupling Coefficient in Sandstones Saturated with Natural and Artificial Brines at High Salinity. *Journal of Geophysical Research: Solid Earth* **2010**, *115* (B12). https://doi.org/10.1029/2010JB007593.
(243) McCleskey, R. B. Electrical Conductivity of Electrolytes Found In Natural Waters from (5 to 90) °C. *J. Chem. Eng. Data* **2011**, *56* (2), 317–327. https://doi.org/10.1021/je101012n.
(244) Sen, P. N.; Goode, P. A. Influence of Temperature on Electrical Conductivity on Shaly Sands. *GEOPHYSICS* **1992**, *57* (1), 89–96. https://doi.org/10.1190/1.1443191.
(245) Kestin, J.; Sokolov, M.; Wakeham, W. A. Viscosity of Liquid Water in the Range −8 °C to 150 °C. *Journal of Physical and Chemical Reference Data* **1978**, *7* (3), 941–948. https://doi.org/10.1063/1.555581.
(246) Stogryn, A. Equations for Calculating the Dielectric Constant of Saline Water (Correspondence). *IEEE Transactions on Microwave Theory and Techniques* **1971**, *19* (8), 733–736. https://doi.org/10.1109/TMTT.1971.1127617.
(247) Machesky, M. L. Influence of Temperature on Ion Adsorption by Hydrous Metal Oxides. In *Chemical Modeling of Aqueous Systems II*; ACS Symposium Series; American Chemical Society, 1990; Vol. 416, pp 282–292. https://doi.org/10.1021/bk-1990-0416.ch022.
(248) Rodriguez-Santiago, V.; Fedkin, M. V.; Lvov, S. N. Protonation Enthalpies of Metal Oxides from High Temperature Electrophoresis. *Journal of Colloid and Interface Science* **2012**, *371* (1), 136–143. https://doi.org/10.1016/j.jcis.2012.01.002.
(249) Fokkink, L. G. J.; de Keizer, A.; Lyklema, J. Temperature Dependence of the Electrical Double Layer on Oxides: Rutile and Hematite. *Journal of Colloid and Interface Science* **1989**, *127* (1), 116–131. https://doi.org/10.1016/0021-9797(89)90012-X.
(250) Blesa, M. A.; Figliolia, N. M.; Maroto, A. J. G.; Regazzoni, A. E. The Influence of Temperature on the Interface Magnetite—Aqueous Electrolyte Solution. *Journal of Colloid and Interface Science* **1984**, *101* (2), 410–418. https://doi.org/10.1016/0021-9797(84)90052-3.
(251) Millero, F.; Huang, F.; Zhu, X.; Liu, X.; Zhang, J.-Z. Adsorption and Desorption of Phosphate on Calcite and Aragonite in Seawater. *Aquatic Geochemistry* **2001**, *7*, 33–56.
(252) Appel, C.; Rhue, D.; Kabengi, N.; Harris, W. Calorimetric Investigation of the Nature of Sulfate and Phosphate Sorption on Amorphous Aluminum Hydroxide. *Soil Science* **2013**, *178* (4), 180–188. https://doi.org/10.1097/SS.0b013e3182979e93.
(253) Silva, A. M.; Lima, R. M. F.; Leão, V. A. Mine Water Treatment with Limestone for Sulfate Removal. *Journal of Hazardous Materials* **2012**, *221–222*, 45–55. https://doi.org/10.1016/j.jhazmat.2012.03.066.
(254) Wynn, P. M.; Fairchild, I. J.; Borsato, A.; Spötl, C.; Hartland, A.; Baker, A.; Frisia, S.; Baldini, J. U. L. Sulphate Partitioning into Calcite: Experimental Verification of PH Control and Application to

Seasonality in Speleothems. *Geochimica et Cosmochimica Acta* **2018**, *226*, 69–83. https://doi.org/10.1016/j.gca.2018.01.020.
(255) Pingitore, N. E.; Meitzner, G.; Love, K. M. Identification of Sulfate in Natural Carbonates by X-Ray Absorption Spectroscopy. *Geochimica et Cosmochimica Acta* **1995**, *59* (12), 2477–2483. https://doi.org/10.1016/0016-7037(95)00142-5.
(256) Staudt, W. J.; Reeder, R. J.; Schoonen, M. A. A. Surface Structural Controls on Compositional Zoning of SO2−4 and SeO2−4 in Synthetic Calcite Single Crystals. *Geochimica et Cosmochimica Acta* **1994**, *58* (9), 2087–2098. https://doi.org/10.1016/0016-7037(94)90287-9.
(257) Johnson, P. R.; Sun, N.; Elimelech, M. Colloid Transport in Geochemically Heterogeneous Porous Media: Modeling and Measurements. *Environ. Sci. Technol.* **1996**, *30* (11), 3284–3293. https://doi.org/10.1021/es960053+.
(258) Song, Lianfa.; Johnson, P. R.; Elimelech, Menachem. Kinetics of Colloid Deposition onto Heterogeneously Charged Surfaces in Porous Media. *Environ. Sci. Technol.* **1994**, *28* (6), 1164–1171. https://doi.org/10.1021/es00055a030.
(259) Williams, D. J. A.; Williams, K. P. Electrophoresis and Zeta Potential of Kaolinite. *Journal of Colloid and Interface Science* **1978**, *65* (1), 79–87. https://doi.org/10.1016/0021-9797(78)90260-6.
(260) Feick, J. D.; Velegol, D. Electrophoresis of Spheroidal Particles Having a Random Distribution of Zeta Potential. *Langmuir* **2000**, *16* (26), 10315–10321. https://doi.org/10.1021/la001031a.
(261) Sachdeva, J. S.; Nermoen, A.; Korsnes, R. I.; Madland, M. V. Impact of Initial Wettability and Injection Brine Chemistry on Mechanical Behaviour of Kansas Chalk. *Transport in Porous Media* **2019**, *128* (2), 755–795. https://doi.org/10.1007/s11242-019-01269-z.
(262) Kallesten, E. I.; Cherif, Y.; Madland, M. V.; Korsnes, R. I.; Omdal, E.; Andersen, P. Ø.; Zimmermann, U. Validation Study of Water Weakening Research from Outcrop Chalks Performed on Eldfisk Reservoir Cores. *Journal of Petroleum Science and Engineering* **2021**, *198*, 108164. https://doi.org/10.1016/j.petrol.2020.108164.
(263) Prelot, B.; Lantenois, S.; Charbonnel, M.-C.; Marchandeau, F.; Douillard, J. M.; Zajac, J. What Are the Main Contributions to the Total Enthalpy of Displacement Accompanying the Adsorption of Some Multivalent Metals at the Silica–Electrolyte Interface? *Journal of Colloid and Interface Science* **2013**, *396*, 205–209. https://doi.org/10.1016/j.jcis.2012.12.049.
(264) Jurinak, J. J.; Bauer, N. Thermodynamics of Zinc Adsorption on Calcite, Dolomite and Magnesite-Type Minerals. *Soil Science Society of America Journal* **1956**, *20* (4), 466–471. https://doi.org/10.2136/sssaj1956.03615995002000040006x.
(265) Marcus, Y. Ionic Radii in Aqueous Solutions. *Chemical Reviews* **1988**, *88* (8), 1475–1498. https://doi.org/10.1021/cr00090a003.
(266) Marcus, Y. *Ions in Solution and Their Solvation*; John Wiley&Sons, 2015.
(267) Allen, N.; Dai, C.; Hu, Y.; Kubicki, J. D.; Kabengi, N. Adsorption Study of Al3+, Cr3+, and Mn2+ onto Quartz and Corundum Using Flow Microcalorimetry, Quartz Crystal Microbalance, and Density Functional Theory. *ACS Earth Space Chem.* **2019**, *3* (3), 432–441. https://doi.org/10.1021/acsearthspacechem.8b00148.
(268) Allen, N.; Machesky, M. L.; Wesolowski, D. J.; Kabengi, N. Calorimetric Study of Alkali and Alkaline-Earth Cation Adsorption and Exchange at the Quartz-Solution Interface. *Journal of Colloid and Interface Science* **2017**, *504*, 538–548. https://doi.org/10.1016/j.jcis.2017.06.005.
(269) Lantenois, S.; Prélot, B.; Douillard, J.-M.; Szczodrowski, K.; Charbonnel, M.-C. Flow Microcalorimetry: Experimental Development and Application to Adsorption of Heavy Metal Cations on Silica. *Applied Surface Science* **2007**, *253* (13), 5807–5813. https://doi.org/10.1016/j.apsusc.2006.12.064.
(270) Forbes, T. Z.; Radha, A. V.; Navrotsky, A. The Energetics of Nanophase Calcite. *Geochimica et Cosmochimica Acta* **2011**, *75* (24), 7893–7905. https://doi.org/10.1016/j.gca.2011.09.034.
(271) Srinivasan, S. G.; Shivaramaiah, R.; Kent, P. R. C.; Stack, A. G.; Riman, R.; Anderko, A.; Navrotsky, A.; Bryantsev, V. S. A Comparative Study of Surface Energies and Water Adsorption on Ce-Bastnäsite, La-Bastnäsite, and Calcite via Density Functional Theory and Water Adsorption

Calorimetry. *Phys. Chem. Chem. Phys.* **2017**, *19* (11), 7820–7832. https://doi.org/10.1039/C7CP00811B.
(272) Garcia-Olvera, G.; Reilly, T. M.; Lehmann, T. E.; Alvarado, V. Effects of Asphaltenes and Organic Acids on Crude Oil-Brine Interfacial Visco-Elasticity and Oil Recovery in Low-Salinity Waterflooding. *Fuel* **2016**, *185*, 151–163. https://doi.org/10.1016/j.fuel.2016.07.104.
(273) Zahid, A.; Sandersen, S. B.; Stenby, E. H.; von Solms, N.; Shapiro, A. Advanced Waterflooding in Chalk Reservoirs: Understanding of Underlying Mechanisms. *Colloids and Surfaces A: Physicochemical and Engineering Aspects* **2011**, *389* (1–3), 281–290. https://doi.org/10.1016/j.colsurfa.2011.08.009.
(274) Alvarado, V.; Moradi Bidhendi, M.; Garcia-Olvera, G.; Morin, B.; Oakey, J. S. Interfacial Visco-Elasticity of Crude Oil - Brine: An Alternative EOR Mechanism in Smart Waterflooding; Society of Petroleum Engineers, 2014. https://doi.org/10.2118/169127-MS.
(275) Jackson, M. D.; Al-Mahrouqi, D.; Vinogradov, J. Zeta Potential in Oil-Water-Carbonate Systems and Its Impact on Oil Recovery during Controlled Salinity Water-Flooding. *Scientific Reports* **2016**, *6*, 37363. https://doi.org/10.1038/srep37363.
(276) Chávez-Miyauchi, T. E.; Firoozabadi, A.; Fuller, G. G. Nonmonotonic Elasticity of the Crude Oil–Brine Interface in Relation to Improved Oil Recovery. *Langmuir* **2016**, *32* (9), 2192–2198. https://doi.org/10.1021/acs.langmuir.5b04354.
(277) Myint, P. C.; Firoozabadi, A. Thin Liquid Films in Improved Oil Recovery from Low-Salinity Brine. *Current Opinion in Colloid & Interface Science* **2015**, *20* (2), 105–114. https://doi.org/10.1016/j.cocis.2015.03.002.
(278) Okasha, T. M.; Alshiwaish, A. Effect of Brine Salinity on Interfacial Tension in Arab-D Carbonate Reservoir, Saudi Arabia. In *SPE Middle East Oil and Gas Show and Conference*; Society of Petroleum Engineers: Manama, Bahrain, 2009. https://doi.org/10.2118/119600-MS.
(279) Chakravarty, K. H.; Fosbøl, P. L.; Thomsen, K. Brine Crude Oil Interactions at the Oil-Water Interface. *Proceedings of the SPE Asia Pacific Enhanced Oil Recovery Conference* **2015**, 817–836. https://doi.org/10.2118/174685-MS.
(280) Buckley, J. S.; Liu, Y. Some Mechanisms of Crude Oil/Brine/Solid Interactions. *Journal of Petroleum Science and Engineering* **1998**, *20*, 155–160.
(281) Abitbol, T.; Kam, D.; Levi-Kalisman, Y.; Gray, D. G.; Shoseyov, O. Surface Charge Influence on the Phase Separation and Viscosity of Cellulose Nanocrystals. *Langmuir* **2018**, *34* (13), 3925–3933. https://doi.org/10.1021/acs.langmuir.7b04127.
(282) Zhao, L. H.; Hu, J. R.; He, B. H. Effect of Electrical Characteristics Modification on Viscosity of Kaolin Suspension. *Advanced Materials Research* **2011**, *335–336*, 1262–1266. https://doi.org/10.4028/www.scientific.net/AMR.335-336.1262.
(283) Kontogeorgis, G. M.; Kiil, S. *Introduction to Applied Colloid and Surface Chemistry*, First.; Wiley, 2016.
(284) Sari, A.; Xie, Q.; Chen, Y.; Saeedi, A.; Pooryousefy, E. Drivers of Low Salinity Effect in Carbonate Reservoirs. *Energy & Fuels* **2017**, *31* (9), 8951–8958. https://doi.org/10.1021/acs.energyfuels.7b00966.
(285) Xie, Q.; Liu, Y.; Wu, J.; Liu, Q. Ions Tuning Water Flooding Experiments and Interpretation by Thermodynamics of Wettability. *Journal of Petroleum Science and Engineering* **2014**, *124*, 350–358. https://doi.org/10.1016/j.petrol.2014.07.015.
(286) Moradi, M.; Topchiy, E.; Lehmann, T. E.; Alvarado, V. Impact of Ionic Strength on Partitioning of Naphthenic Acids in Water–Crude Oil Systems – Determination through High-Field NMR Spectroscopy. *Fuel* **2013**, *112*, 236–248. https://doi.org/10.1016/j.fuel.2013.05.024.
(287) Ayirala, S. C.; Yousef, A. A.; Li, Z.; Xu, Z. Coalescence of Crude Oil Droplets in Brine Systems: Effect of Individual Electrolytes. *Energy & Fuels* **2018**, *32* (5), 5763–5771. https://doi.org/10.1021/acs.energyfuels.8b00309.
(288) Mohammad Salehi, M.; Omidvar, P.; Naeimi, F. Salinity of Injection Water and Its Impact on Oil Recovery Absolute Permeability, Residual Oil Saturation, Interfacial Tension and Capillary

Pressure. *Egyptian Journal of Petroleum* **2017**, *26* (2), 301–312. https://doi.org/10.1016/j.ejpe.2016.05.003.
(289) Lashkarbolooki, M.; Ayatollahi, S. Effects of Asphaltene, Resin and Crude Oil Type on the Interfacial Tension of Crude Oil/Brine Solution. *Fuel* **2018**, *223*, 261–267. https://doi.org/10.1016/j.fuel.2018.03.029.
(290) Gachuz-Muro, H.; Sohrabi, M. Effects of Brine on Crude Oil Viscosity at Different Temperature and Brine Composition - Heavy Oil/Water Interaction. In *EAGE Annual Conference & Exhibition incorporating SPE Europec*; Society of Petroleum Engineers: London, UK, 2013. https://doi.org/10.2118/164910-MS.
(291) Perles, C. E.; Guersoni, V. C. B.; Bannwart, A. C. Rheological Study of Crude Oil/Water Interface – The Effect of Temperature and Brine on Interfacial Film. *Journal of Petroleum Science and Engineering* **2018**, *162*, 835–843. https://doi.org/10.1016/j.petrol.2017.11.010.
(292) Perles, C. E.; Volpe, P. L. O.; Bombard, A. J. F. Study of the Cation and Salinity Effect on Electrocoalescence of Water/Crude Oil Emulsions. *Energy & Fuels* **2012**, *26* (11), 6914–6924. https://doi.org/10.1021/ef301433m.
(293) Takamura, K.; Chow, R. S. The Electric Properties of the Bitumen/Water Interface Part II. Application of the Ionizable Surface-Group Model. *Colloids and Surfaces* **1985**, *15*, 35–48. https://doi.org/10.1016/0166-6622(85)80053-6.
(294) Chow, R. S.; Takamura, K. Electrophoretic Mobilities of Bitumen and Conventional Crude-in-Water Emulsions Using the Laser Doppler Apparatus in the Presence of Multivalent Cations. *Journal of Colloid and Interface Science* **1988**, *125* (1), 212–225. https://doi.org/10.1016/0021-9797(88)90070-7.
(295) Das, S.; Thundat, T.; Mitra, S. K. Analytical Model for Zeta Potential of Asphaltene. *Fuel* **2013**, *108*, 543–549. https://doi.org/10.1016/j.fuel.2013.01.002.
(296) Szymula, M.; Janusz, W.; Jabloriski, J. Electrochemical Properties of Asphaltene Particles in Aqueous Solutions. *Journal of Dispersion Science and Technology* **2000**, *21* (6), 785–802. https://doi.org/10.1080/01932690008913308.
(297) Chen, Y.; Xie, Q.; Sari, A.; Brady, P. V.; Saeedi, A. Oil/Water/Rock Wettability: Influencing Factors and Implications for Low Salinity Water Flooding in Carbonate Reservoirs. *Fuel* **2018**, *215*, 171–177. https://doi.org/10.1016/j.fuel.2017.10.031.
(298) Xie, Q.; Sari, A.; Pu, W.; Chen, Y.; Brady, P. V.; Al Maskari, N.; Saeedi, A. PH Effect on Wettability of Oil/Brine/Carbonate System: Implications for Low Salinity Water Flooding. *Journal of Petroleum Science and Engineering* **2018**, *168*, 419–425. https://doi.org/10.1016/j.petrol.2018.05.015.
(299) Brady, P. V.; Krumhansl, J. L. A Surface Complexation Model of Oil–Brine–Sandstone Interfaces at 100°C: Low Salinity Waterflooding. *Journal of Petroleum Science and Engineering* **2012**, *81*, 171–176. https://doi.org/10.1016/j.petrol.2011.12.020.
(300) Creux, P.; Lachaise, J.; Graciaa, A.; Beattie, J. K.; Djerdjev, A. M. Strong Specific Hydroxide Ion Binding at the Pristine Oil/Water and Air/Water Interfaces. *J. Phys. Chem. B* **2009**, *113* (43), 14146–14150. https://doi.org/10.1021/jp906978v.
(301) Marinova, K. G.; Alargova, R. G.; Denkov, N. D.; Velev, O. D.; Petsev, D. N.; Ivanov, I. B.; Borwankar, R. P. Charging of Oil−Water Interfaces Due to Spontaneous Adsorption of Hydroxyl Ions. *Langmuir* **1996**, *12* (8), 2045–2051. https://doi.org/10.1021/la950928i.
(302) Stachurski, J.; MichaŁek, M. The Effect of the ζ Potential on the Stability of a Non-Polar Oil-in-Water Emulsion. *Journal of Colloid and Interface Science* **1996**, *184* (2), 433–436. https://doi.org/10.1006/jcis.1996.0637.
(303) Dunstan, D. E.; Saville, D. A. Electrophoretic Mobility of Colloidal Alkane Particles in Electrolyte Solutions. *J. Chem. Soc., Faraday Trans.* **1992**, *88* (14), 2031–2033. https://doi.org/10.1039/FT9928802031.
(304) Kallay, N.; Kovačević, D.; Žalac, S. Chapter 6 - Thermodynamics of the Solid/Liquid Interface - Its Application to Adsorption and Colloid Stability. In *Interface Science and Technology*;

Lützenkirchen, J., Ed.; Surface Complexation Modelling; Elsevier, 2006; Vol. 11, pp 133–170. https://doi.org/10.1016/S1573-4285(06)80050-5.
(305) *Interfacial Electrokinetics and Electrophoresis*; Delgado, A. V., Ed.; CRC Press: Boca Raton, 2014. https://doi.org/10.1201/9781482294668.
(306) Wang, M.; Revil, A. Electrochemical Charge of Silica Surfaces at High Ionic Strength in Narrow Channels. *Journal of Colloid and Interface Science* **2010**, *343* (1), 381–386. https://doi.org/10.1016/j.jcis.2009.11.039.
(307) Mugele, F.; Bera, B.; Cavalli, A.; Siretanu, I.; Maestro, A.; Duits, M.; Cohen-Stuart, M.; van den Ende, D.; Stocker, I.; Collins, I. Ion Adsorption-Induced Wetting Transition in Oil-Water-Mineral Systems. *Sci Rep* **2015**, *5* (1), 10519. https://doi.org/10.1038/srep10519.
(308) Borkovec, M.; Westall, J. Solution of the Poisson-Boltzmann Equation for Surface Excesses of Ions in the Diffuse Layer at the Oxide-Electrolyte Interface. *Journal of Electroanalytical Chemistry and Interfacial Electrochemistry* **1983**, *150* (1), 325–337. https://doi.org/10.1016/S0022-0728(83)80214-9.
(309) Parkhurst, D. L.; Appelo, C. A. J. *User's Guide to PHREEQC (Version 2): A Computer Program for Speciation, Batch-Reaction, One-Dimensional Transport, and Inverse Geochemical Calculations*; 99–4259; USGS, 1999. https://doi.org/10.3133/wri994259.
(310) Attard, P.; Antelmi, D.; Larson, I. Comparison of the Zeta Potential with the Diffuse Layer Potential from Charge Titration. *Langmuir* **2000**, *16* (4), 1542–1552. https://doi.org/10.1021/la990487t.
(311) Andelman, D. Electrostatic Properties of Membranes: The Poisson-Boltzmann Theory. In *Handbook of Biological Physics*; Elsevier, 1995; Vol. 1, pp 603–642. https://doi.org/10.1016/S1383-8121(06)80005-9.
(312) Cavalli, A.; Bera, B.; van den Ende, D.; Mugele, F. Analytic Model for the Electrowetting Properties of Oil-Water-Solid Systems. *Phys. Rev. E* **2016**, *93* (4), 042606. https://doi.org/10.1103/PhysRevE.93.042606.
(313) Wang, M.; Chen, Shiyi. On Applicability of Poisson-Boltzmann Equation for Micro- and Nanoscale Electroosmotic Flows. *Communications in Computational Physics* **2008**, *3* (5), 1087–1099.
(314) Ikeda, S. The Gibbs Adsorption Isotherm for Aqueous Electrolyte Solutions. *Advances in Colloid and Interface Science* **1982**, *18* (1–2), 93–130. https://doi.org/10.1016/0001-8686(82)85032-X.
(315) Farooq, U.; Simon, S.; Tweheyo, M. T.; Sjöblom, J.; Øye, G. Electrophoretic Measurements of Crude Oil Fractions Dispersed in Aqueous Solutions of Different Ionic Compositions—Evaluation of the Interfacial Charging Mechanisms. *Journal of Dispersion Science and Technology* **2013**, *34* (10), 1376–1381. https://doi.org/10.1080/01932691.2012.747739.
(316) Sheng, J. J. Investigation of Alkaline–Crude Oil Reaction. *Petroleum* **2015**, *1* (1), 31–39. https://doi.org/10.1016/j.petlm.2015.04.004.
(317) Kokal, S.; Tang, T.; Schramm, L.; Sayegh, S. Electrokinetic and Adsorption Properties of Asphaltenes. *Colloids and Surfaces A: Physicochemical and Engineering Aspects* **1995**, *94* (2), 253–265. https://doi.org/10.1016/0927-7757(94)03007-3.
(318) Chaverot, P. Interfacial Tension of Bitumen-Water Interfaces. Part 1: Influence of Endogenous Surfactants at Acidic PH. *Energy and Fuels* **2008**, *22* (2), 790–798. https://doi.org/10.1021/ef7004892.
(319) Dubey, S. T.; Doe, P. H. Base Number and Wetting Properties of Crude Oils. *SPE Reservoir Engineering* **1993**, *8* (03), 195–200. https://doi.org/10.2118/22598-PA.
(320) Andersson, M. P.; Olsson, M. H. M.; Stipp, S. L. S. Predicting the PKa and Stability of Organic Acids and Bases at an Oil–Water Interface. *Langmuir* **2014**, *30* (22), 6437–6445. https://doi.org/10.1021/la5008318.
(321) Bertheussen, A.; Simon, S.; Sjöblom, J. Equilibrium Partitioning of Naphthenic Acids and Bases and Their Consequences on Interfacial Properties. *Colloids and Surfaces A: Physicochemical and Engineering Aspects* **2017**, *529*, 45–56. https://doi.org/10.1016/j.colsurfa.2017.05.068.
(322) Andersen, S. I.; Chandra, M. S.; Chen, J.; Zeng, B. Y.; Zou, F.; Mapolelo, M.; Abdallah, W.; Buiting, J. J. Detection and Impact of Carboxylic Acids at the Crude Oil–Water Interface. *Energy Fuels* **2016**, *30* (6), 4475–4485. https://doi.org/10.1021/acs.energyfuels.5b02930.

(323) Guo, J. X. The Effect of Alkali on Crude Oil/Water Interfacial Properties and the Stability of Crude Oil Emulsions. *Colloids and Surfaces A-physicochemical and Engineering Aspects* **2006**, *273* (1–3), 213–218. https://doi.org/10.1016/j.colsurfa.2005.10.015.
(324) Rønningsen, H. P. Water-in-Crude Oil Emulsions from the Norwegian Continental Shelf 11. Ageing of Crude Oils and Its Influence on the Emulsion Stability. *Colloids and Surfaces A: Physicochemical and Engineering Aspects* **1995**, *97* (2), 119–128. https://doi.org/10.1016/0927-7757(94)03039-3.
(325) Havre, T. E.; Sjöblom, J.; Vindstad, J. E. Oil/Water-Partitioning and Interfacial Behavior of Naphthenic Acids. *Journal of Dispersion Science and Technology* **2003**, *24* (6), 789–801. https://doi.org/10.1081/DIS-120025547.
(326) Nenningsland, A. L.; Simon, S.; Sjöblom, J. Surface Properties of Basic Components Extracted from Petroleum Crude Oil. *Energy Fuels* **2010**, *24* (12), 6501–6505. https://doi.org/10.1021/ef101094p.
(327) Varadaraj, R.; Brons, C. Molecular Origins of Crude Oil Interfacial Activity. Part 4: Oil–Water Interface Elasticity and Crude Oil Asphaltene Films. *Energy Fuels* **2012**, *26* (12), 7164–7169. https://doi.org/10.1021/ef300830f.
(328) Saliu, F.; Della Pergola, R. Organic Bases, Carbon Dioxide and Naphthenic Acids Interactions. Effect on the Stability of Petroleum Crude Oil in Water Emulsions. *Journal of Petroleum Science and Engineering* **2018**, *163*, 177–184. https://doi.org/10.1016/j.petrol.2017.12.094.
(329) Hutin, A.; Argillier, J.-F.; Langevin, D. Mass Transfer between Crude Oil and Water. Part 1: Effect of Oil Components. *Energy Fuels* **2014**, *28* (12), 7331–7336. https://doi.org/10.1021/ef501751b.
(330) Hutin, A.; Argillier, J.-F.; Langevin, D. Mass Transfer between Crude Oil and Water. Part 2: Effect of Sodium Dodecyl Benzenesulfonate for Enhanced Oil Recovery. *Energy Fuels* **2014**, *28* (12), 7337–7342. https://doi.org/10.1021/ef5017522.
(331) Czarnecki, J. Stabilization of Water in Crude Oil Emulsions. Part 2. *Energy Fuels* **2009**, *23* (3), 1253–1257. https://doi.org/10.1021/ef800607u.
(332) Yang, F.; Tchoukov, P.; Pensini, E.; Dabros, T.; Czarnecki, J.; Masliyah, J.; Xu, Z. Asphaltene Subfractions Responsible for Stabilizing Water-in-Crude Oil Emulsions. Part 1: Interfacial Behaviors. *Energy Fuels* **2014**, *28* (11), 6897–6904. https://doi.org/10.1021/ef501826g.
(333) Yang, F.; Tchoukov, P.; Dettman, H.; Teklebrhan, R. B.; Liu, L.; Dabros, T.; Czarnecki, J.; Masliyah, J.; Xu, Z. Asphaltene Subfractions Responsible for Stabilizing Water-in-Crude Oil Emulsions. Part 2: Molecular Representations and Molecular Dynamics Simulations. *Energy Fuels* **2015**, *29* (8), 4783–4794. https://doi.org/10.1021/acs.energyfuels.5b00657.
(334) Kolltveit, Y. Relationship Between Crude Oil Composition and Physical-Chemical Properties., University of Bergen, Bergen, 2016.
(335) Nasralla, R. A.; Nasr-El-Din, H. A. Impact of Cation Type and Concentration in Injected Brine on Oil Recovery in Sandstone Reservoirs. *Journal of Petroleum Science and Engineering* **2014**, *122*, 384–395. https://doi.org/10.1016/j.petrol.2014.07.038.
(336) Takeya, M.; Shimokawara, Mai; Elakneswaran, Yogarah; Nawa, Toyoharu; Takahashi, Satoru. Predicting the Electrokinetic Properties of the Crude Oil/Brine Interface for Enhanced Oil Recovery in Low Salinity Water Flooding. *Fuel* **2019**, *235*, 822–831. https://doi.org/10.1016/j.fuel.2018.08.079.
(337) Bezanson, J.; Edelman, A.; Karpinski, S.; Shah, V. B. Julia: A Fresh Approach to Numerical Computing. *SIAM Review* **2017**, *59* (1), 65–98. https://doi.org/10.1137/141000671.
(338) Levenberg, K. A Method for the Solution of Certain Non-Linear Problems in Least Squares. *Quart. Appl. Math.* **1944**, *2* (2), 164–168. https://doi.org/10.1090/qam/10666.
(339) Marquardt, D. An Algorithm for Least-Squares Estimation of Nonlinear Parameters. *Journal of the Society for Industrial and Applied Mathematics* **1963**, *11* (2), 431–441. https://doi.org/10.1137/0111030.
(340) Hajari, T.; Ganguly, P.; van der Vegt, N. F. A. Enthalpy–Entropy of Cation Association with the Acetate Anion in Water. *J. Chem. Theory Comput.* **2012**, *8* (10), 3804–3809. https://doi.org/10.1021/ct300074d.

(341) Park, S. H.; Nap, R. J.; Szleifer, I. Association Free Energies of Metal Cations with Mesylate and Acetate in Brine Calculated via Molecular Dynamics Simulation. *arXiv:1801.05888 [physics]* **2018**.
(342) Nasralla, R. A.; Nasr-El-Din, H. A. Double-Layer Expansion: Is It a Primary Mechanism of Improved Oil Recovery by Low-Salinity Waterflooding? *SPE Reservoir Evaluation & Engineering* **2014**, *17* (01), 49–59. https://doi.org/10.2118/154334-PA.
(343) Pouryousefy, E.; Xie, Q.; Saeedi, A. Effect of Multi-Component Ions Exchange on Low Salinity EOR: Coupled Geochemical Simulation Study. *Petroleum* **2016**, *2* (3), 215–224. https://doi.org/10.1016/j.petlm.2016.05.004.
(344) Awolayo, A. N.; Sarma, H. K.; Nghiem, L. X. Brine-Dependent Recovery Processes in Carbonate and Sandstone Petroleum Reservoirs: Review of Laboratory-Field Studies, Interfacial Mechanisms and Modeling Attempts. *Energies* **2018**, *11* (11), 3020. https://doi.org/10.3390/en11113020.
(345) Derkani, M. H.; Fletcher, A. J.; Abdallah, W.; Sauerer, B.; Anderson, J.; Zhang, Z. J. Low Salinity Waterflooding in Carbonate Reservoirs: Review of Interfacial Mechanisms Colloids and Interfaces https://www.mdpi.com/2504-5377/2/2/20/htm (accessed 2019 -01 -01).
(346) Sohal, M. A.; Thyne, G.; Søgaard, E. G. Review of Recovery Mechanisms of Ionically Modified Waterflood in Carbonate Reservoirs. *Energy & Fuels* **2016**, *30* (3), 1904–1914. https://doi.org/10.1021/acs.energyfuels.5b02749.
(347) Strand, S.; Henningsen, S. C.; Puntervold, T.; Austad, T. Favorable Temperature Gradient for Maximum Low-Salinity Enhanced Oil Recovery Effects in Carbonates. *Energy & Fuels* **2017**, *31* (5), 4687–4693. https://doi.org/10.1021/acs.energyfuels.6b03019.
(348) Puntervold, T.; Strand, S.; Austad, T. Water Flooding of Carbonate Reservoirs: Effects of a Model Base and Natural Crude Oil Bases on Chalk Wettability. *Energy Fuels* **2007**, *21* (3), 1606–1616. https://doi.org/10.1021/ef060624b.
(349) Puntervold, T.; Strand, S.; Ellouz, R.; Austad, T. Modified Seawater as a Smart EOR Fluid in Chalk. *Journal of Petroleum Science and Engineering* **2015**, *133*, 440–443. https://doi.org/10.1016/j.petrol.2015.06.034.
(350) Yu, L.; Evje, S.; Skjaeveland, S.; Kaarstad, T.; Kleppe, H.; Yu, L. Modelling of Wettability Alteration Processes in Carbonate Oil Reservoirs. *Networks and Heterogeneous Media* **2008**, *3* (1), 149–183. https://doi.org/10.3934/nhm.2008.3.149.
(351) Evje, S.; Hiorth, A. A Mathematical Model for Dynamic Wettability Alteration Controlled by Water-Rock Chemistry. *Networks and Heterogeneous Media* **2010**, *5* (2), 217–256. https://doi.org/10.3934/nhm.2010.5.217.
(352) Andersen, P. Ø.; Evje, S. A Mathematical Model for Interpretation of Brine-Dependent Spontaneous Imbibition Experiments; 2012. https://doi.org/10.3997/2214-4609.20143217.
(353) Anderson, W. G. Wettability Literature Survey- Part 1: Rock/Oil/Brine Interactions and the Effects of Core Handling on Wettability. *Journal of Petroleum Technology* **1986**, *38* (10), 1,125-1,144. https://doi.org/10.2118/13932-PA.
(354) Amott, E. Observations Relating to the Wettability of Porous Rock. **1959**.
(355) Donaldson, E. C.; Thomas, R. D.; Lorenz, P. B. Wettability Determination and Its Effect on Recovery Efficiency. *Society of Petroleum Engineers Journal* **1969**, *9* (01), 13–20. https://doi.org/10.2118/2338-PA.
(356) Abdallah, W.; Gmira, A. Wettability Assessment and Surface Compositional Analysis of Aged Calcite Treated with Dynamic Water. *Energy Fuels* **2014**, *28* (3), 1652–1663. https://doi.org/10.1021/ef401908w.
(357) Sari, A.; Chen, Y.; Xie, Q.; Saeedi, A. Low Salinity Water Flooding in High Acidic Oil Reservoirs: Impact of PH on Wettability of Carbonate Reservoirs. *Journal of Molecular Liquids* **2019**, *281*, 444–450. https://doi.org/10.1016/j.molliq.2019.02.081.

(358) Tetteh, J. T.; Alimoradi, S.; Brady, P. V.; Barati Ghahfarokhi, R. Electrokinetics at Calcite-Rich Limestone Surface: Understanding the Role of Ions in Modified Salinity Waterflooding. *Journal of Molecular Liquids* **2019**, 111868. https://doi.org/10.1016/j.molliq.2019.111868.
(359) Karoussi, O.; Hamouda, A. A. Imbibition of Sulfate and Magnesium Ions into Carbonate Rocks at Elevated Temperatures and Their Influence on Wettability Alteration and Oil Recovery. *Energy Fuels* **2007**, *21* (4), 2138–2146. https://doi.org/10.1021/ef0605246.
(360) Morrow, N. R. Wettability and Its Effect on Oil Recovery. *Journal of Petroleum Technology* **1990**, *42* (12), 1,476-1,484. https://doi.org/10.2118/21621-PA.
(361) Morrow, N. R.; Mason, G. Recovery of Oil by Spontaneous Imbibition. *Current Opinion in Colloid & Interface Science* **2001**, *6* (4), 321–337. https://doi.org/10.1016/S1359-0294(01)00100-5.
(362) Rabbani, H. S.; Zhao, B.; Juanes, R.; Shokri, N. Pore Geometry Control of Apparent Wetting in Porous Media. *Sci Rep* **2018**, *8*. https://doi.org/10.1038/s41598-018-34146-8.
(363) Anderson, W. Wettability Literature Survey- Part 2: Wettability Measurement. *Journal of Petroleum Technology* **1986**, *38* (11), 1,246-1,262. https://doi.org/10.2118/13933-PA.
(364) Zhou, X.; Morrow, N. R.; Ma, S. Interrelationship of Wettability, Initial Water Saturation, Aging Time, and Oil Recovery by Spontaneous Imbibition and Waterflooding. *SPE Journal* **2000**, *5* (02), 199–207. https://doi.org/10.2118/62507-PA.
(365) Graue, A.; Viksund, B. G.; Eilertsen, T.; Moe, R. Systematic Wettability Alteration by Aging Sandstone and Carbonate Rock in Crude Oil. *Journal of Petroleum Science and Engineering* **1999**, *24* (2), 85–97. https://doi.org/10.1016/S0920-4105(99)00033-9.
(366) Ma, S. M.; Zhang, X.; Morrow, N. R.; Zhou, X. CHARACTERIZATION OF WETTABILITY FROM SPONTANEOUS IMBIBITION MEASUREMENTS. *Journal of Canadian Petroleum Technology* **1999**, *38* (13), 8.
(367) Morrow, N. R.; Xie, X. Oil Recovery By Spontaneous Imbibition From Weakly Water-Wet Rocks. *Petrophysics* **2001**, *42* (04).
(368) Fernø, M. A.; Torsvik, M.; Haugland, S.; Graue, A. Dynamic Laboratory Wettability Alteration. *Energy Fuels* **2010**, *24* (7), 3950–3958. https://doi.org/10.1021/ef1001716.
(369) Morrow, N. R.; Ma, S.; Zhou, X.; Zhang, X. Characterization of Wettability From Spontaneous Imbibition Measurements; Petroleum Society of Canada, 1994. https://doi.org/10.2118/94-47.
(370) Anderson, W. G. Wettability Literature Survey- Part 4: Effects of Wettability on Capillary Pressure. *Journal of Petroleum Technology* **1987**, *39* (10), 1,283-1,300. https://doi.org/10.2118/15271-PA.
(371) Anderson, W. G. Wettability Literature Survey-Part 6: The Effects of Wettability on Waterflooding. *Journal of Petroleum Technology* **1987**, *39* (12), 1,605-1,622. https://doi.org/10.2118/16471-PA.
(372) Mungan, N. Certain Wettability Effects In Laboratory Waterfloods. *Journal of Petroleum Technology* **1966**, *18* (02), 247–252. https://doi.org/10.2118/1203-PA.
(373) Jia, D.; Buckley, J. S.; Morrow, N. R. Control of Core Wettability With Crude Oil; Society of Petroleum Engineers, 1991. https://doi.org/10.2118/21041-MS.
(374) Puntervold, T.; Strand, S.; Austad, T. New Method To Prepare Outcrop Chalk Cores for Wettability and Oil Recovery Studies at Low Initial Water Saturation. *Energy Fuels* **2007**, *21* (6), 3425–3430. https://doi.org/10.1021/ef700323c.
(375) Fathi, S. J.; Austad, T.; Strand, S. Water-Based Enhanced Oil Recovery (EOR) by "Smart Water": Optimal Ionic Composition for EOR in Carbonates. *Energy Fuels* **2011**, *25* (11), 5173–5179. https://doi.org/10.1021/ef201019k.
(376) Zhang, P.; Austad, T. The Relative Effects of Acid Number and Temperature on Chalk Wettability; Society of Petroleum Engineers, 2005. https://doi.org/10.2118/92999-MS.
(377) Tweheyo, M. T.; Zhang, P.; Austad, T. The Effects of Temperature and Potential Determining Ions Present in Seawater on Oil Recovery From Fractured Carbonates. *SPE Symposium on Improved Oil Recovery held in Tulsa, Oklahoma, USA, 22-26 April 2006* **2006**, *99438*, 10.

(378) Fernø, M. A.; Grønsdal, R.; Åsheim, J.; Nyheim, A.; Berge, M.; Graue, A. Use of Sulfate for Water Based Enhanced Oil Recovery during Spontaneous Imbibition in Chalk. *Energy & Fuels* **2011**, *25* (4), 1697–1706. https://doi.org/10.1021/ef200136w.
(379) Hognesen, E. J.; Strand, S.; Austad, T. Waterflooding of Preferential Oil-Wet Carbonates: Oil Recovery Related to Reservoir Temperature and Brine Composition; Society of Petroleum Engineers, 2005. https://doi.org/10.2118/94166-MS.
(380) Al Harrasi, A.; Al-maamari, R. S.; Masalmeh, S. K. Laboratory Investigation of Low Salinity Waterflooding for Carbonate Reservoirs; Society of Petroleum Engineers, 2012. https://doi.org/10.2118/161468-MS.
(381) Mohanty, K. K.; Chandrasekhar, S. Wettability Alteration with Brine Composition in High Temperature Carbonate Reservoirs; Society of Petroleum Engineers, 2013. https://doi.org/10.2118/166280-MS.
(382) Karimi, M.; Al-Maamari, R. S.; Ayatollahi, S.; Mehranbod, N. Wettability Alteration and Oil Recovery by Spontaneous Imbibition of Low Salinity Brine into Carbonates: Impact of Mg2+, SO42− and Cationic Surfactant. *Journal of Petroleum Science and Engineering* **2016**, *147*, 560–569. https://doi.org/10.1016/j.petrol.2016.09.015.
(383) Bartels, W.-B.; Mahani, H.; Berg, S.; Hassanizadeh, S. M. Literature Review of Low Salinity Waterflooding from a Length and Time Scale Perspective. *Fuel* **2019**, *236*, 338–353. https://doi.org/10.1016/j.fuel.2018.09.018.
(384) Sorop, T. G.; Masalmeh, S. K.; Suijkerbuijk, B. M. J. M.; van der Linde, H. A.; Mahani, H.; Brussee, N. J.; Marcelis, F. A. H. M.; Coorn, A. Relative Permeability Measurements to Quantify the Low Salinity Flooding Effect at Field Scale; Society of Petroleum Engineers, 2015. https://doi.org/10.2118/177856-MS.
(385) Lin, Q.; Bijeljic, B.; Berg, S.; Pini, R.; Blunt, M. J.; Krevor, S. Minimal Surfaces in Porous Media: Pore-Scale Imaging of Multiphase Flow in an Altered-Wettability Bentheimer Sandstone. *Physical Review E* **2019**, *99* (6). https://doi.org/10.1103/PhysRevE.99.063105.
(386) Sohal, M. A.; Thyne, G.; Søgaard, E. G. Novel Application of the Flotation Technique To Measure the Wettability Changes by Ionically Modified Water for Improved Oil Recovery in Carbonates. *Energy & Fuels* **2016**, *30* (8), 6306–6320. https://doi.org/10.1021/acs.energyfuels.6b01008.
(387) Aladasani, A.; Bai, B.; Wu, Y.-S.; Salehi, S. Studying Low-Salinity Waterflooding Recovery Effects in Sandstone Reservoirs. *Journal of Petroleum Science and Engineering* **2014**, *120*, 39–51. https://doi.org/10.1016/j.petrol.2014.03.008.
(388) Sohal, M. A.; Kucheryavskiy, S.; Thyne, G.; Søgaard, E. G. Study of Ionically Modified Water Performance in the Carbonate Reservoir System by Multivariate Data Analysis. *Energy Fuels* **2017**, *31* (3), 2414–2429. https://doi.org/10.1021/acs.energyfuels.6b02292.
(389) Yu, L.; Evje, S.; Kleppe, H.; Kårstad, T.; Fjelde, I.; Skjaeveland, S. M. Spontaneous Imbibition of Seawater into Preferentially Oil-Wet Chalk Cores — Experiments and Simulations. *Journal of Petroleum Science and Engineering* **2009**, *66* (3), 171–179. https://doi.org/10.1016/j.petrol.2009.02.008.
(390) Sanaei, A.; Sepehrnoori, K. Implication of Oil/Brine/Rock Surface Interactions in Modeling Modified Salinity Waterflooding in Carbonate and Sandstone Reservoirs. *SPE Annual Technical Conference and Exhibition, 24-26 September, Dallas, Texas, USA* **2018**, 26.
(391) Chandrasekhar, S.; Sharma, H.; Mohanty, K. K. Wettability Alteration with Brine Composition in High Temperature Carbonate Rocks; Society of Petroleum Engineers, 2016. https://doi.org/10.2118/181700-MS.
(392) Usui, S. Interaction of Electrical Double Layers at Constant Surface Charge. *Journal of Colloid and Interface Science* **1973**, *44* (1), 107–113. https://doi.org/10.1016/0021-9797(73)90197-5.
(393) Shehata, A. M.; Alotaibi, M. B.; Nasr-El-Din, H. A. Waterflooding in Carbonate Reservoirs: Does the Salinity Matter? *SPE Reservoir Evaluation & Engineering* **2014**, *17* (03), 304–313. https://doi.org/10.2118/170254-PA.

(394) Yousef, A. A.; Al-Saleh, S.; Al-Kaabi, A. U.; Al-Jawfi, M. S. Laboratory Investigation of Novel Oil Recovery Method for Carbonate Reservoirs; Society of Petroleum Engineers, 2010. https://doi.org/10.2118/137634-MS.
(395) Eftekhari, A. A.; Nick, H.; Bonto, M. An Overview of the Thermodynamic Models for the Chalk Surface Reactions with Brine; 2018. https://doi.org/10.3997/2214-4609.201800760.
(396) Ikeda, S. The Gibbs Adsorption Isotherm for Aqueous Electrolyte Solutions. *Advances in Colloid and Interface Science* **1982**, *18* (1–2), 93–130. https://doi.org/10.1016/0001-8686(82)85032-X.
(397) Guo, J.; Liu, Q.; Li, M.; Wu, Z.; Christy, A. A. The Effect of Alkali on Crude Oil/Water Interfacial Properties and the Stability of Crude Oil Emulsions. *Colloids and Surfaces A: Physicochemical and Engineering Aspects* **2006**, *273* (1–3), 213–218. https://doi.org/10.1016/j.colsurfa.2005.10.015.
(398) Appelo, C. A. J. Principles, Caveats and Improvements in Databases for Calculating Hydrogeochemical Reactions in Saline Waters from 0 to 200°C and 1 to 1000atm. *Applied Geochemistry* **2015**, *55*, 62–71. https://doi.org/10.1016/j.apgeochem.2014.11.007.
(399) Pauling, L. THE PRINCIPLES DETERMINING THE STRUCTURE OF COMPLEX IONIC CRYSTALS. *Journal of the American Chemical Society* **1929**, *51* (4), 1010–1026. https://doi.org/10.1021/ja01379a006.
(400) Zhang, P.; Tweheyo, M. T.; Austad, T. Wettability Alteration and Improved Oil Recovery by Spontaneous Imbibition of Seawater into Chalk: Impact of the Potential Determining Ions Ca2+, Mg2+, and SO42−. *Colloids and Surfaces A: Physicochemical and Engineering Aspects* **2007**, *301* (1–3), 199–208. https://doi.org/10.1016/j.colsurfa.2006.12.058.
(401) Zhang, P.; Tweheyo, M. T.; Austad, T. Wettability Alteration and Improved Oil Recovery in Chalk: The Effect of Calcium in the Presence of Sulfate. *Energy and Fuels* **2006**, *20* (5), 2056–2062. https://doi.org/10.1021/ef0600816.
(402) Cicerone, D. S.; Regazzoni, A. E.; Blesa, M. A. Electrokinetic Properties of the Calcite/Water Interface in the Presence of Magnesium and Organic Matter. *Journal of Colloid and Interface Science* **1992**, *154* (2), 423–433. https://doi.org/10.1016/0021-9797(92)90158-I.
(403) Pierre, A.; Lamarche, J. M.; Mercier, R.; Foissy, A. Calcium as Potential Determining Ion in Aqueous Calcite Suspensions. *j.Dispersion science and technology* **1990**, *6*, 611–635.
(404) Freeman, C. L.; Asteriadis, I.; Yang, M.; Harding, J. H. Interactions of Organic Molecules with Calcite and Magnesite Surfaces. *J. Phys. Chem. C* **2009**, *113* (9), 3666–3673. https://doi.org/10.1021/jp807051u.
(405) Ataman, E.; Andersson, M. P.; Ceccato, M.; Bovet, N.; Stipp, S. L. S. Functional Group Adsorption on Calcite: II. Nitrogen and Sulfur Containing Organic Molecules. *J. Phys. Chem. C* **2016**, *120* (30), 16597–16607. https://doi.org/10.1021/acs.jpcc.6b01359.
(406) Chun, B. J.; Lee, S. G.; Choi, J. I.; Jang, S. S. Adsorption of Carboxylate on Calcium Carbonate (10 $\bar{1}$ 4) Surface: Molecular Simulation Approach. *Colloids and Surfaces A: Physicochemical and Engineering Aspects* **2015**, *474*, 9–17. https://doi.org/10.1016/j.colsurfa.2015.03.003.
(407) Ataman, E.; Andersson, M. P.; Ceccato, M.; Bovet, N.; Stipp, S. L. S. Functional Group Adsorption on Calcite: I. Oxygen Containing and Nonpolar Organic Molecules. *J. Phys. Chem. C* **2016**, *120* (30), 16586–16596. https://doi.org/10.1021/acs.jpcc.6b01349.
(408) Ghatee, M. H.; Koleini, M. M.; Ayatollahi, S. Molecular Dynamics Simulation Investigation of Hexanoic Acid Adsorption onto Calcite (10$\bar{1}$4)Surface. *Fluid Phase Equilibria* **2015**, *387*, 24–31. https://doi.org/10.1016/j.fluid.2014.11.029.
(409) Budi, A.; Stipp, S. L. S.; Andersson, M. P. The Effect of Solvation and Temperature on the Adsorption of Small Organic Molecules on Calcite. *Phys. Chem. Chem. Phys.* **2018**, *20* (10), 7140–7147. https://doi.org/10.1039/C7CP06747J.
(410) Freeman, S. R.; Jones, F.; Ogden, M. I.; Oliviera, A.; Richmond, W. R. Effect of Benzoic Acids on Barite and Calcite Precipitation. *Crystal Growth & Design* **2006**, *6* (11), 2579–2587. https://doi.org/10.1021/cg060186z.

(411) Torsaeter, O. A Comparative Study of Wettability Test Methods Based on Experimental Results From North Sea Reservoir Rocks; Society of Petroleum Engineers, 1988. https://doi.org/10.2118/18281-MS.
(412) Rücker, M.; Bartels, W.-B.; Garfi, G.; Shams, M.; Bultreys, T.; Boone, M.; Pieterse, S.; Maitland, G. C.; Krevor, S.; Cnudde, V.; Mahani, H.; Berg, S.; Georgiadis, A.; Luckham, P. F. Relationship between Wetting and Capillary Pressure in a Crude Oil/Brine/Rock System: From Nano-Scale to Core-Scale. *Journal of Colloid and Interface Science* **2020**, *562*, 159–169. https://doi.org/10.1016/j.jcis.2019.11.086.
(413) Viksund, B. G.; Morrow, N. R.; Ma, S.; Wang, W.; Graue, A. 1998: Initial Water Saturation and Oil Recovery from Chalk and Sandstone by Spontaneous Imbibition. **1998**, 9.
(414) Ahkami, M.; Chakravarty, K. H.; Xiarchos, I.; Thomsen, K.; Fosbøl, P. L. Determining Optimum Aging Time Using Novel Core Flooding Equipment; Society of Petroleum Engineers, 2016. https://doi.org/10.2118/180054-MS.
(415) Kovscek, A. R.; Wong, H.; Radke, C. J. A pore-level scenario for the development of mixed wettability in oil reservoirs. *AIChE Journal* **1993**, *39* (6), 1072–1085. https://doi.org/10.1002/aic.690390616.
(416) Graue, A.; Aspenes, E.; Bognø, T.; Moe, R. W.; Ramsdal, J. Alteration of Wettability and Wettability Heterogeneity. *Journal of Petroleum Science and Engineering* **2002**, *33* (1), 3–17. https://doi.org/10.1016/S0920-4105(01)00171-1.
(417) Bartels, W.-B.; Rücker, M.; Boone, M.; Bultreys, T.; Mahani, H.; Berg, S.; Hassanizadeh, S. M.; Cnudde, V. Imaging Spontaneous Imbibition in Full Darcy-Scale Samples at Pore-Scale Resolution by Fast X-Ray Tomography. *Water Resources Research* **2019**, *55* (8), 7072–7085. https://doi.org/10.1029/2018WR024541.
(418) Andersson, M. P.; Hem, C. P.; Schultz, L. N.; Nielsen, J. W.; Pedersen, C. S.; Sand, K. K.; Okhrimenko, D. V.; Johnsson, A.; Stipp, S. L. S. Infrared Spectroscopy and Density Functional Theory Investigation of Calcite, Chalk, and Coccoliths—Do We Observe the Mineral Surface? *J. Phys. Chem. A* **2014**, *118* (45), 10720–10729. https://doi.org/10.1021/jp5053858.
(419) Hassenkam, T.; Skovbjerg, L. L.; Stipp, S. L. S. Probing the Intrinsically Oil-Wet Surfaces of Pores in North Sea Chalk at Subpore Resolution. *Proc Natl Acad Sci U S A* **2009**, *106* (15), 6071–6076. https://doi.org/10.1073/pnas.0901051106.
(420) Bonto, M.; Eftekhari, A. A.; Nick, H. Reactive Transport Modeling in Carbonate Reservoirs and Assessment of the Adsorption of Oil Polar Components on the Rock Surface; Book of Abstracts: Valencia, Spain: Universitat Politecnica de Valencia, 2019; pp 80–80.
(421) Zullig, J. J.; Morse, J. W. Interaction of Organic Acids with Carbonate Mineral Surfaces in Seawater and Related Solutions: I. Fatty Acid Adsorption. *Geochimica et Cosmochimica Acta* **1988**, *52* (6), 1667–1678. https://doi.org/10.1016/0016-7037(88)90235-9.
(422) Bovet, N.; Yang, M.; Javadi, M. S.; Stipp, S. L. S. Interaction of Alcohols with the Calcite Surface. *Physical Chemistry Chemical Physics* **2015**, *17* (5), 3490–3496. https://doi.org/10.1039/C4CP05235H.
(423) Lakshtanov, L. Z.; Bovet, N.; Stipp, S. L. S. Inhibition of Calcite Growth by Alginate. *Geochimica et Cosmochimica Acta* **2011**, *75* (14), 3945–3955. https://doi.org/10.1016/j.gca.2011.04.014.
(424) Puntervold, T.; Mamonov, A.; Piñerez Torrijos, I. D.; Strand, S. Adsorption of Crude Oil Components onto Carbonate and Sandstone Outcrop Rocks and Its Effect on Wettability. *Energy Fuels* **2021**, *35* (7), 5738–5747. https://doi.org/10.1021/acs.energyfuels.0c03003.
(425) Kaminsky, R.; Radke, C. J. Asphaltenes, Water Films, and Wettability Reversal. *SPE Journal* **1997**, *2* (04), 485–493. https://doi.org/10.2118/39087-PA.
(426) Thomas, M. M.; Clouse, J. A.; Longo, J. M. Adsorption of Organic Compounds on Carbonate Minerals: 3. Influence on Dissolution Rates. *Chemical Geology* **1993**, *109* (1), 227–237. https://doi.org/10.1016/0009-2541(93)90072-Q.

(427) Havre, T. E.; Sjöblom, J.; Vindstad, J. E. Oil/Water-Partitioning and Interfacial Behavior of Naphthenic Acids. *Journal of Dispersion Science and Technology* **2003**, *24* (6), 789–801. https://doi.org/10.1081/DIS-120025547.
(428) Andersen, S. I.; Chandra, M. S.; Chen, J.; Zeng, B. Y.; Zou, F.; Mapolelo, M.; Abdallah, W.; Buiting, J. J. Detection and Impact of Carboxylic Acids at the Crude Oil–Water Interface. *Energy & Fuels* **2016**, *30* (6), 4475–4485. https://doi.org/10.1021/acs.energyfuels.5b02930.
(429) Golmohammadi, M.; Mohammadi, S.; Mahani, H.; Ayatollahi, S. The Non-Linear Effect of Oil Polarity on the Efficiency of Low Salinity Waterflooding: A Pore-Level Investigation. *Journal of Molecular Liquids* **2021**, 117069. https://doi.org/10.1016/j.molliq.2021.117069.
(430) Morrow, N. R.; Buckley, J. S. *Wettability and Oil Recovery by Imbibition and Viscous Displacement from Fractured and Heterogeneous Carbonates*; DE-FC26-02NT15344; Chemical & Petroleum Engineering, University of Wyoming, 2006; p 184.
(431) Geffroy, C.; Foissy, A.; Persello, J.; Cabane, B. Surface Complexation of Calcite by Carboxylates in Water. *Journal of Colloid and Interface Science* **1999**, *211* (1), 45–53. https://doi.org/10.1006/jcis.1998.5966.
(432) Valiya Parambathu, A.; Wang, L.; Asthagiri, D.; Chapman, W. G. Apolar Behavior of Hydrated Calcite ($10\bar{1}4$) Surface Assists in Naphthenic Acid Adsorption. *Energy Fuels* **2019**, *33* (7), 6119–6125. https://doi.org/10.1021/acs.energyfuels.9b00877.
(433) Thomas, M. M.; Clouse, J. A.; Longo, J. M. Adsorption of Organic Compounds on Carbonate Minerals: 1. Model Compounds and Their Influence on Mineral Wettability. *Chemical Geology* **1993**, *109* (1), 201–213. https://doi.org/10.1016/0009-2541(93)90070-Y.
(434) Fathi, S. J.; Austad, T.; Strand, S. Effect of Water-Extractable Carboxylic Acids in Crude Oil on Wettability in Carbonates. *Energy Fuels* **2011**, *25* (6), 2587–2592. https://doi.org/10.1021/ef200302d.
(435) Madsen, L.; Lind, I. Adsorption of Carboxylic Acids on Reservoir Minerals From Organic and Aqueous Phase. *SPE Reservoir Evaluation & Engineering* **1998**, *1* (01), 47–51. https://doi.org/10.2118/37292-PA.
(436) Fuerstenau, M. C.; Miller, J. D. THE ROLE OF THE HYDROCARBON CHAIN IN ANIONIC FLOTATION OF CALCITE. *AIME Transactions* **1967**, *238*, 8.
(437) Fenter, P.; Sturchio, N. C. Structure and Growth of Stearate Monolayers on Calcite: First Results of an in Situ X-Ray Reflectivity Study. *Geochimica et Cosmochimica Acta* **1999**, *63* (19), 3145–3152. https://doi.org/10.1016/S0016-7037(99)00241-0.
(438) Legens, C.; Toulhoat, H.; Cuiec, L.; Villieras, F.; Palermo, T. Wettability Change Related to the Adsorption of Organic Acids on Calcite: Experimental and Ab Initio Computational Studies; Society of Petroleum Engineers, 1998. https://doi.org/10.2118/49319-MS.
(439) Ivanova, A.; Mitiurev, N.; Cheremisin, A.; Orekhov, A.; Kamyshinsky, R.; Vasiliev, A. Characterization of Organic Layer in Oil Carbonate Reservoir Rocks and Its Effect on Microscale Wetting Properties. *Sci Rep* **2019**, *9* (1), 1–10. https://doi.org/10.1038/s41598-019-47139-y.
(440) Saraji, S.; Goual, L.; Piri, M. Dynamic Adsorption of Asphaltenes on Quartz and Calcite Packs in the Presence of Brine Films. *Colloids and Surfaces A: Physicochemical and Engineering Aspects* **2013**, *434*, 260–267. https://doi.org/10.1016/j.colsurfa.2013.05.070.
(441) Dudášová, D.; Simon, S.; Hemmingsen, P. V.; Sjöblom, J. Study of Asphaltenes Adsorption onto Different Minerals and Clays: Part 1. Experimental Adsorption with UV Depletion Detection. *Colloids and Surfaces A: Physicochemical and Engineering Aspects* **2008**, *317* (1), 1–9. https://doi.org/10.1016/j.colsurfa.2007.09.023.
(442) Al-Balushi, M. A.; Karimi, M.; Al-Maamari, R. S. Impact of Acid and Base Numbers and Their Ratios on Wettability Alteration of the Calcite Surface. *Energy Fuels* **2020**, *34* (1), 245–257. https://doi.org/10.1021/acs.energyfuels.9b03538.
(443) Young, C. A.; Miller, J. D. Effect of Temperature on Oleate Adsorption at a Calcite Surface: An FT-NIR/IRS Study and Review. *International Journal of Mineral Processing* **2000**, *58* (1), 331–350. https://doi.org/10.1016/S0301-7516(99)00057-5.

(444) Mohammed, M. A.; Sorbie, K. S. Thermodynamic Modelling of Calcium Naphthenate Formation: Model Predictions and Experimental Results. *Colloids and Surfaces A: Physicochemical and Engineering Aspects* **2010**, *369* (1), 1–10. https://doi.org/10.1016/j.colsurfa.2010.08.034.
(445) Beneventi, D.; Carré, B.; Gandini, A. Precipitation and Solubility of Calcium Soaps in Basic Aqueous Media. *J Colloid Interface Sci* **2001**, *237* (1), 142–144. https://doi.org/10.1006/jcis.2001.7431.
(446) Somasundaran, P. Adsorption of Starch and Oleate and Interaction between Them on Calcite in Aqueous Solutions. *Journal of Colloid and Interface Science* **1969**, *31* (4), 557–565. https://doi.org/10.1016/0021-9797(69)90056-3.
(447) Kulkarni, R. D.; Somasundaran, P. Flotation Chemistry of Hematite/Oleate System. *Colloids and Surfaces* **1980**, *1* (3), 387–405. https://doi.org/10.1016/0166-6622(80)80025-4.
(448) Rao, K. H.; Cases, J. M.; Forssberg, K. S. E. Mechanism of Oleate Interaction on Salt-Type Minerals: V. Adsorption and Precipitation Reactions in Relation to the Solid/Liquid Ratio in the Synthetic Fluorite—Sodium Oleate System. *Journal of Colloid and Interface Science* **1991**, *145* (2), 330–348. https://doi.org/10.1016/0021-9797(91)90365-F.
(449) Meyers, P. A.; Quinn, J. G. Interaction between Fatty Acids and Calcite in Seawater1. *Limnology and Oceanography* **1971**, *16* (6), 992–997. https://doi.org/10.4319/lo.1971.16.6.0992.
(450) Suess, E. Interaction of Organic Compounds with Calcium Carbonate—I. Association Phenomena and Geochemical Implications. *Geochimica et Cosmochimica Acta* **1970**, *34* (2), 157–168. https://doi.org/10.1016/0016-7037(70)90003-7.
(451) Mishra, S. K. Electrokinetic Properties and Flotation Behaviour of Apatite and Calcite in the Presence of Sodium Oleate and Sodium Metasilicate. *International Journal of Mineral Processing* **1982**, *9* (1), 59–73. https://doi.org/10.1016/0301-7516(82)90006-0.
(452) Bertheussen, A.; Simon, S.; Sjöblom, J. Equilibrium Partitioning of Naphthenic Acid Mixture Part 2: Crude Oil-Extracted Naphthenic Acids. *Energy Fuels* **2018**, *32* (9), 9142–9158. https://doi.org/10.1021/acs.energyfuels.8b01870.
(453) Bertheussen, A.; Simon, S.; Sjöblom, J. Equilibrium Partitioning of Naphthenic Acid Mixture, Part 1: Commercial Naphthenic Acid Mixture. *Energy Fuels* **2018**, *32* (7), 7519–7538. https://doi.org/10.1021/acs.energyfuels.8b01494.
(454) Sarac, S.; Civan, F. Mechanisms, Parameters, and Modeling of Naphthenate-Soap-Induced Formation Damage. *SPE Journal* **2009**, *14* (02), 259–266. https://doi.org/10.2118/112434-PA.
(455) Palandri, J. L.; Kharaka, Y. K. *A Compilation of Rate Parameters of Water-Mineral Interaction Kinetics for Application to Geochemical Modeling*; Open-File Report; Open-File Report 1068; 2004.
(456) Dyer, S. J.; Graham, G. M.; Arnott, C. Naphthenate Scale Formation - Examination of Molecular Controls in Idealised Systems; OnePetro, 2003. https://doi.org/10.2118/80395-MS.
(457) Osman, M. A.; Suter, U. W. Surface Treatment of Calcite with Fatty Acids: Structure and Properties of the Organic Monolayer. *Chem. Mater.* **2002**, *14* (10), 4408–4415. https://doi.org/10.1021/cm021222u.

List of Publications

Journal publications (included in the thesis)

1. **Bonto**, **M**., Eftekhari, A.A., Nick, H.M. (2019). An overview of the oil-brine interfacial behavior and a new surface complexation model. Scientific Reports *9*, 1–16.
2. **Bonto**, **M**., Eftekhari, A.A., Nick, H.M. (2020). Wettability indicator parameter based on the thermodynamic modeling of chalk-oil-brine systems. Energy & Fuels 34 (7), 8018-8036.
3. **Bonto, M.**, Nick, H.M., Eftekhari, A.A. (2021). Thermodynamic analysis of the temperature effect on calcite surface reactions in aqueous environments. Energy & Fuels 35 (20) 16677-16692
4. **Bonto**, **M**., Eftekhari, A.A., Nick, H.M. Electrokinetic behavior of artificial and natural calcites: a review of experimental measurements and surface complexation models. In revision.
5. **Bonto**, **M**., Eftekhari, A.A., Nick, H.M. Modelling the adsorption of carboxylates on calcite: coupled effect of calcite-brine and brine-oil interactions. Under review.

Journal publications (not included in the thesis):

6. Taheriotaghsara, M., **Bonto, M**., Eftekhari, A.A., Nick, H.M. (2020). Prediction of oil breakthrough time in modified salinity water flooding in carbonate cores. Fuel 274, 117806.
7. Taheriotaghsara, M., **Bonto, M.**, Nick, H.M., Eftekhari, A.A. (2021). Estimation of calcite wettability using surface forces. Journal of Industrial and Engineering Chemistry, 98, 444–57.
8. **Bonto, M.,** Welch, M., Lüthje, M., Andersen, S.I., Veshareh, M.J. et al. (2021). Challenges and enablers for large-scale CO_2 storage in chalk formations. Earth-Science Reviews, 222, 103826.

Conference Proceedings (not included in the thesis):

9. **Bonto**, **M**., Eftekhari, A.A., Nick, H.M. (2019, April). A Calibrated Model for the Carbonate-Brine-Crude Oil Surface Chemistry and its Effect on the Rock Wettability, Dissolution, and Mechanical Properties. In SPE Reservoir Simulation Conference. Society of Petroleum Engineers, 193865-MS.
10. **Bonto**, **M**., Eftekhari, A.A., Nick, H.M. (2019, April). A Mechanistic Model for the Fines-migration During the Modified-salinity Waterflooding in Carbonate Reservoirs. European Association of Geoscientists & Engineers, pp. 1–18.
11. Taheri, M., **Bonto**, **M**., Eftekhari, A.A., Nick, H.M. (2019, April). Analyzing the Production Chemistry Data of the North Sea Chalk Reservoirs with a Multiphase Reactive Transport Model. European Association of Geoscientists & Engineers, pp. 1–15.
12. Taheri, M., **Bonto**, **M**., Eftekhari, A., Torrijos, I.D.P., Puntervold, T., Strand, S., Nick, H.M. (2019, April). Analyzing the Smart Water Core-flooding Data in Carbonates by Modelling the Oil Breakthrough Time Using a Novel Reactive Transport Model. European Association of Geoscientists & Engineers, pp. 1–21.
13. Amour, F., **Bonto, M.**, Hajiabadi, M.R., Nick, H.M. (2021). Sensitivity Study of Chemical Effects on the Compaction Behavior of Reservoir Chalk (Dan Field, Danish North Sea). In 55th US Rock Mechanics/Geomechanics Symposium, OnePetro.

MARIA BONTO

Gladsaxevej 400 C, Copenhagen, Denmark, 2860
(+45) 50252556 ◦ maria.bonto23@yahoo.com

EDUCATION

Technical University of Denmark, Denmark 2018-2021
Doctor of Philosophy in Applied Mathematics and Computer Science

Technical University of Denmark, Denmark 2016-2018
Master of Science in Petroleum Engineering

Rey Juan Carlos University, Spain 2010-2016
Joint degree in Chemical Engineering and Energy Engineering

DTU Compute

Richard Petersens Plads
Building 324
2800 Kongens Lyngby

www.compute.dtu.dk

Danish Hydrocarbon
Research and Technology
Centre

Elektrovej
Building 375
2800 Kongens Lyngby

www.oilgas.dtu.dk